CRANFIELD UNIVERSITY

MUHAMMAD ILHAM ADHYNUGRAHA

LONGITUDINAL DYNAMICS OF WING IN GROUND EFFECT CRAFT IN WAVES

ENERGY AND POWER THEME
Offshore and Renewable Energy

PhD Thesis
Academic Year: 2016 - 2017

Supervisor:
Dr Maurizio Collu
Prof Feargal Brennan

June 2017

CRANFIELD UNIVERSITY

ENERGY AND POWER THEME
Offshore and Renewable Energy

PhD Thesis

Academic Year 2016 - 2017

MUHAMMAD ILHAM ADHYNUGRAHA

Longitudinal Dynamics of Wing in Ground Effect Craft in Waves

Supervisor:
Dr Maurizio Collu
Prof Feargal Brennan

June 2017

This thesis is submitted for the degree of Doctor of Philosophy

ABSTRACT

An assessment of the longitudinal motion of a hybrid configuration called the aerodynamically alleviated marine vehicle (AAMV) with the presence of waves, is demonstrated in the thesis. The development of this type of vehicle requires a mathematical framework to characterise its dynamics with the influence of external forces due to the waves' motion.

An overview of the effect of waves towards the models of dynamics developed for wing in ground effect (WIGE) craft and high-speed marine vehicles (planing craft) is carried out. However, the overview only leads to a finding that the longitudinal stability of a lifting surface over wavy ground effect is not entirely established.

Taking this fact into account, the analysis of the model is proposed for a WIGE craft configuration. A simplification is adopted considering heave motion only in the modelling of oscillation. The simplification is made to thoroughly capture the effect of oscillation toward dynamic stability of the vehicle.

To support the model verification, a numerical simulation followed by a semi-empirical design method was adopted to produce aerodynamic data, both in two-dimensional and three-dimensional domains, respectively. The results show that the combination of underpinning parameters, i.e. ride height, frequency and amplitude of oscillation, remarkably influence the aerodynamics.

The characteristics in aerodynamics affect the production of stability derivatives and eventually stability behaviour of the chosen configuration. Some patterns in the results are identified but there also some data that show the peculiarity. Thus further investigation is needed.

Keywords:

Aerodynamics, stability derivatives, dynamic stability, oscillation

ACKNOWLEDGEMENTS

All praises are due to Allah, the Lord of the universe. I sincerely offer my humble submission to Him. I bear witness no god has the right to be worshipped but He, and Muhammad (peace be upon him) is His slave and messenger. There are not enough words to convey my gratitude for the immeasurable grace so I can reach this accomplishment.

The greatest achievement of this research is that I ended up with a mindfulness that the work I have been engaged in is like a drop of water in the ocean of knowledge. It is true that my name is written on the cover of this thesis as the author, but the research itself has involved many people who have supported me in the best way they could. I send my appreciation to all those people, especially Dr Maurizio Collu as my supervisor, and Dr Takafumi Nishino as the subject advisor of this research.

I want to give acknowledgements to the Ministry of Research Technology and Higher Education (Kemenristekdikti), the Agency for the Assessment and Application of Technology (BPPT) – especially the Centre for Industrial Machinery Technology (PTI Permesinan) - and Cranfield University for giving me the opportunity to pursue the degree of Doctor of Philosophy.

Finally, I want to send my salaam to my late father, Mukhdar Bakara Soegi *rahimahullah*, and my mother, Sumarni Jasin Soegi. They have been giving their best, so I can still stand firm up to this point of life.

TABLE OF CONTENTS

LIST OF FIGURES

LIST OF TABLES

LIST OF EQUATIONS

LIST OF NOTATIONS AND ABBREVIATIONS

$[0]_{i\times j}$	Zeros matrix, i row times j column
a_{ah}, a_F, a_{ws}	Pitch moment arm of the corresponding parameter, i.e. D_{ah}, D_F, D_{ws}
a	Real component of characteristic roots
A	Amplitude, sometimes written in A/c to indicate the parameter is nondimensionalised
$AAMV$	Aerodynamically Alleviated Marine Vehicle
AAZ	Aerodynamic Alleviated Zone
AR	Wing aspect ratio
$\mathbb{A}, \mathbb{B}, \mathbb{C}, \mathbb{D}, \mathbb{E}, \mathbb{F}, \mathbb{G}$	Characteristic polynomial coefficients
$[A]$	Mass + Added mass matrix. When it excludes the effect of system mass, the matrix denotes as $[A^{\dagger}]$
$[A_s]$	Left state space matrix
b	Wing span
$\mathscr{b}$	Imaginary component of characteristic roots
$[B]$	Damping matrix
$[B_s]$	Right state space matrix
c (see context)	• Pitch moment arm of N – related to equilibrium attitude • Chord length – related to aerofoil/wing aerodynamics • Spring coefficient – related to system dynamics
c_d	Drag coefficient of an aerofoil
c_{d_α}, c_{d_h}	The slope of drag coefficient of an aerofoil against the corresponding parameter
$c_{d_{ig}}$	Drag coefficient of an aerofoil in ground effect
c_l	Lift coefficient of an aerofoil
c_{l_α}, $c_{l_{\alpha_{eff}}}$, c_{l_h}	The slope of lift coefficient of an aerofoil against the corresponding parameter
$c_{l_{og}}$	Lift coefficient of an aerofoil out of ground effect
c_m	Pitch moment coefficient of an aerofoil
c_{m_α}, c_{m_h}	The slope of pitch coefficient of an aerofoil against the corresponding parameter
C_D	Drag coefficient of a vehicle
C_{D_0}	Parasite drag coefficient

C_{D_i}	Induced drag coefficient
$C_{D_{L\&P}}$	Drag coefficient due to the contribution of leakages and protuberances
$C_{D_{Misc.}}$	Miscellaneous drag components for special features, e.g. flaps, etc.
C_{D_α}, C_{D_h}	The slope of drag coefficient of a vehicle against the corresponding parameter
C_f	Skin friction coefficient (general)
C_{f_e}	Equivalent skin friction coefficient
C_{f_c}	Skin friction coefficient of a component, e.g. tail, fuselage, etc.
C_L	Lift coefficient of a vehicle
C_{L_α}, C_{L_h}	The slope of lift coefficient of a vehicle against the corresponding parameter
C_m	Pitch moment coefficient of a vehicle
C_{m_α}, C_{m_h}	The slope of pitch moment coefficient of a vehicle against the corresponding parameter
$[C]$	Restoring stability matrix
d	Fuselage diameter
d_s	Submerged depth in water
D	Drag (general)
D_{ah}	Aerodynamic drag experienced by the dry section of the hull
$D_{a1,2}$	Aerodynamic drag experienced by aerodynamic surfaces ($a1$ for the first surface and $a2$ for the second surface)
D_F	Hydrodynamic frictional drag
D_{ws}	Whisker spray drag force (due to the hull)
$[D]$	Aerodynamic ground effect matrix
e	Oswald number
F	Force (general kind)
F_{FK}	Froude-Krylov forces
F_w	External forces due to the presence of waves, $F_w = F_w^a + F_w^h$
F_{w_A}	Amplitude of external forces due to the presence of waves
F_w^a	Induced aerodynamic forces due to the motion of waves
F_w^h	Induced hydrodynamic forces due to the motion of waves
FF_c	Form factor of a component, e.g. tail, fuselage, etc.

FLF	Fuselage lift factor
g	Gravitational constant acceleration
h	Ride height, sometimes written in h/c to indicate the parameter is nondimensionalised
H	$\partial(h)/\partial t$
$H_{1/3}$	Significant wave height
$HSMV$	High-speed Marine Vehicle
$[H_s]$	State space matrix
IMO	International Maritime Organization
$[I]$	Matrix of identity
I_y	Pitching moment of inertia
k	Reduced frequency
$\not{k}$	Wave number (general), $2\pi/\lambda$
$\not{k}_j$	Wave number of the j[th] wave, $2\pi/\lambda_j$
K (see context)	• Kinetic energy – related to turbulence model • Drag-due-to-lift factor – related to design configuration
K_{eff}	Effective drag-due-to-lift factor
ℓ	Reference length; differ for each component, e.g. wing mac, tail mac, and the length of fuselage
L	Lift force (general)
$L_{a1,2}$	Aerodynamic lift experienced by aerodynamic surfaces ($a1$ for the first surface and $a2$ for the second surface)
m	Mass of the system
mac	Mean aerodynamic chord
M	Pitch moment (general)
Ma	Mach number
$M_{a1,2}$	Aerodynamic pitch moments of aerodynamic surfaces ($a1$ for the first surface and $a2$ for the second surface)
M_h^a, M_q^a,M_u^a, M_w^a, $M_{\dot{w}}^a$	Derivative of aerodynamic pitch moment with respect to the corresponding variable, i.e. ride height (h), pitch rate (q), axial velocity (u), normal velocity (w), and normal acceleration ($\dot{w}$); applicable for AAMV/WIGE craft case
M_q^h, M_u^h, M_w^h, $M_{\dot{q}}^h$, $M_{\dot{u}}^h$, $M_{\dot{w}}^h$, M_z^h, M_θ^h	Derivative of hydrodynamic pitch moment with respect to the corresponding variable, i.e. pitch rate (q), axial velocity (u), normal velocity (w), pitch angular acceleration ($\dot{q}$), axial

	acceleration ($\dot{u}$), normal acceleration ($\dot{w}$), heave displacement (z), and pitch angle (θ); applicable for AAMV/HSMV case
N	Hydrodynamic potential force
q	Pitch rotation velocity
$\dot{q}$	Pitch rotation acceleration
Q_c	Interference factor in drag calculation of a component, e.g. tail, fuselage, etc.
Re	Reynolds number
Re_{cut}	Fictitious cut-off Reynolds number of a component
$RULM$	Rectilinear Uniform Level Motion
s	Laplace variable, roots of the mode of oscillation
S	Area (general)
$S_{Exp.}$	Exposed area of wing, in accordance to wetted area
$S_{Ref.}$	Reference area of wing (clean without additional devices)
$S_{Wet.}$	Wetted area (general)
$S_{Wet.c}$	Wetted area of a component, e.g. tail, fuselage, etc.
SM	Static margin
SR	Skin roughness factor
t	Time
(t/c)	thickness ratio against chord length
T	Propulsion force (thrust)
TAP	Transport Amphibious Platform
u	Axial velocity
$\dot{u}$	Axial acceleration
U_e	Forward velocity at equilibrium
w	Normal velocity
$\dot{w}$	Normal acceleration
W	Gravitational force (weight)
$WIGE$	Wing in Ground Effect
WMO	World Maritime Organization
x (see context)	• Surge displacement (small disturbance variable, positive forward) – related to dynamic • Position in the direction of the wave propagation – related to wave function

$(x/c)_m$	Chord wise location of the aerofoil maximum thickness point
X_h^a, X_q^a, X_u^a, X_w^a, $X_{\dot{w}}^a$	Derivative of aerodynamic surge force with respect to the corresponding variable, i.e. ride height (h), pitch rate (q), axial velocity (u), normal velocity (w), and normal acceleration ($\dot{w}$); applicable for AAMV/WIGE craft case
X_q^h, X_u^h, X_w^h, $X_{\dot{q}}^h$, $X_{\dot{u}}^h$, $X_{\dot{w}}^h$, X_z^h, X_θ^h	Derivative of hydrodynamic surge force with respect to the corresponding variable, i.e. pitch rate (q), axial velocity (u), normal velocity (w), pitch angular acceleration ($\dot{q}$), axial acceleration ($\dot{u}$), normal acceleration ($\dot{w}$), heave displacement (z), and pitch angle (θ); applicable for AAMV/HSMV case
z	Heave displacement (small disturbance variable, positive downward)
Z_h^a, Z_u^a, Z_w^a, Z_q^a, $Z_{\dot{w}}^a$	Derivative of aerodynamic heave force with respect to the corresponding variable, i.e. ride height (h), axial velocity (u), normal velocity (w), pitch rate (q); applicable for AAMV/WIGE craft case
Z_q^h, Z_u^h, Z_w^h, $Z_{\dot{q}}^h$, $Z_{\dot{u}}^h$, $Z_{\dot{w}}^h$, Z_z^h, Z_θ^h	Derivative of hydrodynamic heave force with respect to the corresponding variable, i.e. pitch rate (q), axial velocity (u), normal velocity (w), pitch angular acceleration ($\dot{q}$), axial acceleration ($\dot{u}$), normal acceleration ($\dot{w}$), heave displacement (z), and pitch angle (θ); applicable for AAMV/HSMV case
α	Angle of attack
α_{eff}	Effective angle of attack
α_ω	Relative angle of attack due to the oscillation of the system
ε	• Phase lags (general) – related to wave function • Energy dissipation – related to turbulence model
ε_j	Random wave phase for the j[th] wave
ϵ	Angle between the mac and the keel
ζ	Wave elevation (as a function of position and time)
ζ_A	Wave amplitude (general)
ζ_{Aj}	Wave amplitude for the j[th] wave
$\underline{\eta}$	Small disturbance vector, $[x \quad z \quad \theta]^T$
$\underline{\dot{\eta}}$	$\partial\underline{\eta}/\partial t = [u \quad w \quad q]^T$
$\underline{\ddot{\eta}}$	$\partial\underline{\dot{\eta}}/\partial t = [\dot{u} \quad \dot{w} \quad \dot{q}]^T$
θ	Pitch rotation angle (small disturbance variable, positive bow-up)
λ	Wavelength (general)

λi	i[th] position in a wavelength
λ_j	Wavelength for the j[th] wave
Λ	Wing sweep angle (general)
$\Lambda_{\max t}$	Wing sweep angle where aerofoil section is the thickest
μ (see context)	• Angle between wave speed and speed vector, course angle – related to wave motion • Fluid viscosity – related to fluid flow analysis)
μ_t	Kinematic eddy viscosity
$\underline{\nu}$	State space vector
$\dot{\underline{\nu}}$	$\partial \underline{\nu} / \partial t$
ρ	Fluid density (water/air – see the context)
$\xi_{ac1,2}$	Aerodynamic centres' location in axial direction relative to the body-fixed axes system ($ac1$ for the first surface and $ac2$ for the second surface)
ξ_{TP}	Thrust point in axial direction relative to the body-fixed axes system
ς_s, ς_p	Damping ratio of the SPPO and Phugoid mode
τ	Trim angle
$\phi_{ac1,2}$	Aerodynamic centres' location in normal direction relative to the body-fixed axes system ($ac1$ for the first surface and $ac2$ for the second surface)
ϕ_{TP}	Thrust point in normal direction relative to the body-fixed axes system
ω (see context)	• Circular wave frequency (general) – related to wave function • Specific dissipation rate – related to turbulence model
ω_e	Frequency of encounter
ω_j	Frequency for the j[th] wave
ω_n	Natural frequency
ω_s, ω_p	Natural frequency of the SPPO and Phugoid mode
$\mathfrak{N}$	Aerofoil efficiency

1 INTRODUCTION

This chapter introduces focal information which is the foundation of this thesis document. The chapter comprises seven sections, and those are *(1) Background*; *(2) Context*; *(3) Problem statement*; *(4) Aim and objectives*; *(5) Research methodology*; *(6) Thesis organisation*; and *(7) Conclusion*.

1.1 Background

The technology of water transportation modes has reached a level where hybrid concepts become a new option in their development. One of the perspectives in this regard is focused on the combination of external forces to sustain the weight of marine vehicles.

Revisiting the sustention concept of marine vehicles depicted by the weight sustention triangle is one way to understand the concept of hybrid in weight sustention of marine vehicles. From a traditional viewpoint, the weight of a water vehicle is supported by either hydrostatic lift, powered aerostatic lift or hydrodynamic lift.

The next development was to combine those forces to sustain the weight of new generation marine vehicles. The combination has led the emergence of a variety of marine vehicles in the market, see Figure 1-1. One of the reasons behind the endeavour of manufacturing marine vehicles with hybrid characteristics is to carry more payloads and to cruise further and faster.

The use of the aerodynamic lift to sustain the weight of marine vehicles was presented with the appearance of wing in ground effect (WIGE) craft in the 1960s; one of the examples is depicted in Figure 1-3. However, the study of the ground effect phenomenon came earlier enough (Raymond, 1921). Despite major resemblances to aircraft, WIGE has been considered as a type of marine vehicle rather than aircraft, thus adopts IMO regulations in most of its operating modes.

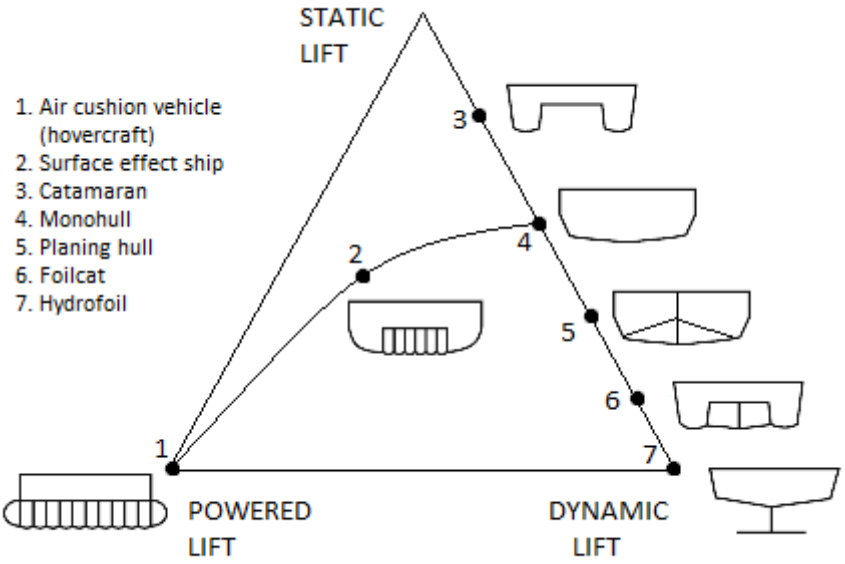

Figure 1-1 Lift sustention triangle

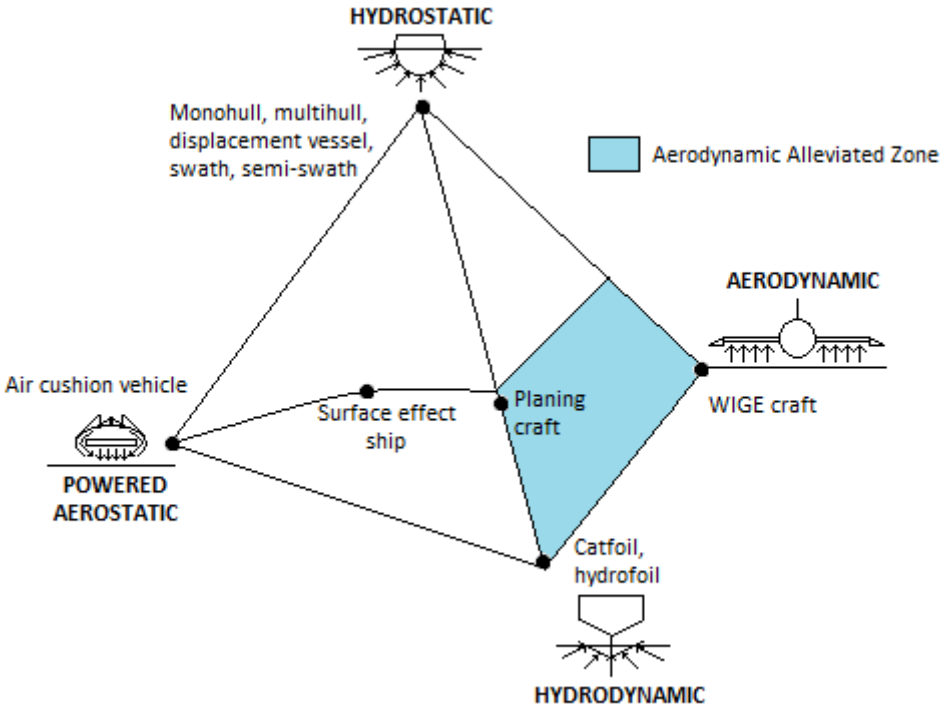

Figure 1-2 Lift sustention pyramid

The introduction of aerodynamics in the weight-sustaining concept has forced a modification of the weight sustention triangle into the weight sustention pyramid, see Figure 1-2. It also creates an outlook for further development in marine vehicles' technology. One of the examples is a newly introduced idea of aerodynamically alleviated marine vehicles - AAMV (Collu, 2008), see Figure 1-4. The concept is one of the future options for sea transportation modes (www.lemarin.fr, 2015; www.meretmarine.com, 2015). Considering the features it offers, AAMV may secure a niche place in the market for seagoing vessels. In the approach formulated by Gabrielli and von Karman (1950) and expanded by Yong et al. (2005), AAMV is projected to fill in the gap between conventional high-speed marine vehicle (HSMV) technology and low-speed aircraft. Hence, the benefit offered by this concept is, profitably, about overcoming the issues of operational costs because of the higher speed and less fuel consumption it offers. However, albeit AAMV is relatively new terminology, the study in the area started not as recently as it seemed. A study on the stability characteristics of KUDU II was done by Kallio (1978) and Ward et al. (1978); that the conceptual vehicle utilised both hydrodynamics and aerodynamics in its manoeuvre.

1.1.1 Aerodynamically Alleviated Marine Vehicles: General concept

When the idea of combining aerodynamics and hydrodynamics in sustaining the weight of marine vehicles emerged, the direct implication was that two terminologies were derived. First was the AAMV itself and the other one was Aerodynamically Alleviated Zone (AAZ) (Collu, 2008).

An AAMV is defined as:

> *"a high-speed marine vehicle designed to exploit, in its cruise phase, the aerodynamic lift force, using one or more aerodynamic surfaces."*

While the terminology of AAZ can be elaborated as:

"the area represents the points where a combination of buoyancy, hydrodynamic lift and aerodynamic lift is used to sustain the weight of a vehicle."

In Figure 1-2, the blue highlighted area between hydrostatic, hydrodynamics and aerodynamic corners illustrates the AAZ.

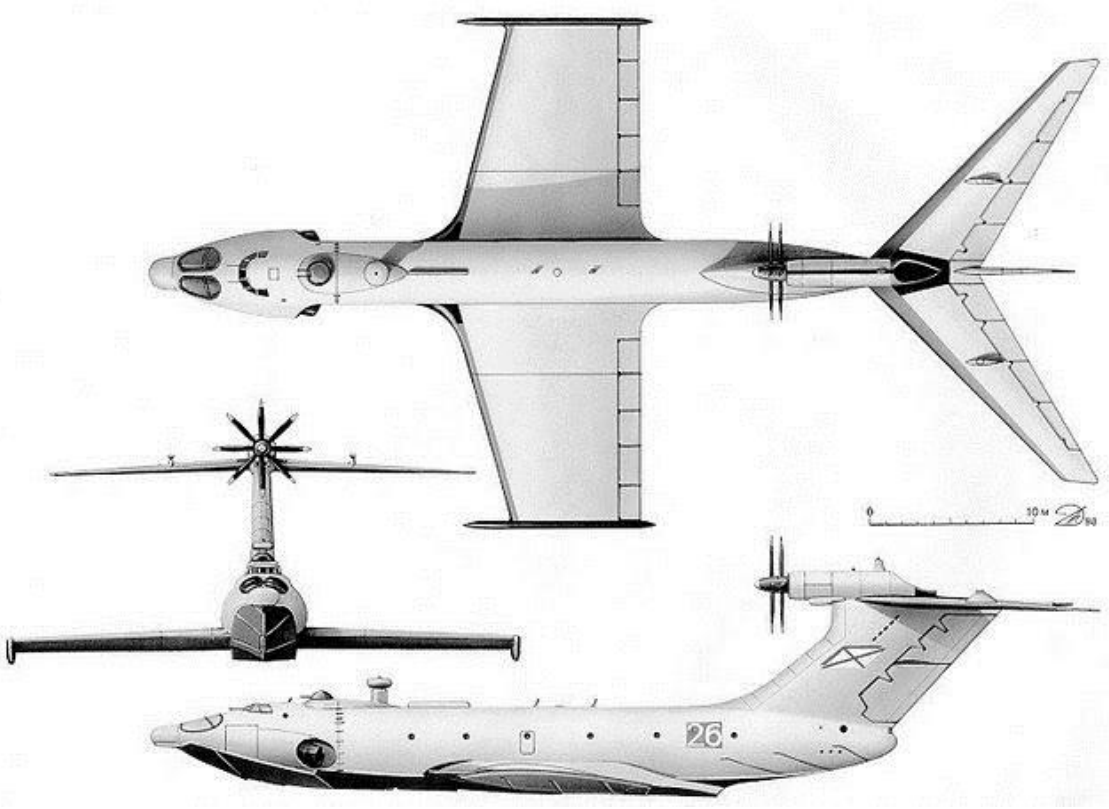

Figure 1-3 Orlyonok Ekranoplan, an example of WIGE craft

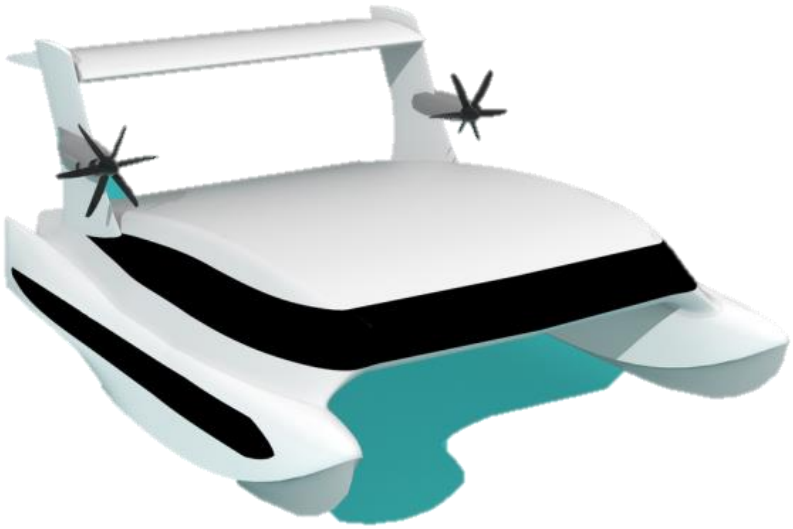

Figure 1-4 Example of AAMV configuration

1.1.2 Aerodynamically Alleviated Marine Vehicles: Further outlook

There is a great prospect to carry out research in the AAMV realm, and it is reasonable from two aspects. Firstly, reflecting the situation of the current condition that AAMV is one of the future alternatives in water transportation. Secondly, at this stage, only a small number of academic articles discuss the aerodynamics-hydrodynamics' utilisation in marine vehicles. The topics of research in the field are also plentiful, covering broad areas including aerodynamics, hydrodynamics, design configuration, structural integrity, material, stability, ergonomics, and economics.

Before stepping into those research topics in the AAMV realm, it is essential to identify possible problems that may occur with the vehicle. A brief hypothesis in this regard is that AAMV is likely to experience similar problems encountered by conventional HSMV and WIGE craft. However, the possibility that the vehicle may undergo unique problems does exist.

Distinctive behaviours may arise from many aspects, for instance, a constant aerodynamic-hydrodynamic interaction. Further discussion of the challenges is available in Chapter 2.

1.2 Context

As explained in Section 1.1, the research in AAMV covers a broad range of study. Amongst the topics related to the AAMV, the author decided **to focus on the dynamics of the vehicle with the consideration of operation under wavy environment**. The focus was considered after an extensive examination of a nine-month literature review.

One of the issues encountered in this research was related to the insufficiency of scholarly resources available in the area. The impediment is not exclusive to the dynamics field but also other areas related. In the case of the dynamics of AAMV, one of the reasonable methods to analyse it is by examining and then combining the dynamics of WIGE craft and HSMV. This method was proposed by Collu et al. (2008a). However, there was also a disclaimer concerning the level of accuracy between aerodynamic and hydrodynamic forces in the analysis (Collu, 2008, p.5). From this standpoint, it was decided for the present work **to focus on the analysis of the longitudinal dynamics over wavy surfaces**. The lateral-directional motion is, of course, necessary, especially how it affects the ergonomics of human beings (Journee and Pinkster, 2002). However, the longitudinal movement became the focus due to the reason to maintain the continuation of preceding study.

During the completion of the research programme, the author realised that the chosen topic was still too broad. It was found that the available literature on the longitudinal dynamics of WIGE craft over wavy surfaces was insufficient and it became an obstacle to comprehend the longitudinal dynamics of an AAMV configuration in a similar situation. This limitation **led to the decision to observe the topic toward WIGE craft instead of AAMV**. Examining longitudinal motion

of WIGE craft in such conditions would also benefit the comprehension of the dynamics of AAMV.

The decision to focus on WIGE craft also brought forward another consequence, of executing additional work, namely Computational Fluid Dynamic (CFD) analysis of an aerofoil oscillating in ground effect. The CFD analysis consumed nearly a one-year period. Unfortunately, due to the time constraint of the programme, the CFD analysis was not escalated to investigate the aerodynamics of the wing configuration or full configuration of the chosen vehicle. To provide three-dimensional aerodynamic analyses, another approach was carried out.

Acknowledging the numerical study that had been carried out, **this thesis includes the discussion about it** in one dedicated chapter. The significance of CFD analysis is about recognition of the behaviour of aerodynamic derivatives for dynamic analysis purpose. Also, from this work, a contribution to knowledge in the field is derived.

It has been mentioned that some limitations had prevented further CFD study to obtain three-dimensional data and led to the use of a different approach. The approach was a **semi-empirical approach used to transform aerofoil aerodynamic data into wing-tail-fuselage aerodynamic data and, conclusively, the aerodynamic derivatives of the designated configuration**. This arrangement, however, was not intended to provide high fidelity data but more about capturing the trend of the configuration in oscillation modes.

The configuration to be adopted by the current research is a WIGE craft design based on Orlyonok Ekranoplan A-90. The choice is based on the data and discussion available in Delhaye's (1997) thesis.

The present study, as available in this document, has demonstrated the significances of waves' parameters to the ground effect phenomenon and its implications on dynamics. **The ride height, frequency, and amplitude of oscillation** affect aerodynamic behaviour and stability characteristics.

1.3 Problem statement

"Do waves affect the longitudinal stability of an aerodynamically alleviated marine vehicle?"

The formulation of the problem statement for this research was a product of the literature review. As a relatively new area, AAMV offers many options for research activities.

Reflecting previous research by Collu (2008) and Collu et al. (2007, 2008a, 2008b, 2010), the discussion is about the stability and the development of mathematical models of dynamics of the vehicle. These are an excellent pivotal point to prompt further research. Besides, without disavowing the importance of other aspects, the dynamic study determines whether the vehicle as a system works as desired or not. In the present work, the novelty instead consists of the modelling and analysis of the effect of the waves on the dynamics of WIGE/AAMV.

The decision to involve the effect of waves imposed many implications at many levels. Deriving a set of questions is a way to examine those effects. The questions below have been the guidelines to establish a clear problem statement and determine a methodology to answer the problem statement. The list of the questions is as follows:

a. What is the influence of waves in the stability analysis of an AAMV?
b. How can the effect of the waves be formulated into the equations of motion?
c. How would the derivatives of forces and moments be affected by the movement?
d. To what extent do the waves influence the longitudinal stability of an AAMV?
e. Is there any difference in the analysis without the excitation of waves?
f. If there is a difference, how is it different and how much is the difference?

The list of questions above was summarised into one general problem statement question at the beginning of this section.

As previously mentioned in Section 1.2, the research required to narrow down the scope because one of the focal concepts was not well-established, i.e. the dynamics of WIGE in wavy conditions. To answer the problem statement above, initial steps to comprehend the dynamics of WIGE in waves are vital. Fortunately, the set of questions above is also applicable to the needs of dynamics of WIGE in wavy conditions. Thus, this thesis discusses findings in the perspective of WIGE. Despite the consideration to focus on WIGE, the results are valuable to support the understanding the dynamics of AAMV.

1.4 Aim and objectives

1.4.1 Aim

The main aim is *to understand the longitudinal stability characteristics of an AAMV configuration while operating in waves.*

1.4.2 Objectives

To achieve the aim above, the following objectives have been defined:

- To investigate the effect of water waves on the dynamic behaviour of WIGE craft;
- To develop a set of equations of motion of a vehicle operating in ground effect condition with a consideration of waves' occurrence;
- To produce some aerodynamic data and dynamic stability derivatives of the vehicle for oscillating state in ground effect;
- To perform longitudinal stability analyses of the vehicle.

As may be noticed, the objectives of this thesis are on WIGE craft instead of AAMV. This difference was intentional, and it was due to the idea that the dynamics of WIGE craft in waves supports the understanding of the dynamic

concept of AAMV. However, unfortunately, the discussion of WIGE craft in such a state has been the overlooked part of the ground effect realm. In the end, the goals of this research are not only designated to widen the horizon on dynamics of WIGE craft but also to establish a strong knowledge foundation of AAMV.

1.5 Methodology

Initially, the agenda of the research covered two main activities. The first activity was a literature review, and the other one was the development of the model of dynamics of an AAMV configuration in wavy condition. The latter part of the methodology was decided based on pieces of information collected from doing the literature survey.

1.5.1 Literature review

A thorough literature survey was conducted covering WIGE, HSMV, and AAMV fields and related topics. The primary purposes of this activity were to determine the research focus, to define aim and objectives, and to organise the methodology. The first nine-month period of this research programme was dedicated to this part with no technical work involved. Later, the activity was continued in parallel with the technical work.

During the literature review, the primary challenge was the scarcity of references that mainly discuss the AAMV. Another concern was related to the virtual absence of studies on the dynamic stability of AAMV/WIGE in the presence of waves. Also, the availability of data had been problematic to verify the model of dynamics. Thus, adjustments had to be made.

The literature review also determined the way of conducting the research. The work comprises three main parts:

- part I: development of a model of dynamics for AAMV and WIGE craft with the influence of wave;

- part II: definition of derivatives of the system, determined from a sequence of computational and semi-empirical processes;
- part III: implementation of the developed approach and the analysis of a chosen configuration (a wing-tail-fuselage WIGE configuration).

1.5.2 Part I: Model development

This part discusses the kinematic framework and the development of a system of equations of motion. Here, the external forces and moments due to the occurrence of waves are considered. The system of equations has been focused on the longitudinal motions following the prior research in the area. Part I is covered in Chapter 4.

1.5.3 Part II: Data acquisition

This part discusses the procedure of obtaining data. The data in this regard include configuration information, aerodynamic forces and moments, and stability derivatives. There were several approaches to collecting data including numerical simulation and semi-empirical formulation. Here, the numerical simulation was initially not programmed in the project, but then it was inserted to aid the completeness of the proposed plan. The part II is available in Chapter 5 and Chapter 6.

1.5.4 Part III: Implementation and analysis

After the attaining aerodynamic data, especially the stability derivatives, the next stage was to obtain a solution in a dynamic analysis of a WIGE craft configuration over wavy surfaces. The hypothesis was that the waves would induce a range of hysteresis of the characteristic roots compared to what the vehicle produced when it flew over flat surfaces. This part is explained in Chapter 7 in this thesis.

1.6 Thesis organisation

This thesis comprises eight chapters excluding the abstract and appendices. The logic of the chapters is the reflection of methodology section above. Figure 1-5 illustrates the flow of the thesis.

The first three chapters provide the foundation of the thesis. **Chapter 1 INTRODUCTION** describes the core information about how the research is built, from the background to the production of the thesis. The chapter briefly includes the context of the study, problem definition, the methodology used, and how all pieces of information in the research are constructed into the thesis. **Chapter 2 LITERATURE REVIEW** comprehends the information collected from academic resources. The importance of the chapter is laid upon the fact that the availability of the academic resources encountered influences all aspects of the research. Even though the literature survey is a part of methodology conducted in the research, it is given one dedicated chapter due to its importance, and the formulation of the method itself was the result of the literature study. The following chapter is **Chapter 3 RESEARCH APPROACH**. The chapter thoroughly explains the methodology. The programme comprises three parts of methodology, including the literature survey, core research programme, and the extended research programme. The core programme covers the development of a model of dynamics in the form of a system of equations of motion, stability derivatives data acquisition, and model implementation toward a modified existing vehicle configuration. The extended programme is about generating aerodynamic data needed for the attainment of stability derivatives.

The development of the model of dynamics is presented in one chapter, **Chapter 4 MODEL OF DYNAMICS IN WAVY CONDITIONS**. The chapter presents a mathematical expression of the movement experience by WIGE craft with the external influence of waves. Before introducing the model, a review of the system of equations of motion of related vehicles is available. The model is focused in longitudinal motions.

Data acquisition was not initially a part of the programme, but due to the limitation of information obtained from the literature study, it was then included in the

programme. The data mentioned here are meant as the set of aerodynamic coefficients of forces and the stability derivatives in wavy ground effect condition. The discussion of data acquisition is available in this report in two chapters. **Chapter 5 AERODYNAMICS OF OSCILLATING PROFILE IN GROUND EFFECT** provides a study of an aerofoil treated in oscillation near to the surface by the use of the computational approach. In **Chapter 6 STABILITY DERIVATIVES**, the discussion is about how the two-dimensional aerodynamic data was transformed into full configuration aerodynamic data by using a semi-empirical method. Further, the full configuration data is used to obtain the stability derivatives of a chosen configuration. The investigation into the behaviour of these derivatives due to the presence of the waves is also available in the chapter.

The verification of the model is presented in one chapter only, **Chapter 7 STABILITY ANALYSES**. It discusses the utilisation of a model on a case study. An existing configuration is chosen, and the analyses are done for several underpinning parameters, i.e. ride height, frequency, and amplitude of oscillation.

The discussion in this thesis is disseminated in all chapters, especially Chapters 4, 5, 6 and 7. The decision not to provide the discussion in a single chapter is due to the broad range of topics covered by this thesis. In those chapters, the author presents the novelty and contribution to the knowledge in the related topics. The focus, of course, is on dynamics of AAMV.

The last chapter is **Chapter 8 RESEARCH CONCLUSIONS AND FUTURE DEVELOPMENT**. It sums up all the information within the thesis and also the development that may be attempted in future research. This chapter is available at the end of this report, before the References and Appendices sections.

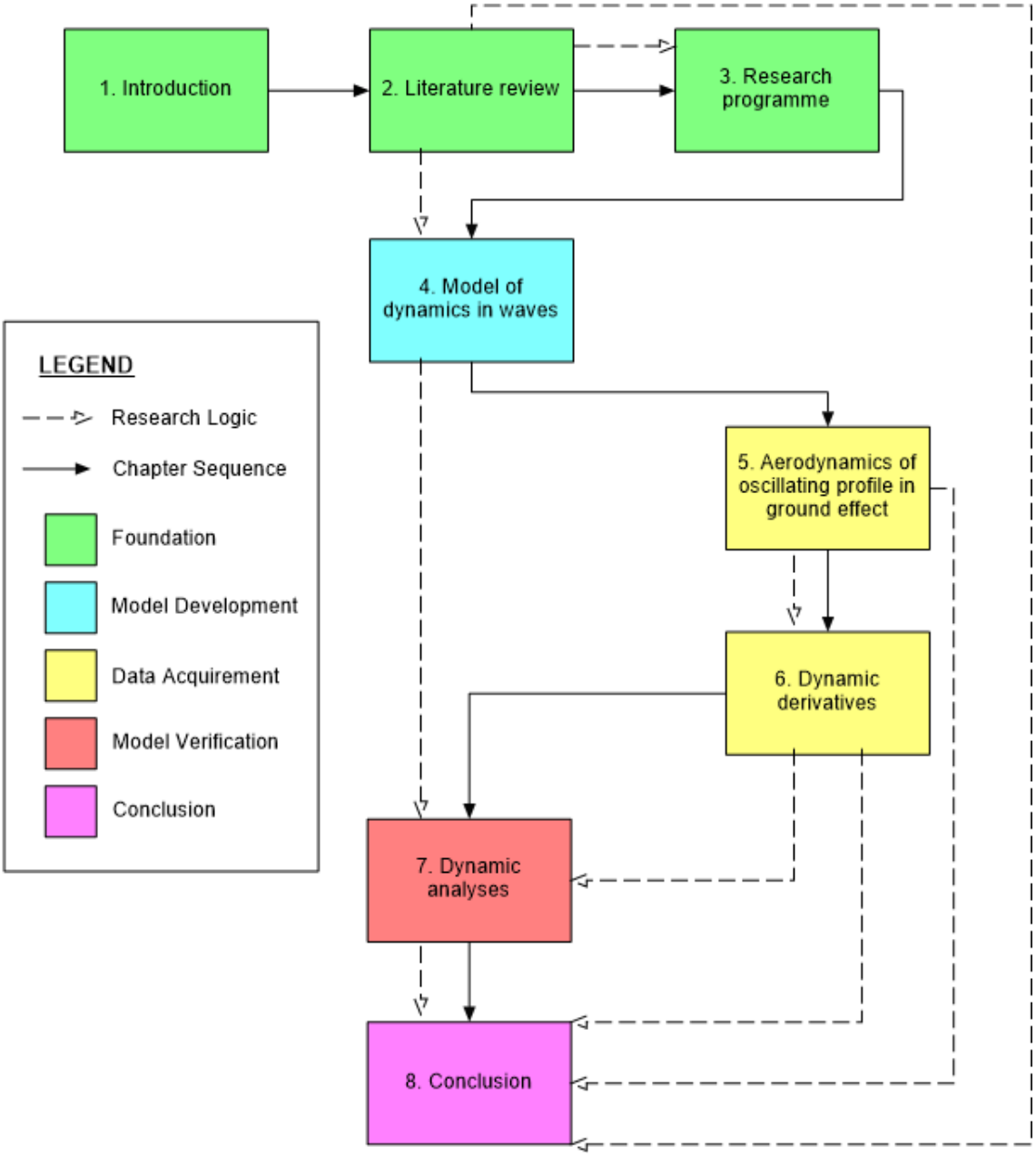

Figure 1-5 Thesis organisation

1.7 Conclusion

The current chapter points out that AAMV is a new generation of high-speed water vehicles that conceptually adopts conventional HSMV and WIGE craft. There is a big gap of understanding in the field that led the author to pursue research in the area. Context and problem statements are about dynamics with external forces and moments that are engaged due to the motion of waves.

The formulation of the methodology is briefly discussed here, which is divided into three parts and expressed in four out of eight chapters (Chapters 4, 5, 6 and 7). Beforehand, there are foundation chapters (Chapters 1, 2 and 3). The conclusion of the thesis is available at the end of the report (Chapter 8).

2 LITERATURE REVIEW

This chapter comprehensively gives details of the literature survey done for this research. A full nine-month period was dedicated to this activity concentrating on many aspects of discussion for airborne and waterborne vehicles resulting in a map of problems identification for AAMV and the methodology carried out to answer each chosen problem. After this period, the literature investigation was still maintained even though it was not the primary focus anymore. This chapter comprises ten sections. The sections are: *(1) Introduction to AAMV literature review; (2) High-speed marine vehicle (HSMV)*; *(3) Wing in ground effect (WIGE) craft*; *(4) AAMV: a hybrid HSMV*; *(5) Problems' identification*; *(6) Critical review on the current AAMV model of dynamics*; *(7) Critical review of the literature on the ground effect aerodynamics over wavy surfaces*; *(8) Critical review of the literature on the aerodynamics of oscillating lifting surface in ground effect*; *(9) Critical review of the literature on numerical technique for transient CFD analyses*; and *(10) Conclusion*.

2.1 Introduction to AAMV literature review

The history of water transportation dates back to the 4th millenium BC to the ancient Egyptians even though the possibility of much earlier rudimentary technology might exist (Casson, 1991). Since then, the development of the technology has been expanding and, today, people can enjoy high-speed transportation on water. However, a thirty-knot speed is the minimum standard for a vehicle to be in the category of high-speed marine vehicles (Baird, 1998); rather slow compared to other high-speed transportation modes. In the Gabrielli-von Karman (1950) diagram, see Figure 2-1, marine vehicles are positioned at the left part of the chart, which means in terms of speed they are less competitive. This fact has pushed more attempts to design a much higher speed HSMV.

A more general definition of HSMV is related to the Froude number. A Froude number is less than 0.4, and the buoyancy force due to the hydrostatic pressure has a dominant portion to determine the velocity of marine vehicles. At this range

of speed, the buoyancy force of marine vehicles is proportional to its displacement under the water or the submerged volume thus called displacement ships. In contrary, when the Froude number is more than 1.0–1.2, the hydrodynamic lift mainly holds the weight of a marine vehicle, and such a vehicle is known as a planing vessel. The marine vehicle that is dominantly influenced by hydrodynamic force tends to have higher speeds but then also may encounter a problem of cavitation (Faltinsen, 2005, chap.1). The cavitation not only affects the drop of lift of the vehicle but also can escalate into other problems, such as structural damages and a decrease in its performance.

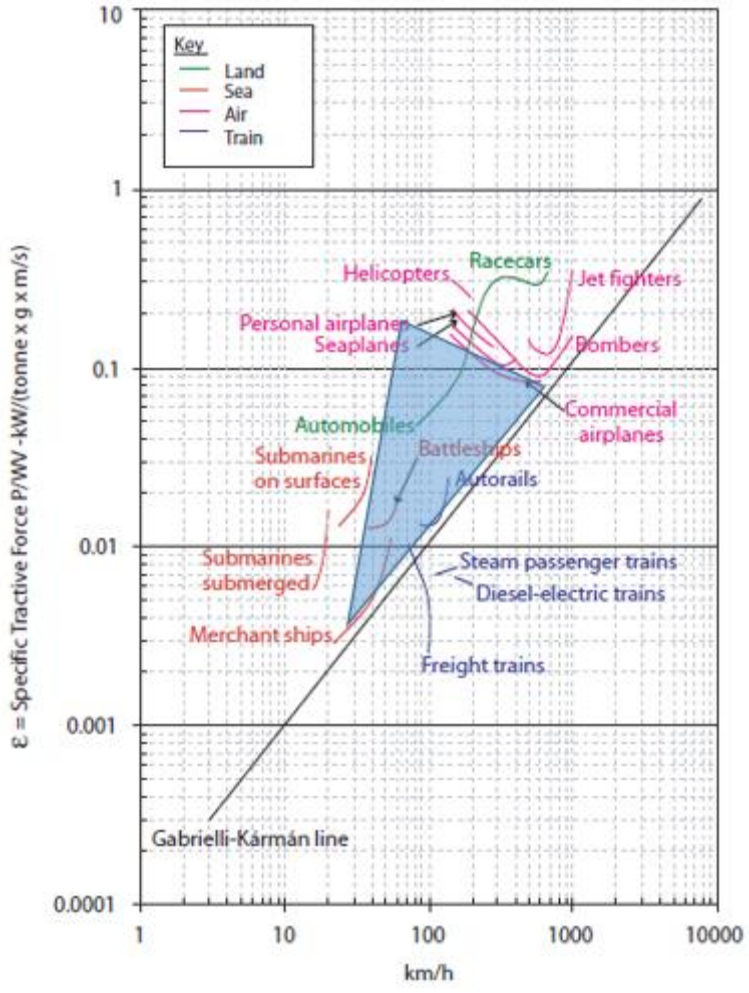

Figure 2-1 Gabrielli-von Karman diagram (Yong et al., 2005), with a projection for AAMV (highlighted in blue)

One of the ideas to alter the operability of marine vehicles is to use aerodynamics to sustain the weight of the vehicles, and this has expanded the options in how to support the weight of marine vehicles. The WIGE craft configuration uses aerodynamics to lift the body and has features closer to an aircraft. Still, it has been categorised as HSMV and seemed promising to diminish the gaps between marine vehicles and other high-speed transportation modes.

The next development in weight the sustention conception appears to be the combination of aerodynamics and hydrodynamics. In the WIGE craft itself, there is a phase when the aerodynamics and hydrodynamics are employed together to sustain the weight of it but not more than ten percent during its operation. The hybrid concept of aerodynamics and hydrodynamics starts drawing attention as the future potential in the HSMV technology.

At present, academic references that discuss the concept are insufficient. Some hints of the concept are scattered but mentioned in some academic work, but there are no adequate dedicated resources that talk about the field. In those small number of studies, there was no given nomenclature describing the concept until the term ‘aerodynamically alleviated marine vehicle’ (AAMV) was introduced by Collu (2008).

With the small number of references available, it is difficult to gather much information, proven data, or even a rigorous idea about the concept. However, as a hybrid derived from long-existing concepts, a new understanding might be built upon integrating those concepts. Therefore, at this point, literature surveys on WIGE and HSMV are still the most relevant way to figure out the nature of the technology. This approach was adopted for the literature review of this programme.

2.2 High-speed marine vehicle (HSMV)

From a speed point of view, Baird (1998) determined that a 30-knot speed is the standard for a marine vehicle to be categorised as a high-speed marine vehicle. The topic is more complicated concerning the way the vehicle is supported.

Faltinsen (2005, chap.1) divided HSMV into four categories, i.e. submerged hulls, hydrofoils, air cushions, and a combination between those three. The division is similar to the lift sustention triangle provided in Appendix E - a Naval Architecture Technical Memorandum Plan Formulation (Art Anderson Associates, 2004) with more general terms. A marine vehicle may be supported by buoyant lift, (hydro)-dynamic lift, and powered (aerostatic) lift. Later, considering the aerodynamic lift as the way to sustain the weight marine vehicles, the concept of the lift sustention pyramid appeared. Variety in the nomenclatures, as well as the advantages and disadvantages of different vessels including hybrid configurations, have been briefly discussed by Papanikolaou (2002). However, he skipped vehicles that employ aerodynamics.

From a brief explanation in the paragraph above, one may draw a conclusion that the HSMV may cover a broad range of discussions and WIGE craft is a subset of it. Due to the wide range of this research area, it is wise to limit the discussion in this section only to the vehicles that employ entirely or mostly hydrodynamics.

Hydrofoil vessels are an example of marine vehicles that employ hydrodynamics entirely in its cruise. The vehicles have characteristics of good seakeeping and efficiency with regard to speed loss in waves. Johnston (1985) indicated that fully submerged hydrofoils could maintain lateral-directional stability, to have a stable recovery when broaches occur, to show little deterioration of performance in severe waves, and to comply with safety requirements. One of the concerns is about the impact of loads on the structure during the operation of the vessels. For instance, for monohulled hydrofoils, the slamming and bending moment on the hull may become an issue as Abramson (1974) discussed.

The concept of static equilibrium of a hydrofoil vessel is related to its geometry. In a simple illustration, the equilibrium is reached when the mass of the vessels is equal to the displaced fluid mass at zero forward speed. Of course, the interdependence between one parameter with other parameters may complicate the calculation. The complexity of attaining the static stability is well-illustrated in determining the trim condition. In that analysis, the calculation of lift for fore and aft foils may need to be done separately. Furthermore, just like an aircraft, the lift

calculation involves meticulous factors including the angle of attack, flap angle, camber, thickness ratio, aspect ratio, Froude number, cavitation number, and Reynolds number. Not only the geometry but also the surrounding condition may affect the result considerably. For instance, the analysis in shallow water will produce a different outcome to the deep water.

The effect of surrounding implies the treatment of an active control system. For example, the use of platforming and contouring modes of an active control system exists in different conditions. The contouring mode is used in longer waves to minimise relative vertical motion between the vessel and the waves. It also avoids ventilation and broaching of the foils. The platforming mode is used to minimise vertical accelerations of the craft in relatively short waves.

Figure 2-2 Carl XCH-4 "Canard" hydrofoil in the 1950s

Cavitation is another possible phenomenon that may occur in hydrofoil vessels. If the condition appears, it may jeopardise the foil and propeller structure, which leads to deterioration of lift production. One way to avoid the situation is to use supercavitating foils, especially for vehicles that exceed beyond fifty knots.

Planing vessels are another type of HSMV that employ hydrodynamics but having less importance on the buoyancy effect. It is a Froude number of 1.2 that distinguishes a marine vehicle characterised as a displacement ship or a planing vessel (Savitsky, 1992). However, sometimes a Froude number of 1.0 also becomes the threshold of a planing craft (Faltinsen, 2005, chap.9).

The research on fast planing vessels was initially aimed at the seaplane design but later focused on the design of planing boats and hydrofoil craft. In its development, several approaches explain the relationship between the configuration of a planing boat and the forces and moments acting on it. Savitsky (1964) offered one of the approaches; an empirical approach derived from extensive experimental data obtained in preceding years. The method also includes a set of computational procedures that are also available to calculate running attitude, power requirements and stability characteristics.

Martin (1976) demonstrated the equations of motion of planing boat. Interestingly, he showed that motion decoupling is possible. Zarnick (1978) employed the equation of Martin to end up with a set of nonlinear integrodifferential equations of motion. The study on the equations of motions has been continued by, among others, Troesch (1992), and Troesch and Falzarano (1993).

The discussion on stability often links with the possible risks that may occur during an operation of a planing vessel. One of the risks is porpoising. The phenomenon is due to the instability of coupled heave and pitch motions. Blount and Codega (1992) presented a design guideline to predict and avoid the hazard.

Another occurrence that may happen in the operation of a planing vessel is wave-induced motions and loads. The occurrence is interconnected with many parameters including speed, the centre of gravity position, trim angle, and deadrise angle, as investigated by Fridsma (1969).

Katayama et al. (2000) indicated that jumping in a seaway may occur as the investigation on model tests over regular waves were carried out. In further discussion, jumping may lead to slamming loads. These are responsible for the undesirable effect on structural strength and vertical accelerations.

Figure 2-3 Royal Navy MTB 5 in the 1940s: an example of a planing boat

2.3 Wing in ground effect (WIGE) craft

There are some definitions derived for WIGE craft along with many different names referring to the vehicle. However, the definition by Rozhdestvensky (2006) covers all relevant aspects and is brief enough to describe the craft.

A WIGE craft is:

> "*a heavier than air vehicle with an engine, which is designed to operate in proximity to an underlying surface for efficient utilisation of the ground effect.*"

The definition covers several aspects that can be elaborated as follows:

1. WIGE craft is a heavier than air vehicle – means that it needs to find a way to sustain its weight so it can fly upwards. From this point of view, it shares the same conception with general aircraft, that to produce dynamic up-thrust it employs aerodynamic lift and powered lift. The use of powered lift has the significance that is related to the following point of the definition.
2. A WIGE craft is equipped with at least an engine – means that the vehicle is powered, which in this case is provided by an engine (or more). Referring to the first point, a heavier than air vehicle WIGE craft has narrower options than general aircraft which may be unpowered (e.g. sailplanes, paragliders). Due to the nature of its operation, it is unlikely for a WIGE craft to be without powering devices.
3. The nature of operation of a WIGE craft is to fly in the proximity of an underlying surface – meaning that the vehicle travels close to a surface. The term ‘surface’ shows a general idea that the surface might be earth ground, water, or ice. The consequence of this operation includes the difference in design configuration between WIGE craft and general aircraft.
4. To operate in the abovementioned nature is intentional to get benefits of ground effect. The ground effect is engineered in a way, so it gives the vehicle optimum performance.

The explanation above indicates a long journey in research in the area. The journey started early enough when aviators encountered a peculiar phenomenon when they flew near the ground. At that time, the phenomenon was called a ‘cushion effect’, as an aircraft experienced a sensation of bouncing up when it flew near to the ground or ‘pancake landing’, as happened mostly in its landing manoeuvre.

The first, academic credit for an article providing a theoretical study of the phenomenon went to a paper by Betz (1912). He discussed experimental results

associated with the ground effect showing a decrease in drag and an increase in lift. A quite solid resume, from more than 365 pieces of literature on the phenomenon and related issues, is available in a report by Foshag (1966). He showed the evolution of understanding and the approaches to explain the phenomenon. Later, more study was performed and led to an adequate idea of the phenomenon. Even though more discussions of the phenomenon are on the aerodynamics, it surely covers broader topics of discussion. Reeves (1993) covered these topics in a comprehensive definition of the phenomenon – saying that ground effect is a phenomenon of aerodynamic, aeroelastic, and aeroacoustic impacts on platforms flying in proximity to an underlying surface.

As an application in flight, the first designed ground effect vehicle was the Aeroslegde No.8 in 1935 (Kaario, 1959), which was capable of transporting a man up to 12 knots over snow surfaces. In the 1960s, Lockheed had been involved in the development of WIGE craft and flying catamaran. Also, around that time, other attempts to develop WIGE craft also appeared in some places around the world. In 1963, Günther Jörg built a series of tandem-airfoil-flairboats (TAF). In the same year, Lippisch built the first X-112 'Airfoil Boat', and the development continued for a decade. The attempts also arose in Japan, notably by the Japanese company, Kawasaki, with its KAG series.

Despite the endeavour to develop WIGE vehicles, an outstanding success was demonstrated by the Russian's Ekranoplan series. The Ekranoplan project was initiated in 1958 by R. Y. Alexeyev. In the 1960s the first set, called SM, was built and tested. This endeavour continued with the next development, called Project KM. The achievement of the project was remarkable, and the vehicles from this project gained their fame and were known as Caspian Sea Monster. The craft from this project is still extensively discussed these days. Today, the development of new the WIGE craft generation continues in many countries including Australia, China, Germany, Japan, Korea, Russia, Singapore, and the USA. More discussions on the historical review of WIGE vehicles are available in Ollila (1980) and section 2 and 3 in Rozhdestvensky (2006).

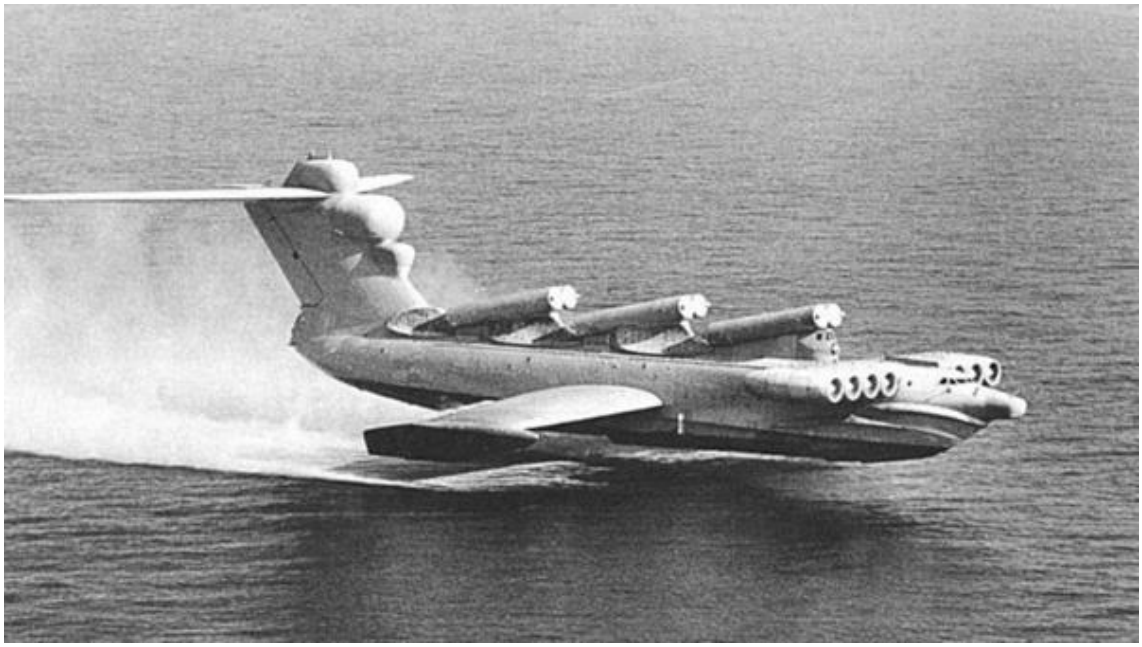

Figure 2-4 Lun Ekranoplan in the 1980s, an example of a WIGE craft

With regard to the advantage of WIGE crafts, it becomes a common understanding that such vehicles have better lift-to-drag ratio than the similar size conventional aircraft. However, what is the implication of this benefit? Maskalik et al. (2000) gave a perspective regarding the development of Ekranoplan, which more related to the military operation. The first implication is that the craft has a higher speed that overshadows surface ships and boats. The advantage reduces the decision-making time, provides freedom of manoeuvring and quick redeployment.

Aside from the aerodynamic and performance virtues it offers, Ekranoplan may have a quality of stealth, invulnerability to mines and torpedo weapons, effective combat capability, a wide range of missions (i.e. as a cargo vehicle, missile vehicle, anti-submarine vehicle, and amphibian vehicle). All the advantages are also supported by the possibility of dispersing without runways and expensive stationary airfield facilities.

It has been claimed that with its virtues the WIGE craft is projected to be the future of sea transportation technology. However, some difficulties are identified. The

main issue is about the configuration design as each option may have consequences in other aspects. Some options of configuration are available in Table 2-1 that is based on discussion by Rozhdestvensky (2006).

Table 2-1 WIGE craft configuration design

Configuration	Benefit	Drawback	Implementation	Remark
Wing tail (conventional)	• Large range of height. • Large height-pitch combination to sustain stable flight. • The capability of making 'dynamic jump'. • The capability of 'hopping' and banking (for efficient turning). • The capability of efficiently applying power augmentation at take-off. • Large wing loading helps high-speed (as counterbalances	• A significant weight penalty. • The tail unit does not contribute significantly to lifting capacity. • Tail unit adds additional viscous drag. • Relatively low lift-to-drag ratio (due to the large non-lifting area fraction). • Large structural weight. • Large empty weight fraction.	Tailplane mounted on a vertical stabiliser outside the influence of ground effect, thus shifting the centre of pitch downstream.	It is a configuration with a feature of a large main wing and a horizontal tail plane.

	the loss of the transport).			
Wing tail (reverse delta)	• High lift-to-drag ratio. • A wide range of heights and pitch angle of stable height. • The capability of making 'dynamic jump' and efficient turning.	• Advantages are unique to this configuration. • Overpowering due to inefficient take-off aids and the absence of power augmentation.	• A linear decrease of the local chord of the main wing from the root chord section toward the tips. • Small tail unit.	An attempt to restrict the longitudinal shifting of the centre of pressure of the vehicle in response to variation of height.
Tandem wing	• Allows shifting the aerodynamic centres in a proper way for stability. • Simple construction. • Simple tuning of the configuration to secure a given	• High take-off speed. • The height of the motion stability is too narrow. • The rigidity of flight. • It operates only in ground effect.	The configuration is designed by • adjusting design pitch angle; • using wing profile with a maximum capacity to exploit the ground effect;	The configuration is developed to resolve the problem of stability.

	static stability margin. • Effective one-channel (throttle) control. • Small span.	• Sensitive static stability due to the combination of pitch angle and ground clearance. • For a small vehicle, limited operational height and seaworthiness.	• adjusting the geometry of the fore and aft wing element.	
Flying wing	• Can have inherent stability due to smart profiling. • Efficient utilisation of the vehicle to take maximum advantage of ground effect. • Low empty-weight fractions, in particular for the small-aspect-ratio vehicle.	• The low range of height-pitch combinations to achieve longitudinal stability. • Relatively low operational flight height. • Difficulties in providing structural integrity of a water-based all-wing vehicle. • The inefficiency of use of flaps which	The configuration is identified by: • reducing non-lifting components, very small or absent horizontal tail; • special profiling of the lower side of the wing or/and by making use of an automatic stabilisation/ damping system.	Converting the whole craft into a lifting surface, resolving longitudinal stability problems.

		may deteriorate the static stability.		
Composite wing	• Higher lift-to-drag ratio. • Combining with s-shape of the wing sections provides higher efficiency and range. • Small aspect ratio maximises the efficiency of the power-augmented take-off.	• Sensitive to transverse flow that leads to a decrease in lift and an increase in drag. • The transverse flow also leads to an early flow separation over lifting surfaces.	• Central wing with small aspect ratio with endplates and side wings of high aspect ratio. • Employing the idea of profiling the lower side to reduce the tail unit.	The configuration is about combining the advantages of aeroplane configuration and flying wing configuration.

2.4 AAMV: a hybrid HSMV

The terminology of the aerodynamically alleviated marine vehicle (AAMV) was firstly coined by Collu (2008). AAMV is a subset of HSMV that employs both aerodynamics and hydrodynamics in its manoeuvres. AAZ is the operational area of the vehicle. Along with AAMV, the terminology of the aerodynamic alleviated zone (AAZ) was also introduced, describing the operational area of the vehicle.

As recently coined, the concept apparently has been studied over several decades although not to a large extent. Shipps (1976) analysed an outboard tunnel hull that could be considered as an aerodynamic-supported marine vehicle. The craft is identified as having a feature of a catamaran configuration acting as aerodynamic end plates of the ram wing. The vehicle demonstrated better performance than other conventional hull race boats in that era. The advantage is related to the increase in lift forces, up to eighty percent of the total weight, which gives the further benefit of decreasing hydrodynamic drag. In addition, the construction of the boat makes it possible to dampen the effect of heave and pitch motions. However, some issues are also anticipated from such a configuration, mainly related to stability and safety.

Ward et al. (1978) conducted a study on the design and performance of a ram wing planing vessel, known as KUDU II. The vehicle has the configuration of an AAMV as it owns two planing pontoons separated by a wing profile. It means the vehicle has both aerodynamic and hydrodynamic surfaces, thus is designated to employ aerodynamic and hydrodynamic lift.

Kiryllovikh and Privalov (1996) exhibited a design and performance estimation of a vehicle called Transport Amphibious Platform (TAP), which presented a trait of a proper AAMV. It comprises two hulls, a fuselage, a wing and an aerodynamic tail between the hulls. During its operation, it always keeps contact with the water, and aerodynamic cushion effect is employed. Unfortunately, there was no further information about the dynamic model adopted by the craft.

Doctors (1997) proposed a configuration named ‘Ekranocat’ and adopted ‘an aerodynamic alleviated concept’. The configuration is sustained by aerodynamic

lift, thanks to its streamlined structure. A decline in total drag of up to fifty percent is obtained at very high speed.

Figure 2-5 Ram wing planing craft KUDU II, an example of AAMV

Along with the introduction of AAMV and AAZ as mentioned, Collu (2008) also developed a mathematical model to estimate the equilibrium attitude and a system of equations of motion of such a configuration. The equilibrium state was formulated by adopting Savitsky's (1964) approach in planing vessel design with some additions to include the ground effect. Later, the system of equations of motions was developed combining the known systems of equations for AAMV and the planing boat.

2.5 Problem identification

The literature survey was not only about giving a perspective of the concept of AAMV but also drawing an idea about problems that may occur in the vehicles

adopting it. The problems mentioned in this section were identified from in-depth problem evaluation on WIGE craft and HSMVs in general.

The identification of challenges in AAMV can cover a broad range of topics. However, the author limited the discussion to eight topics, i.e. aerodynamics, hydrodynamics, stability, structure and material, design, power, performance and safety, and economics and other related aspects. The division of the topic areas is depicted in Figure 2-6.

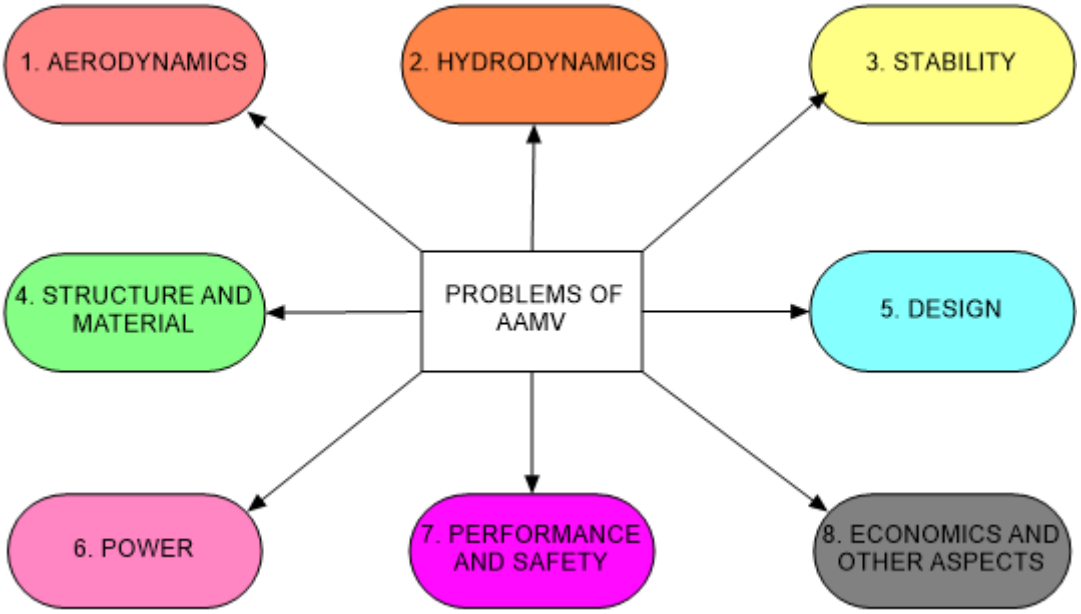

Figure 2-6 Possible problem areas of the AAMV

To explain the figure, it might be identified that each item may have different characteristics. There are areas possess specific problems. However, there is also an area affecting other areas drawing problems. On the contrary, there is a field that possesses problems only due to what takes place in other areas.

2.5.1 Aerodynamic problems

In the AAMV case, the approach to designing the aerodynamic lifting surfaces is similar to WIGE craft. It considers the augmentation of lift in the ground effect zone. The virtues in the aerodynamics of ground effect have been massively discussed, but there are also issues about the vehicles adopting the phenomenon. An illustration of aerodynamic problems that may occur is depicted in Figure 2-7. The author tried to categorised the problems into several big chunks which are expressed in rectangular boxes in the figure. Of course, in some way, these categories are still related to each other. The circles describe the cause of those problems.

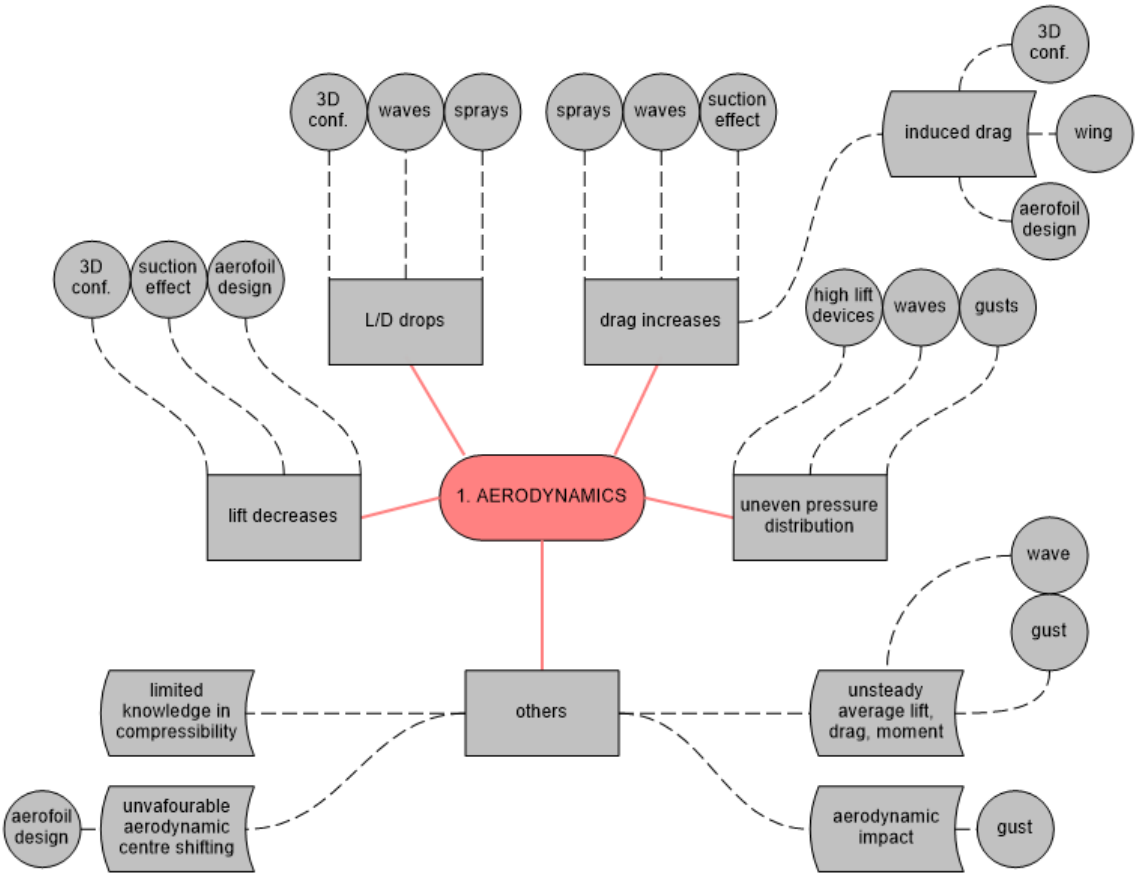

Figure 2-7 Related problems in aerodynamics

The first observation was about the lift generation as the increase in it is always being promoted as the virtue of WIGE craft.

In fact, the increase in lift in a ground-effect-adopting vehicle is a result of thorough configuration layout of the vehicle. The drop of lift is due to the interference of other parts of non-lifting surfaces (Rozhdestvensky, 2006).

The decrease of lift may also be caused by the suction effect. It occurs due to the creation of a convergent-divergent channel leading to drop of pressure. The phenomenon itself has been identified in the two-dimensional study, for example by Kikuchi et al. (2002), Ahmed and Sharma (2005), Ahmed et al. (2007) and Qu et al. (2014a, 2014b) – all authors discussed an aerofoil flying over ground effect. From the study, a conclusion can be derived that in some conditions an aerofoil experiences suction effect in ground effect.

Another challenge about lift is its peculiarity due to some circumstances. This challenge is better explained by a series of events affecting pressure distribution. One can expect uneven pressure distribution due to, among others, the existence of high lift devices, waves and gusts.

The following problem is related to the drag production. It is known that a portion of drag of an aerodynamic lifting surface, called induced drag, is linked to the lift production. Having a consistent manner towards lift production, it also has the same causes of the problem with lift production.

In WIGE craft, the linearity between the generation of lift and the growth of drag is not always the case. Even, the common understanding is that the increase in lift and the decrease of induced drag occur mutually. However, this advantage only applies for span dominated WIGE craft and not for chord dominated ones. Here, one can see the importance of thorough profiling of an aerofoil and in-depth setting of wing configuration in a vehicle adopting the ground effect concept.

Aside from the possibility of increasing induced drag, another aspect that contributes to the drag growth is the suction effect in some instances, as previously discussed.

In addition, the operating environment may also have the discouraging effect on the drag. The occurrence of waves and sprays, for example, may create the unpredicted situation.

In the case of waves, a Knoller (1909) – Betz (1912) effect may occur. It is a thrust generating effect due to the oscillation motion. The issue is not about the production thrust itself but, instead, the fluctuation of drag experienced by the vehicle. The fluctuation of drag may cause further problems in terms of dynamic stability.

The effect of sprays toward aerodynamic drag is related to the fairness of lifting surfaces during the operation. The sprays deteriorate the general aerodynamic characteristics of the surfaces. The effect is similar to what happens in the hull of a boat.

In further discussion, the issue is about the aerodynamic efficiency or lift-over-drag ratio. Rozhdestvensky (2006) claimed that a drop of up to sixty to seventy percent is possible in WIGE craft due to the presence of hull, PAR engine, and a non-lifting tail.

A fluctuation of the lift-over-drag ratio in wavy conditions is also expected. This condition is due to the fluctuation that also occurs in lift and drag forces. The problem is one cannot see the similar pattern between these three parameters as they have a different periodic function (mostly because of different phase lags). In the case of gusts, the fluctuation of these parameters also may occur.

The gusts also may create an aerodynamic impact on the structure. The impact is unfavourable from a structural integrity viewpoint.

Another undesired event is the shifting of the aerodynamic centre in pitch and aerodynamic centre in height. This situation may present due to the careless use of an aerofoil.

A poor aerofoil design in a vehicle adopting ground effect not only affects the production of lift but also the unnecessary movement of aerodynamic centres (Maskalik et al., 2000, pp.58–59). For example, the increase of profile thickness

reduces the coefficient of lift and shifts the aerodynamic centre of height towards the leading edge. In another instance, the profile concavity also influences the shifting of aerodynamic centres, especially the aerodynamic centre in pitch. The increase in concavity may draw the aerodynamic centre in pitch nearer towards the leading edge.

Also, a challenge in ground effect aerodynamics is the limitation of knowledge regardless of many studies in the area that have been carried out. The situation gives the opportunity to conduct more research in the field including the implementation to AAMV.

2.5.2 Hydrodynamic problems

Figure 2-8 presents a brief review of possible problems that may occur in hydrodynamics. It seems the topic is not as broad as aerodynamics, but the problems in hydrodynamics are highly nonlinear and should be looked after carefully.

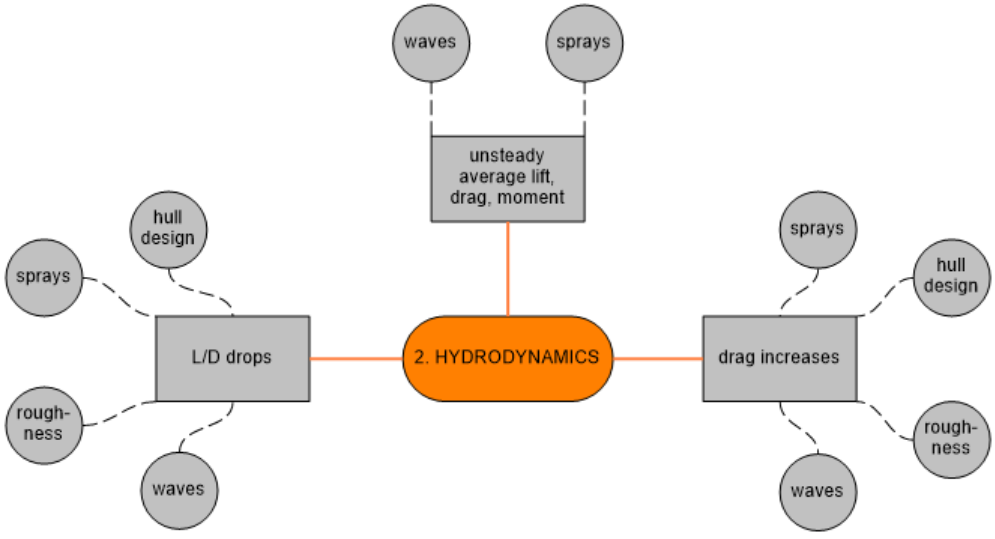

Figure 2-8 Related problems in hydrodynamics

In the literature survey, the author limited the discussion in drag, and lift-to-drag ratio, the oscillation of forces and moments acting on AAMV.

The first two topics, drag and lift-to-drag ratio, have similar problem causes. First, it is about the hull design. It is desirable to have a reduced area of the hull to obtain smaller drag. A smaller hull area means a smaller wetted area that contributes to the friction drag. However, reducing the size of the hull is not always applicable due to design objectives and requirements. More often, the endeavour is restricted by the sizing limitation to comply with, for example, the seaworthiness and payloads. This idea was suggested by Truscott et al. (1938).

The drag is not solely about the design but also the operating environment of the vehicle. As mentioned by Husa (2000), the sprays affect the combination of induced and pressure drag. The more intensity of the sprays, the more drag of the vehicle is generated.

The existence of waves can also be problematic to AAMV. A marine vehicle system will experience periodic additional forces and moments due to the waves. Problematically, these periodic forces have a dependency on the depth of the water. Shallow water will give different results from deep water.

2.5.3 Stability problems

The stability encompasses a broad range of discussion in conventional HSMV and WIGE craft; hence also applies to AAMV. It would be expected that a variety of issues do exist. The real problem for AAMV, of course, is the minuscule understanding in the area. Very few researchers in the field despite the concept of aerodynamic alleviated vehicles have been published in the recent past. Collu et al. (2007, 2008a, 2008b, 2010) initiated analysis in AAMV stability, especially in the longitudinal plane. In understanding the challenges faced by AAMV, one may expect that the causes of problems in the field are from configuration and operation.

Starting from the stability derivatives, AAMV has more objects of interest. Aerodynamic design (both in two-dimensional profiling and three-dimensional setting up), hydrodynamic design, configuration, the height between the aerodynamic surface(s) and water surface have a contribution to the derivatives. Having taken a look at Collu's (2008) thesis, one can see the significance of the parameters in the system of equations of motion. Like WIGE craft, AAMV has the mass, damping, restoring, and ground effect matrix. The difference between WIGE craft and the AAMV system is about the matrices' components. In the AAMV, the mass, damping and restoring matrix consider both aerodynamic and hydrodynamic force derivatives. This complexity leaves a difficulty in providing the solution.

In his thesis, Collu disregarded the effect of waves. The neglect, instead, shows the importance of wave analysis in the dynamics of AAMV. What to expect is that the external forces and moments should be considered.

Moving forward to another problem, i.e. longitudinal stability, one may expect it to be complex based on its extensive discussion both in traditional HSMV and WIGE craft. In the past, there were many endeavours to provide longitudinal stability for WIGE craft. Most of the attempts were made by engineering the configuration, especially about the wings. Unfortunately, as reviewed by Rozhdestvensky (2006), the efforts had trade-offs in other aspects.

The longitudinal stability problem is also shared in the hull design. The planing hull has to be carefully designed to attain stability in the longitudinal plane. As shown by Faltinsen (2005, p.267), longitudinal instability may come in the form of non-oscillatory trim instability bow drop or dynamic pitch-heave oscillation, known as porpoising. The existence of waves during operation increases the possibility of dynamic instability.

The hull design, as well as the existence of waves, is also essential to determine the lateral-directional stability. In Faltinsen (2005, p.267), it is mentioned that non-oscillatory roll instability and dynamic roll oscillation (or chine walking) are the problems in transversal motion. These forms of instability are unfavourable

toward aerodynamics and hydrodynamics due to uneven pressure distribution along the hull.

Besides the traditional stability analysis, AAMV is similar to WIGE craft with regard to the existence of height stability. Actually, the height stability is a subset of longitudinal stability. The separation relates to acknowledging the ground effect phenomenon that takes place in the system. Again, this stability is dependent on the design of the vehicle. Subsection 2.5.1 mentioned aerodynamic problems whereby certain choices in design determine the location of neutral points, i.e. aerodynamic centre in pitch and aerodynamic centre in height. The position between these two neutral points determines the static stability of the vehicle. It is easy to draw a conclusion that a careful design is needed to not jeopardise the stability of the vehicle.

Talking about neutral points, the AAMV has more complexity than the traditional HSMV or WIGE craft. A vehicle adopting the aero-hydrodynamic hybrid concept has three neutral points. Aside from two already mentioned points, it possesses a hydrodynamic centre. The existence of three neutral points raises the bar of complexity about dynamics. The neutral points should be appropriately located to reach static stability and, ultimately, dynamic stability (Collu, 2008).

Maskalik et al. (2000) identified a problem related to the insensitivity of the control system to deal with a disturbance during the operation of WIGE craft. The causes of the insensitivity are still obscured. However, the possibility came from the environment during the operation. One may expect more chaotic events during the operation in an open sea due to, for instance, waves, gusts, and tides.

Another problem related to the stability is reliability. In this case, the reliability has been discussed more qualitatively by a few articles on stability problems. As one may realise, the discussion in this subsection mostly is from WIGE craft or HSMV points of view. There is no such evidence that a specific configuration is fit for AAMV design purposes, not to mention the inclusion of waves in the analysis, which even in the realm of WIGE craft and HSMV still become a challenge.

All the aspects that have been discussed here are briefly depicted in Figure 2-9.

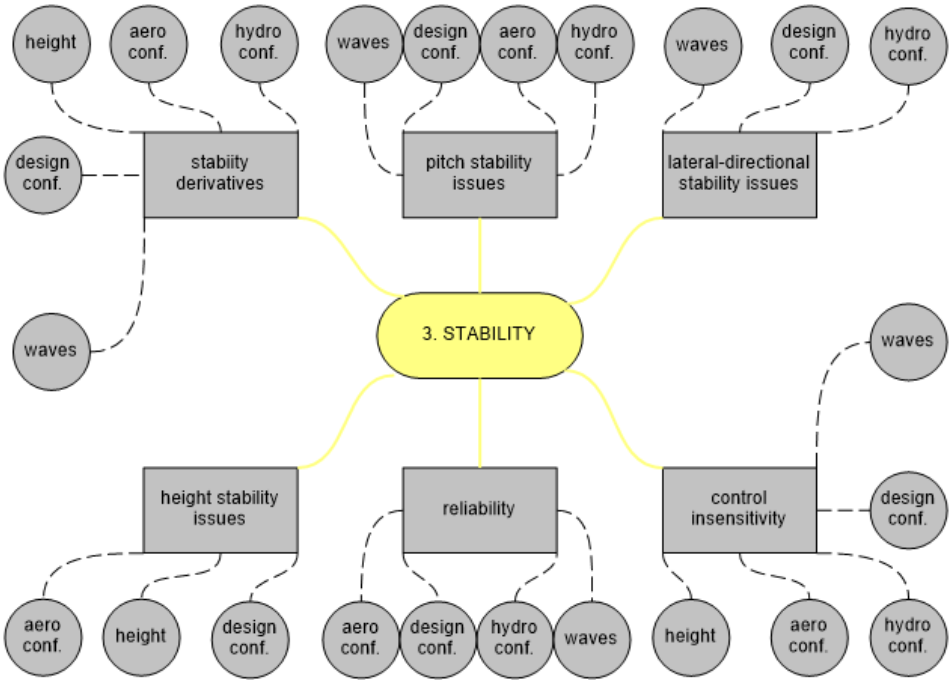

Figure 2-9 Related problems in stability

2.5.4 Structure and material problems

The topics on structural integrity and material being used for manufacturing a vehicle also promise to be valuable for research. While the centre of attention of stability is the operability, the structure and material, in the end, safety has to be addressed. The problems in the area may comprise many branches of discussion, as depicted in Figure 2-10.

One given situation that AAMVs may face is the operation in the corrosive environment. Material selection becomes very crucial. One of the options is to design composite material for this purpose. However, the problem does not stop there. In general, regardless of whether a material has a resistance to corrosion, it may not be robust enough to handle the load. Other than the characteristic of load handling, the use of a composite may not be promoted at this stage as its manufacturing involves more advanced and costly technology.

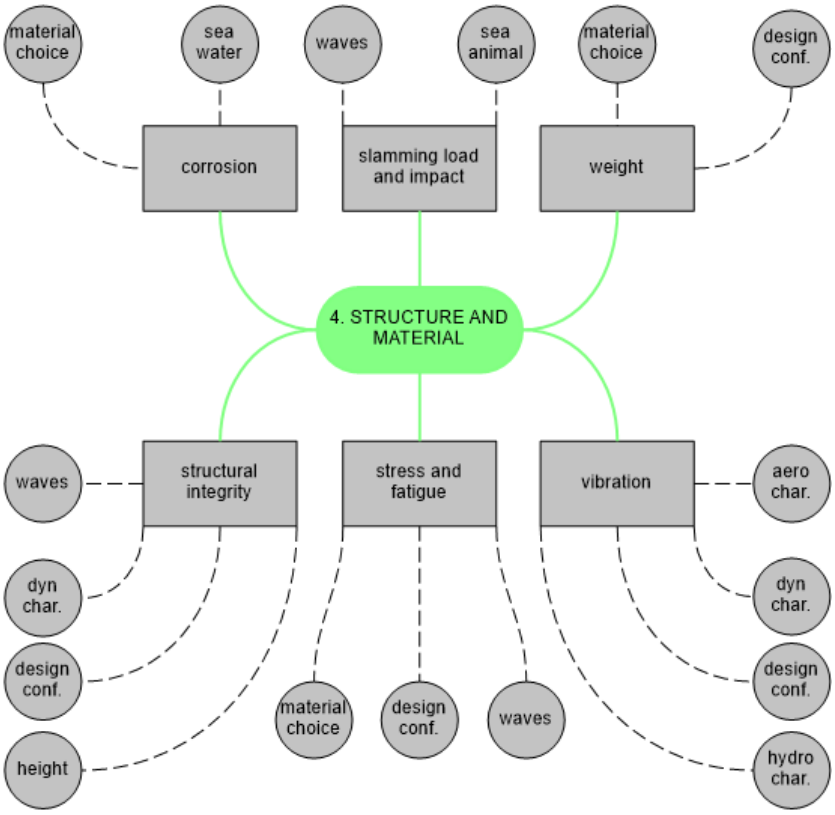

Figure 2-10 Related problems in structure and material

With regard to load handling, the open sea is a perfect place to anticipate a variety of loads and slamming action on the structure. Aside from the loads from the configuration, the vehicle is likely to experience a periodic load from the motion of waves or sometimes slamming or sudden impact due to gusts. All the loads need to be carefully examined in the first place.

There is always a concern with any vehicle regarding weight. The weight problem in AAMVs is due to configuration and material choices. An example of the significance of configuration is shown from the previous development of WIGE craft. As mentioned by Rozhdestvenksy (2006), the wing-tail configuration tends to have a greater weight than other configurations due to the need of a large horizontal tail to counterbalance the pitch moment of the craft. Also, different materials present different weights due to various characteristics among them.

Other challenges are typical structural problems, for example, structural integrity, stress and fatigue, and vibration.

2.5.5 Design problems

There is a unique trait about the design. Rather than having certain problems in the field, it is likely that what happens during design determines the problems that may occur in other areas of discussion, see Figure 2-11. This statement has already been proven in previous subsections.

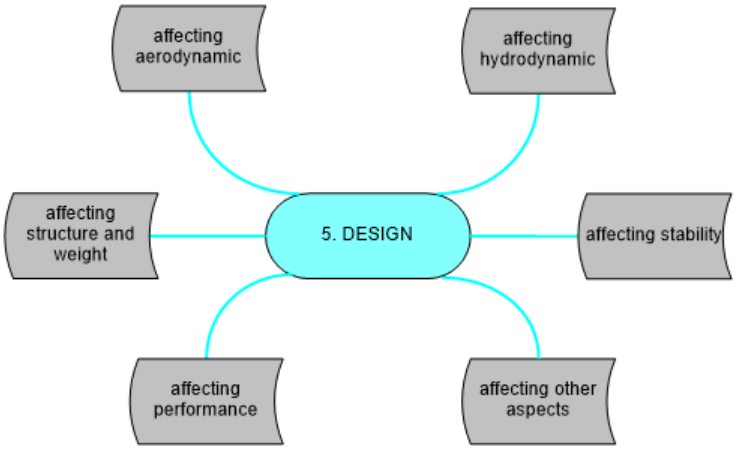

Figure 2-11 Affecting areas due to design choices

As an illustration of the consequences of the choice of configuration, one can perform a review of the paper by Rozhdestvensky (2006). The paper points out the effects of several configurations that have been used in the development of WIGE craft.

Starting from a traditional wing-tail configuration; WIGE craft may encounter some problems in aerodynamics and the structure field. In aerodynamics, the configuration tends to have high viscous drag and low lift-over-drag ratio. From a structural viewpoint, the vehicle may have a significant weight penalty and high empty weight fraction.

Lippisch proposed a special case of wing-tail WIGE craft in 1963. The craft is a sort of reverse delta wing vehicle. The problem with this kind of configuration is related to the structure; it has considerable weight. More than that, the versatility of operation is also limited due to the design.

There have been some proposals to resolve the problems in wing-tail configuration. One of them is tandem wing planform. However, up until now, there is no evidence of success about this design. Instead, one may expect some difficulties with regard to taking off speed, the versatility of manoeuvre, and the range of ride height. The configuration restricts the area of operation only in ground effect, but then it has an extreme sensitivity to the condition of the surface.

WIGE craft with flying wing configuration has several challenges including a low range of height-pitch stability, limitation in the operational ride height, and structural integrity. The addition of flaps can also be problematic. When they are not properly installed, there is deterioration of the static stability of the vehicle.

The composite wing planform also suffers from some disadvantages despite its superiority to many configurations (Yun et al., 2009, p.186). It is sensitive to transverse flow. The flow leads to a decrease in lift and an increase in drag. Also, it forces the separation over lifting surfaces.

In the case of power augmentation ram, the attachment of such a device raises some concern about operability, the risk of collision at low speed, and reducing the pilot’s vision.

Reflecting what happens in WIGE craft, one may see the impact of design choices on other aspects of the vehicle. Similarly, challenges to produce an appropriate design for AAMV do exist. The challenges may involve, but not limited, hull design, aerodynamic profiling and setting, and maybe the involvement of stabilising surfaces in some cases. Considerations in design, in some way, affect other aspects of the vehicle. Thus, trade-offs are inevitable as one cannot accommodate all those considerations.

2.5.6 Power and propulsion problems

Not very many discussions were found during the initial literature survey. Moreover, once the focus of research was chosen, there was no further investigation on the topic. The illustration of what happens in the power and propulsion area is available in Figure 2-12.

One of the challenges is about sprays. The problems due to the occurrence of sprays, most of the time, are linked with the deterioration of aerodynamic or hydrodynamic characteristics. However, the event is also unfavourable to the power production' sprays reduce engine performance.

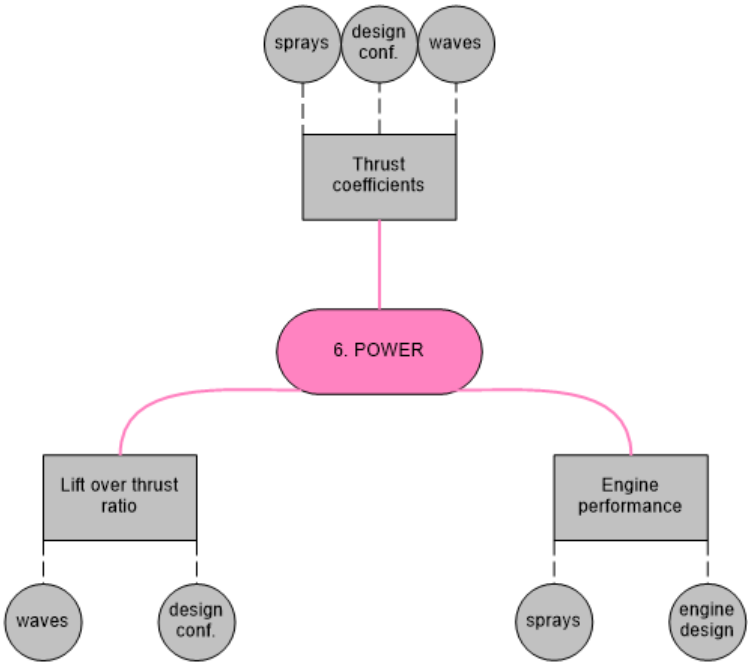

Figure 2-12 Related problems in power (propulsion)

When the event of waves occurs, one may expect that the engine experiences the fluctuation of thrust coefficient and lift-over-thrust ratio. This situation requires a suitable control system.

The layout can also contribute to the decrease of engine effectiveness. In the case of bow-thrusters, a poorly positioned one may yield in a reduction in static lift-over-thrust ratio.

Also, there is a need to improve the quality of fuel consumption. The need means a right combination of the engine design and the full configuration. The improvement in fuel consumption means improvement in costs.

2.5.7 Performance and safety problems

The area of performance, as well as safety, is unique because all the problems are the consequences of what happened in other areas. So, the character is different from a design viewpoint, as described above in subsection 2.5.5. The depiction on how performance and safety are affected by other fields is available in Figure 2-13. The insight into how those encircled fields in that figure have been suitably discussed in the previous subsections.

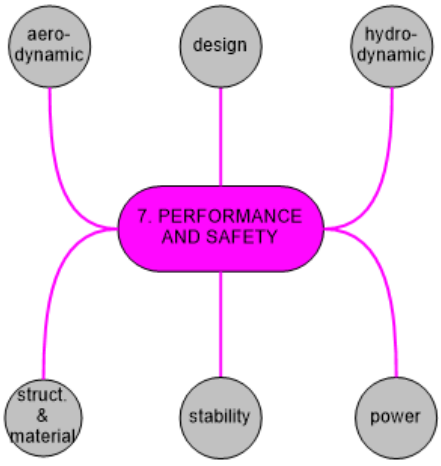

Figure 2-13 Areas affecting performance and safety

In aerodynamics and hydrodynamics, forces' and moments' production is paramount. The composition of forces and moments determine the operability of

the vehicle. From the stability perspective, the static and dynamic stability criteria govern the movement of the vehicle.

In structure and material, a thorough analysis should be made to provide structural integrity; failing to do so jeopardises the performance as well as safety. In design, it is clear that every option brings forward specific issues. The power and propulsion also have a contribution to performance in the form of a lift-over-thrust ratio.

2.5.8 Economics and other related problems

Regarding economics, the concept of the AAMV has not proven itself yet as a promising option in the market of marine vehicles. The latest development of such a vehicle is the French A2V that has reached the prototyping stage (www.lemarin.fr, 2015; www.meretmarine.com, 2015). Its designers boast about the profitably as a result of higher speed and less fuel consumption that the vehicle offers. However, only time will reveal the truth.

At the current stage, it is difficult to find a scholarly study that mainly discusses economics or feasibility of the AAMV. Even in the WIGE craft realm, the author could only find one thesis that talks particularly about economics (Paek, 2006). The document provides some measurements to estimate the economic rationality of WIGE craft technology. The measurements are the comparison between cost-effectiveness and the specific power required, transport productivity, transport effectiveness and other related factors. The transport productivity comprises several branches, i.e. payload ratio, the ratio between fuel consumption against total weight. The WIGE craft has superiority over the general marine vehicle regarding cost-effectiveness, fuel consumption, and transport effectiveness. Conversely, regarding aircraft, the WIGE craft wins in the production costs as it is based on the ship development method.

The thesis also demonstrated several scenarios of cost analysis. It considers model configurations and some cost sources. These components are implemented into a formulation. From the analysis, it was stated that it is not easy

to estimate the cost due to no reliable information being available. However, there is a prediction that the cost of WIGE craft will be affected by what is called direct operating cost (DOC). At this stage, there is no competition for WIGE craft as, in terms of the cost, it may be differentiated from aircraft or other marine vehicles. The problem is the range of costs can be unrestricted. A thorough cost analysis needs to be done to secure price competitiveness between high-speed marine vehicles.

Reflecting on what is provided in the thesis, one may draw a prediction that the AAMV will have the very same challenges as WIGE craft.

Aside from what has been discussed above, another aspect to consider is ergonomics, especially when the objective of the vehicle is to transport people. This topic is close to the discussion about safety but ergonomics has a meaning more toward the convenience and comfortability of human beings. In some way, it also related to the design and stability.

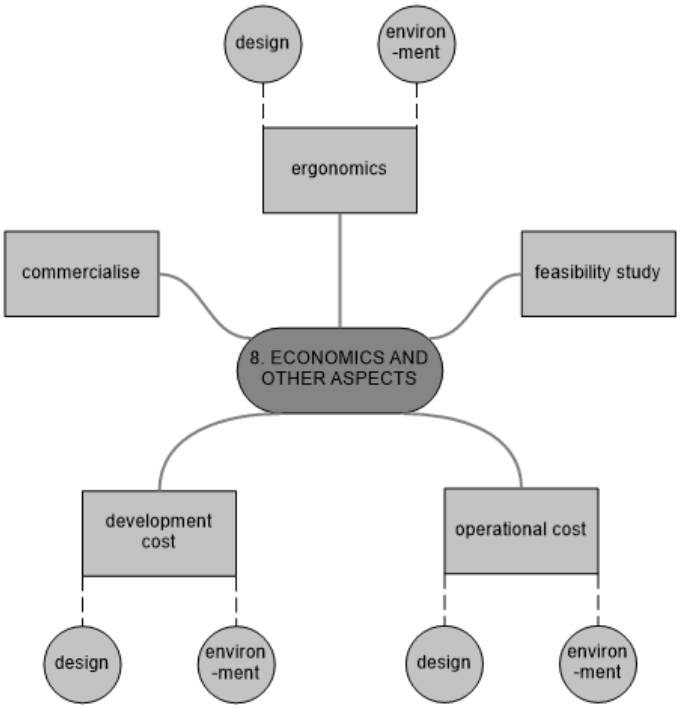

Figure 2-14 Related problems in economics and other aspects

In Introduction of Ship Hydromechanics by Journeé and Pinkster (2002), a combination of dynamic acceleration and frequency of oscillation govern the level of comfort. There are situations where the combination is out of the acceptance zone of human beings, marked by what is known as seasickness. Seasickness is a result of excessive stimulation of the internal balance organ. The AAMV may also encounter the very same situation in its operation.

2.6 Critical review of the current AAMV model of dynamics

In the previous sections, it has been mentioned that Collu (2008) did not only coin the terminology of the AAMV but also proposed a system of equations of motion for a configuration adopting the concept.

The model he developed was based on the system of equations of motion for WIGE craft and planing vessels. However, before talking further about the system of equations of motions, Collu carefully determined the equations of equilibrium of an AAMV configuration. Of course, the equations of equilibrium might differ from one configuration to another, but what he conducted was establishing the idea of how to draw the equilibrium state out of a system. The idea he proposed is based on the 'Savitsky long-form method' (Doctors, 1985, chap.4; Savitsky and Brown, 1976).

The consequence of the use of the approach based on the Savitsky method is that there are two stages of iterative processes as there are two parameters to be considered. Firstly, the determination of the equilibrium attitude starts from guessing the ride height of the aerodynamic surface(s). The next step is guessing the trim angle. Following this, one can determine the aerodynamic forces and also the weight to be sustained hydrodynamically. The use of the 'Savitsky long-form method' is then carried out. Then the equations from the method should be assessed first with the guessed trim angle and then the guessed height. If the equations satisfy both parameters, the equilibrium attitude is achieved. It is an iterative process that may take time thus the use of a computer is recommended. The illustration of the process is depicted in Figure 2-15.

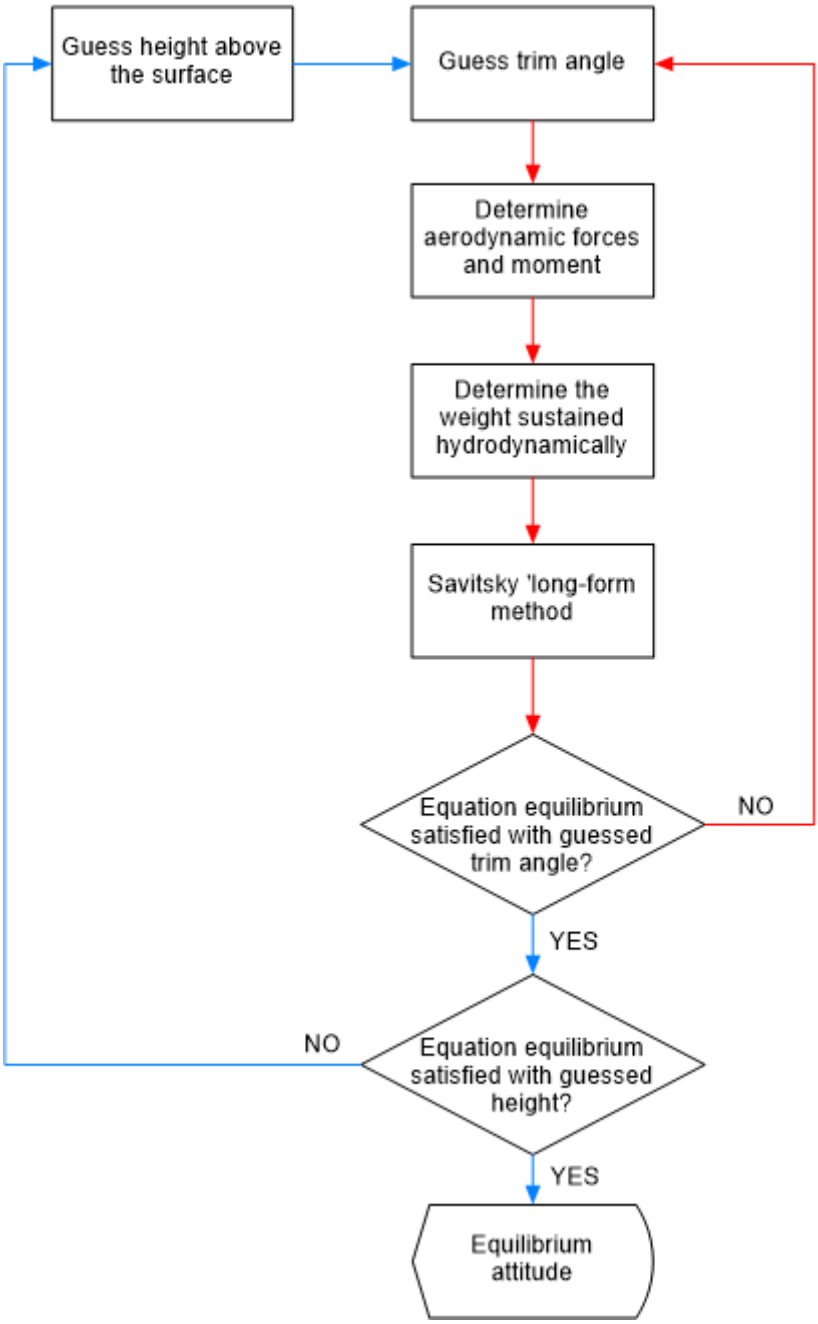

Figure 2-15 Logic flow of determining AAMV equilibrium state

Returning to the discussion about the system of equations of motion for the AAMV, in general, it shows similarities with the WIGE craft. For non-forced conditions and no input from control systems, the equations comprise four matrices on the left-hand side and matrix zero on the right-hand side. The four matrices are the mass matrix, damping matrix, restoring matrix and ground effect matrix. What differentiates the system for WIGE craft and the AAMV is down to the components of their mass matrix, damping matrix, and restoring matrix. For WIGE craft the components of those matrices are from the derivative of aerodynamic forces and moments. However, AAMV considers not only the derivatives from forces and moments produced by aerodynamic surfaces but also those generated by hydrodynamic surfaces.

The complexity of the system of equations of motion for AAMV increases and the comparison of the characteristic roots explains it all. In the planing boat, there are two pairs of complex roots. In WIGE craft, it has two pairs of complex roots and one real root. Eventually, in the AAMV, it has three pairs of complex roots (or probably two pairs and two real roots).

Collu (2008) thoroughly adopted the reduced order system in the planing boat so that the solutions of the system become less complicated. The reduced system results in two pairs of complex roots and one real root only. Not only reducing the number of the characteristic roots, but the approximation also brings forward the similarities between WIGE craft and the AAMV in determining the static stability criteria.

In WIGE craft, static stability criterion is defined as:

$$\frac{M_w}{Z_w} - \frac{M_h}{Z_h} > 0 \qquad (2\text{-}1)$$

and, similarly, in the AAMV:

$$\frac{M_h^a}{Z_h^a} - \frac{M_z^h}{Z_z^h} > 0 \qquad (2\text{-}2)$$

Both criteria above describe the position of the aerodynamic centre in height toward other neutral points. In WIGE craft, to be statically stable, it is important to assure the aerodynamic centre in height is located upstream of the aerodynamic centre in pitch. In the AAMV, that criterion between two aerodynamic centres is applied but needs to be complemented with another criterion, that the hydrodynamic centre in heave has to be located downstream of the aerodynamic centre in height to remain statically stable.

Despite what has been discussed above, there is a concern about the formulation of the systems available in Collu's thesis (2008). There is a mistake in the component of restoring matrix. The weight component described in the matrix has an incorrect sign (it should be positive but negative is written in the document). This error is started very early in the explanation of the system of equations of motion for WIGE craft, and propagates with the system for planing boats and eventually for the AAMV. Despite the mistake, the code that was built to test the model turned out to be correctly developed and gave appropriate results, as shown in the document.

The characteristics of the present system of equations of motion for the AAMV are that it is developed in a condition of a rectilinear trajectory, a constant speed and at a constant altitude above the surface. Also, the equations do not consider the existence of external forces acting on the vehicle nor input from the control systems. From this viewpoint only, the journey of perfecting the system equation of motion is still long.

The literature review that has been done resulted in concern about the presence of waves. Qualitatively, it has been concluded from most of the discussion in section 2.5 that the effect of waves is important to consider in the analyses of the related aspects, including dynamics. The dynamics is the subset of the stability area that focuses on the stability in its motion when a disturbance occurs. Both, WIGE craft and conventional HSMV, face challenges about the subject, and apparently so does the AAMV.

The acknowledgement of waves in affecting the stability of an AAMV configuration will be transformed into its system of equations of motions. Looking

ahead, the rectilinear uniform level motion (RULM) characteristics abovementioned are no longer applicable.

Nebylov and Wilson (2002, chap.4) pointed out active progress in the statistical theory for shipbuilding and ship dynamics with regard to acknowledging the presence of waves. The noteworthy success of this approach was in perfecting the roll calculation. In addition, there are more problems that remain unsolved. They also proposed that system control must consider the effect of waves. However, the idea was only to determine positional reference and relative velocity of the wavy ground. There is no further explanation how the waves affect the aerodynamics and its consequences on the stability derivatives or dynamic behaviour.

Most recently, Kosari and Chamanpara (2016) conducted an investigation of the dynamics of WIGE craft over a wavy surface. They inferred that the stability of WIGE craft configurations is a function of wavelength, cruise speed, wave amplitude, mass, moment of inertia, wing chord, and wing aspect ratio. The instability is likely to occur but is difficult to predict due to the high nonlinearity involved in the analysis, especially when dealing with the time-dependent factors. Such concerns may also be raised in the dynamic analysis of AAMV.

2.7 Critical review of the literature on the ground effect aerodynamics over wavy surfaces

Many studies have focused on the ordinary ground effect problem, i.e. the cases of the flat surface ground. Even in the common problem, the cases cover a wide range of discussions, for example, two-dimensional and three-dimensional cases or steady and unsteady cases. In terms of the application, the study also includes, among others, the aerodynamics of ground effect craft, the aerodynamics of racing cars, gust response, and dynamic stability. With regard to conducting approaches, one may find articles on analytical, experimental or numerical techniques.

For the wavy wall surfaces, however, there are very few studies on the area. One of the reasons is the not-so-extensive applications compared to the ordinary ground effect problem. The demand of the research is related to the operation of WIGE craft or air cushion vehicle (ACV) or, recently, the AAMV with regard to the presence of waves. Another reason for the scarcity of discussions about the problem is its complexity that leads many researchers choosing to simplify it into the ordinary ground effect problem with the addition of certain conditions in order to model the effect of the wavy surfaces.

Ichikawa and Ando (1991) investigated the aerodynamic response of a thin aerofoil flying over a wavy wall surface. The investigation was characterised with the difference between the freestream velocity and the speed of the surface. In the article, they confronted the use of a mirroring technique to model the ground effect case. This is regardless the results from their investigation showed a good agreement with the mirroring method. It is not right to use the mirroring approach for wavy wall problems. Two parameters of wavelength and speed ratio show a great impact on the ground effect characteristics.

While the idea of the inapplicability of the mirroring method for the wavy condition can be adopted, there is a noteworthy difference on the point of interest between the current study and the investigation by Ichikawa and Ando. A part of the interest of the present research is the aerodynamics of an aerofoil, which to some extent is identified as a thick aerofoil compared to the thin aerofoil assumption by Ichikawa and Ando (1991). The thin aerofoil theory idealises the flow around an aerofoil as a two-dimensional flow thus it can be imagined as addressing the aerofoil as having a zero thickness and infinite wingspan. Conversely, from another review on the ground effect (Rozhdestvensky, 2006), the thickness plays an important role in the aerodynamic characteristics.

Nitta (1994) carried out a study on the aerodynamics of a flat plate aerofoil flying over a wavy wall. She investigated the 3–DOF motions and their aerodynamic characteristics of the body using a finite difference method at relatively low speeds ($Ma = 0.1 - 0.3$). In that case, the components of the 3–DOFs were the ride height, incidence angle and the control surface pitching. Initially, she

conducted the analysis for a flat surface problem and then raised the concern of the poor results in low Mach number. It was related to the approach that fitted more to the transonic rather than low speed problem which can be concluded from the improvement of the accuracy by the increase in Mach number validated against another approach. Conversely, a completely different situation appeared when the moving wavy wall was considered. Lower speed demonstrated better results, which may due to the high frequency of the wall. Even though the nonlinearity was neglected in the calculation, it still raised concerns including the scaling of vertical axes that differed from one case to another to accommodate the aeroelastic analysis. The convergence of some parameters, subject to question, with the control surface pitching is the worst of all. The numerical instability and the mixture of aerodynamic and aeroelastic responses are to blame for the occurrence of the situation. Here, Nitta contributed a well-discussed understanding about the difficulties that may be encountered for a low Mach number case of a wing in oscillating ground effect. This is good information for the present study about handling the low speed condition in the aerodynamic analysis. However, the case is also considered as a thin aerofoil theory case, concluded from the use of the finite difference method over a line projected as the aerofoil in Nitta's investigation.

Im and Chang (2000) numerically investigated the aerodynamic characteristic of NACA 6409 aerofoil flying over wavy ground. The approach used Euler code based on the lower/upper-factored algorithm and the high-order upwind scheme. Beforehand, other sets of analyses were also carried out as benchmarks, i.e. a NACA 4412 flying over flat ground, a heave-oscillating NACA 4412 in freestream conditions, and a NACA 0012 flying over wavy ground.

The effects of different wavelengths toward the normal force and pitching moment of NACA 6409 aerofoil were identified. In one case ($h = 0.1$ and $A = 0.025$), the average normal force coefficient (c_n) tends to increase with the increase in the wavelength. In contrast, the time-averaged pitching moment coefficient at the quarter chord point ($c_{m_{1/4}}$) shows a decrease by the increase in the wavelength (it means become more negative). Interestingly, the increase in the wavelength

is followed by the decrease in the range between maximum and minimum values, both for normal force and pitching moment at the quarter chord point. The second case, where the ride height is tripled from abovementioned case, shows the trend for the average normal force decreases and then stable with increasing wavelength. On the other hand, the time-averaged pitching moment starts to increase with the increase in wavelength but the drops afterward. Another peculiarity is the time-averaged pitching moment for $\lambda = 5$ that overlaps with the minimum value of pitching moment. Here one can conclude that while the periodic manner of pitching moment is expected to occur, it was less sinusoidal. The last case, the amplitude is increased fourfold from the second case. The trends shows different behaviour which the average of normal force and pitching moment coefficients show opposite trends from the second case.

One primary concern about the study by Im and Chang is the number of observation points that were carried out. Despite some trends being identifiable, more behaviours cannot be drawn due to the small number of observation points. Also, the height derivative and incidence derivative cannot be appropriately determined because only two ride heights and one angle of attack have been considered.

Moore (2005) carried out a series of experiments to analyse the aerodynamic behaviours of the DHMTU aerofoil in ground effect over flat and wavy surfaces. Beforehand, a series of tests were also done for the NACA 0012 aerofoil as a control during the investigation of the flat surface problem. In wavy conditions, the aerodynamic forces, aerodynamic efficiency and effective angle of attack resemble the wave function. However, no evidence was provided as to when the amplitudes of these parameters occurred. The values of forces were subject to wavelength; the wider it was, the amplitude of the lift forces decreased, and the amplitude of drag forces increased. This condition led to a lower aerodynamic efficiency by the narrowing wavelength. With regard to the precision and accuracy of the results, a concern is raised. The fact that the study over a wavy surface was not validated against other data is one of the causes. However, the apprehension may be questionable even from the study on a flat surface. The

comparison conducted for NACA 0012 and DHMTU aerofoils was done without any validation. For one case of the NACA 0012 aerofoil in out of ground effect conditions, after an assessment of his results, it turned out that considerably underestimated values were produced from his experiment compared to another more established source (Abbott and Doenhoff, 1959). From this standpoint, it is more difficult to rely on the results of Moore's investigation of the wavy case.

Yang et al. (2010) carried out a numerical approach to investigate the aerodynamic study of WIGE craft near wavy ground. Interestingly, the study adopted sliding mesh and dynamic meshing. The combination of these techniques enables the course angle of WIGE craft over the wavy surface effect to be simulated. Also, it gave more stable results to cancel the effect of $K-\varepsilon$ turbulence model. In other simulations (only sliding mesh cases), the results showed less precision. In the simulation that the author ran later, the $K-\omega\,SST$ turbulence model showed more reliability than the $K-\varepsilon$ turbulence model. Nishino (2016) mentioned the lack of the standard $K-\varepsilon$ turbulence model in handling the calculation near the wall. The limitations of $K-\varepsilon$ turbulence model are also mentioned in Pope (2000, p.433), including issues in handling low turbulence Reynolds number and shear stress near the wall. Another limitation in this study is the range of angle of attack run for the simulation. The sets of simulations were only done for one angle of attack ($\alpha = 5°$). Aside from the type of mesh abovementioned, the only parameter being varied was the course angle ($\gamma = 180°$ and $185°$ in the original document addressed as β and calculated from the nose, thus giving $0°$ and $5°$). There is no explanation for the effect of ride height, frequency and amplitude because the variation was not made for these parameters.

Liang et al. conducted an investigation on nonlinear lifting theory for WIGE craft in the case of water waves both for a two-dimensional case (2013a) and three-dimensional case (2013b) in high Reynolds number. In the two-dimensional analysis, the most important finding is that the parameters of waves cannot affect the time-averaged lift coefficient, but they do affect the amplitude, frequency and phase lag of the coefficients. No further explanation is provided for drag

coefficient and pitch moment coefficient. In the three-dimensional analysis, the wave parameters affect the alteration of the time-averaged force coefficients, both for lift coefficient and drag coefficient by the change in aspect ratio. The increase in aspect ratio increases the time-averaged lift but decreases the time-averaged drag. There was no explanation about the effect of frequency and amplitude of the wave. The lift tends to gain higher values when the position of the wing is over convex waves and, vice versa, to decrease over the concave waves. They also confirmed the shifting of the centre of pressure of the wing in a cyclic manner due to the incidence of waves. This may lead to a hazard for the stability of WIGE craft.

Regarding stability, less research has been done for the wavy condition. One of the discussions related to the waves other than aerodynamics is available in a book titled *Ekranoplanes, Controlled Flight Close to the Sea* (Nebylov and Wilson, 2002). However, rather than discussing the effect of the wave toward the controllability of WIGE craft, it merely discussed the probability characteristics of sea waves in space and times and a moving frame. The impact of the study is only about determining the relative position of the craft to the surface as an input to the control system.

More recently, Ito and Iwashita (2016) carried out numerical and experimental studies on two wing configurations, rectangular wing and tapered wing with endplates. The study confirmed the fluctuation of forces around the steady positions with a tendency of nonlinearity. The drag force presented the strongest linearity, marked by the less sinusoidal function of its coefficients. The position of the centre of pressure also demonstrated the similar trend of nonlinearity fluctuation. From the study, it can be concluded that the fluctuation of forces and centre of pressure are strongly affected by the amplitude and ride height. The thrust generation also appeared, and its averaged value increased by increasing frequency. From the comparison that was carried out, Ito and Iwashita stated that computed and measured results were in agreement. While the work presented a reasonable explanation for the effect of several parameters, such as ride height, and amplitude and frequency of wave elevation, to the aerodynamic

characteristic of studied wings, there was no clarification about the angle of attack thus some aerodynamic derivatives could not be drawn from the results presented.

A general conclusion from conducting a literature review of WIGE craft over wavy surfaces, or merely aerofoil over wavy ground effect, is not many studies have been carried out. The typical earlier studies in the 1990s were the aerodynamic characteristics in wavy ground effect for a thin aerofoil. At this stage, the focus was on the effect of general parameters like speed, angle of attack, and ride height in the case of aerofoil flying in proximity to wavy walls. Also, there was a new understanding that the use of traditional methods, such as the mirroring approach in ground effect analysis, may not be applicable. Following the use on the assumption of a thin aerofoil theory, the numerical method adopted was the finite difference method. The next development was the analysis for thick aerofoils. However, the number of investigations was still limited thus the characteristic of aerofoil flying in proximity to wavy walls was not properly identified. One of the reasons was regarding the parameters involved being too many. Some researchers have been trying to propose the best parameter combination in order to capture the aerodynamics of aerofoils in such conditions, but the attempts still leave some gaps to be examined. The number of analytical and experimental approaches in the field is even scarcer, yet the attempts on these have been initiated recently showing the progression of interest in the area.

2.8 Critical review of the literature on aerodynamics of oscillating lifting surface in ground effect

It has been mentioned before that, in appropriate circumstances, one can draw out the effect of waves on the lifting body using a simpler approach, i.e. to assume the system oscillates over a flat surface. This may be considered when the waves have low frequency thus the effect of ride height changing can still be felt by the body. This idea is also agreed by Matsuzaki et al. (2008) and Molina and Zhang (2011), conveying that the unsteady flow of a body may be considered as quasi-steady when the sinking or climbing rates of the system are very small. The

approach may be useful for the analysis of the AAMV in waves. Moreover, the studies of WIGE craft over wavy surfaces are still limited and have not converged to a single direction as the studies were done independently with different parameters of interests.

When the assumption is taken, more possibilities of research may be available. One can conduct research in heave motion over a flat surface, which means to examine the alteration of the relative position of the system toward the surface. Another option is to investigate the pitch motion in ground effect to assess the angular attitude of the system toward the surface. Alternatively, the combination of the two motions can be studied to gain a better approximation of the attitude of the system when it moves on wavy surfaces.

Fortunately, many studies about oscillating body have been conducted for many applications. At small Reynolds number, they have benefited the development of bio-inspired robotic technology. The research in the field has also impacted the aircraft development, especially the high-speed ones. In another automotive field, the analyses are used for the aerodynamics of racing cars. The latter field is also linked with the realm of the ground effect phenomenon. Although the studies that are particularly discussed about WIGE craft are limited, the general idea may be captured from other applications.

Nelson (1951) reported the effect of harmonic pitching and heaving for triangular wing flying at supersonic speed. In a two-dimensional section analysis, the solution of motion proportionally affects the aerodynamic damping both for lift and pitch moment that are associated with respective motion. In a three-dimensional analysis, the total lift and moment have linear dependence on the semiapex angle of the wing. The negative values of the moment do not contribute to the damping of the system but act as the resource of energy for the system. This result indicates the possibility of single-torsional flutter. Due to the supersonic flow regime, the analyses of the upper and lower surfaces are treated separately. Instability may occur depending on the configuration, the values of wavelength, and the Mach number.

Runyan et al. (1955) presented a comparison study between theory and experiment of the effect of tunnel walls on the air forces on an oscillating wing in a two-dimensional subsonic compressible flow. To some extent, this study resembles how an aerofoil oscillates in ground effect. It was shown that the enlargement of wind tunnel or the increase in height had affected the decrease in critical frequency. It means that the effect of the wall to the wing is reduced by increasing height giving the convenience of a small range of resonant region. In other words, the oscillation near the ground leads to a range of natural frequencies rather than a single natural frequency.

The effect of oscillations or periodic motions may lead to the modification of the characteristics of the system. It applies even due to the oscillation of one part of the system, for example, the oscillation of the elevator in aircraft dynamics, as confirmed by Neumark (1956). The modification of the characteristics is marked by the addition of a degree of freedom. It involves great complexity and most of the time the solutions are barely suitable for use as compared with the flight test.

Koochesfahani (1989) investigated the vortical pattern in the wake of an oscillating NACA 0012 aerofoil. The experiment was carried out for small amplitude pitching motion in a low-speed water tunnel. The study confirmed the impact of amplitude, frequency and motion function on the structure of the wake. At a higher frequency, a propulsive characteristic was identified. Interestingly, the critical frequency seemed to depend on the magnitude of the amplitude. Despite the identification of thrust, no further explanation is provided of the parameters toward lift and drag.

Tuncer and Platzer (1996) studied the thrust generation produced by a flapping NACA 0012 aerofoil using computational fluid dynamics (CFD). It was found that the propulsive efficiency has a strong relationship with the reduced frequency and the amplitude of motion. It was also remarked that a flapping/stationary combination in tandem might significantly augment the propulsive efficiency by up to 40%.

Durand (1998) carried out work on the time domain modelling of flapping flat plate aerofoil, which was set for freestream conditions. He concluded that the optimal

cases correspond to the cases where pitch and heave are simultaneous and opposite. The function of motion showed an impact toward the thrust generation. Interestingly, a harmonic squared function generates thrust more than the sinusoidal function. The phenomenon can be explained that the squared motion has higher pitch and heave rates. However, the sinusoidal function has better virtue in the smoother phase transition from time to time.

The propulsive effect of oscillating lifting body that has been previously mentioned in this section is known as the Knoller (1909) – Betz (1912) effect or sometimes also addressed as the Katzmayr (1922) effect. The phenomenon was also identified by Jones et al. (1998) in their investigation of the effect toward the NACA 0012 wing. It was found that the thrust generation is related to the Strouhal number. In larger Strouhal numbers (>0.3), the thrust is generated. There was a difference between the results from experiment and theory. In the experiment that they carried out, it showed more asymmetrical velocity than the panel method, which indicated the viscousity affecting the wake formation.

Lai and Platzer (1999) set an experiment to investigate the effect of the plunge (or heave) velocity to the oscillating NACA 0012 aerofoil. The investigation was run for a range of combinations of parameters (i.e. freestream speeds – Reynolds number of 500-50,000; frequencies; and amplitudes). There was a transition from drag generation to thrust generation for nondimensionalised plunge velocity between 0.2 and 0.4. At higher plunge velocities, the mean streamwise, the velocity field shows as a jet instead of a wake. Another work on the oscillating NACA 0012 was also performed by Young and Lai (2004) focusing on the effect of the plunging motion frequency and amplitude. The work was a numerical simulation to solve a compressible two-dimensional Navier-Stokes solver at a Reynolds number of 20,000. The results showed a good agreement with Lai and Platzer.

Moryossef and Levy (2004) carried out a different investigation focusing on the plunging motion of an inverted aerofoil, Tyrrell 026, in extreme ground effect out of the interest in the race car performances. It was a numerical scheme based on Euler/Navier–Stokes equations. The simulations exhibited a wide variety of

interesting phenomena. It was found that the time-averaged lift of the oscillating aerofoil gives similar results to the non-oscillating one. However, the drag shows a different situation where, in the oscillating case, the Knoller–Betz or Katzmayr effect occurs. The increase in the frequency of oscillation and the decrease in ride height, both induce the increase in the thrust generation. The frequency of oscillation also has the impact on the phase lag and amplitude. The decrease in frequency of oscillation pushes the phase lag approaching zero and also lower amplitude.

Iosilevskii (2008) theoretically addressed the production of aerodynamic lift and moment of an oscillating wing in weak ground effect. Started from minimum references, Iosilevskii stated that the normalisation of the ratio of the wing transversal displacement to its semi-chord is essential in separating time-dependent aerodynamic loads from time-independent ones. The solution of the problem of a wing with an infinitesimally thin aerofoil is asymptotically influenced by the ratio of the wing quarter-chord (mac) to the average ride height ($\bar{h}$). Aside from mac and $\bar{h}$, the structure of integral equation proposed by this study is affected by the wavelength (λ). The approach seems promising as it showed good agreement with a numerical simulation, but, as Iosilevskii (2008) mentioned in the article, more evidence is needed. Also, the approach offers versatility as it may be applicable for aircraft wings during ground roll and low flight, and even for high set front wings of racing cars.

Molina and Zhang (2010, 2011) presented a numerical study on a heaving inverted aerofoil in ground effect. Based on the phase lag analysis of the aerodynamic coefficients from the aerofoil motion, the aerodynamic behaviours may be categorised into three regions, i.e. ground effect bound, incidence angle bound, and added mass bound. At low frequencies, when the case is considered quasi-stationary, the ground governs the flow. At medium frequencies, the effect of incidence angle is apparent, which is marked with the effective angle of attack. At higher frequencies, the effect of added mass is more dominant and less effect of ground effect. Interestingly, the behaviours abovementioned are independent of Reynold number.

The continuation of Molina and Zhang's investigation was continued by Molina et al. (2011), adding the stability analysis to the study. Molina et al. remarked on the occurrence of instability when the aerofoil is at low ride heights and low frequencies, leading to stall flutter occurrences. In this case, the heaving motion in ground effect is comparable to the pitching motion in which dynamic stall occurs at high frequency.

In terms of involving motion, Molina et al. (2016) stepped further by investigating the effect of pure pitching motion and the combination of heaving–pitching motion of an inverted aerofoil. In the pure pitching motion case, the hysteresis of the results widens compared to what pure heaving motion produces. The characteristic occurs due to the separation at the suction side that comes earlier, which may lead to the stall at low frequencies. For the combined heaving and pitching motion, it seems that the heaving motion has more impact at high frequencies, whereas the pitching motion influences more at low frequencies. The interaction between both modes is governed by the difference in their phase lags.

The investigation of oscillating inverted wings in ground effect is related to the automotive research area. Such investigations in an experimental manner also have been carried out at Cranfield University (Mistry, 2012; Plensky, 2012; Fernández-Soto, 2013; Pietrzak, 2013).

Mistry (2012) discussed the effect on the wake of oscillating wings in ground effect. The configuration was a double element of wings. They were varied in the angle of attack and slot gap between each other. The variation was also placed for the ride height and wind tunnel speed. However, there was no explanation about the value of the frequency of oscillation – apparently, it was a single high frequency. The variety of results was obtained as a result of the underpinning parameter. The interesting point that Mistry conveyed in the study was the occurrence of the Venturi effect when the configuration was in the trough position. The Venturi effect causes the wake profile attached to the ground for a longer time during the upward motion.

Plensky (2012) also carried out an investigation on a double element of wings, but with static angle of attack ($\alpha_1 = \alpha_2 = 0$). The oscillation influences the values of normal forces of the wing system where the decrease in ride height leads to the amplification in its normal force. In high lift over drag ratio and high lift configuration, discontinuity occurs. The discontinuity leads to the separation of the merging boundary layer, thus less sinusoidal lift function. However, the effect of discontinuity is less with high frequencies as well as the maximum normal force.

Pietrzak (2013) continued the work on oscillation of double elements of wing focusing on the effect of the transition point of the wing. For the free-transition point case, the amplification of the amplitude of the normal force was observed for lower heights. Therefore wing in ground effect is more sensitive to the ride-height change. On the other hand, the transition fixing reduces the level of normal force generated by the model. Moreover, change in Reynolds number indicated that the force distribution is slightly reduced.

Different from the other three, Fernández-Soto (2013) investigated a single element wing. In general, there is no significant difference in behaviours from the previous discussion in the area. However, one interesting phenomenon is the occurrence of stall in extreme ground proximity before the wing reaches its lowest position. Hence, flow separation is likely to occur during the middle stages of the cycle. At high angles of attack, flow separation must also take place at the first and last stages of the cycle, according to the low magnitude of the forces, in comparison with that at lower angles of attack. Here, it may be concluded that full separation in ground effect occurs in extreme ground effect and only part of the flow reattaches when the wing moves further from the ground. Increase in the frequency of oscillation leads to the increase in phase lag and greater changes in the effective angle of attack. The same effect is caused by increasing the oscillation amplitude. The fixing transition in ground effect leads to a reduction in normal force as flow separation may occur.

More recently, Liang et al. (2014) carried out a numerical study on heaving 2D aerofoils in ground effect. The investigation was performed for two conditions, i.e.

flat surface and wavy surface (the latter case means that two oscillations are occurring at the same time, the motion of the aerofoil and the periodic elevation of the surface). It can be observed that the time-averaged lift coefficient increases rapidly as the ride height decreases when the reduced frequency is fixed. The same increasing manner is true for the amplitude of the lift coefficient. Therefore, the ground effect is significant when the clearance is low. The reduced frequency does not have a significant influence on the time-averaged lift coefficient. However, the reduced frequency significantly affects the amplitude of the lift coefficient curve. The greater the reduced frequency, the larger is the lift coefficient amplitude. It is also observed that the ride height is independent of the frequency of the lift coefficient curve. Differently, when the wave occurs, taking the aerofoil as the frame of reference, the harmonic waves appear to undergo a change in frequency. The frequency experienced by the aerofoil is denoted as the encounter frequency which is different from the frequency of the wave. The lift coefficient curve varies harmonically. The general tendency of the lift is that the time-averaged lift coefficient increases slightly with the heaving frequency. Something missing in the study is that there was no variance in the angle of attack and the position was set only for two ride heights and one freestream condition.

From the literature observation that has been conducted, the trend of investigation in the area is mainly divided into two categories. The first category is the investigation of the cases of the small Reynolds number ($< 50{,}000$), high frequency and low amplitude. The other category is for the cases of inverted wings, high frequencies, very low amplitudes and in extreme ground effect. Examining the trends, one can conclude the characteristic differences that are not applicable to the present research. The first category is the extension of research on the aerodynamics of bio-inspired robotics. The irrelevance in the present research is mainly on the Reynold number. There are, of course, similar shared characteristics between the two. However, the difference will affect the flow regime involved (laminar or turbulent) and eventually affect the forces production. As for the second category, the difference is the object being investigated and nature of treatment. Inverted wings, mainly used in the research on racing cars, are often carried out for extreme ground effect conditions as a

result of structural vibration that may lead to fluid-structure interaction. Also, the frequency is considerably high compared to the present research. Based on the trends available, it is necessary to carry out a new investigation that is suitable for the case of WIGE craft.

2.9 Critical review of the literature on numerical technique for transient CFD analysis

Transient CFD analysis is a broad topic, thus in this section, the author only limited the topic to the ground effect or oscillating wing/aerofoil cases. This critical review is mainly to examine the most suitable approach for the aerodynamic study case in the present research.

One of the earliest numerical approaches of unsteady analysis in ground effect is the vortex lattice method (VLM). The method models a lifting body as an infinitely thin sheet of discrete vortices to compute lift and induced drag. Chen and Schweikhard (1985) and Katz (1985) used the approach for a case of the aerodynamics of a standard flat wing and the aerodynamics of a wing for racing cars, respectively. The ground effect was approached using the mirror image technique. In the discussion, Katz also considered the effect of heaving. In the study carried out by Katz, the calculation was done by using a 13x4 elements vortex. The addition of numbers of vortex elements did not give a difference in the results.

Mook and Nuhait (1989) also utilised the unsteady VLM in a study on aerodynamics in ground effect. Regarding the mirror image technique, they pointed out that when the ground is rough (not as a plane), images can be omitted and instead replace with panels on the ground. The credibility of the approach was validated against an earlier study and gives an excellent agreement. It is noteworthy to mention that the use of VLM is not limited to two-dimensional steady flows.

One of the limitations of the use of VLM is the absence of thickness even though the three-dimensional can still be performed. Also, the effect of viscosity in the

analysis is neglected. These are drawbacks in producing a reliable result because these parameters (i.e. thickness and viscosity) matter in ground effect analysis. Hence, the approach is suitable for the calculation of aerodynamic lift and drag in potential flow during the initial design phase.

The finite difference method (FDM) started being used at the beginning of the 1990s. Nitta (1994) adopted the approach for the analysis of flat plate aerofoil moving over a wavy wall. The wavy wall surface here was modelled to have vertical displacement as a harmonic function for simplicity reasons. The whole grid shape in the computational domain was squared. Particular attention is in the generating of the polynomial that should be rewritten to accommodate the expression of the wave. The approach was checked by doing some comparisons against the least square method (LSM) using the mirroring wing. In the low-speed condition ($M_\infty = 0.1$), the assessment showed poor agreement. The fact that the LSM was developed for a transonic case was to blame for the difference. This was strengthened with better agreement in results with the increase of speed to $M_\infty = 0.3$. However, this hypothesis does not explain how the speed is affecting the accuracy in Nitta's case. There is no clear evidence in the low speed that the approach by Nitta would give good results unless it is validated against an experiment or other proven approach for such a case.

The application of the finite volume method came later, for instance as shown by Hsiun and Chen (1996) for a steady case, and Tuncer and Platzer (1996) for an unsteady one. Some comments on Hsiun and Chen's work were produced due to taking the wrong assumption in the computational modelling thus it did not correspond with the physical experience and theoretical background of ground effect aerodynamics (Steinbach, 1997).

The case discussed by Tuncer and Platzer is the combination of aerofoils in tandem. Three different approaches are adopted, i.e. Navier–Stokes, unsteady potential flow, and Navier–Stokes/potential flow solutions. The challenges in these approaches are about the development of computational domain and its boundary condition.

For the Navier–Stokes solution, Tuncer and Platzer adopted C-grids blocks to compute the flow field around the aerofoil system. Due to the flapping/stationary motion of the system, the computational domain was discretised with an overlapping uniform grid around each aerofoil. An interpolation across overlapping grid boundaries was taken into account due to the circumstance. The development of grids was problematic as the upstream grid suffered having poor orthogonality. Several attempts to generate a better orthogonal domain were not fruitful except by using an algebraic grid generator. The heaving motion of one of the aerofoils imposed that the computational grid around the aerofoil must move in the same manner. Another attention was also given to the overlapping grid by applying interpolation flow variables across the boundary at every time step. As the grid moved relative to each other, overlapping boundary points were localised of the neighbouring grid before the interpolation made. This approached was claimed robust and efficient by the authors themselves. As for the implementation, the case was run in an upwind biased, factorised, iterative and implicit scheme.

The unsteady potential flow is an approach based on the panel method. The unsteady flow field was represented by distributing source and vortex sheets on the aerofoil's surface and concentrated vortices in the wake region. The superimposition of the source/sink and vorticity was used to determine the boundary condition on the aerofoil surface.

In the Navier–Stokes/potential flow solution, the domain is portioned into two zones, i.e. near-field and far-field zone. The Navier–Stokes equation was solved in the entire near-field zone, and potential flow solution was used to solve flow field in the far-field zone. The source and vortex were calculated in the near-field zone rather than on the surface of the aerofoil. The flow field in the far-field region was computed using the potential flow solution. The baseline of the computational grid of this approach is obtained from the grid of the Navier–Stokes solution mentioned previously. The difference was the exclusion of the grid lines beyond the specific outer boundary in the transversal direction for the Navier–Stokes/potential flow solution.

The three approaches, despite the overall agreement, showed differences in the results. The pure unsteady potential flow solution deviated the most, which can be immediately comprehended because of the assumption of incompressibility and fully attached flow field. A better agreement was demonstrated by the other two solutions. However, the Navier–Stokes/potential flow solution was built in a smaller computational size, thus has faster computational time than the pure Navier–Stokes solution.

The use of Navier-Stokes inspired solutions is also found for the low Reynolds number and high frequency (Young and Lai, 2004), inverted aerofoils (Moryossef and Levy, 2004) – which is actually a hybrid between the Navier-Stokes and Euler solutions, and when the encounter frequency is considered (Yang et al., 2010).

Another approach using pure Euler solutions is also available (Im and Chang, 2000). The investigation was on the unsteady aerodynamics of an aerofoil flying in proximity from wavy walls. Im and Chang employed the H-grid system for the case. The code was validated against an experimental result and gives good agreement except for high angles of attack. Regarding time accuracy (which leads to the definition of wavelength afterwards), it also gave agreeable results against other studies. As the wavy wall is modelled as a travelling sine function, readjustment of inner grid points in the computational domain occurred at every time step. Some limitations that may occur by adopting the approach are the range of cases that give accurate results. When it comes to high angles of attack and long wavelength, deviations may be expected. This is probably because of the absence of viscosity effect in the calculation.

When it comes to the Navier–Stokes solutions, there is an approximated method that is called Reynolds–averaged Navier–Stokes (RANS). This RANS approach is the approach being used in the cases above even though it has been termed as simply Navier–Stokes in the articles. The equations involved in RANS are pretty similar to the original Navier–Stokes except for the addition of Reynolds stress. This addition has implications for the use of a turbulence model being used during the computational process. As far as the author is concerned, the

turbulence methods that are used in the case of ground effect and oscillation may vary.

One of the turbulence methods adopted is the realisable $K-\varepsilon$ turbulence model for a case of wavy ground effect with frequency of encounter consideration (Yang et al., 2010). Pope (2000, p.433) and Nishino (2016) mentioned some limitations of the model especially when handling the effect of the wall. In the case carried out by Yang et al., the difference in adaptive grids was to blame for the fluctuation of results. However, the effect may also be caused by the choice of turbulence model. The author did some tests on the turbulence model and found that the fluctuation even occurs in the pressure distribution. From the test, the author found that Yang et al. probably took the $K-\varepsilon$ turbulence model from the fact that it is widely used in many oscillation cases.

Another model used for modelling turbulent flow is the Spalart–Allmaras model, and it has been adopted in the investigation of ground effect, for example by Qu et al., both for the 2D case (2014a, 2014b) and 3D case (2014a). The Spalart–Allmaras turbulence model is a one-equation turbulence model. It solves a modelled transport equation for the kinematic eddy turbulent viscosity. Originally the model is effectively a low-Reynolds number, requiring the viscosity-affected region of the boundary layer to be properly resolved. In the 2D case, the author managed to reproduce of the case but with a different turbulence model, i.e. SST $K-\omega$ turbulence model, giving good agreement in lift force at low angles of attack. In higher angle of attack, the SST $K-\omega$ turbulence model has more agreeable results in lift than Spalart–Allmaras compared against experimental data (Kikuchi et al., 2002). The deviation is probably because the computational error of the Spalart-Allmaras model is higher in this case.

The other thing that is likely to be considered is the use of dynamic mesh and adaptive grid. The cases abovementioned (Yang et al., 2010; Qu et al., 2014b) also paid attention to the effect of dynamic mesh. In the case discussed by Yang et al., the results from dynamic mesh may differ significantly rather than using simple sliding mesh (which also can be considered a dynamic characteristic in the computational domain). The dynamic ground effect, as the term Qu et al.

(2014b) used, explains the block grid near the ground wall that moves dynamically thus the definition of ground velocity is placed in the grid block and not in the wall boundary itself. It was found that in the ground effect area, the dynamic ground effect results differ from the static ground effect results. The difference gets smaller as the ride height increases away from ground effect region. This affirms the importance of the usage of dynamic mesh in the investigation of ground effect in a transient mode.

2.10 Conclusion

This chapter discusses the literature survey that has been undertaken for the research. The survey was a part of the investigation methodology where the first nine-months were solely dedicated to the activity. The literature investigation was started from the literature on HSMVs and WIGE craft.

In order to culminate the focus of the research, the literature review was categorised into several main related topics. After careful thought, the focus was directed on the longitudinal stability of WIGE craft in waves along with the methodology implemented during the programme. The objectives were given to WIGE craft, instead of AAMV, due to the lack of knowledge in the area.

Special attention was given to the aerodynamic data acquisition by means of CFD. From the literature survey conducted, the author assessed the essential computational parameters in the acquisition processes.

One of the significances of the literature investigation was the conference paper presented at the 10th Symposium on High Speed Marine Vehicles in Naples, Italy in 2014 (James et al., 2014). The paper, in which the author of this research becomes the second author, is about challenges, especially in the hydrodynamic aspect of AAMV. The abstract of the paper is available in Appendix A.

3 RESEARCH APPROACH

This chapter presents the methodology adopted in this study. As mentioned in section 1.5, the research methodology has been defined based on the literature review. This chapter is composed of four stages: *(1) Research design*; *(2) Methodology implementation*; *(3) Methodology evaluation*; and *(4) Conclusion*.

3.1 Research design

The first step in formulating the research design is to understand the broader context and how this study fits in the realm of study. Figure 3-1 depicts the current investigation in the HSMV area. Moreover, a detailed context of the research is presented in Figure 3-2.

The scheme of how the research was carried out is presented in Figure 3-3. The research was divided into three main stages, i.e. the literature review, the core programme, and the extended programme.

Firstly, the figure demonstrates that a robust literature review was a fundamental part of the methodology since it supported the research programme. The literature review was done throughout the three-year study, but was the main activity during the first nine months. It not only identified the main challenges, but also gave inspiration on how to tackle these challenges.

The core research programme has been focusing on the development of a dynamic model of AAMV/WIGE craft in wavy conditions. The programme was carried out in several stages in order to meet the objectives of this study. A review on kinematics was performed before the mathematical and numerical models were developed. Eventually, verification was carried out and recorded in a thesis document. Unfortunately, no validation could be performed as no single study has been undertaken in the field.

During the completing of the programme, some obstacles occurred preventing the author to see immediate outcomes of the research. It has been mentioned before about the scarcity of academic resources on the discussion of the problem

raised by this study. The literature shortage revealed further issues regarding the availability of data to be used. The author found difficulties in obtaining the stability derivatives that might be used in the dynamic analysis of AAMVs or WIGE craft in wavy conditions.

To determine stability derivatives, the configuration and aerodynamic data are needed. This pushed the author to find information in ground effect aerodynamics, especially in the influence of waves. However, the attempt only resulted in a finding with little discussion hence no adequate data can be utilised.

Facing the issue has led to a decision to produce aerodynamic and stability derivatives data which initially were not parts of the programme. This is what is referred to as an extended research programme in this document. The extension of the programme was not only the benefit of the data acquisition but also contributed to the knowledge in ground effect aerodynamics.

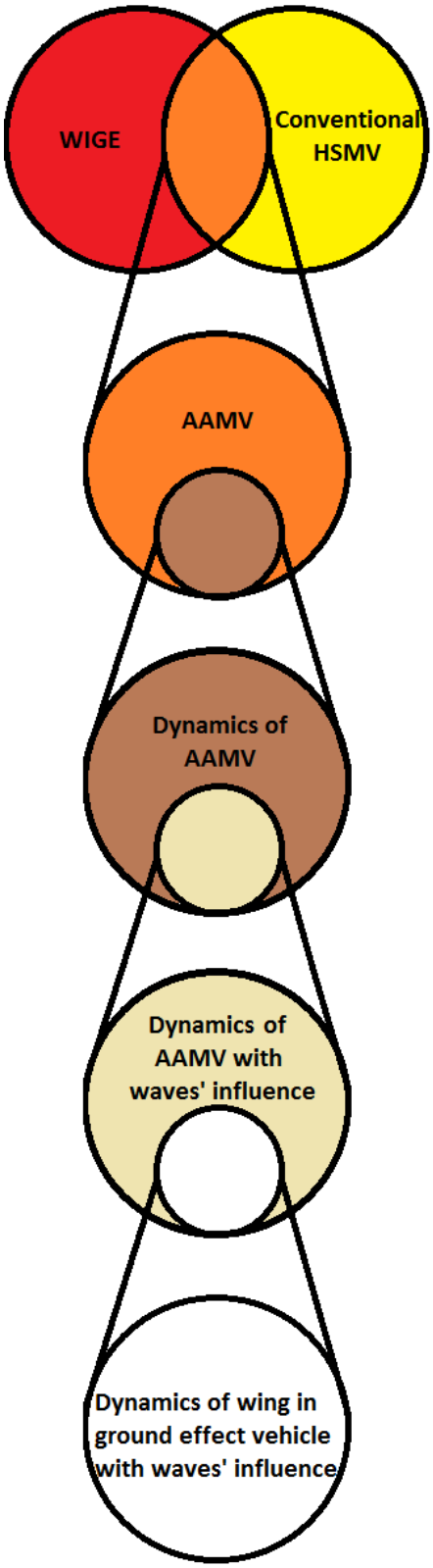

Figure 3-1 Position of the research in the HSMV realm

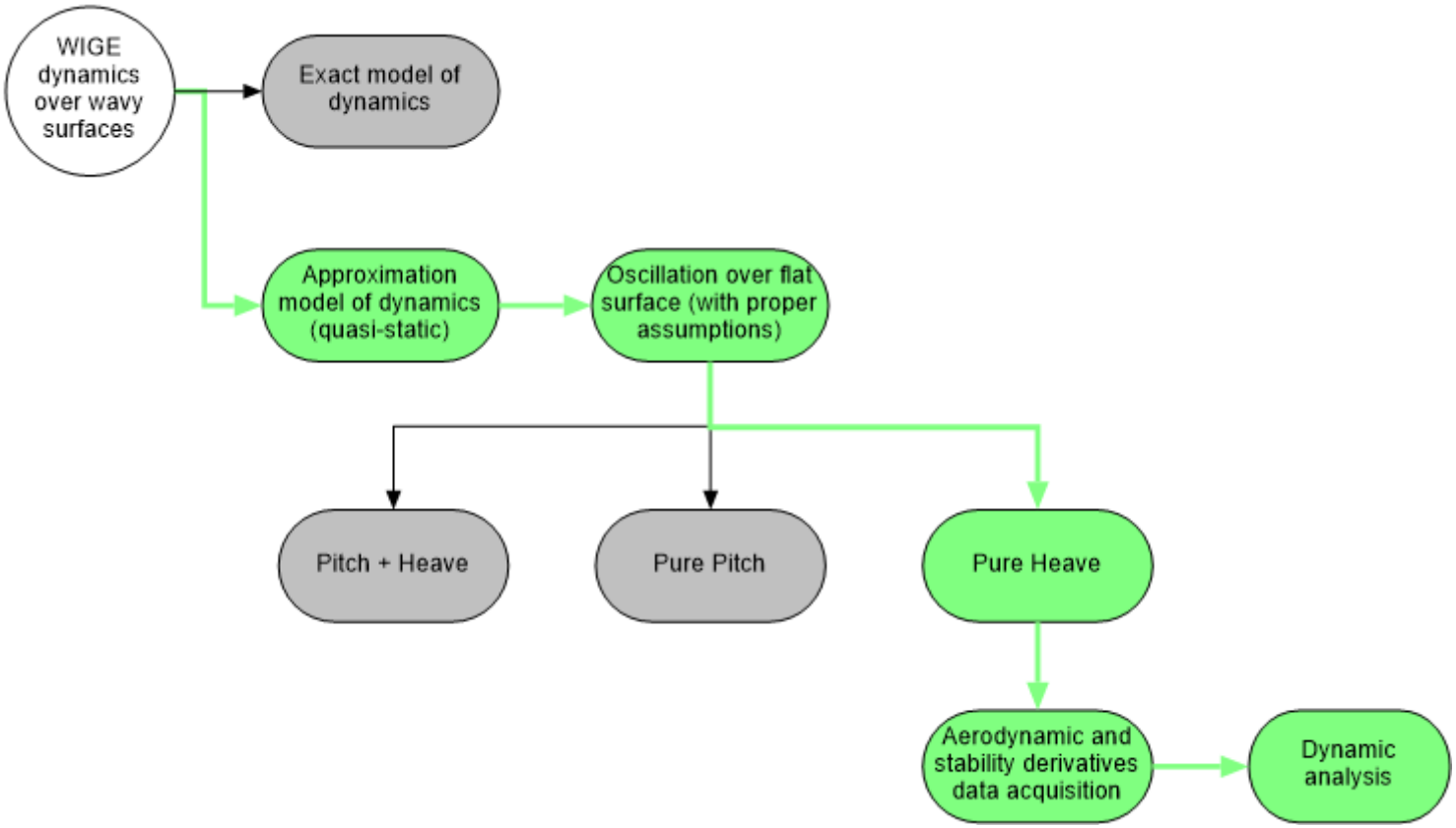

Figure 3-2 Detailed research context

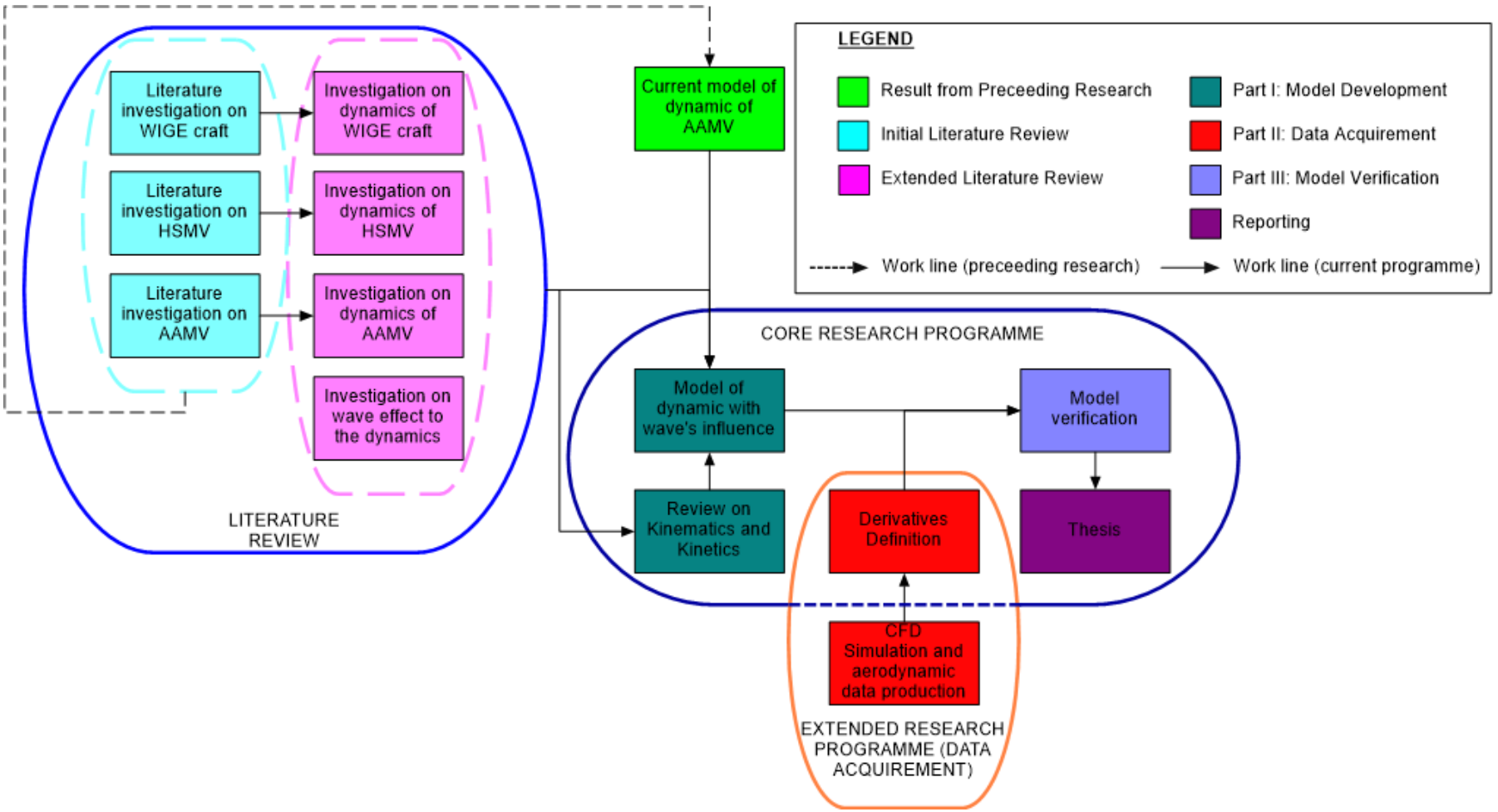

Figure 3-3 Methodology of the research

3.2 Methodology implementation

3.2.1 Literature review

The research started investigating a new generation of a water transportation mode, called AAMV. The first draft was to conduct a systematic literature review assuming the number of literature would be sufficient. However, the number of references that straightforwardly discuss the topic was very limited thus the method was not directly applicable. The literature review was then conducted by reviewing the literature available for WIGE and conventional HSMVs.

Figure 3-4 shows the four stages of the literature review. The first nine months focused on the first three steps, i.e. initial, expanded, and focused literature review.

The initial literature review was about understanding the realm that the author would engage. Some literature was assigned to read, especially the doctoral thesis, *Dynamics of Marine Vehicles with Aerodynamic Surfaces* (Collu, 2008).

The expanded literature review resulted in problem identification and an initial implementation model of dynamics in the form of a flowchart. The problem identification was presented in the Year 1 Review Meeting (Adhynugraha, 2014) and the flowchart was presented in the Year 2 Review Meeting (Adhynugraha, 2015). The first flowchart was very complex as various scenarios were considered. With the complexity shown, its viability was questioned including the time that would be consumed and the number of supporting data available to fulfil all the circumstances proposed.

The second iteration of the literature survey resulted in a more focused research topic and an initially proposed methodology where the main focus is on the influence of waves on the dynamics of AAMVs. The continuation of the review process allowed a more reasonable model to be approached.

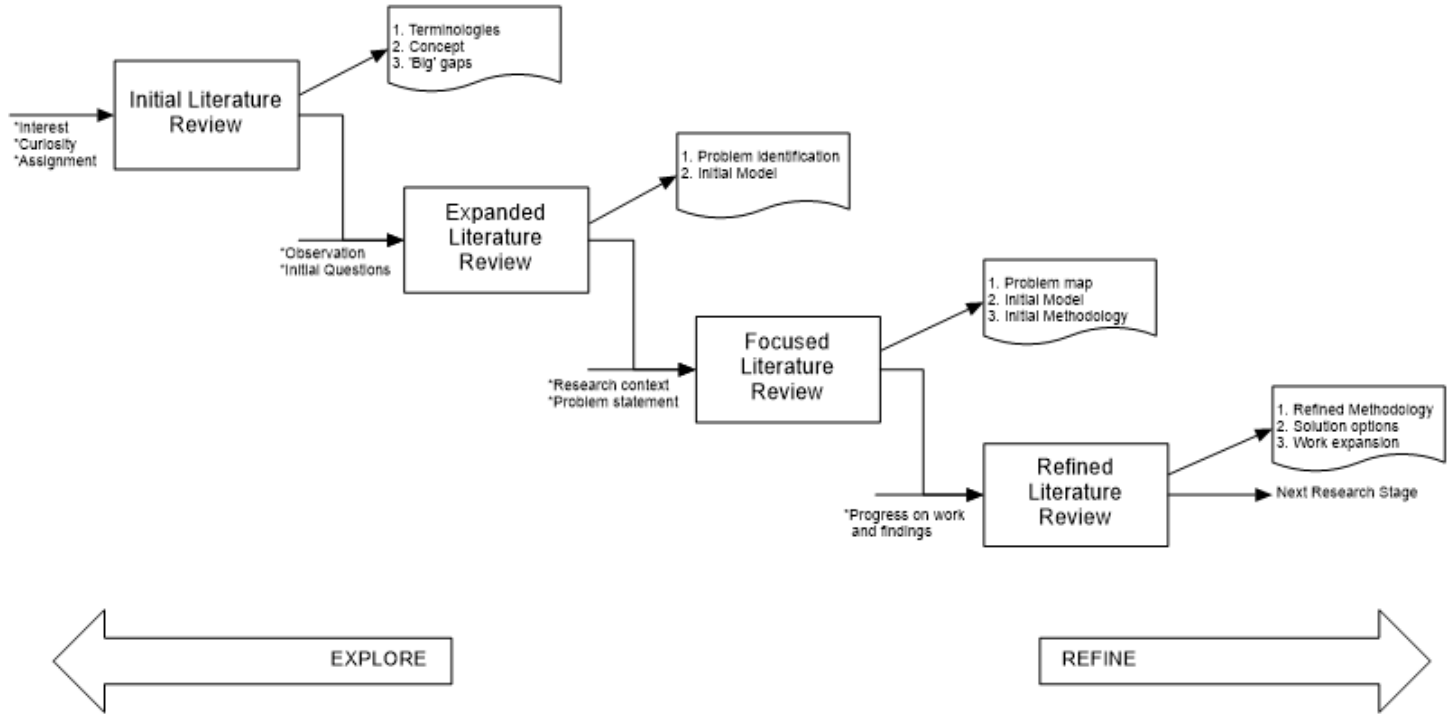

Figure 3-4 Literature review sequence

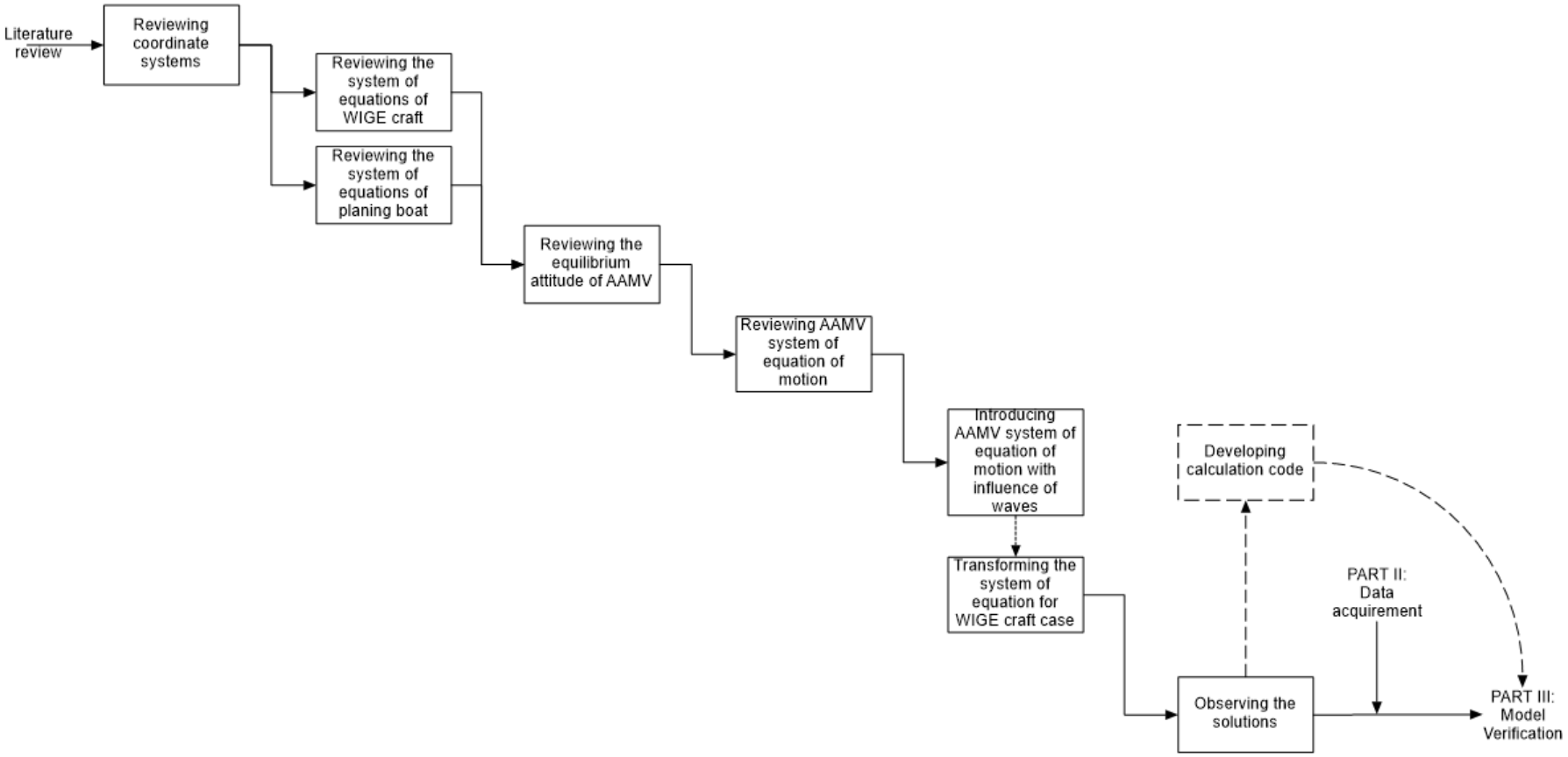

Figure 3-5 Part I: Model development

In the last stage, the literature review resulted in the idea to solve the problem and improve the methodology, as presented in this thesis. The final stage also identified the need to conduct a numerical simulation to aid the investigation process.

3.2.2 Core research programme

The core programme encompasses several parts. There are three technical parts and one reporting part. The technical parts are model development, numerical and experimental data production and collection, and verification. This thesis provides the last element related to the documentation of the project.

3.2.2.1 Part I: model development

This part comprises two steps, i.e. review on kinematics and elaboration of the model of dynamics of the vehicle in the presence of waves. The illustration of this part is depicted in Figure 3-5.

Review on kinematics

Collu (2008) discussed the kinematics framework of WIGE craft, planing boat and AAMVs. He pointed out that the investigation on kinematics played an important part in defining the model of dynamics and how to represent it in a mathematical expression. This part has the purpose of reviewing the work and seeing the connection with the current research.

Even though the kinematics is not put in the main body of the thesis (but in 0), its importance should be not underestimated. It determines the reference framework where the model is built, thus affecting the formulation of the system of equations of motion.

Development of the system of equations of motions

The mathematical formulation of the longitudinal motion of an AAMV configuration operating in wavy conditions was developed and are presented in Chapter 4.

The formulation was started from reviewing the equations of equilibrium of AAMVs proposed by Collu (2008, chap.6). Even though the formulation for a configuration can be different from another, the forces and moments acting on a vehicle can be divided into four groups, i.e. gravitational, thrust, aerodynamic, and hydrodynamic. The choice of configuration will affect those forces and moments.

After reviewing the equations of equilibrium, the next step is to examine the systems of equations of motion, focusing on the longitudinal motion, for HSMVs, WIGE craft, and AAMVs, respectively. This activity did not only capture the idea how the system of equations of the AAMV was built, but also apprehended the relationship and similarities of it with the other two systems of equations.

The final step was to introduce the effect of waves into the system of equations of motions. One of the consequences of considering external forces is the complexity to draw the conclusion increases. To handle the complexity, the author proposed an approach of ‘quasi-static’ dynamic analysis. The approach can be explained as a set of homogeneous solutions of dynamic analysis for several points of observation as a function of position relative to the surface. The approach has been assessed that it is only fit for low (encounter) frequencies. Fortunately, many HSMVs operate in this condition.

As repetitively mentioned that the dynamic stability concept in the presence of waves for WIGE craft is not well established thus the verification was applied to a WIGE craft configuration instead. This decision was expected to be beneficial for both WIGE craft and AAMVs. For AAMVs, it is simply because a part of the idea adopts the WIGE craft conception.

3.2.2.2 Part II: data acquisition

Due to the lack of experimental and numerical data about the aerodynamic performance (lift, drag, moment coefficients) of profiles operating in ground effect, and over a wavy surface, during the PhD, it was decided to introduce the additional task of deriving the necessary data through Computational Fluid Dynamics simulations. The process was unfortunately not straightforward. Some approaches involved the acquisition of data on configuration, aerodynamics, and stability derivatives of a chosen vehicle. The detail of this part is shown in Figure 3-6.

Acquisition of configuration data

There were some options of WIGE craft that were considered for the dynamic analyses; however, the decision was on the Ekranoplan 'Orlyonok' A-90 that was also adopted by Delhaye (1997). In the document, the difficulties in obtaining more comprehensive data on the vehicle are mentioned. Out of this limitation, Delhaye used a semi-empirical method, based on the conceptual design method provided by Roskam (1989, 1990) and Torenbeek (1982) to produce reference configuration data.

This reference configuration data was used for this project, due to time-saving reasons and also the fact that many subsequent investigations in the dynamics of WIGE have referred to it. The difference between this study and Delhaye's consists in the use of different aerodynamic profiles, resulting in different aerodynamic characteristics. The method to acquire the aerodynamic data is available in the discussion below.

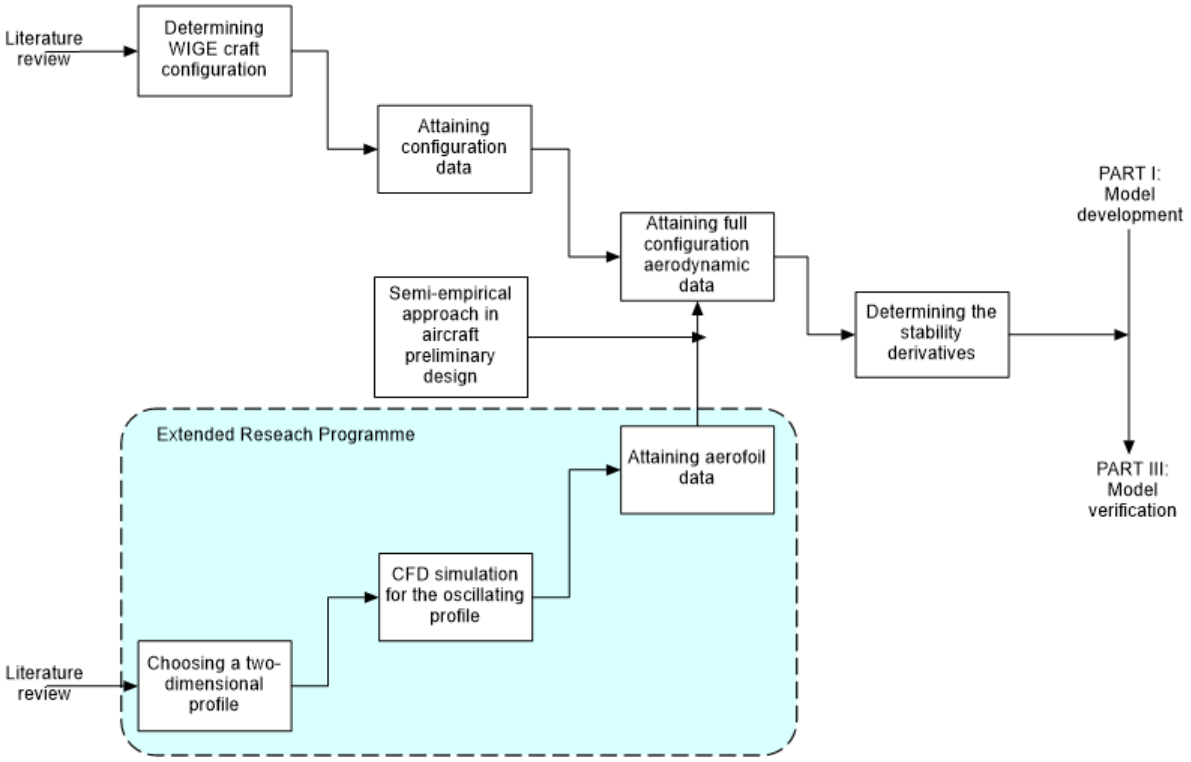

Figure 3-6 Part II: Data acquisition

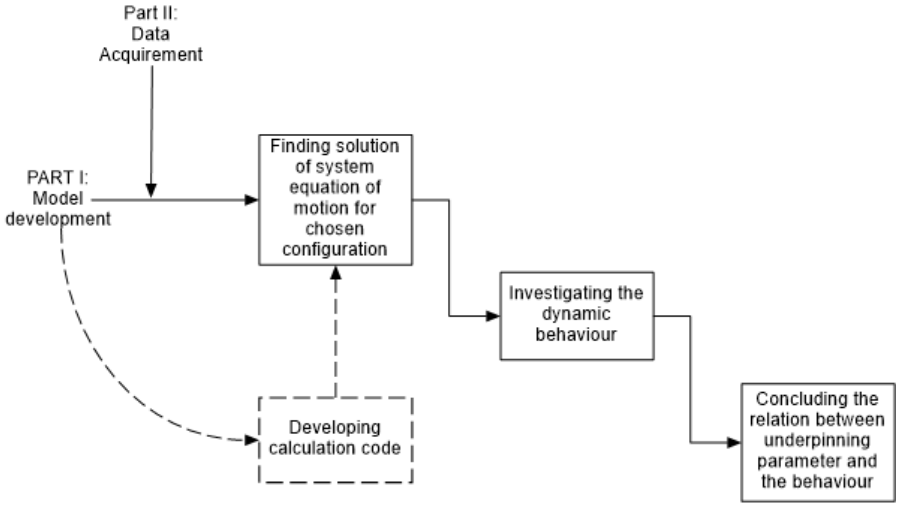

Figure 3-7 Part III: Model verification

Acquisition of aerodynamic data

Aerodynamic data are required to provide aerodynamic derivatives of a WIGE craft. Due to the small number of records obtainable from open literature, the author decided to produce a set of aerodynamic data through a series of CFD simulations; more details about the simulation are presented in chapter 5. The approach was used focusing on two-dimensional profile oscillating in ground effect.

Later, the two-dimensional data was transformed into the aerodynamics of the wing and eventually the aerodynamics of the vehicle. The approach, more details of which are available in section 6.1, was the empirical approach for a conceptual design based on the techniques in *Aircraft design: a conceptual approach* (Raymer, 1999).

Acquisition of dynamic derivatives

Obtaining the dynamic derivatives of a 'modified' Ekranoplan is quite straightforward. Some approaches can be used, but this study adopted the UK-style to provide the derivatives. More explanation is in Chapter 6 of this thesis.

3.2.2.3 Part III: model verification

A MATLAB code has been implemented to estimate the dynamic stability of the chosen vehicle. The program calculates the roots of the modes of oscillation and the time response to an external disturbance. The execution of the program followed several scenarios including an initial comparison between the configuration of Delhaye and current research. The detail of this part is available in Figure 3-7.

3.2.2.4 Reporting

This thesis is the most important document produced being a comprehensive recording of the research since it was started. It provides a sequence flow of how the research was done, formulated, performed and at the end produced results for discussion.

There are other documentation during the programme including progress reports, review reports, and papers. However, these documents only give partial information about the research and possess different objectives, as does the thesis.

3.2.3 Extended research programme

The extension of the research programme was particularly about producing aerodynamic data through computational fluid dynamics and in an extended point of view was a portion of Part II of the core research programme about data acquisition, see Figure 3-6. The reason behind the extension endeavour was the inadequacy of available aerodynamic data records for the case with the influence of waves' motions. Most of the literature that the author encountered has been limited to small range parameters thus no further derivatives could be obtained.

The CFD focused only on the two-dimensional profile due to the complexity involved with a three-dimensional analysis and the time limit. The simulation was run with advance virtues of CFD including transient analysis and dynamic mesh.

The set of 2D data was transformed into a set of 3D aerodynamic data of wing and wing-fuselage-tail configuration. The transformation was done by using an approach that usually is used for initial design of an aircraft. It should be noted the tail analysis uses a different aerofoil with an assumption out of ground effect.

The approach confirmed the significance of a two-dimensional profile to the dynamic stability derivatives, as later in the verification processes, an initial comparison is made between the derivatives of the present study and Delhaye's (1997) work.

3.3 Methodology evaluation

The methodology of this study has been evaluated by three reviews done during the programme. However, more importantly, the deliverables from each component of the action plan show its robustness from an academic point of view.

One of the deliverables of the literature review activity is the map of identified challenges that an AAMV may encounter. It encapsulates pieces of information in the numbers of sources of WIGE craft and HSMVs. The map itself has been a contribution to the new realm of AAMVs as a guideline for future researchers. Also, the literature survey had contributed to the discussion in a conference paper (James et al., 2014).

The core research has developed an approach to perform a dynamic analysis on a WIGE craft in the condition of external forces from the waves involved. The approach is also compatible with a dynamic analysis for the AAMV in waves. Two scholarly articles have been prepared aimed for journal submissions.

The extended research programme also has contributed to the field of ground effect aerodynamics. This part of the present study enriches the prior knowledge, especially for the case of oscillation in ground effect for WIGE purposes; most of the previous studies have focused on oscillation (due to structural vibrations) inverted wings for racing cars. This work also was presented at a conference (Adhynugraha et al., 2016). The paper was requested for publication in a journal, but the author personally declined in order to refine the discussion before it is properly issued for academic use.

With regard to the whole project, the deliverable is this thesis.

3.4 Conclusion

This chapter particularises the methodology adopted for the research. It follows a traditional way in defining a model of dynamics of a system. Starting from a

literature survey, the author decided to put the focus on one particular problem (i.e. longitudinal dynamic stability of WIGE craft in waves) and strive to obtain the solutions for it. It is followed by formulation of the programme including the development of the model and its verification. With regard to the verification, it turned out that the research should be furnished with a set of aerodynamic data. Therefore, the CFD simulation was inserted in the programme.

4 MODEL OF DYNAMICS IN WAVY CONDITIONS

This chapter discusses the development of a mathematical model of the longitudinal dynamics of WIGE craft. This chapter comprises five sections, which are *(1) Introduction*; *(2) Generic mathematical model for the non-forced AAMV*; *(3) Mathematical model of the longitudinal dynamics of an AAMV when the impact of the waves is considered*; *(4) Quasi-static approach for WIGE craft*; and *(5) Conclusion.*

4.1 Introduction

A stability analysis of a vehicle starts from determining an equilibrium state of the vehicle and how it reacts to a disturbance. Collu (2008, chap.6) demonstrated an approach to estimate the equilibrium attitude of an AAMV. The approach considers the geometric, inertia, aerodynamic and hydrodynamic parameters of the vehicle.

A rectilinear uniform level motion (RULM) condition is considered as the equilibrium state. It means that the vehicle is in a rectilinear trajectory, with constant attitude in height and speed. Also, the vehicle is over calm water, and no effect of waves is considered.

Once the equilibrium state is obtained, a system of equations of motions is needed to determine the static and dynamic stability of the vehicle. The system of equations of motion was also presented by Collu (2008, chap.7).

This thesis proposes the next level of stability analysis by acknowledging the waves' influence in the system of equations of motion.

4.2 Generic mathematical model for the non-forced AAMV

4.2.1 Equations of equilibrium

The stability analysis of a vehicle starts from an equilibrium state and how it reacts to a disturbance. Collu (2008, chap.6) exhibited a mathematical approach to estimate the equilibrium attitude of an AAMV. It should be noted that the forces and moments involved have an explicit dependency on the configuration. In this case, the external effects are disregarded.

The solution is developed from adopting the 'Savitsky long-form method' (Doctors, 1985, chap.4; Savitsky and Brown, 1976). When considering an AAMV configuration, the aerodynamic forces and moment are also considered. Since there are a higher number of unknown variables than the equations involved, it is necessary to adopt an iterative approach. The process is started by guessing the height and the trim angle. The logic of this approach is presented in Figure 2-15.

In the longitudinal plane, there are three conditions to reach the equilibrium state, and they are:

- The total of the vertical forces is equal to zero;
- The total of the horizontal forces is equal to zero; and
- The total of pitch moments is equal to zero.

The résumé of the equilibrium condition for an AAMV with two aerodynamic surfaces is available in Table 4.1.

Motion	Equation	
Surge	$-D_{a1} - D_{a2} - D_{ah} - N\sin(\tau) - D_F\cos(\tau) - D_{ws} + T\cos(\tau+\epsilon) = 0$	(4-1)
Heave	$L_{a1} + L_{a2} + N\cos(\tau) - D_F\sin(\tau) - W + T\sin(\tau+\epsilon) = 0$	(4-2)

Pitch $$L_{a1} * [\xi_{ac1} \cos(\tau) + \phi_{ac1} \sin(\tau)] + D_{a1} * [\xi_{ac1} \sin(\tau) - \phi_{ac1} \cos(\tau)] + M_{a1} + L_{a2} * [\xi_{ac2} \cos(\tau) + \phi_{ac2} \sin(\tau)] + D_{a2} * [\xi_{ac1} \sin(\tau) - \phi_{ac2} \cos(\tau)] + M_{a2} + D_{ah} * a_{ah} + D_{ws} * a_{ws} - N * c - D_F * a_F + T * [\xi_{TP} \cos(\epsilon) + \phi_{TP} \sin(\epsilon)] = 0$$ (4-3)

The components of the equations of equilibrium above are explained as follows:

- $D_{a1,2}$ are the aerodynamic drag experienced by aerodynamic surfaces ($a1$ for the first surface and $a2$ for the second surface);
- D_{ah} is the aerodynamic drag experienced by the dry section of the hull;
- D_F is the hydrodynamic frictional drag;
- D_{ws} is the whisker spray drag force (due to the hull);
- $L_{a1,2}$ is the aerodynamic lift experienced by aerodynamic surfaces ($a1$ for the first surface and $a2$ for the second surface);
- $M_{a1,2}$ are the aerodynamic pitching moments of aerodynamic surfaces ($a1$ for the first surface and $a2$ for the second surface);
- N is hydrodynamic potential force;
- T is the propulsion force (thrust);
- W is the gravitational force (weight);
- a_F is the pitch moment arm of D_F;
- a_{ah} is the pitch moment arm of D_{ah};
- a_{ws} is the pitch moment arm of D_{ws};
- c is pitch moment arm of N;
- $\xi_{ac1,2}$ are the aerodynamic centres' location in axial direction relative to the body-fixed axes system ($a1$ for the first surface and $a2$ for the second surface);
- ξ_{TP} is the thrust point in axial direction relative to the body-fixed axes system;

- $\phi_{ac1,2}$ are the aerodynamic centres' location in normal direction relative to the body-fixed axes system ($a1$ for the first surface and $a2$ for the second surface);
- ϕ_{TP} is the thrust point in normal direction relative to the body-fixed axes system.

The equations also involve some angles, which are:

- ϵ is the angle between the mac and the keel;
- τ is the trim angle.

Along with other forces, one can figure out that aerodynamic and hydrodynamic forces and moments compose the set of the questions above. In this work, there is an assumption that takes place about aerodynamic forces, that they are dependent on the trim angle, τ, and ride height, h.

Following the designation of equilibrium state, the next step of stability analysis may be carried out. It is conducted by formulating the system of equations of motion. When considering an AAMV configuration, its system of equations of motion is, at first approximation, a composition of the systems of WIGE craft and other HSMVs (planing boat, in this case).

4.2.2 System of equations of motion

4.2.2.1 WIGE craft

Etkin (2012, pp.162–163) provided a comprehensive system of equations of motion for a case of nonzero z-derivatives. The system applies to the case of WIGE craft. Also, there have been academic discussions on longitudinal motion of WIGE craft, for instance by Kumar (1967), Staufenbiel and Kleineidam (1980), Hall (1994), Gera (1995), Delhaye (1997), Chun and Chang (2002), and Boschetti and Cárdenas (2012).

The system of equations of longitudinal motion is:

$$[A]\underline{\ddot{\eta}} + [B]\underline{\dot{\eta}} + [C]\underline{\eta} + [D]h = \mathbf{0} \tag{4-4}$$

where,

$$\underline{\eta} = \begin{bmatrix} x \\ z \\ \theta \end{bmatrix}; \qquad \underline{\dot{\eta}} = \begin{bmatrix} u \\ w \\ q \end{bmatrix}; \qquad \underline{\dot{\eta}} = \begin{bmatrix} \dot{u} \\ \dot{w} \\ \dot{q} \end{bmatrix} \tag{4-5}$$

and h is the ride height above the water surface.

The matrix $[A]$ represents the mass matrix and is elaborated as:

$$[A] = \begin{bmatrix} m & -X_{\dot{w}}^{a} & 0 \\ 0 & m - Z_{\dot{w}}^{a} & 0 \\ 0 & -M_{\dot{w}}^{a} & I_y \end{bmatrix} \tag{4-6}$$

The matrix $[B]$ denotes the damping matrix and is defined as:

$$[B] = \begin{bmatrix} -X_{u}^{a} & -X_{w}^{a} & -X_{q}^{a} \\ -Z_{u}^{a} & -Z_{w}^{a} & -\left(Z_{q}^{a} + mU_e\right) \\ -M_{u}^{a} & -M_{w}^{a} & -M_{q}^{a} \end{bmatrix} \tag{4-7}$$

The matrix $[C]$ is the restoring matrix and characterised as:

$$[C] = \begin{bmatrix} 0 & 0 & mg \\ 0 & 0 & 0 \\ 0 & 0 & 0 \end{bmatrix} \tag{4-8}$$

Eventually, the matrix $[D]$ indicates the aerodynamic matrix of WIGE craft following influence of the ride height above the surface. It is described as:

$$[D] = \begin{bmatrix} -X_{h}^{a} \\ -Z_{h}^{a} \\ -M_{h}^{a} \end{bmatrix} \tag{4-9}$$

In finding the solution of the system of equations (4-4), a transformation into the state-space form may be used by firstly defining the state-space vector, $\underline{\nu}$.

$$\underline{\nu} = [u \quad w \quad q \quad \theta \quad H]^T \tag{4-10}$$

The state-space vector above has five components while the system of equations of motion (4-4) comprises three equations. Hence, two additional equations are provided, and those are:

$$\begin{cases} \dfrac{\partial(\theta)}{\partial t} = q \\ \dfrac{\partial(h)}{\partial t} = -w + U_e\theta \end{cases} \tag{4-11}$$

The first part of (4-11) is the time derivative of pitch rotation angle which known as pitch rate and denoted by q. The second part of the equation is the time derivative of ride height. It is a superposition of the heave velocity and the normal component of the free stream velocity as experienced by the system.

Following the definition above, one may obtain the state-space system as:

$$[A_s]\dot{\underline{\nu}} = [B_s]\underline{\nu} \tag{4-12}$$

Further, the system of equations (4-12) can be manipulated as:

$$\dot{\underline{\nu}} = [A_s]^{-1}[B_s]\underline{\nu} \tag{4-13}$$

or,

$$\dot{\underline{\nu}} = [H_s]\underline{\nu} \tag{4-14}$$

Fourier transformation can be conveniently used to determine the modes of oscillation. Hence the equation (4-14) becomes:

$$\begin{gathered} s \cdot \underline{\nu} = [H_s]\underline{\nu} \\ (s[I]_{5\times5} - [H_s])\underline{\nu} = [0]_{5\times1} \end{gathered} \tag{4-15}$$

Excluding the trivial solution of $\underline{\nu} = [0]_{5\times1}$, the equation (4-15) gives polynomial characteristic as follows:

$$\mathbb{A} * s^5 + \mathbb{B} * s^4 + \mathbb{C} * s^3 + \mathbb{D} * s^2 + \mathbb{E} * s + \mathbb{F} = 0 \tag{4-16}$$

The roots of modes of oscillation are the solutions of the equation (4-16).

$$\begin{cases} s_{1,2} = a_1 \pm i \cdot b_1 \\ s_{3,4} = a_2 \pm i \cdot b_2 \\ s_5 = a_3 \end{cases} \tag{4-17}$$

Traditionally, one can deduce that the solutions, as seen in the set of equations (4-17), are grouped in three modes of oscillation, i.e. phugoid, short period and speed subsidence. The last mode is exclusive to WIGE craft.

4.2.2.2 Planing vessels

For planing boats, Martin (1976) presented a mathematical model depicting the system of equations of motion. One can right away identify its similarity with the system of equations of motion of WIGE craft. The dissimilarity is the system does not have a matrix ground effect as the WIGE craft.

$$[A]\underline{\ddot{\eta}} + [B]\underline{\dot{\eta}} + [C]\underline{\eta} = \mathbf{0} \tag{4-18}$$

Looking further, the components of displacement vector $\underline{\eta}$, velocity vector $\underline{\dot{\eta}}$, and acceleration vector $\underline{\ddot{\eta}}$ are similar to the ones adopted for WIGE craft. As for the components of the matrix $[A]$, $[B]$, and $[C]$, they are defined as follows:

$$[A] = \begin{bmatrix} m - X_{\dot{u}}^h & -X_{\dot{w}}^h & -X_{\dot{q}}^h \\ -Z_{\dot{u}}^h & m - Z_{\dot{w}}^h & -Z_{\dot{q}}^h \\ -M_{\dot{u}}^h & -M_{\dot{w}}^h & I_y - M_{\dot{q}}^h \end{bmatrix} \tag{4-19}$$

$$[B] = \begin{bmatrix} -X_u^h & -X_w^h & -X_q^h \\ -Z_u^h & -Z_w^h & -Z_q^h \\ -M_u^h & -M_w^h & -M_q^h \end{bmatrix} \tag{4-20}$$

$$[C] = \begin{bmatrix} 0 & -X_z^h & mg - X_\theta^h \\ 0 & -Z_z^h & -Z_\theta^h \\ 0 & -M_z^h & -M_\theta^h \end{bmatrix} \tag{4-21}$$

Similar to the procedure in solving the system of equations in WIGE craft, one can easily adopt the state-space form. In finding the solution of the system of equations (4-18), a transformation into the state-space form may be used by firstly defining the state-space vector, $\underline{\nu}$. Here the state-space vector is defined as:

$$\underline{\nu} = [u \quad w \quad q \quad z \quad \theta]^T \tag{4-22}$$

The state-space vector above has five components, while the system of equations of motion (4-18) comprises three equations. Hence two additional equations are provided, and those are:

$$\begin{cases} \dfrac{\partial(z)}{\partial t} = w \\ \dfrac{\partial(\theta)}{\partial t} = q \end{cases} \tag{4-23}$$

The first part of (4-23) is the time derivative of heave displacement or the normal velocity. The second part of the equation above is the time derivative of pitch rotation angle of the system.

The definition of the five components of state-space subsequently shows a similar scheme, as shown in the equations (4-12), (4-13) and (4-14).

In determining the solution of the system of equations of motion of a planing boat, Martin (1976) exhibited decoupling of the systems that can be treated separately, i.e. the surge motion and the heave-pitch motions. This approach has been adopted by Troesch (1992), Troesch and Falzarano (1993), and Faltinsen (2005, pp.370–372). With this assumption, one may approach the problem in equations (4-18) with reduced form of displacement vector $\underline{\eta}$, velocity vector $\underline{\dot{\eta}}$, and acceleration vector $\underline{\ddot{\eta}}$, elaborated as follows:

$$\underline{\eta} = \begin{bmatrix} z \\ \theta \end{bmatrix}; \qquad \underline{\dot{\eta}} = \begin{bmatrix} w \\ q \end{bmatrix}; \qquad \underline{\dot{\eta}} = \begin{bmatrix} \dot{w} \\ \dot{q} \end{bmatrix} \tag{4-24}$$

Thus, the matrix $[A]$, $[B]$, and $[C]$ become:

$$[A] = \begin{bmatrix} m - Z_{\dot{w}}^{h} & Z_{\dot{q}}^{h} \\ -M_{\dot{w}}^{h} & I_y - M_{\dot{q}}^{h} \end{bmatrix} \tag{4-25}$$

$$[B] = \begin{bmatrix} -Z_{w}^{h} & -Z_{q}^{h} \\ -M_{w}^{h} & -M_{q}^{h} \end{bmatrix} \tag{4-26}$$

$$[C] = \begin{bmatrix} -Z_{z}^{h} & -Z_{\theta}^{h} \\ -M_{z}^{h} & -M_{\theta}^{h} \end{bmatrix} \tag{4-27}$$

From this point, it follows the procedure equation (4-15) and gives:

$$\begin{gathered} s \cdot \underline{\nu} = [H_s]\underline{\nu} \\ (s[I]_{4\times4} - [H_s])\underline{\nu} = [0]_{4\times1} \end{gathered} \tag{4-28}$$

where,

$$\underline{\nu} = [\, w \quad q \quad z \quad \theta]^T \tag{4-29}$$

Excluding the trivial solution of $\underline{\nu} = [0]_{4\times1}$, the equation (4-28) gives a polynomial characteristic, as follows:

$$\mathbb{A} * s^4 + \mathbb{B} * s^3 + \mathbb{C} * s^2 + \mathbb{D} * s + \mathbb{E} = 0 \tag{4-30}$$

The roots of modes of oscillation are the solutions of the equation (4-30):

$$\begin{cases} s_{1,2} = a_1 \pm i \cdot b_1 \\ s_{3,4} = a_2 \pm i \cdot b_2 \end{cases} \tag{4-31}$$

In the stability analysis of a planing boat, just like other dynamic systems, the focus is on whether the solutions decay (stable) or increase with time (unstable). The criteria of stability are fulfilled when all root characteristics are negative. If a positive root occurs, instability may occur.

4.2.2.3 AAMV

The system of equations of motion of AAMV can now be developed. The novelty of the new hybrid system is the partaking of aerodynamic and hydrodynamic elements. It is apparent to observe that the system would have expanded components and give more complex solutions.

In general, the system of equations of motion for an AAMV is somewhat similar to the one of a WIGE craft system, as shown in equation (4-4). The differences lay on the details of components in the matrix $[A]$ and $[B]$, as the matrix $[C]$ has conveniently the same components of the planing vessel system and the matrix $[D]$, the ground effect matrix has no difference being the WIGE craft system.

The matrix $[A]$ still expresses the mass matrix but now with the addition of aerodynamic and hydrodynamic added mass. The added mass can physically be interpreted as a particular volume of fluid particles that are accelerated with a moving system. In principle, every fluid particle will accelerate to some extent as the body moves, and the added mass is the integration of the entire particles' mass (Newman, 1977, p.141). A little bit insight about the added mass or virtual mass, in practice it is most common for marine vehicle. In an earlier case when the concept was introduced, a treatment was done to a pendulum in the fluid and the vacuum. It turned out the period of motion in the fluid was even longer than expected (note that here the buoyancy effect which also delayed the period of motion in the fluid was already accounted in the first place). This as if that the pendulum received an 'additional' inertia. In this event the virtual increase of the inertia has a linear proportion to the mass of the displaced fluid (Stokes, 1851). This idea then has been adopted and acknowledged as added mass.

The matrix $[A]$, here can be described as:

$$[A] = \begin{bmatrix} m - X_{\dot{u}}^{h} & -X_{\dot{w}}^{a} - X_{\dot{w}}^{h} & -X_{\dot{q}}^{h} \\ -Z_{\dot{u}}^{h} & m - Z_{\dot{w}}^{a} - Z_{\dot{w}}^{h} & -Z_{\dot{q}}^{h} \\ -M_{\dot{u}}^{h} & -M_{\dot{w}}^{a} - M_{\dot{w}}^{h} & I_y - M_{\dot{q}}^{h} \end{bmatrix} \quad (4\text{-}32)$$

The matrix $[B]$ is defined as:

$$[B] = \begin{bmatrix} -X_u^a - X_u^h & -X_w^a - X_w^h & -X_q^a - X_q^h \\ -Z_u^a - Z_u^h & -Z_w^a - Z_w^h & -Z_q^a - Z_q^h \\ -M_u^a - M_u^h & -M_w^a - M_w^h & -M_q^a - M_q^h \end{bmatrix} \quad (4\text{-}33)$$

The matrix $[C]$ and $[D]$ are:

$$[C] = \begin{bmatrix} 0 & -X_z^h & mg - X_\theta^h \\ 0 & -Z_z^h & -Z_\theta^h \\ 0 & -M_z^h & -M_\theta^h \end{bmatrix} \quad (4\text{-}34)$$

$$[D] = \begin{bmatrix} -X_h^a \\ -Z_h^a \\ -M_h^a \end{bmatrix} \quad (4\text{-}35)$$

The matrices $[A]$, $[B]$, $[C]$, and $[D]$ may be converted into:

$$[A] = \begin{bmatrix} m + A_{11} & A_{13} & A_{15} \\ A_{31} & m + A_{33} & A_{35} \\ A_{51} & A_{53} & I_y + A_{55} \end{bmatrix} \quad (4\text{-}36)$$

$$[B] = \begin{bmatrix} B_{11} & B_{13} & B_{15} \\ B_{31} & B_{33} & B_{35} \\ B_{51} & B_{53} & B_{55} \end{bmatrix} \quad (4\text{-}37)$$

$$[C] = \begin{bmatrix} 0 & C_{13} & mg + C_{15} \\ 0 & C_{33} & C_{35} \\ 0 & C_{53} & C_{55} \end{bmatrix} \quad (4\text{-}38)$$

$$[D] = \begin{bmatrix} D_{10} \\ D_{30} \\ D_{50} \end{bmatrix} \tag{4-39}$$

Implementing the same procedure to transform the system into a state-space form, thus:

$$\underline{\nu} = [x \quad w \quad q \quad z \quad \theta \quad H]^T \tag{4-40}$$

As there are six components of state-space vector while, on the other hand, only three equations are provided by the system of equations of motion, three new equations are needed. Those equations are given by:

$$\begin{cases} \dfrac{\partial(z)}{dt} = w \\ \dfrac{\partial(\theta)}{dt} = q \\ \dfrac{\partial(h)}{\partial t} = -w + U_e\theta \end{cases} \tag{4-41}$$

Disregarding the trivial solution of $\underline{\nu} = [0]_{5\times1}$, the equation (4-40) gives polynomial characteristic as follows:

$$\mathbb{A} * s^6 + \mathbb{B} * s^5 + \mathbb{C} * s^4 + \mathbb{D} * s^3 + \mathbb{E} * s^2 + \mathbb{F} * s + \mathbb{G} = 0 \tag{4-42}$$

The static stability of the system is given by:

$$\frac{\mathbb{G}}{\mathbb{A}} > 0 \tag{4-43}$$

Assuming $\mathbb{A} = 1$, the static stability is assured when:

$$\mathbb{G} = \frac{N_0}{\Delta} > 0 \tag{4-44}$$

where,

$$N_0 = U_e[D_{10}(B_{31}C_{53} - B_{51}C_{33}) - B_{11}(C_{33}D_{50} - C_{53}D_{30})] \tag{4-45}$$

and,

$$\begin{aligned}\Delta = \left(I_y + A_{55}\right)[m^2 + m(A_{11} + A_{33}) + A_{11}A_{33} - A_{31}A_{13}] \\ + (m + A_{11})A_{53}A_{35} - (m + A_{33})A_{51}A_{15} + A_{53}A_{31}A_{15} \\ + A_{51}A_{13}A_{35}\end{aligned} \tag{4-46}$$

From equation (4-42), six roots are expected, linked to the relative modes of oscillation. However, as mentioned by Collu (2008, chap.8), a reduced order system may be considered to ease the complexity. Similar to the reduced system considered for planing vessels, the surge degree of freedom (x) may be separated from the heave (z) and pitch (θ) degrees of freedom. Of course, the assumption needs validation against experimental data that, unfortunately, is not available yet.

By decoupling the surge motion from heave and pitch, the state-space vector becomes:

$$\underline{\nu} = [\, w \quad q \quad z \quad \theta \quad H]^T \tag{4-47}$$

thus, the characteristic polynomial becomes:

$$\mathbb{A} * s^5 + \mathbb{B} * s^4 + \mathbb{C} * s^3 + \mathbb{D} * s^2 + \mathbb{E} * s + \mathbb{F} = 0 \tag{4-48}$$

The equation (4-48) above leads to static stability criterion, as in Collu (2008a) given by:

$$\frac{N_0}{\Delta} > 0 \tag{4-49}$$

$$\frac{U_e(C_{33}D_{50} - C_{53}D_{30})}{(I_y + A_{55})(m + A_{33}) - A_{53}A_{35}} > 0$$

If the denominator is larger than zero, the stability criterion becomes:

$$\frac{D_{50}}{D_{30}} - \frac{C_{53}}{C_{33}} > 0 \qquad (4\text{-}50)$$

or in notations of stability derivatives being used in this document:

$$\frac{M_h^a}{Z_h^a} - \frac{M_z^h}{Z_z^h} > 0 \qquad (4\text{-}51)$$

The expression of the equation (4-51) is similar to the static stability criteria, as presented by Irodov (1974). However, they are slightly different with regards to the physical meaning of both criteria. In WIGE craft, the criterion expresses that static stability can be reached if the aerodynamic centre in height is located upstream of the aerodynamic centre in pitch. Rozhdestvensky (2006) also derived this interpretation. For an AAMV configuration, the additional criterion is that the hydrodynamic centre should be located downstream of the aerodynamic centre in height to attain static stability.

With regards to the AAMV dynamic stability, the characteristic roots' equation of the systems should be analysed. Just like other systems, an AAMV is defined as dynamically stable if it is statically stable and all the roots have a real negative component. However, determining the roots is still a complicated task even for a case of the reduced order system.

4.3 Mathematical model of the longitudinal dynamics of an AAMV when the impact of the waves is considered

4.3.1 Overview waves modelling

In many cases of HSMV operation, the occurrence of waves is unavoidable, and this also valid for the AAMV. The behaviour of the wave is mostly always irregular. However, the irregularities of waves can be seen as a superposition of many regular harmonic waves, each with its characteristics.

A general equation expressing the elevation of the waves can be written as:

$$\zeta(x,t) = \sum_{j=1}^{J} \zeta_{Aj} \cos\left(\omega_j t - \hbar_j x + \varepsilon_j\right) \tag{4-52}$$

where,

- ζ is the elevation of the superposition of regular wave functions;
- ζ_{Aj} is the wave amplitude for the j[th] wave (m);
- ω_j is the wave frequency for the j[th] wave (rad/s);
- $\hbar_j$ is the wave number for the j[th] wave, equal to $2\pi/\lambda_j$ (rad/m);
- λ_j is the wavelength for the j[th] wave (m);
- t is time (s);
- x is the position in the direction of the wave propagation (m);
- ε_j is random wave phase for the j[th] wave (rad).

In a case of regular waves, the equation (4.52) becomes:

$$\zeta = \zeta_A \cos(\omega t - \hbar x) \tag{4-53}$$

where,

- ζ_A is the wave amplitude (m);
- ω is the wave frequency (rad/s);
- $\hbar$ the is wave number (rad/m);
- t is time (s);

- x is the position in the direction of the wave propagation (m).

In regular waves, the motions of a system can be divided into three perpendicular translations of the centre of gravity, i.e. surge, sway and heave, and three rotations around the centre of gravity, i.e. roll, pitch and yaw.

In the longitudinal plane, one can reduce the system into three motions only, as follows:

$$\begin{cases} x = x_A \cos(\omega_e t + \varepsilon_{x\zeta}) \\ z = z_A \cos(\omega_e t + \varepsilon_{z\zeta}) \\ \theta = \theta_A \cos(\omega_e t + \varepsilon_{\theta\zeta}) \end{cases} \quad (4\text{-}54)$$

Each of the ε value represents a different phase angle. The phase shifts are related to the harmonic wave elevation at the origin of body axis system. The wave elevation at the centre of gravity is defined as:

$$\zeta = \zeta_A \cos(\omega_e t) \quad (4\text{-}55)$$

Following the definition of the motions above, the harmonic velocities and accelerations are obtained:

$$\begin{cases} u = -\omega_e x_A \sin(\omega_e t + \varepsilon_{u\zeta}) \\ w = -\omega_e z_A \sin(\omega_e t + \varepsilon_{w\zeta}) \\ q = -\omega_e \theta_A \sin(\omega_e t + \varepsilon_{q\zeta}) \end{cases} \quad (4\text{-}56)$$

$$\begin{cases} \dot{u} = -{\omega_e}^2 x_A \cos(\omega_e t + \varepsilon_{\dot{u}\zeta}) \\ \dot{w} = -{\omega_e}^2 z_A \cos(\omega_e t + \varepsilon_{\dot{w}\zeta}) \\ \dot{q} = -{\omega_e}^2 \theta_A \cos(\omega_e t + \varepsilon_{\dot{q}\zeta}) \end{cases} \quad (4\text{-}57)$$

The ω_e describes the frequency of encounter not the actual frequency of the waves. Frequency of encounter is the frequency that is felt by the vehicle due to the difference between the direction of wave propagation and the course of the

vehicle. Further explanation of frequency of encounter and its calculation are available in Appendix D and Appendix E.

In hydrodynamics, besides the motions' characteristics, i.e. displacements, velocities and accelerations mentioned above, one can also identify the load acting on the vessels due to the unsteady pressure field generated by undisturbed waves, known as Froude-Krylov forces. In one degree of freedom, one can draw Froude-Krylov force as the expression of a spring coefficient, c, of the system multiplied by effective wave elevation ζ^* (Journee and Pinkster, 2002, p.42). It is expressed as:

$$F_{FK} = c\zeta^* \tag{4-58}$$

where,

$$\begin{aligned} c &= \rho g S \\ \zeta^* &= e^{-\hbar d_s} \cdot \zeta_A \cos(\omega_e t) \end{aligned} \tag{4-59}$$

while noting that,

- ρ is water density;
- g is gravitational acceleration;
- S is wetted surface area;
- $\hbar$ is wave number; and
- d_s is the submerged depth in water.

When the characteristic dimension of the system is large with respect to the wavelength, the Froude-Krylov forces require a correction to complete the total wave force. The correction is due to the diffraction of the waves by the presence of the vehicle in the water. This correction is applicable only for the systems with large characteristic length compared to the wavelength. Otherwise, the diffraction is negligible thus only Froude-Krylov forces are considered.

The total wave forces when Froude-Krylov forces and diffraction are considered can be expressed as:

$$F_\zeta = [A^\dagger]\ddot{\zeta}^* + [B]\dot{\zeta}^* + [C]\zeta^* \tag{4-60}$$

where,

$$\begin{aligned} \zeta^* &= e^{-\hbar d_s} \cdot \zeta_A \cos(\omega_e t) \\ \dot{\zeta}^* &= -e^{-\hbar d_s} \cdot \zeta_A \omega_e \sin(\omega_e t) \\ \ddot{\zeta}^* &= -e^{-\hbar d_s} \cdot \zeta_A {\omega_e}^2 \cos(\omega_e t) \end{aligned} \tag{4-61}$$

To be aware of the matrix $[A^\dagger]$ in the equation (4-60), it is not the same with the matrix $[A]$ of the system of equations of motion. In that particular situation, there is no component of mass of the system involved. The matrix $[A^\dagger]$ expresses the virtual mass caused by deflection of some volume of fluid due to the motion of the system. Respectively, the matrix $[B]$ states the damping matrix and the matrix $[C]$ declares the spring or restoring matrix.

4.3.2 System equation of motion of the AAMV with waves

The core of this research is presented in this subsection. In order to reach the goal of the study, the author proposed a system of equations of motion with the influence of waves. The system of equations is derived from preceding studies that have been reviewed earlier.

In general, the system of equations of motion of the AAMV with waves' influence is similar to any other system with externally-induced forces. In a very simple approach, it is none but the application of Newton's second law that:

$$m_j \frac{\partial u_j}{\partial t} = sum\ of\ all\ forces\ on\ the\ system\ j \tag{4-62}$$

Respectively, one may define a new system of equations of motion for the AAMV with regards to the occurrence of the waves as follows:

$$[A]\underline{\ddot{\eta}} + [B]\underline{\dot{\eta}} + [C]\underline{\eta} + [D]h = [F_w] \tag{4-63}$$

where,

$$F_w = F_w^a + F_w^h \tag{4-64}$$

and F_w^a is the induced aerodynamic forces due to the waves' motion and F_w^h is the additional hydrodynamic forces due to the waves. The wave load acting on the hydrodynamic surface of an AAMV configuration is simply the representation of the equation (4-60),

$$F_w^h = \left[A^{\dagger^h}\right]\ddot{\zeta}^* + [B^h]\dot{\zeta}^* + [C^h]\zeta^* \tag{4-65}$$

or by neglecting the diffraction, the equation above becomes:

$$F_w^h = [C^h]\zeta^* \tag{4-66}$$

By using similar approaches, one can get the load due to waves working on an aerodynamic surface as:

$$F_w^a = \left[A^{\dagger^a}\right]\ddot{\zeta}^{\oplus} + [B^a]\dot{\zeta}^{\oplus} + [C^a]\zeta^{\oplus} \tag{4-67}$$

By default, the matrix $\left[A^{\dagger^a}\right]$ is zero because there is no aerodynamic added mass or is very small, thus $\left[A^{\dagger^a}\right]\ddot{\zeta}^{\oplus}$ is zero. The component of $[B^a]\dot{\zeta}^{\oplus}$ in the equation is also negligible as other components outweigh the contribution of aerodynamic damping due to the waves. The important part is the latter part, $[C^a]\zeta^{\oplus}$, that gives the spring-like forces. Thus:

$$F_w^a = [C^a]\zeta^{\oplus} \tag{4-68}$$

with $\zeta^{\oplus}$ being the effective wave elevation as felt by the aerodynamic surfaces of the AAMV.

One can appropriately assume that the equation (4-64) can still be seen as a harmonic function. Thoughtfully, it may be written as:

$$F_w = F_w^a + F_w^h$$

$$F_w = [C^a]\zeta^{\oplus} + [C^h]\zeta^* \tag{4-69}$$

$$F_w = F_{w_A}\cos\left(\omega_e t + \varepsilon_{F_w\zeta}\right)$$

Thus,

$$[A]\underline{\ddot{\eta}} + [B]\underline{\dot{\eta}} + [C]\underline{\eta} + [D]h = F_{w_A}\cos\left(\omega_e t + \varepsilon_{F_w\zeta}\right) \tag{4-70}$$

4.3.3 Solution of system of equations of motion: General approach

Obtaining the solution of the system of equations of motion for this circumstance involves high complexity. Modal analysis can be used to fulfil this objective. Combining two identity equations:

$$\begin{gathered}[A]\underline{\dot{\eta}} - [A]\underline{\dot{\eta}} = \mathbf{0} \\ [I]\underline{\dot{\eta}} - [I]\underline{\dot{\eta}} = \mathbf{0}\end{gathered} \tag{4-71}$$

with the system of equations (4-63), one can obtain the relationship as follows:

$$\begin{bmatrix}[A] & [B] & \mathbf{0}\\ \mathbf{0} & [A] & \mathbf{0}\\ \mathbf{0} & [I] & \mathbf{0}\end{bmatrix}\begin{bmatrix}\ddot{\eta}\\ \dot{\eta}\\ \dot{h}\end{bmatrix} + \begin{bmatrix}\mathbf{0} & [C] & [D]\\ -[A] & \mathbf{0} & \mathbf{0}\\ -[I] & \mathbf{0} & \mathbf{0}\end{bmatrix}\begin{bmatrix}\dot{\eta}\\ \eta\\ h\end{bmatrix} = \begin{bmatrix}[F_w]\\ \mathbf{0}\\ \mathbf{0}\end{bmatrix} \tag{4-72}$$

It is convenient to represent the system of equations (4-72) in the following manner:

$$[\mathbb{a}]\left[\dot{\vartheta}\right] + [\mathbb{b}][\vartheta] = [\mathbb{z}] \tag{4-73}$$

To solve the system of equations (4-73), the first step is to find their homogeneous solutions by letting the matrix $[\mathbb{z}] = \mathbf{0}$.

$$[\mathbb{a}]\left[\dot{\vartheta}\right] + [\mathbb{b}][\vartheta] = \mathbf{0} \tag{4-74}$$

By seeking a solution of the form $[\vartheta] = [\vartheta^*]e^{st}$ and $\left[\dot{\vartheta}\right] = s[\vartheta^*]e^{st}$, thus the system of equations (4-74) becomes:

$$s[\mathbb{a}][\vartheta^*] + [\mathbb{b}][\vartheta^*] = \mathbf{0} \tag{4-75}$$

or,

$$\left[s[\mathbb{a}] + [\mathbb{b}]\right][\vartheta^*] = \mathbf{0} \tag{4-76}$$

The set of equations (4-76) has the solution if the determinant of the coefficient is zero.

$$\det\left[s[\mathbb{a}] + [\mathbb{b}]\right] = 0 \tag{4-77}$$

The approach above leads to a set of 2N characteristic roots, which occur in conjugate pairs. Corresponding to each root, an eigenvector with 2N components exists satisfying the following condition:

$$\left[[\mathbb{b}] + s_n[\mathbb{a}]\right]\underline{\nu}^n = \mathbf{0} \tag{4-78}$$

Once the homogeneous solutions are obtained, the next step is to acquire the forced solutions. Let:

$$[\mathbb{z}(t)] = [\mathbb{z}^*]e^{j\omega t} \tag{4-79}$$

and

$$\begin{aligned} [\vartheta(t)] &= [\vartheta^*]e^{j\omega t} \\ \left[\dot{\vartheta}(t)\right] &= j\omega[\vartheta^*]e^{j\omega t} \end{aligned} \tag{4-80}$$

therefore, the system of equations (4-73) becomes:

$$j\omega e^{j\omega t}[\mathbb{a}][\vartheta^*] + e^{j\omega t}[\mathbb{b}][\vartheta^*] = e^{j\omega t}[\mathbb{z}^*]$$
$$j\omega[\mathbb{a}][\vartheta^*] + [\mathbb{b}][\vartheta^*] = [\mathbb{z}^*] \tag{4-81}$$

Since the eigenvector has been defined over 2N space, the solution of the system above may be written as:

$$[\vartheta^*] = \sum_{n=1}^{2N} \gamma_n \underline{\nu}^n \tag{4-82}$$

where,

$$\gamma_n = \frac{\underline{\nu}^{n^T}[\mathbb{z}^*]}{j\omega\mathbb{a}_n + \mathbb{b}_n} \tag{4-83}$$

Thus:

$$[\vartheta^*] = \sum_{n=1}^{2N} \frac{\underline{\nu}^{n^T}[\mathbb{z}^*]\underline{\nu}^n}{j\omega\mathbb{a}_n + \mathbb{b}_n} \tag{4-84}$$

One of the essentials of eigenvectors is about its orthogonality and reversal law, which agrees with the following conditions:

$$\underline{\nu}^{m^T}[\mathbb{b}]\underline{\nu}^n + s_n\underline{\nu}^{m^T}[\mathbb{a}]\underline{\nu}^n = \mathbf{0} \tag{4-85}$$

$$\underline{\nu}^{n^T}[\mathbb{b}]\underline{\nu}^m + s_n\underline{\nu}^{n^T}[\mathbb{a}]\underline{\nu}^m = \mathbf{0} \tag{4-86}$$

Applying those conditions (4-82) and (4-83) into the equation (4-81), one can obtain:

$$[\vartheta^*] = \sum_{n=1}^{2N} \frac{\underline{\nu}^{n^T}[\mathbb{Z}^*]\underline{\nu}^n}{\mathbb{a}_n(j\omega - s_n)} \tag{4-87}$$

4.3.4 Solution of system of equations of motion: Practical approach

At the current stage, it is challenging to solve the system of equations of motion of an AAMV analytically. The solution is expected to be extremely nonlinear, even for regular waves. To handle the difficulties in solving the system of equations of motion analytically, some approaches can be used to find the solution that generally can be categorised as approximations methods. One of the methods is to use the empirical dynamic analysis approach derived from statistical analysis. Before culminating in the empiric equations, many data sets are required. At this point, due to the requirement above, the option is inapplicable. Another approach is the 'quasi-static' dynamic analysis. The 'quasi-static' term here means that the assumption of the whole system is in equilibrium at any given point that is considered. For this situation, no dynamics effects are taken into account. Consequently, it is necessary to discretise the motion into several points of observation, which each describes a given instant in time. At each point, one can assume the problem is static, and the solution is derived following the homogeneous solution. This approach works well when the inertial effects are very low, thus may be ignored. For the case of an AAMV configuration, it is applicable only when the waves have relatively low frequency and large wavelength.

The quasi-static approach was taken for this research. The decision resulted from several considerations as follows:

- The size of the vehicle. At the current stage, only limited information is available for vehicles adopting the concept of the AAMV. However, an interpretation may be made based on the typical WIGE craft that is available. Most of the configurations have a small up to moderate size and weight (Jane et al., 2009). Typically, the configurations have 300 to 8,000 kg weight; cruise speeds are between 45 and 135 knots; and exposed

surface about 10 to 200 m^3. For an AAMV configuration, it is the reasonable range of sizes and speed to adopt. There are, indeed, configurations that have large dimensions and displacement, but are only available in small numbers.

- The empirical data of typical waves occur in an open sea. Based on the wave forecasting diagram in *Guide to Wave Analysis and Forecasting*, 2nd ed. (WMO, 2008, p.44), the typical wave speeds are between 5 and 30 m/s and wave periods are between 2 and 17 seconds. However, the waves that are created locally can then travel a thousand miles and become swells. This pushes slightly higher periods which in the subsequent verification (Chapter 7) is limited between 5 and 25 seconds or frequency between 0.25 and 1.25 rad/s.
- The amplitude of the waves was assumed small. This is to assure that the static assumption at an instantaneous time is valid. Also, small amplitudes secure the waves from touching the aerodynamic surfaces.

Combining those conditions, the 'quasi-static' approach is now applicable.

In the form of a system of equations, the approach is applied by converting the wave-induced forces' $[F_w]$ components into the mass matrix $[A]$, damping matrix $[B]$, restoring matrix $[C]$ and ground effect matrix $[D]$ into the system of equations in the left-hand side and allowing a zeros-matrix in the right-hand side. This is rather different than keeping wave-induced forces $[F_w]$ in the right-hand side of the system of equations, as shown in equation (4-63). The new system of equations of motion with 'quasi-static' approach thus becomes:

$$[A(\lambda i)]\underline{\ddot{\eta}} + [B(\lambda i)]\underline{\dot{\eta}} + [C(\lambda i)]\underline{\eta} + [D(\lambda i)]h = \mathbf{0} \tag{4-88}$$

where λi is a function of ride height and angle of attack, or can be written as:

$$\lambda i = f(h/c, \alpha) \tag{4-89}$$

The rationale of the system of equations of motion is that at an instantaneous point, the acceleration of wave elevation is very small, thus negligible. At that

minute observation, the vehicle is considered to have internal forces only thus a homogeneous solution serves well to determine the dynamics of it.

Following the traditional method, as shown in the set of equations from (4-4) to (4-17), the solution of equation (4-88) becomes:

$$\begin{cases} s_{\lambda i_{1,2}} = a_{1_{\lambda i}} \pm i \cdot \mathscr{b}_{1_{\lambda i}} \\ s_{\lambda i_{3,4}} = a_{2_{\lambda i}} \pm i \cdot \mathscr{b}_{2_{\lambda i}} \\ s_{\lambda i_5} = a_{3_{\lambda i}} \end{cases} \tag{4-90}$$

One of the consequences of the 'quasi-static' approach is the need for a set of mass matrix $[A]$, damping matrix $[B]$, restoring matrix $[C]$ and ground effect matrix $[D]$ at different positions along the wavelength. The more sets of data used will give a better depiction of the behaviour of the system in waves.

One of the advantages of this approach is that the representation of the position of the vehicle relative toward the surface can be attained as the periodic changes in ride height over the flat surface. Again, this idea is only appropriate when the characteristic length is small compared to the wavelength. This conception, later, also benefited the CFD study in terms of grid generation and the boundary condition definition.

Another positive point of the approach is producing a general idea of dynamic behaviour in the preliminary design phase of the development of an AAMV configuration. The process can be set relatively in parallel with the initial aerodynamic/hydrodynamic analysis. The dynamic behaviour attained from this method may not be the high fidelity one but is fit enough to give an idea of design range of the developed vehicle.

Despite the advantages above, the representation of the vehicle oscillating over a flat surface still leaves a complexity. As one may expect, the attitude of the vehicle is now a function of ride height. However, the attitude as a function of, at least, the angle of attack should also be considered to capture the longitudinal dynamic behaviour, as suggested in (4-89). This is similar to many aerodynamic studies, as reviewed in Section 2.8, which examine the superposition of pitch and

heave. There is also another motion, i.e. surge motion, but the effect is small, thus can be simply overlooked.

As a new concept, it is wise to start the longitudinal dynamic analysis by separating both motions and evaluating each. This attitude is acceptable and has been taken by many researchers. It also benefits in distinguishing the effects of each motion toward longitudinal dynamic behaviour. When the characteristics of each motion are established, the superposition may be performed to examine the result of its stability analysis. At this point, it can be seen whether one motion is dominant against another or the superposition will lead to completely different characteristics.

The explanation above conveys that the practicality of the 'quasi-static' approach that is proposed may not be entirely 'practical'. The approach comprises several meticulous steps to be taken before having the complete idea of longitudinal dynamic behaviour in waves. The practicality of the approach is merely because the problem can be approximated by deriving a set of homogeneous solutions.

4.3.4.1 Applicability in WIGE craft and the impact

A set of appropriate data from experiments or operational tests becomes very useful for the appliance of the 'quasi-static' approach. However, during the research being carried out, relevant experimental data are not available in the public domain. One of the ways to handle the approach is through CFD and semi-empirical methods. The set of methods is a long way from reaching the solution, but by doing so, the solid understandings are obtainable.

Before applying the set of methods to the AAMV case, the author made a quick review of wave-induced forces on WIGE craft and planing vessels. The discussion about the effect of waves for HSMVs is more prominent than for WIGE craft. Most of the time, the stability analyses of WIGE craft only cover a small amount of discussion from a more qualitative point of view or, at best, the mathematical approach presented is just the general system of equations of motions.

At the stage of the writing up of this thesis, the author had hardly encountered a specific study in the field of stability, whether in analytical, empirical or numerical points of view. Up to the present time, noticeable discussions on the effect of waves have only reached the objectives to understand the aerodynamic behaviour of a profile flying over curved surfaces.

The lack of relevant studies on the dynamics of WIGE craft in waves is itself an obstacle towards understanding the behaviour of an AAMV in that state. It is because the AAMV in its operation also experiences what is called ground effect aerodynamics. The essence of investigating the effect of waves toward WIGE craft is to understand the waves affecting the longitudinal dynamics of the system employing ground effect. There are indeed some studies in the stability/control related area on WIGE craft in waves, for instance, how the control system keeps the vehicle in the constant position relative to the significant wave height, $H_{1/3}$. It is to assure the stability and controllability of the vehicle. However, in that study, the kernel is not about how the system behaves with such conditions, which may not be essential for AAMV. Hence, the investigation of the effect of waves toward longitudinal dynamics of WIGE craft, not only benefiting the enrichment of knowledge in the WIGE craft realm but also, more importantly, to understand better the dynamics of vehicles adopting the AAMV concept.

Neglecting the stability derivatives from the hydrodynamic viewpoint, one can right away see the applicability of the ‘quasi-static’ approach shown in equation (4-88) in the case of WIGE craft. From this point on, the discussion in this thesis is about the use of the system of equations of motion for WIGE craft.

4.4 Quasi-static approach for WIGE craft

The Subsection 4.3.4 has explained a ‘quasi-static’ approach in conducting dynamic stability analysis of a system flying in ground effect over wavy surfaces. The ‘quasi-static’ means that a solution is obtainable by using a homogenous solution for several instantaneous observation points. By doing so, the system

will have several sets of homogeneous solutions based on the relative position of it to the surface.

In the WIGE craft case, it is convenient to transform the perspective on how one may handle the approach. Following the explanation in Subsection 4.3.4, the problem of WIGE craft flying over wavy surfaces can be approximated as the oscillating WIGE craft over flat surfaces. Obviously, it can only be true only when the frequency of waves is low enough or, in other words, the wavelength is long enough compared to the referential length (mac). The reasoning of this approximation is that when the frequency of the waves is low, the rate of changes of the attitude of the vehicle can be identified also as a periodic motion with low frequency. At an instantaneous range of time, one may see the vehicle as a system at a certain height with a certain pitch angle. By normalising the series of instantaneous points, it is simply the oscillation of the vehicle over a flat surface. At this stage, the motion of the vehicle is the function of the height and angle of attack.

The oscillation of WIGE craft may be still too complex to be solved as it involves at least two motions, the pitch and heave motion (note that the surge motion is not significant, thus negligible here). In many aerodynamic related studies, especially in the automotive and bio-inspired robotics realms, the separation of the motions is widely conducted. The separation does not only mean to ease the analyses but, more importantly, gives a better understanding of each motion before going further with the superposition motion. In this research, the problem has been set to pay attention to the heave motion. This means that the oscillation of the vehicle is assumed to be the function of height while the angle of attack is stationary. Still, the heave motion has a great deal of influence toward other planes other than the Z-plane. The evolution of modelling of WIGE craft flying over a wavy surface to heaving WIGE craft over a flat surface is shown in Figure 4-1.

When a configuration is assessed under this approximation, the dynamic stability can be done by firstly obtaining stability derivatives. In this research, the acquirement of stability derivatives was through some endeavours including CFD

and a semi-empirical approach of designing aircraft. Unfortunately, due to time and resource constraints, it was not possible for the author to plan and execute an ad-hoc experimental campaign to collect the necessary data. Therefore, a CFD approach has been chosen to estimate the aerodynamic coefficients and, from these, the aerodynamic stability derivatives.

Once the stability derivatives are attained, one can use the derived data to do the dynamic analysis. Traditionally, the dynamic characteristics of a configuration are identified from its characteristic roots. The author developed a simple numerical code built on the MATLAB platform to calculate the characteristic roots based on the stability derivatives obtained from the endeavours mentioned above. The hypothesis was that the dynamic analysis for each observation point would give hysteresis of the characteristic roots, different from what the non-oscillating case produces. More details are available in Chapter 7.

4.5 Conclusion

This chapter describes the mathematical model to analyse the stability of the AAMV configuration operating over waves. Starting from reviewing the equilibrium state, the discussion goes further with the system of equations of motion of the planing boat, WIGE craft and the AAMV. The presence of waves is considered with the insertion of an external force matrix in the right-hand side of the system of equations. With some thorough assumptions, i.e. low frequency, long wavelength and small amplitude of the wave, the system of equations of motion with external forces due to the waves can be approximated into a new system of equations where the external forces are infused as if a part of the forces of the system. This approach gives a more practical solution but is still able to capture the effect of waves on the vehicle.

At this point, the concept of the dynamics of the AAMV in waves is not well established. Unfortunately, the same situation also happens for WIGE craft. The author deliberately decided to focus the objective on the WIGE craft to establish a better understanding of the dynamics of a lifting system flying in ground effect

over wavy surfaces. By doing so, it helps the realisation of the primary goal of the research, i.e. to understand the longitudinal dynamics' characteristics of the AAMV while operating in waves.

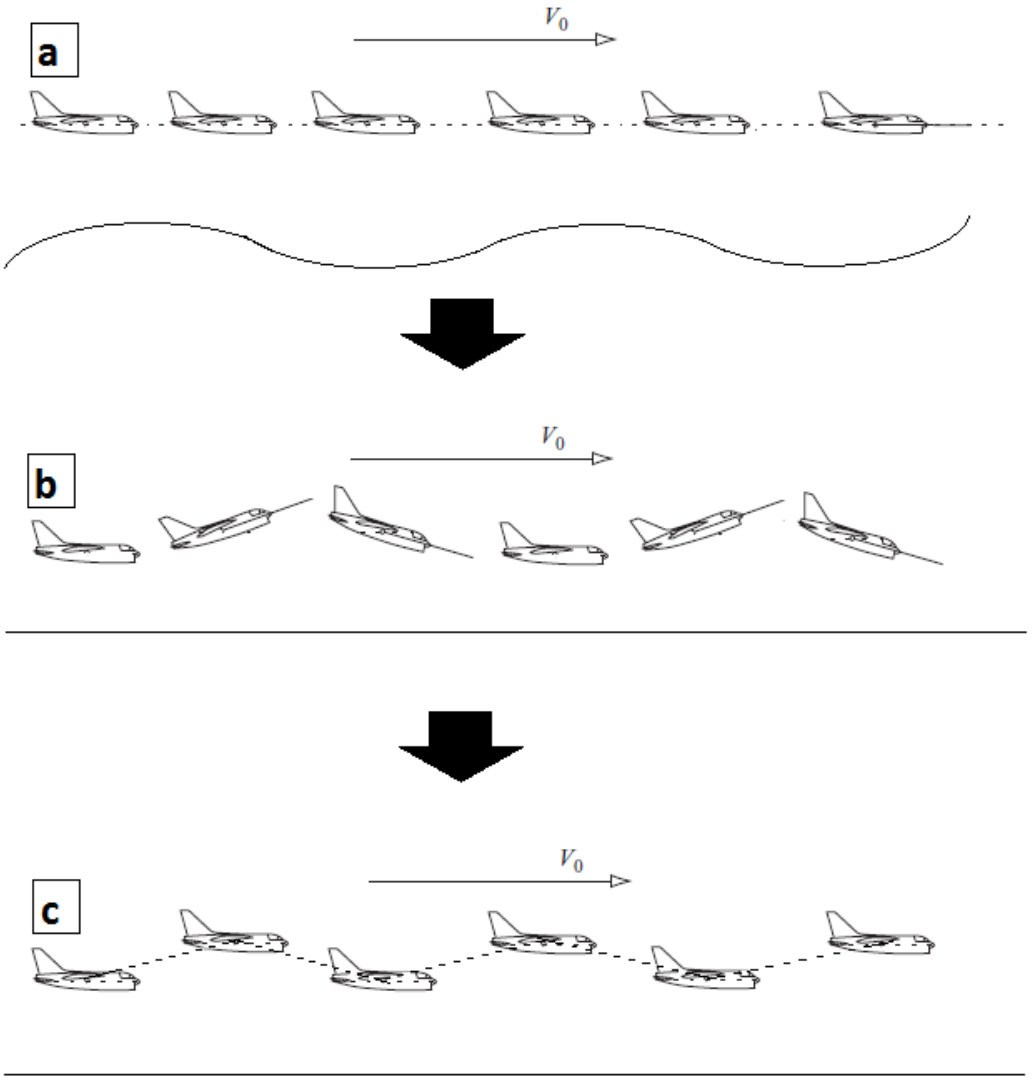

Figure 4-1 Evolution of how the waves being modelled (a. steady flight over curved surfaces; b. oscillatory flight over flat surfaces [pitch + heave]; c, oscillatory flight over flat surfaces [heave only])

5 AERODYNAMICS OF OSCILLATING PROFILE IN GROUND EFFECT

This chapter focuses on the computational fluid dynamics' numerical study of an aerodynamic profile oscillating in the ground effect. It comprises five sections, namely *(1) Introduction*; *(2) Numerical method*; *(3) Aerodynamics of the oscillating profile*; *(4) Main observations;* and *(5) Conclusion.*

5.1 Introduction

One of the main issues emerging during the programme was the scarcity of reliable aerodynamic data available to be used for the dynamic analysis of WIGE craft in waves. This required the author to derive the necessary aerodynamic data before completing the designated dynamic analysis.

Aerodynamic characteristics of a wing flying near the ground have been discussed for nearly a century. Although the research in this field is extensive, the details of the phenomenon have not been fully understood. One of the topics related to the ground effect realm is the aerodynamic ground effect of a lifting surface over wavy walls and oscillating lifting surface in ground effect (both over flat and wavy surfaces).

A number of investigations on the aerodynamics of the wavy ground effect have been carried out, among others by Ichikawa and Ando (1991), Nitta (1994), Im and Chang (2000), Moore (2005), Yang et al. (2010), and Liang et al. (2013a, 2013b). In almost three decades, the prevalence of study does not show improvement or lead to convergence toward practical application.

In term of application, more attention is given to the oscillating body in the ground effect. Combining the ground effect and the effect of wing oscillation is an interesting research topic. The combination has not been discussed much in the development of WIGE craft. One of the cases in the WIGE realm has been carried out by Liang et al. (2014). The main studies about oscillating wing in ground effect are informed in the automotive field (Moryossef and Levy, 2004; Molina and

Zhang, 2010; Mistry, 2012; Plensky, 2012; Fernandez Soto, 2013; Pietrzak, 2013). These studies are mostly related to the design of the rear part of racing cars which resembles an inverted wing. However, more general studies on the symmetric profiles are also available, as in Wu and Zhao (2013).

The importance of conducting CFDs is to aid the dynamic analysis for WIGE craft. However, more than that, the study also has benefits through the enrichment of understanding about ground effect aerodynamics. Thus, not only does this research offer novelty and contribution to knowledge from a dynamics stability point of view but also to aerodynamics.

In the dynamics analysis, the derivatives are obtained for a full configuration. Therefore, full configuration of aerodynamic forces and moments is needed. However, it worth reminding that the CFD study has been limited to a 2D case (i.e. aerofoil heaving in ground effect) due to several reasons. The first reason is due to the scarcity of data. It would be better to derive first the aerofoil's dynamic data followed by a more complex configuration, starting from the wing, wing-tail, wing-tail-fuselage, and eventually to the full configuration. Secondly, this research programme does have a limited time frame that, unfortunately, prevents the author from conducting all the sequences mentioned above. Thirdly, the lack of experimental value to make a comparison will be the obstacle to assess the accuracy of the results. Fourthly, the 2D data are more flexible; with relevant correction factors, one can approximate aerodynamics for many 3D configurations, not only a specific configuration. The 3D data means a wing configuration up to full configuration when the information is appropriate enough. Fifthly, simulating from a 2D case would give better comprehension of the effect of parameters when the next levels are carried out. Conducting simulation for a 3D case immediately only gives limited comprehension as it would be specific to the configuration and remove the opportunity to understand more basic parameters.

The limitation of CFD study has been mentioned previously thus the aerodynamic data for full basic configuration (wing-tail-fuselage) were obtained using a different approach that will be explained later in Section 6.1.

The brief results of the CFD simulation are available in Appendix F.

5.2 Numerical Method

5.2.1 Governing equation

A series of CFD simulations were conducted using a commercial CFD solver "ANSYS FLUENT". The simulation is aimed to solve the form of nondimensionalised two-dimensional unsteady compressible Reynolds-averaged Navier–Stokes equations for the NACA 4412 aerofoil flying near the surface set at a Reynolds number of 3x10^5, based on the chord length of the aerofoil, c.

In general coordinates, the governing equations are expressed as:

$$\frac{\partial U_i}{\partial x_i} = 0 \tag{5-1}$$

$$\frac{\partial U_i}{\partial t} + \frac{\partial \left(U_i U_j\right)}{\partial x_j} = -\frac{1}{\rho}\frac{\partial P}{\partial x_i} + \upsilon \frac{\partial^2 U_i}{\partial x_j \partial x_j} + \frac{\partial}{\partial x_j}\left(-\overline{u_i' u_j'}\right) \tag{5-2}$$

With $-\overline{u_i' u_j'}$ being the Reynolds stress term.

The turbulence model adopted for the simulation was the SST $K-\omega$ model developed by Menter (1993, 1994). The transport equations of turbulence kinetic energy K, is written as:

$$\frac{\partial(\rho K)}{\partial t} + \frac{\partial \left(\rho u_j K\right)}{\partial x_j} = \rho P_K - \beta^* \rho K \omega + \frac{\partial}{\partial x_j}\left[(\mu + \sigma_K \mu_t)\frac{\partial \kappa}{\partial x_j}\right] \tag{5-3}$$

and the specific dissipation rate ω is expressed as follows:

$$\frac{\partial(\rho\omega)}{\partial t} + \frac{\partial \left(\rho u_j \omega\right)}{\partial x_j} = \frac{\gamma}{\nu_t} P - \beta \rho \omega^2 + \frac{\partial}{\partial x_j}\left[(\mu + \sigma_\omega \mu_t)\frac{\partial \omega}{\partial x_j}\right] + 2(1 - F_1)\rho \sigma_{\omega 2}\frac{1}{\omega}\frac{\partial \kappa}{\partial x_j}\frac{\partial \omega}{\partial x_j} \tag{5-4}$$

The variables used in the equations above are described as follows:

$$P = \tau_{ij}\frac{\partial u_j}{\partial x_j}$$

$$\tau_{ij} = -\rho\overline{u_i' u_j'} = \mu_t\left(2S_{ij} - \frac{2}{3}\frac{\partial u_K}{\partial x_K}\delta_{ij}\right) - \frac{2}{3}\rho K\delta_{ij}$$

$$S_{ij} = \frac{1}{2}\left(\frac{\partial u_i}{\partial x_j} + \frac{\partial u_j}{\partial x_i}\right)$$

$$\mu_t = \frac{\rho a_1 K}{\max(\alpha_1\omega; \Omega F_2)}$$

$$F_1 = \tanh\left\{\left\{\min\left[\max\left(\frac{\sqrt{K}}{\beta^*\omega y}, \frac{500\upsilon}{y^2\omega}\right), \frac{4\sigma_{\omega 2}K}{CD_{\kappa\omega}y^2}\right]\right\}^4\right\}$$

$$F_2 = \tanh\left[\left[\max\left(\frac{2\sqrt{K}}{\beta^*\omega y}, \frac{500\upsilon}{y^2\omega}\right)\right]^2\right]$$

$$CD_{K\omega} = \max\left(2\rho\sigma_{\omega 2}\frac{1}{\omega}\frac{\partial K}{\partial x_j}\frac{\partial \omega}{\partial x_j}, 10^{-20}\right)$$

Note that μ_t is the kinematic eddy viscosity.

The equations also have constants that have different values depending on the closure of the problem set. When the part of original $K-\omega$ model is solved, the constants are $\sigma_{k1} = 0.85$, $\sigma_{\omega 1} = 0.5$, $\beta_1 = 0.075$, and when the $K-\varepsilon$ closure is solved, those constants being used are $\sigma_{k2} = 1$, $\sigma_{\omega 2} = 0.856$, $\beta_1 = 0.0828$. The addition to this model is the consideration of shear-stress transport (SST) closure constants as follows, $\beta^* = 0.09$ and $a_1 = 0.31$.

Menter's (1993) SST $K-\omega$ turbulence model offers the blending of the best virtues of both the $K-\omega$ and $K-\varepsilon$ turbulence models. This turbulence model was chosen due to its reliable prediction for flow around an aerofoil in ground effect (Mahon and Zhang, 2004).

5.2.2 Implementation

The equations are solved on a modified, structured H-grids system around the aerofoil, as shown in Figure 5-1. The aforementioned term ‘modified’ relates to the block around the aerofoil. The block is considered as C-grids, built to assure the orthogonality of the grid in the region near the body, see Figure 5-2.

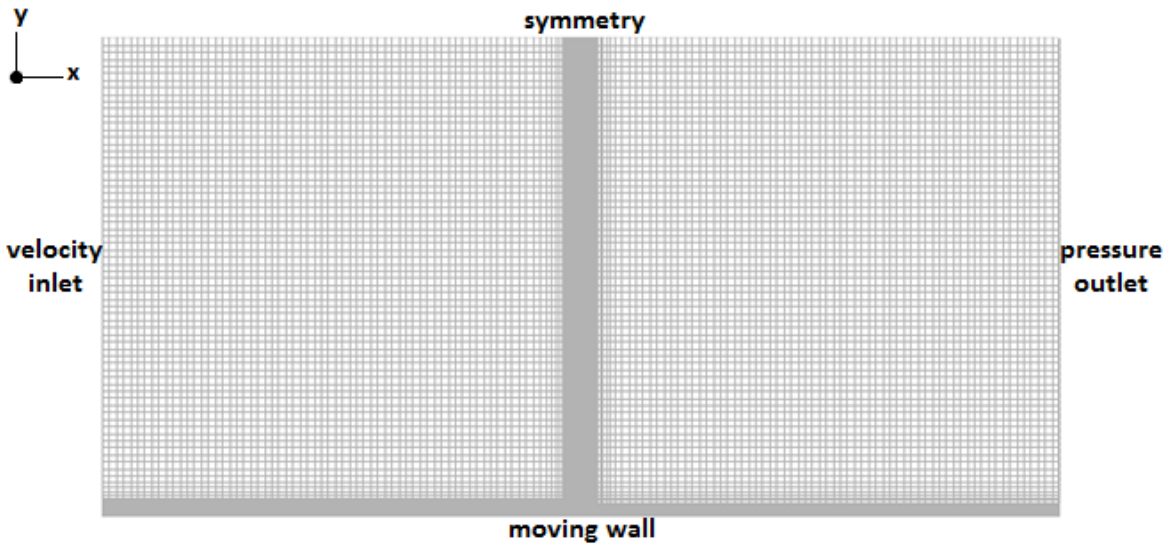

Figure 5-1 Grid block

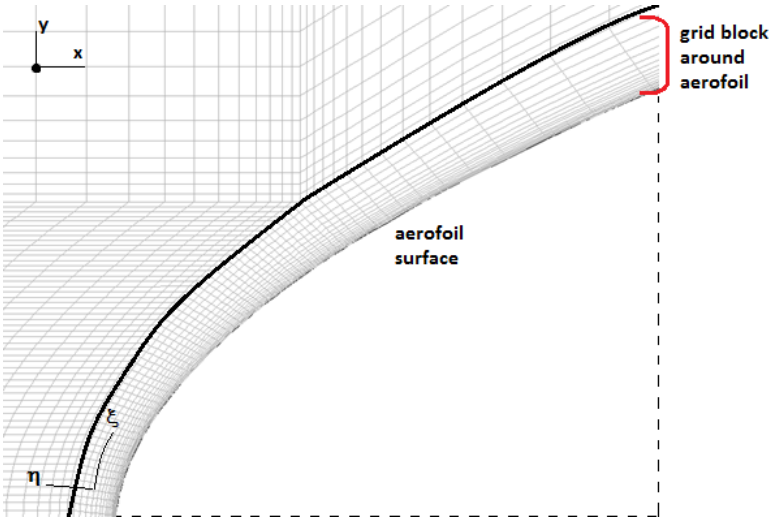

Figure 5-2 Grids near aerofoil surface

As seen in Figure 5-1, the boundary condition for computational domain comprises the inlet, outlet, upper far field and ground moving wall. The inlet is set as the velocity inlet, the outlet as the pressure outlet and the upper boundary as the symmetry, all located $50c$ away from the aerofoil. This distance of the boundary condition followed the preceding research that focused on the effect of dynamic mesh on the aerodynamics of the same aerofoil (Qu et al., 2014b). Meanwhile, the distance between the aerofoil and the ground is the ride height, h, and is offset at 0.3 c, 0.5 c and 1.0 c, as measured from the trailing edge.

When it came to the main purpose of this part, i.e. to simulate the case of the oscillating aerofoil case, transient simulations were carried out to represent the unsteady condition. A FLUENT user-defined function (UDF) file based on C++ programming language was used together with the use of dynamic mesh to capture the characteristics of the aerofoil. A full oscillation in the longitudinal plane would require a periodic movement in the surge, pitch and heave. The oscillatory surge motion can be neglected since the amplitude of the speed oscillations in surge is negligible with respect to the forward speed of the vehicle. The oscillation in pitch can, at first approximation, be captured quasi-statically, analysing the behaviour of the profile at different angles of attack. The oscillation in heave is the one having the most substantial effect on the aerodynamic coefficients, due to the non-linearity of the ground effect. Due to this reason, the UDF program was built considering only the elevation in heave motion.

The unsteady term is discretised with a second-order implicit scheme. The SIMPLE algorithm is adopted to calculate velocity and pressure. The term SIMPLE is an acronym for *Semi-Implicit Method for Pressure Linked Equations*, and the name is related in how the algorithm works. In this approach, the discretised momentum equation and pressure correction equation are solved implicitly, where the velocity correction is solved explicitly. The pressure field and its correction during the iterative process are the centre of attention of this method to obtain the solution of the governing equation. One of the earliest application of this numerical scheme was employed by Patankar and Spalding (1972).

Regarding the use of dynamic mesh, two types of dynamic mesh are being utilised, i.e. smoothing and remeshing. The aerofoil, defined as a rigid body, oscillates based on the equation set in the UDF file, and due to the motion, the mesh will be adjusted per time step. For each case, the number of time steps is 1000, and the size is 0.05 seconds.

5.2.3 Evaluation

In the application of simulations, there were two stages of evaluating the present numerical method. They were the simulations of non-oscillating aerofoil for both freestream and ground effect conditions. The results were validated against existing experimental and numerical studies.

5.2.3.1 Freestream condition

For the validation of the freestream condition, the Reynolds number used is 3×10^6 rather than 3×10^5, following the experimental data to be compared.

The results of the freestream condition for a range of angles of attack were validated against the experimental results presented by Abbott and Doenhoff (1959) and Pinkerton(1963), see Figure 5-3 and Figure 5-4. The lift and moment coefficients from the CFD simulations were in agreement with the experimental data in Abbott and Doenhoff's research with small discrepancies of less than 6% for lift and 3.5% for pitching moment. On the other hand, lack of agreement was shown and, compared with Pinkerton's results, they gave the deviation up to 30% for lift and 10% for pitching moment. The great difference shown by Pinkerton was claimed to be related to the interference of an experimental setting. Another difference is the trend that is shown by the coefficient of pitching moment by the increase in angle of attack. As that is not the concern of this project, the next attempts were limited to the area where the flow still gives linear characteristics in lift and moment.

As for the drag coefficient, CFD simulations give much higher values (47% higher on average) than the data from Abbott and Doenhoff (1959), see Figure 5-5. No

information was given by Pinkerton (1963). The differences in drag can be explained since the aerofoil boundary layer was not “tripped” in the experiments. Differently, the present CFD simulations were set to predict a fully turbulent boundary layer which corresponded to a tripped condition. The difference of tripped and non-tripped experiments has been discussed, e.g. by Rumsey (2014). A comparison of the drag of the NACA 0012 between the non-tripped experiments and tripped experiments by McCroskey (1987) and Ladson (1988) shows a discrepancy of approximately up to 42%.

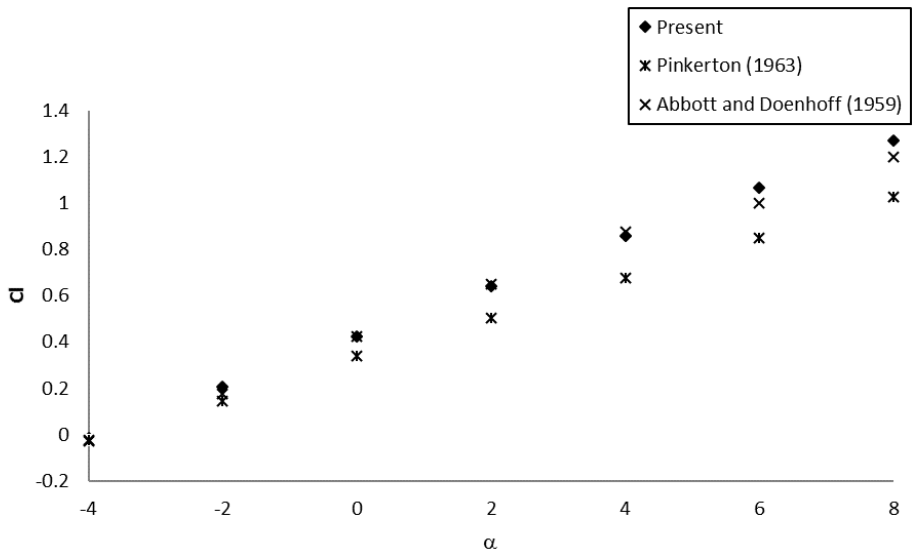

Figure 5-3 c_l against α in freestream condition

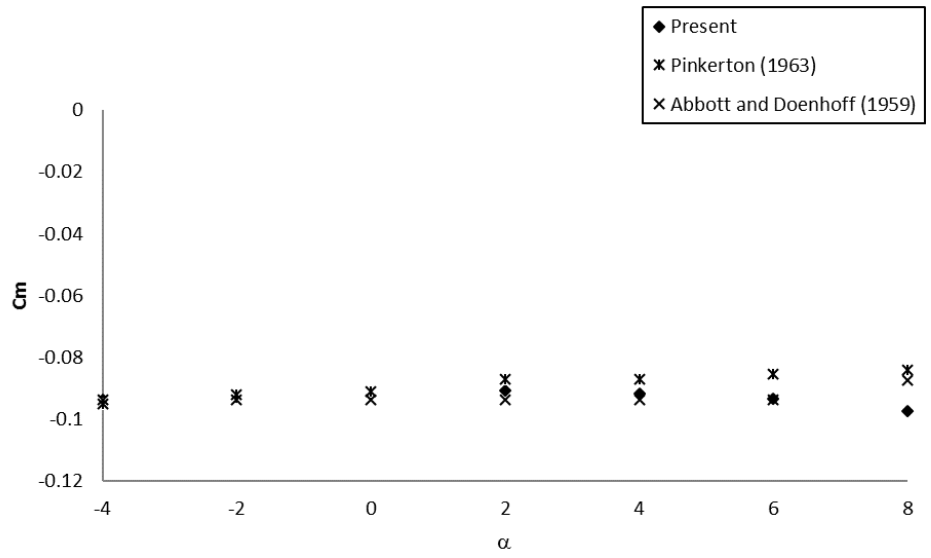

Figure 5-4 c_m at 25%c against α in freestream condition

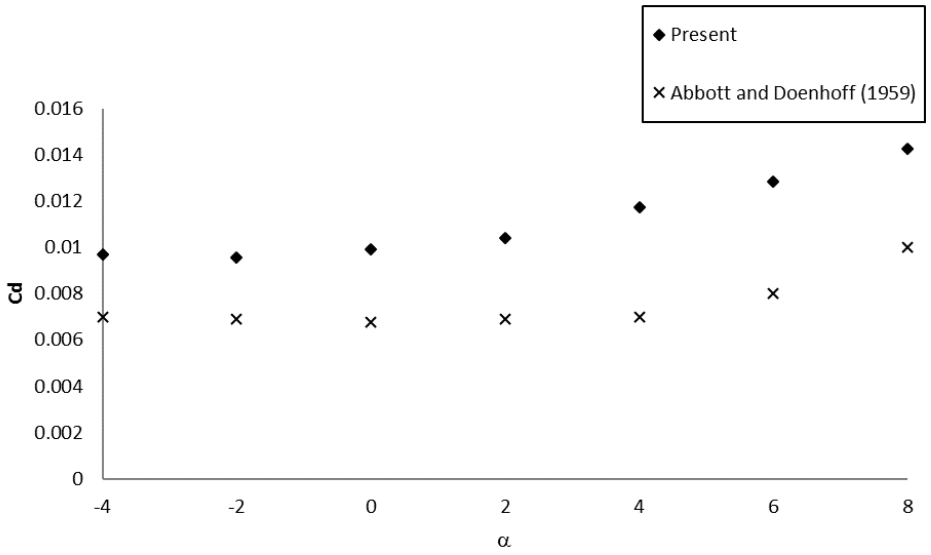

Figure 5-5 c_d against α in freestream condition

5.2.3.2 Ground effect condition

As for the ground effect case, the results were compared against two examples of experimental data (Kikuchi et al., 2002; Ahmed et al., 2007) and numerical simulation data (Qu et al., 2014b). The comparison of lift between these data is shown in Figure 5-6.

Qu et al. (2014b) promoted the use of dynamic mesh in the simulation they carried out. The simulation was run with the Spalart-Allmaras turbulence model. It was assumed the choice was adopted from the fact that the Spalart-Allmaras model is one equation model, thus lighter for computational performance. This is despite the review that they have conducted on the work of Mahon and Zhang (2004), confirming that the SST $K-\omega$ turbulence model to some extent gives better accuracy than the other five models for the case of ground effect.

Differently, the SST $K-\omega$ turbulence model was utilised for the simulations of the present study. For a regular ground effect situation, the present work produced no significant differences in lift forces. The deviation occurs with up to 7% between each other. From Figure 5-6, one may see that the trend by the increase of angle of attack showing that the results in Qu et al. (2014b) slightly overestimate the results of the present study. Here, it is shown that the effect of the turbulence model matters for the condition where the flow starts to abandon the linear characteristics. When the trends are compared against experimental data, as explained later, the present results show a better agreement than the results by Qu et al. (2014b). The difference is probably because the separation start is taking place at higher angles of attack, and the Spalart-Allmaras turbulence model, from experience, is showing the lack of handling flow separation. In contrast, the SST $\kappa-\omega$ turbulence model shows the versatility in handling the flow in ground effect, both in strong ground effect and weak ground effect toward the freestream condition.

Two experiments were referred for the validation at this point. The experiments had different approaches, i.e. by using a towing facility (Kikuchi et al., 2002) and by using a moving ground facility (Ahmed et al., 2007). Interestingly, major discrepancies are shown by both methods. The investigation was carried out by Kikuchi et al. only in the strong ground effect region while Ahmed et al. had a wider range of observations.

At $0°$ of angle of attack, all the investigations, numerical and experimental, give a similar trend showing that the drop of coefficient lift occurs through the decrease of ride height. In the dropping area ($0 < h/c < 0.3$), the results Qu et al.

overestimate the other. The present study also shows higher values than the results from the experiments. The gradient of the present study in that area is closer to the data produced by Ahmed et al (2007).

Before proceeding to the next characteristics, it is necessary to discuss the dropping behaviour shown by the aerofoil in conducting investigations. It is widely known that the ground has a lift-altering effect toward lifting a body, like aerofoils and/or wings. However, that idea is often not furnished with further explanation, that the effect is also affected by other circumstances. The results of the studies described here confirm this. Differently, from the common understanding of ground effect, the lift of the chosen aerofoil in ground effect might be lower than the lift in a freestream condition. In this case, at $0°$ angle of attack, the NACA 4412 creates a convergent-divergent passage leading to the occurrence of the Venturi effect, indicated by the plunge in c_l when the ride height decreases. The lower surface of the NACA 4412 is not completely flat; rather, it has a convex lower surface from the leading edge to $0.4c$. This condition creates a strong suction on the lower surface while the profile approaches the ground.

This consistent trend shown by conducting investigations illustrates the importance of the profile of lifting surfaces. This is also mentioned in Rozhdestvensky (2006), stating that the aerofoil profiling has a great deal of importance in the overall aerodynamics of WIGE craft.

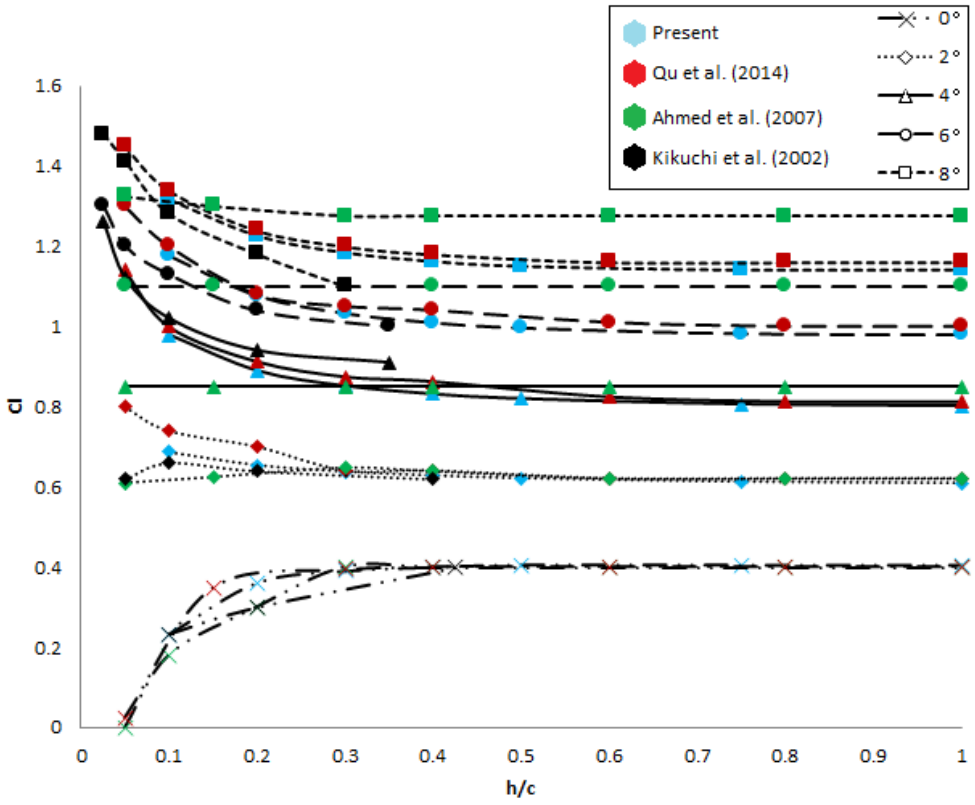

Figure 5-6 c_l at varying h/c for different α

Continuing with characteristics of the results from conducting the investigation, one can distinguish the anomaly shown by Ahmed et al. (2007). At $2°$ angle of attack, the trend still indicates the drop of lift by decreasing height, but the strength of the phenomenon has reduced dramatically. From $4°$ to $6°$ angle of attack, the ground does not seem to give significant changes in lift forces. Only at $8°$ angle of attack do very weak increases by decreasing ride height start to be spotted. The abnormality was not explained very well, and is only based on the difference between the pressure on the upper and lower surfaces.

More reasonable trends are shown in Kikuchi et al. (2002), showing the alteration of lift by the change in ride height. At $2°$ angle of attack, the Venturi effect is only observed in the ride height of less than 0.1c, and at larger ground clearances the coefficient drops by the increasing ride height. At higher angles of attack ($4°$ - $8°$),

the trend is in accordance with the general understanding of ground effect phenomenon.

In the strong ground effect region, the present study indicates better agreement than Qu et al. (2014b) as compared to the experiment carried out by Kikuchi et al. (2002). At $2°$ angle of attack, there is no trace of the Venturi effect shown by Qu et al. and, rather, the values overestimate the experimental data quite significantly. The substantial difference shown by Qu et al. is probably due to the choice of their turbulence model. The Spalart-Allmaras model used by them is not able to capture the effect of the wall, both for the aerofoil and the ground. The SST $K-\omega$ model in the present study has better reliability to handle flow around the wall. When the ground clearance enlarges, there is no significant difference between the results from the present study and from Qu et al. (2014b).

Concerning the characteristic of the drag, the present study shows a difference in the value trend from the experimental results. Both experimental data show a tendency of an increase in drag with reducing ride height for all angles of attack, whereas the numerical results show a slight decrease at 2^o and 4^o of angles of attack. There is no explanation about drag characteristics in the numerical investigation by Qu et al. (2014b).

In conclusion, the experimental data show that the study by Kikuchi et al. (2002) gave more reasonable results than Ahmed et al. (2007) The difference is in the experimental technique matters. Kikuchi et al. claimed that the investigation using the towing facility would give better results than the moving ground technique in the wind tunnel.

Furthermore, from the overall results, the numerical approach of the present study shows better agreement with the results of the experimental done by Kikuchi et al. compared to another numerical study. The main prediction is related to the difference in the turbulence model. It is known that the SST $K-\omega$ model has good performance in the analysis of the ground effect case, and the comparison with the preceding investigations confirms this.

Despite the conducting simulations in the present study gave reasonable trends, the results of the present study slightly overestimate the experimental data. The deviation may occur from the limitation of the computational calculation to capture the flow around the aerofoil.

5.2.3.3 Turbulence model

The previous discussion gives a depiction of the significance of the turbulence model in CFD analysis. Examining the results from two numerical simulations, as explained before, leads to the conclusion that the two-equation SST $K-\omega$ turbulence model is more suitable than the one-equation Spalart-Allmaras turbulence model.

However, before using the SST $K-\omega$ model, the author made some attempts to examine the same problem using another two-equation turbulence model, i.e. the $K-\varepsilon$ turbulence model. It turned out that this turbulence model has some issues regarding the accuracy of the results. The simulation using the $\kappa-\varepsilon$ model shows undesirable fluctuation in the pressure distribution. The fluctuation in the pressure distribution level will affect the production of aerodynamic forces of the aerofoil.

The pressure distribution fluctuation is also demonstrated in a study of a lifting surface over wavy ground (Yang et al., 2010). The fluctuation of the results was claimed as the effect of the meshing technique, which is reasonable to some extent. However, the use of the $K-\varepsilon$ turbulence model probably also contributes to the behaviour.

Based on the trend shown, it can be concluded that the $K-\varepsilon$ turbulence model is not suitable for the ground effect analysis.

In the turbulence model employed, the range of y^+ is consistent in the range of the sub-viscous region where, in this case, $0 < y^+ < 0.8$. This shows that the mesh generated is acceptable for the study, see Figure 5-7 as an example.

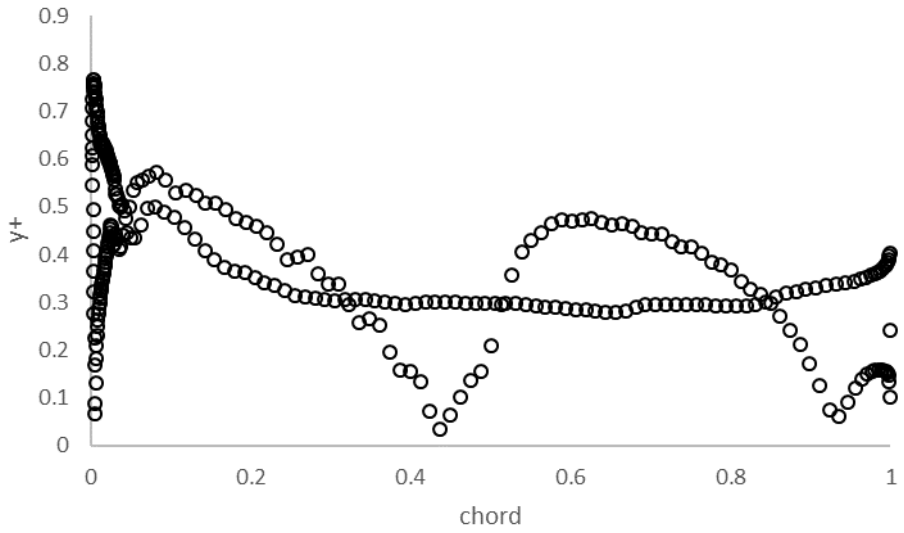

Figure 5-7 y^+ of NACA 4412 at $\alpha = 4$, $h/c = 0.3$, $k = 0.026$, $A/c = 0.05$, and $time\ step = 500$

5.3 Aerodynamics of oscillating profile

The expected results were that the values of the forces and moments would fluctuate periodically. In general, the coefficients of forces and moments should change depending on the frequency and amplitude of the oscillation. A different phase is expected corresponding to the relative phase lag between the vehicle oscillation and the wave oscillation.

With regard to the average values of aerodynamic coefficients, the values present different patterns. The mean value of coefficient of lift, c_l, of the oscillating aerofoil was very close to the c_l produced by the non-oscillating aerofoil. Conversely, the average coefficient of drag, c_d, of the oscillating aerofoil was lower than the c_d of the non-oscillating aerofoil. Furthermore, the average values of c_d shown by the oscillating aerofoil was strongly affected by the frequency and amplitude of the oscillation. The average coefficient of pitching moment, c_m, of the oscillating aerofoil was lower than the c_m of the non-oscillating aerofoil. However, the average c_m did not seem to be influenced by the frequency and amplitude of the

oscillation. These aspects are discussed in more depth in the following subsections.

Before continuing in depth with the discussion, it should be noted that there are two terms related to the frequency used in this chapter. The first term refers to the frequency of the motion, denoted with ω and described in rad/s. The other term is 'reduced frequency', with notation k, which describes the non-dimensional number about frequency, used for the sake of forces' analysis. The parameter is described as:

$$k = \frac{\omega c}{2U_e} \tag{5-5}$$

where ω is the angular frequency of oscillation, c is the chord length and U_e is the freestream velocity.

The 'reduced frequency' term is more used when discussing aeroelasticity or unsteady aerodynamics. It conveys the information about the level of unsteadiness of a system.

In the case of this study, the reduced frequencies used are 0.026, 0.052, 0.103, and 0.129 (corresponding to $\omega = 0.25\,rad/s$, $0.50\,rad/s$, $1.00 rad/s$, and $1.25\,rad/s$). From the reduced frequencies presented, the first two indicate quasi-steady aerodynamics and the other two indicate unsteady aerodynamics. The categorisation is applicable despite the fact that the real frequencies are small.

5.3.1 Lift characteristics

Firstly, as explained in Subsubsection 5.2.3.2 above, it should be understood that, differently from the common understanding of ground effect, the lift of the chosen aerofoil in the ground effect might be lower than the lift in the freestream condition depending on the circumstances that apply to the aerofoil.

With regard to the impact on the aerodynamics, a negligible difference was identified between the c_l of the non-oscillating aerofoil and the average c_l of the oscillating aerofoil in the ground effect, see Figure 5-10, Figure 5-11, and Figure

5-12. This is similar to the lifting theory for an aerofoil flying over a wavy surface (Liang et al., 2013a), confirming that the time-averaged lift for such a condition would give the same lift with the aerofoil flying over a flat surface. On the other hand, it should be noted that a completely different situation should be expected for the 3D case, i.e. there is a difference between the time-averaged lift in the wavy ground effect and the lift in the regular ground effect. The time-averaged lift should be higher (Liang et al., 2013b). Here, one can conclude the influence of the span to the ground effect aerodynamics. The wing span determines the strength of circulation of the vortex ring on the wing surface. Also, there is a similitude shown by another 2D case about the time-averaged lift of an oscillating aerofoil and the lift of the same aerofoil stationary flying over a flat surface (Moryossef and Levy, 2004). This statement indicates that the lift for the 3D body is subject to the encounter frequency felt by the system.

It worth reminding that the scope of the present study does not include the aerodynamic differences in the 2D and 3D cases. Instead, the aerodynamic data for the 3D case is derived from the 2D data with a semi-empirical technique. Exerting the 2D simulation data and transform them into 3D data with the technique may not give the truest result. However, due to the limitation that has been previously explained in Section 5.1, the semi-empirical technique has been employed for this research.

The effect of ride height is depicted in Figure 5-13, showing that there is a change in the gradient of c_l against α. Despite being almost negligible, there is indeed a slight difference between the time-averaged lift from the oscillating case and the lift from the non-oscillating one, especially in the stronger ground effect region. This may be related to the viscosity involved in the analysis. In most oscillating cases, the phenomena that occur are associated with inviscid flow. In the ground effect condition, the flow, to the contrary, is considered to be viscous, which becomes stronger as it approaches the extreme ground effect region. The viscosity is related to the shear stress that energises the flow to remain attached to the surface and lead in the improvement of the pressure distribution and lift of the aerofoil.

Rather than discussing the time-averaged lift, it is much more identifiable to discuss the significance of oscillation on the maximum and minimum c_l of the oscillating aerofoil. As expected, the c_l oscillates in a nearly harmonic manner, with some phase lags, see Figure 5-8 and Figure 5-9. The phase lags demonstrate that the oscillation induces the production of energy of the system. As an instance, when the motion is in its amplitude and starts moving down, the lift still increases for some time before starting to decrease. It shows that even though the relative position of the aerofoil is lower than the amplitude, the lift in this position may be higher than the lift when the aerofoil is at the peak of oscillation. The energy of the flow from the previous instantaneous time is still able to boost the system to produce lift. From this observation, the periodic motion appears to feed the system to maintain the oscillation.

The magnitude of the oscillation frequency has a strong impact on the range of c_l. Figure 5-14 and Figure 5-15 relay that the increase in reduced frequency leads to a higher c_l amplitude. The relationship is mainly due to the increase in the magnitude of vertical velocity experienced by the profile. The vertical velocity magnitude is proportional to the frequency of oscillation. From the angle of attack point of view, the change in the magnitude of vertical velocity leads to the alteration in effective angle of attack, which is quantified in equation (5-6).

$$\alpha_{eff} = \alpha - \alpha_{\omega}$$
$$\alpha_{\omega} = \arctan\frac{-V_{\omega}(t)}{U_e} \tag{5-6}$$

Based on the relationship in equation (5-6) above, one can conclude that the alteration in the frequency of the oscillation leads to the change in the range of effective angles of attack. Thus, a wider c_l range occurs.

The comparison between Figure 5-14 and Figure 5-15 illustrate the characteristics of the amplitude of the motion and also affects the magnitude of the range of c_l. As expected; the higher the amplitude of oscillation, the wider the c_l range becomes. The relationship between the amplitude of oscillation and the

amplitude of the c_l shows a linear trend. By tripling the amplitude of motion, the width between the maximum and minimum c_l also increases threefold at every frequency simulated.

As expected for the cause-effect principle, the phase lag between the motion and the lift force is positive based on the relationship $c_l(t) = c_{l_a} \cos(\omega t + \varphi_\omega)$, i.e. the lift peak comes later than the motion peak. These phase lags tend to decrease by increasing the frequency.

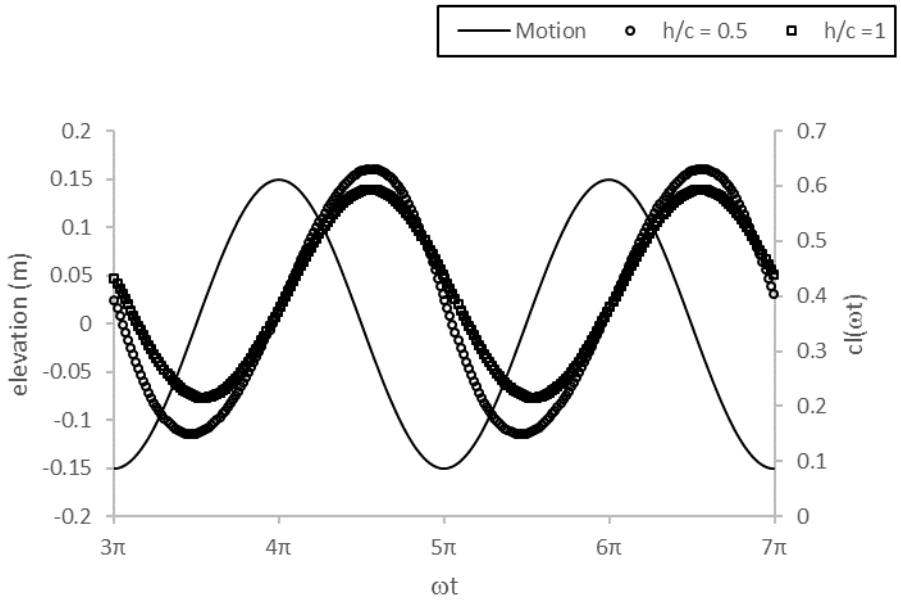

Figure 5-8 Motion and c_l time history in the ground effect for various h/c at $\alpha = 0°$; $A = 0.15c$; $k = 0.103$

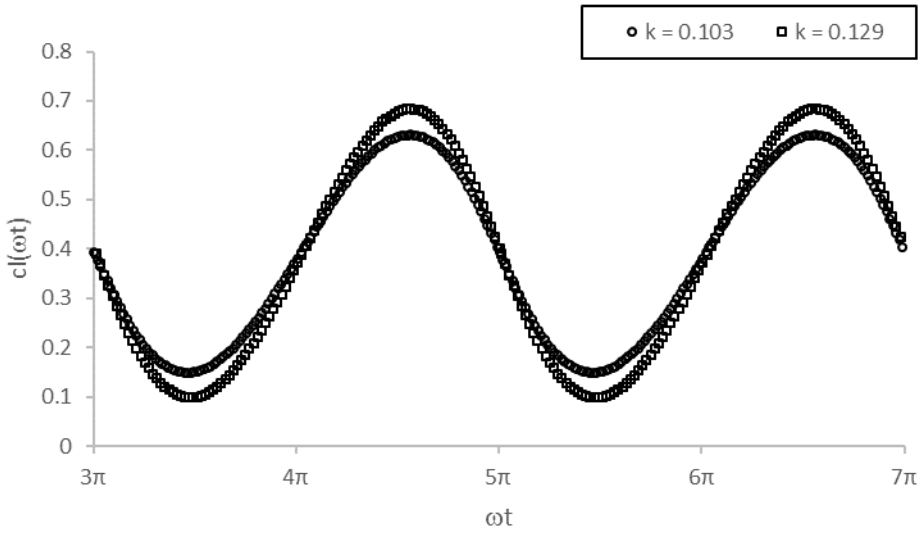

Figure 5-9 c_l time history in the ground effect for k at $\alpha = 0°$; $h = 0.5c$; $A = 0.15c$

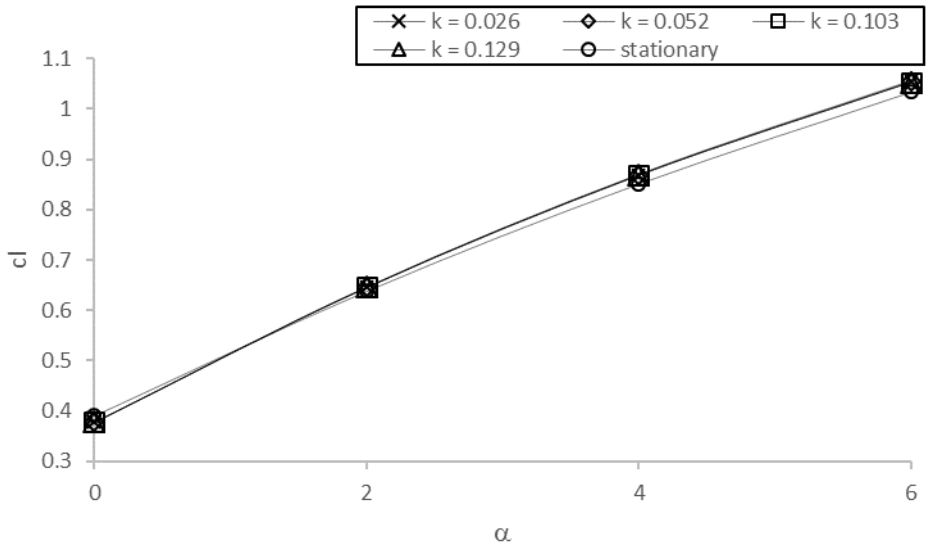

Figure 5-10 Time-averaged c_l against α at h/c = 0.3 and A/c = 0.05

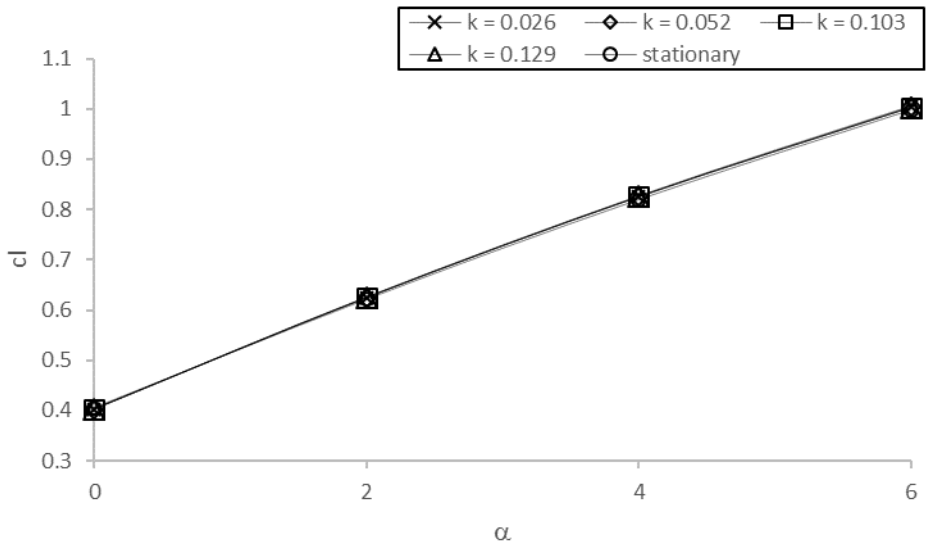

Figure 5-11 Time-averaged c_l against α at h/c = 0.5 and A/c = 0.05

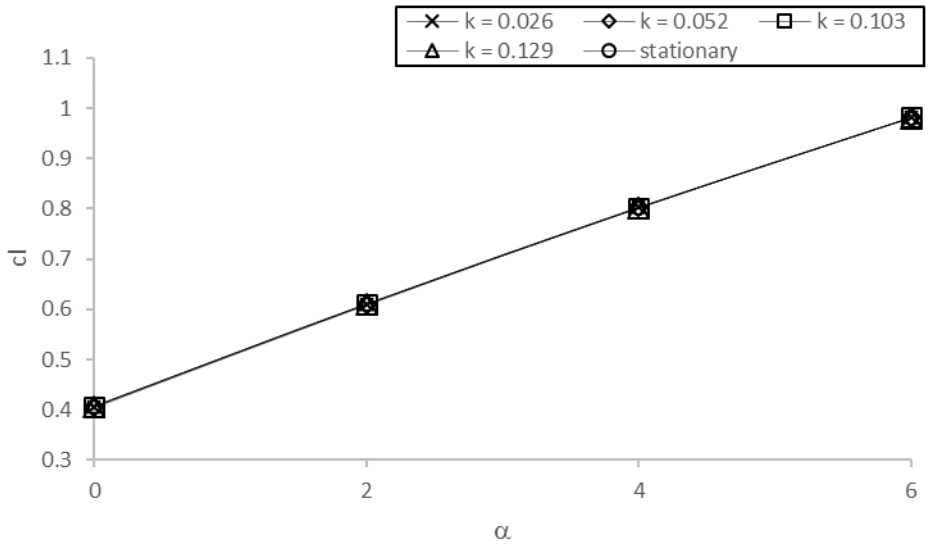

Figure 5-12 Time-averaged c_l against α at h/c = 1.0 and A/c = 0.05

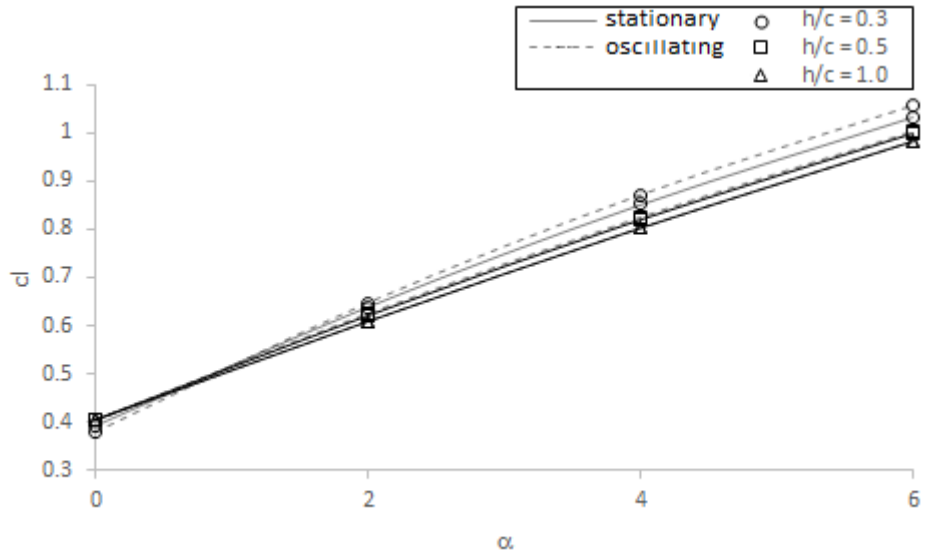

Figure 5-13 $c_l - \alpha$ curve of oscillation (with k = 0.052 and A/c = 0.05) vs. non-oscillating one

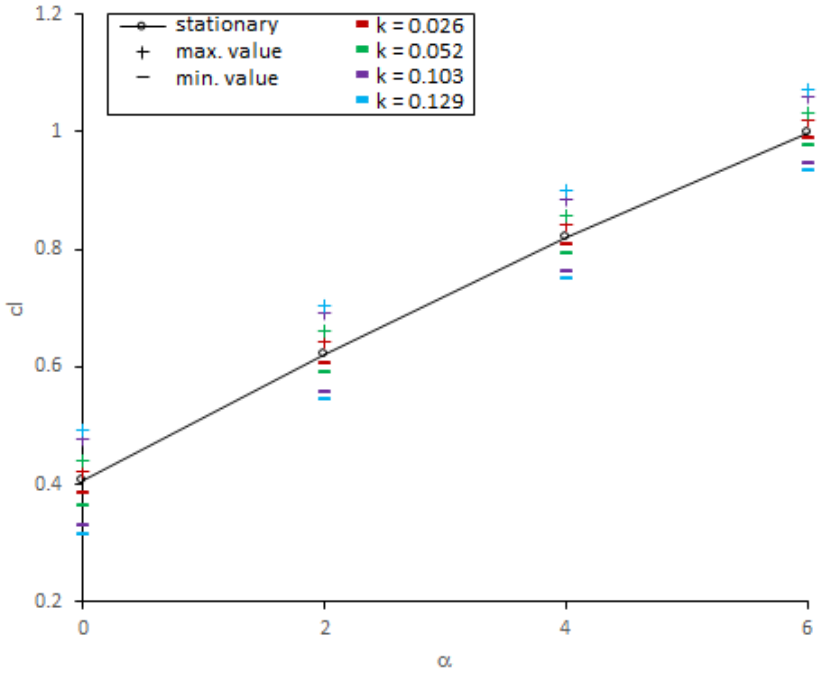

Figure 5-14 Maximum and minimum c_l against α at h/c = 0.5 and A/c = 0.05

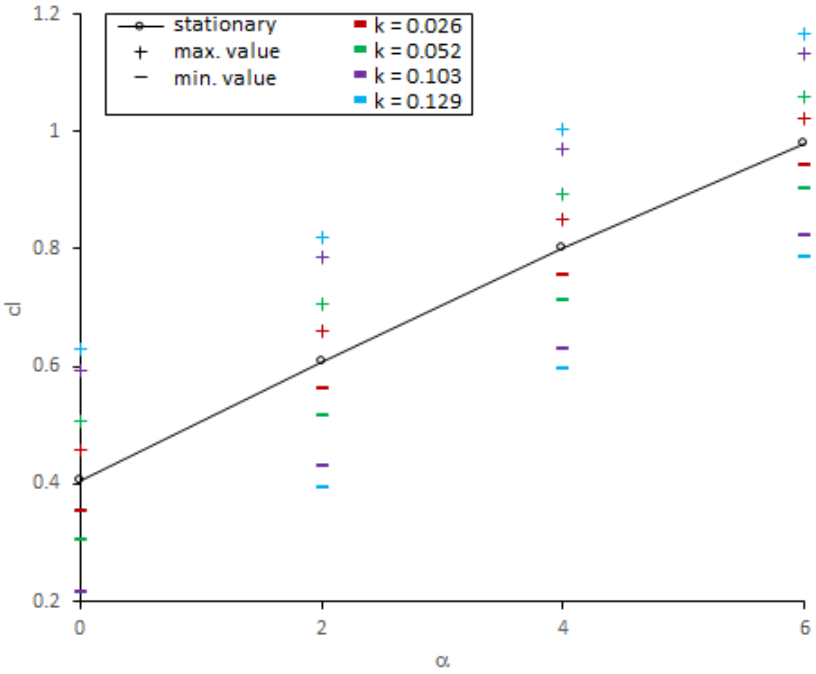

Figure 5-15 Maximum and minimum c_l against α at h/c = 0.5 and A/c = 0.15

5.3.2 Drag characteristics

As expected, c_d also experiences periodic changes in value, see Figure 5-16. Besides the expected periodic change, the drag exhibits many interesting phenomena. Some parts of the phenomena also occur in oscillating cases outside the ground effect. The figure also displays that drag exerts negative phase lags, thus the amplitude of drag comes earlier than the peak position of the aerofoil. At the beginning, at the top position, the aerofoil has initial drag. When the aerofoil starts moving down, the vortex drag also diminishes leading to the decrease in overall drag. However, as the aerofoil descends lower and the lift increases, the system starts gaining drag, as induced by the generation of lift. When the aerofoil is in the through position of its motion, the influence of the previous instantaneous position still pushes the system to produce more drag. Due to the periodic motion of the aerofoil, some amount of kinetic energy in the vortex is stored to maintain the motion, thus the generation of forces is repeated also in the periodic manner. Another factor that the periodic motion also exhibits

is the propulsive forces. Garrick (1936) mentioned the mathematical relationship between the work done, vortex kinetic energy and propulsive forces.

The propulsive characteristic of an oscillating aerofoil is like the Knoller (1909) - Betz (1912) or Katzmayr (1922) effect. The phenomenon has been identified in many cases out of the ground effect, for example, Tuncer and Platzer (1996) and Jones et al. (1998), and in the ground effect, for example, Moryossev and Levy (2004). The results of the present study also confirm the condition. In several circumstances, especially when the motion is highly unsteady, even the negative values of c_d do exist, see Figure 5-17. The decline in the time-averaged drag is influenced by the frequency of the oscillation. The higher the frequency of oscillation, the lower average c_d becomes. It shows that the increase in frequency leads to a higher propulsive effect of the system. The relationship between the averaged c_d and the frequency of oscillation is depicted in Figure 5-18, Figure 5-19, and Figure 5-20. The time-averaged drag shows a decrease by reducing the height ride due to this propulsive effect.

Katzmayr (1922) explained that the oscillation motion implies the change of flow behaviour around the oscillating system. From experiments previously conducted, the flow significantly deflected yet showed synchronous changes from time to time. This has the effect on the 'location' of the leading edge, pressure distribution, and damping mechanism to the body and eventually the fluctuation of the aerodynamic forces. The motion induces a different angle of attack from the real angle of attack. The difference in the perspective of the angle of attack has been discussed earlier in Subsection 5.3.1.

Observing Figure 5-17, it is also discovered that for higher reduced frequencies, the periodic manner slightly bends from a sinusoidal characteristic and is rather considered as a nearly squared periodic change, especially at high frequency and large ride height. A similar trend was also discovered in the inverted aerofoil study, such as in Moryossev and Levi (2004). They suspected that the motion in constant high reduced frequencies enforces the presence of additional frequencies to the drag thus the superposition leads to the presence of the phenomenon.

Moryossef and Levy also expressed general c_d as:

$$c_{d_{ig}}(t) = \omega(A/U_e)\cos(\omega t)\left[c_{l_{\alpha_{eff}}} - c_{l_{og}}\right] - \omega^2\left(A^2/{U_e}^2\right)\cos^2(\omega t)\, c_{l_{\alpha_{eff}}} \qquad (5\text{-}7)$$

where,

- A is amplitude of motion;
- $c_{d_{ig}}$ is drag coefficient in ground effect;
- $c_{l_{\alpha_{eff}}}$ is gradient of lift coefficient against effective angle of attack;
- $c_{l_{og}}$ is lift coefficient out of ground effect;
- U_e is freestream velocity;
- ω is angular frequency.

At a higher ride height, the term $\left[c_{l_{\alpha_{eff}}} - c_{l_{og}}\right]$ is thus the drag response dominated by the squared cosine part. However, when the aerofoil is approaching the ground, the term becomes significant and controls the behaviour of the drag response. It should be noted that the drag is also affected by the frequency, not only as shown by the expressed equation but also further toward a $c_{l_{\alpha_{eff}}}$ component. As shown in equation (5-6), the frequency of oscillation matters for the effective angle of attack.

The oscillation amplitude also has a significant impact on the averaged c_d, see Figure 5-21 and Figure 5-22. The first influence is regarding the averaged c_d. The higher the amplitude of oscillation, the lower the averaged c_d becomes. For instance, at $\alpha = 0°$, $k = 0.129$, and $A = 0.05c$, the average c_d is 8.5×10^{-3}. As the amplitude is tripled, at the same angle of attack and reducd frequency, the average c_d is 2.4 times lower than the previous one. However, the trend becomes less significant by increasing the angle of attack.

The comparison between Figure 5-21 and Figure 5-22 also reveals the severity of the increase in the amplitude of oscillation toward the maximum and minimum c_d. In general, the increase in the amplitude of oscillation boosts the magnitude of both maximum and minimum c_d. However, the minimum c_d appers to have more significant changes than the maximum c_d. However, this situation is

compensated for by the time consumed by the two conditions, i.e. the aerofoil holds the maximum c_d longer than the minimum c_d, see Figure 5-17.

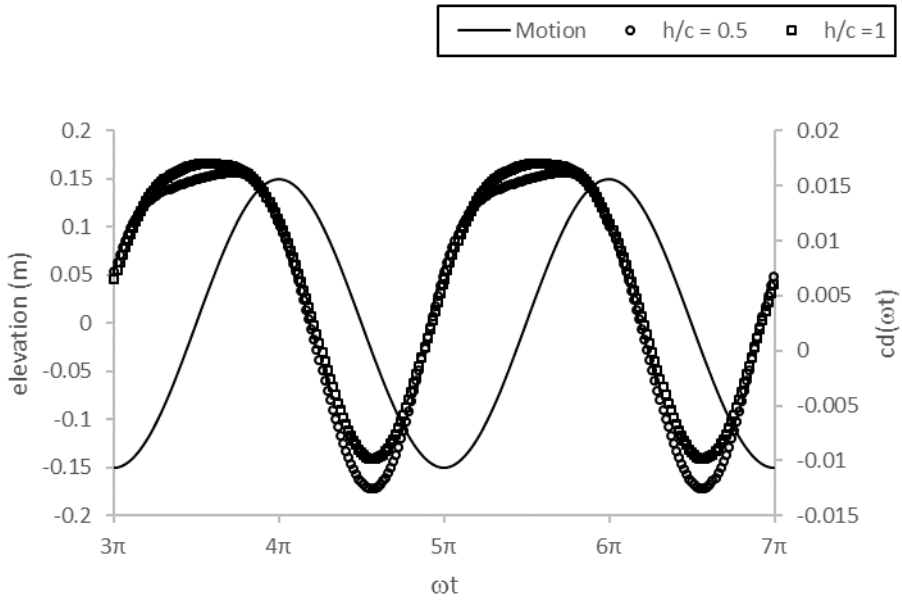

Figure 5-16 Motion and c_d time history in the ground effect for various h/c at $\alpha = 0°$; $A = 0.15c$; $k = 0.103$

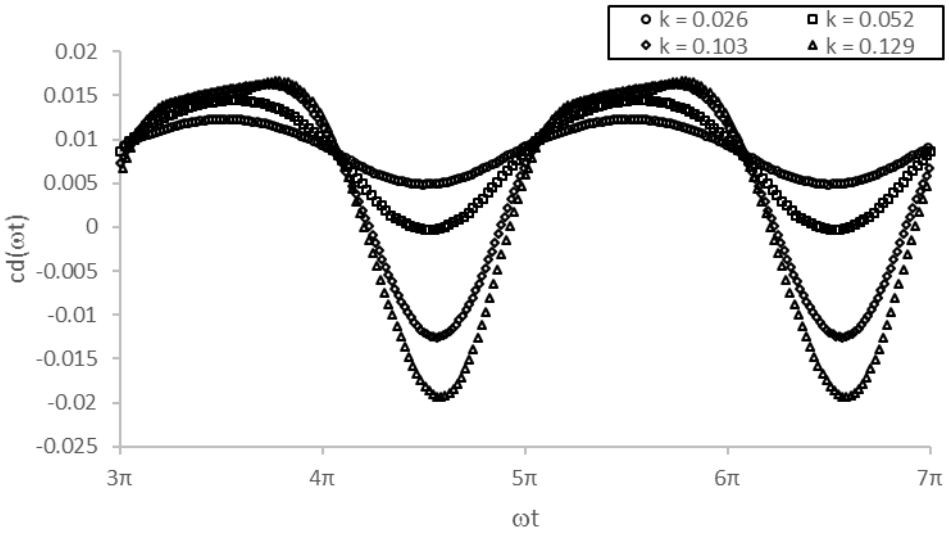

Figure 5-17 c_d time history in the ground effect for k at at $\alpha = 0°$; $h = 0.5c$; $A = 0.15c$

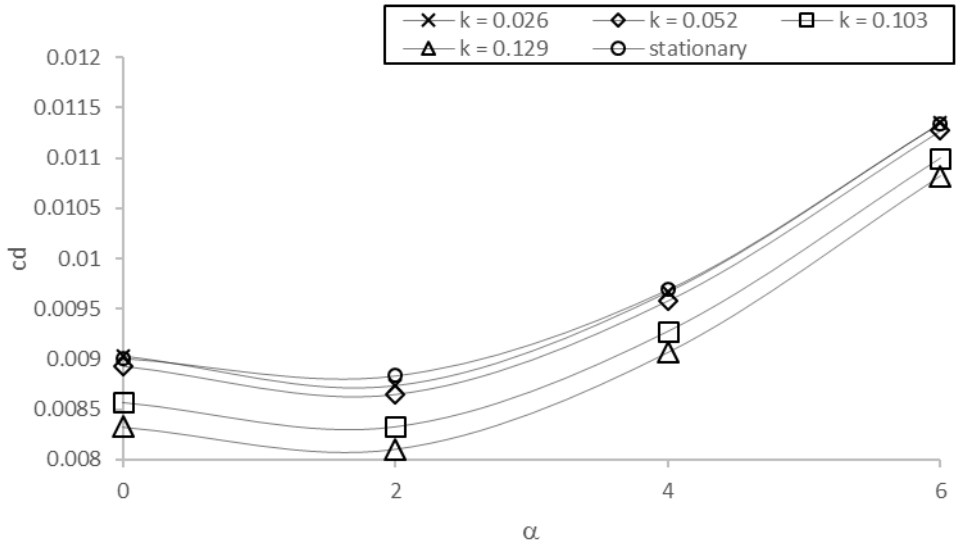

Figure 5-18 Time-averaged c_d against α at h/c = 0.3 and A/c = 0.05

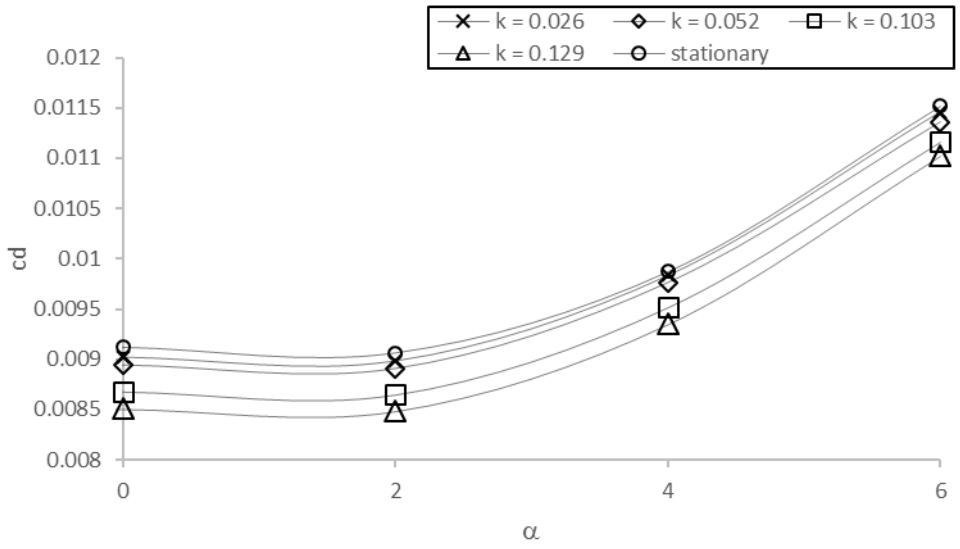

Figure 5-19 Time-averaged c_d against α at h/c = 0.5 and A/c = 0.05

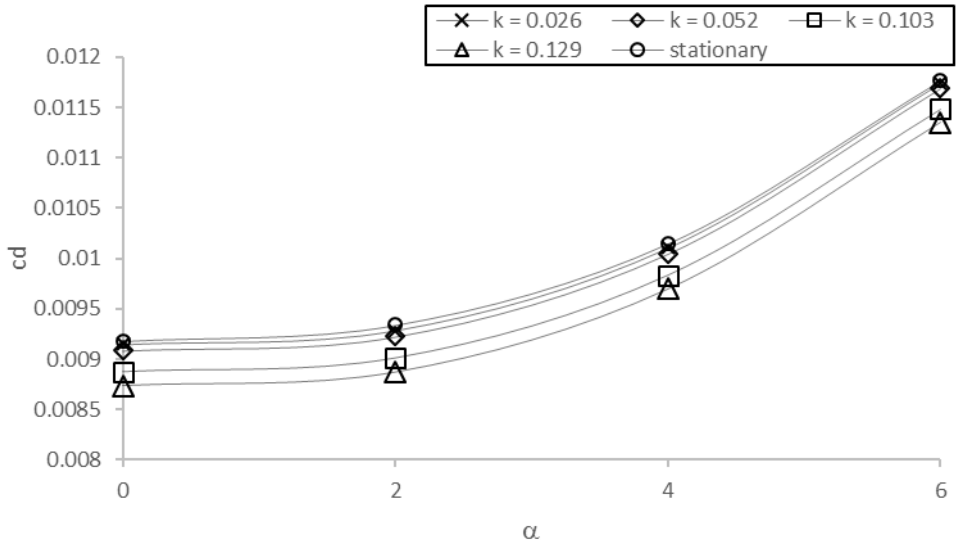

Figure 5-20 Time-averaged c_d against α at h/c = 1.0 and A/c = 0.05

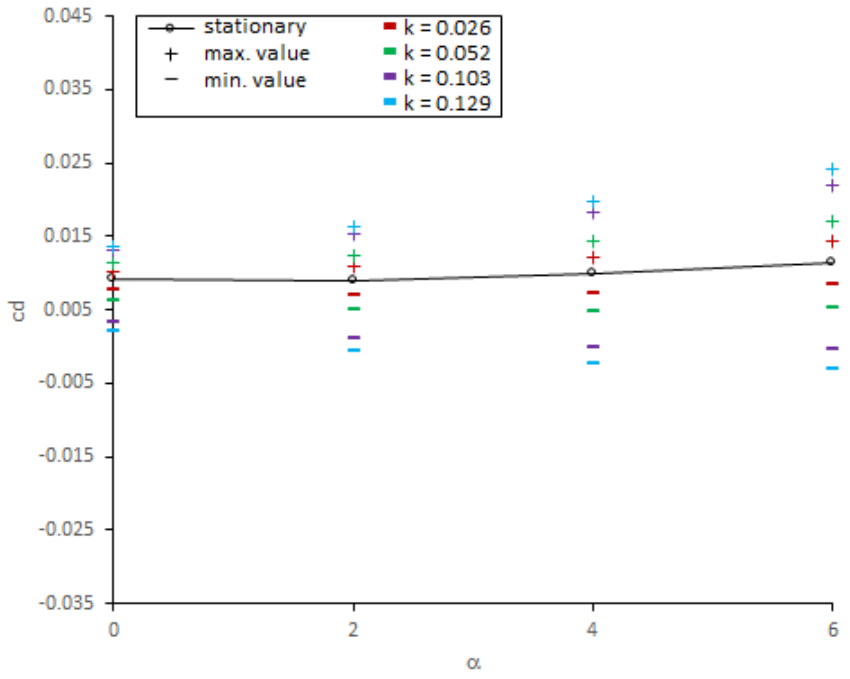

Figure 5-21 Maximum and minimum c_d against α at h/c = 0.5 and A/c = 0.05

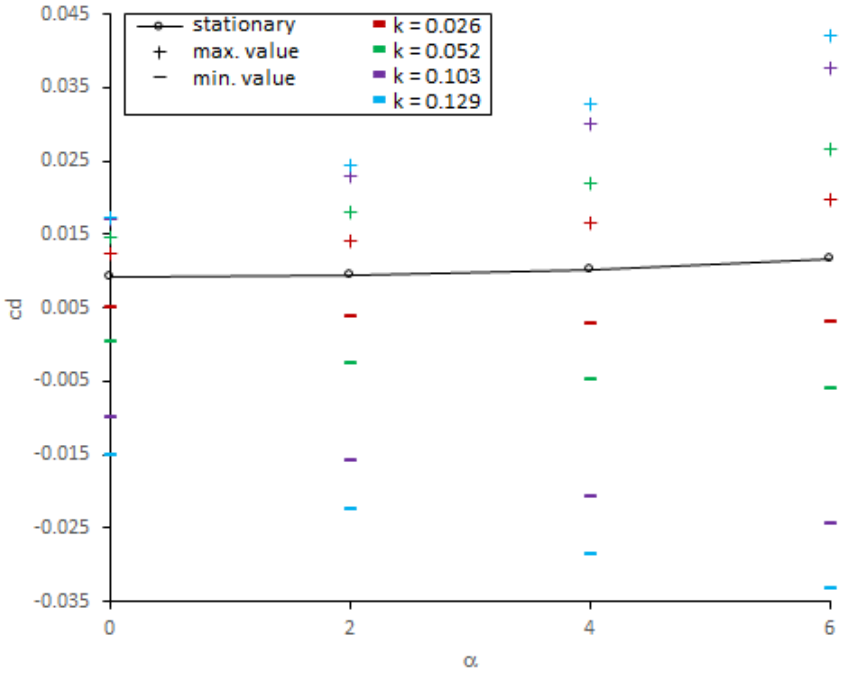

Figure 5-22 Maximum and minimum c_d against α at h/c = 0.5 and A/c = 0.15

5.3.3 Averaged aerodynamic efficiency

The ratio between the average c_l and average c_d is affected by the parameters that have been discussed above for the lift and drag characteristics. As one may see, the polar curves shown in Figure 5-23, Figure 5-24, and Figure 5-25 depict that the decreasing ride height leads the curves to shift toward the left, which means higher efficiency is obtained. This finding agrees with the idea that the aerodynamic efficiency becomes greater when the proximity between the aerofoil and the surface is closer. It is also observed that the maximum averaged aerodynamic efficiencies are shifting to a higher angle of attack as the height ride is decreasing.

However, the changes in aerodynamic efficiency probably become an issue. Looking forward to the difference in phase lags between lift and drag, it is almost 2π rad. This conveys that when the lift is at its peak, drag would be at the lowest point or at least near it. Thus, the discrepancy between the highest and the lowest

aerodynamic efficiency could be very distant and the deviation between each other becomes strongly nonlinear.

The increase in the frequency of oscillation also affects the increase in aerodynamic efficiency. However, the influence of amplitude is more pronounced; compare Figure 5-26 and Figure 5-27.

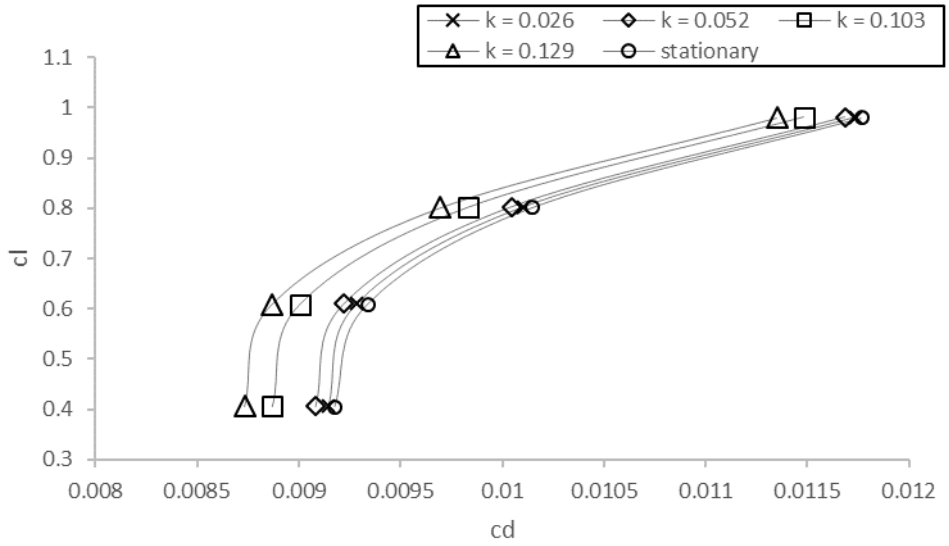

Figure 5-23 Polar curve at h/c = 0.3 ($A/c = 0.05$ for oscillating case)

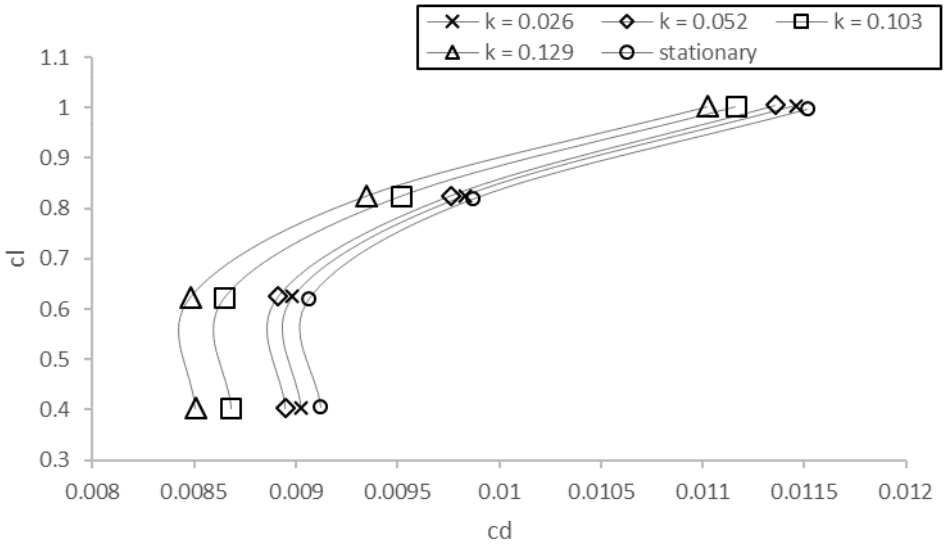

Figure 5-24 Polar curve at h/c = 0.5 ($A/c = 0.05$ for oscillating case)

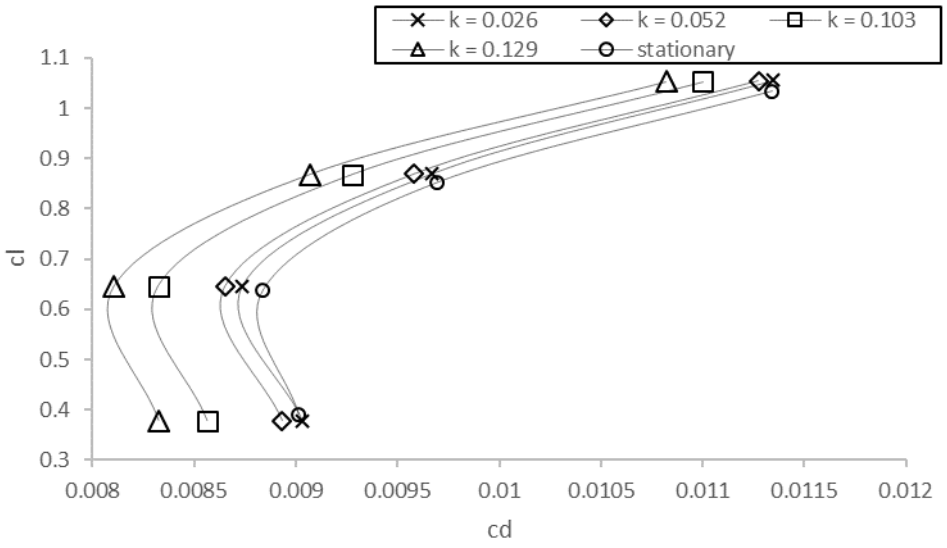

Figure 5-25 Polar curve at h/c = 1.0 ($A/c = 0.05$ for oscillating case)

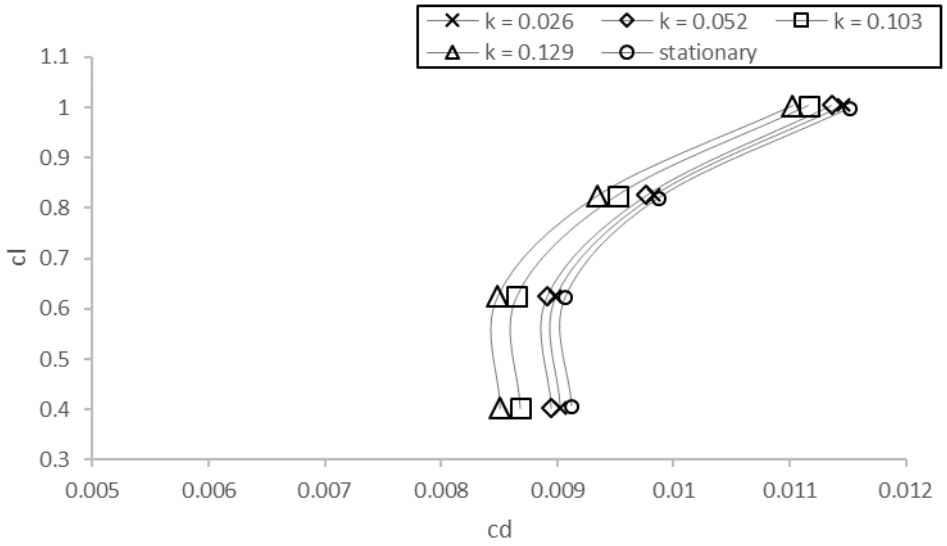

Figure 5-26 Polar curve at h/c = 0.5 ($A/c = 0.05$ for oscillating case)

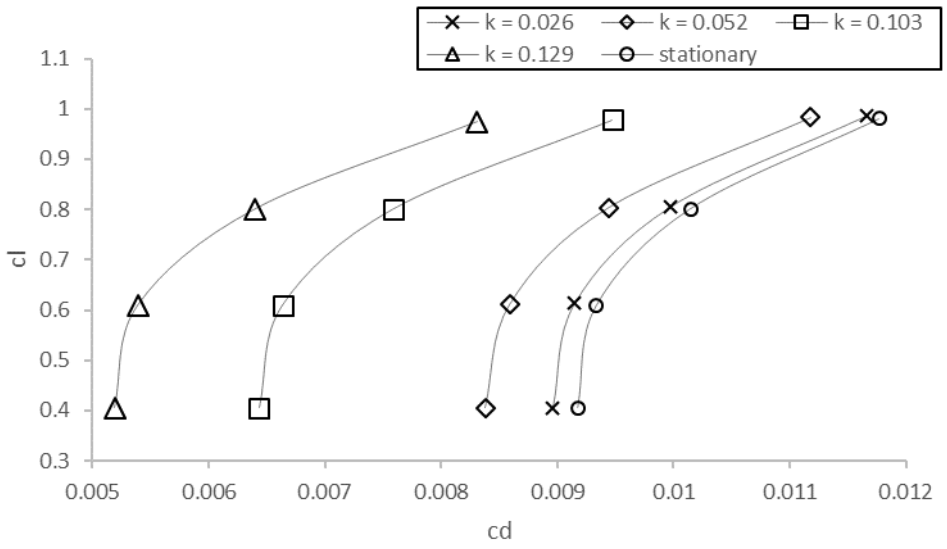

Figure 5-27 Polar curve at h/c = 0.5 ($A/c = 0.15$ for oscillating case)

5.3.4 Pitching moment characteristics

The discussion on pitching moment characteristics in oscillation is not massive as in lift and drag, even though pitching moment exhibits many interesting phenomena. Pitching moment is one of the stability derivatives. The behaviour of the pitching moment right away informs whether the system is statically stable or not.

The first identification from the simulation is that the ride height significantly affects the slope of c_m at $0.25c$ against the angle of attack. For the case of this aerofoil, the decreasing ride height improves the stability behaviour of the aerofoil by imposing a more negative slope. This condition applies for both non-oscillating and oscillating conditions, noting that in this context the averaged values of c_m is considered for the case of oscillation. The presence of the slope also confirms the shift of the centre of pressure, in which the decrease in ride height shifts the centre of pressure backward away from the leading edge.

The effect of the oscillation toward pitching moment is the decrease of its average coefficient. In the weak ground effect region, the decrease in averaged c_m is rather small, see Figure 5-29 and Figure 5-30. However, in the stronger ground effect region, the decrease in pitching moment becomes more pronounced, see Figure 5-28.

Combining the information from the two paragraphs above, one can comprehend that the oscillating aerofoil experiences a significant change in its gradient of c_m curve in the strong ground effect area. Interestingly, however, the decrease in the value seems not to be related with the change in the reduced frequency.

Observing the fluctuation of the c_m through time, the periodic changes give rather consistent averaged values, and even when it comes to the maximum and minimum value, the characteristic might show irregularities.

Figure 5-31 depicts the maximum and minimum pitching moment curve against the angle of attack for various reduced frequencies at $0.3c$ of ride height. At small reduced frequencies ($k = 0.026$ and $k = 0.052$), the discrepancies between maximum and minimum values widen with the increase in angle of attack. On the

other hand, at higher reduced frequencies ($k = 0.103$ and $k = 0.129$), the discrepancies are rather constant. At high angles of attack, the magnitude of maximum and minimum values at small reduced frequencies surpasses magnitude of maximum and minimum values at higher reduced frequencies. The increase in the ride height pushes a similar trend that the discrepancies of maximum and minimum values become more consistent despite the increased angle of attack, see Figure 5-32 and Figure 5-33. One can conclude that in the strong ground effect region the ride height exerts stronger influence than the reduced frequency toward pitching moment. However, as reduced frequencies become higher, there is a point where the oscillation takes control of the behaviour of the pitching moment.

One of the explanations regarding the differences in maximum and minimum pitching moment coefficient is referred as the concept of reduced frequency itself. The definition of unsteadiness of the flow is determined by the range of reduced frequency, k. Based on the criteria, the first two reduced frequencies are in the range of quasi-steady flow and the latter two, which are higher, are considered as unsteady flow.

At quasi-steady flow condition, as experienced by the aerofoil, the effect of ground proximity is still strong. When the c_m is measured at 25% of the aerofoil chord, it will exert the fluctuation of lift to contribute to the reading of pitching moment. This is because 25% chord is no longer functioning as the aerodynamic centre. Thus, the discrepancies of maximum and minimum c_m are visible by the increase in the angle of attack.

On the contrary, at unsteady flow, the effect of oscillation overshadows the influence of height. In many unsteady aerodynamic studies, the oscillation forces the fluctuation of separation point. The importance of this fluctuation most of the time is related to the dynamic stall of a lifting system (McCroskey and Philippe, 1975; Sears, 1976). In a case of the ground effect, the fluctuation of separation gives new insight. It seems that the changes in location of separation have the same rate with the fluctuation of the centre of pressure, which leads to a

consistent range between maximum and minimum c_m, regardless of the increase in the angle of attack.

The effect of the amplitude of oscillation on pitching moment is similar as is its effect toward lift and drag. The range between maximum and minimum c_m is amplified considerably, see Figure 5-34.

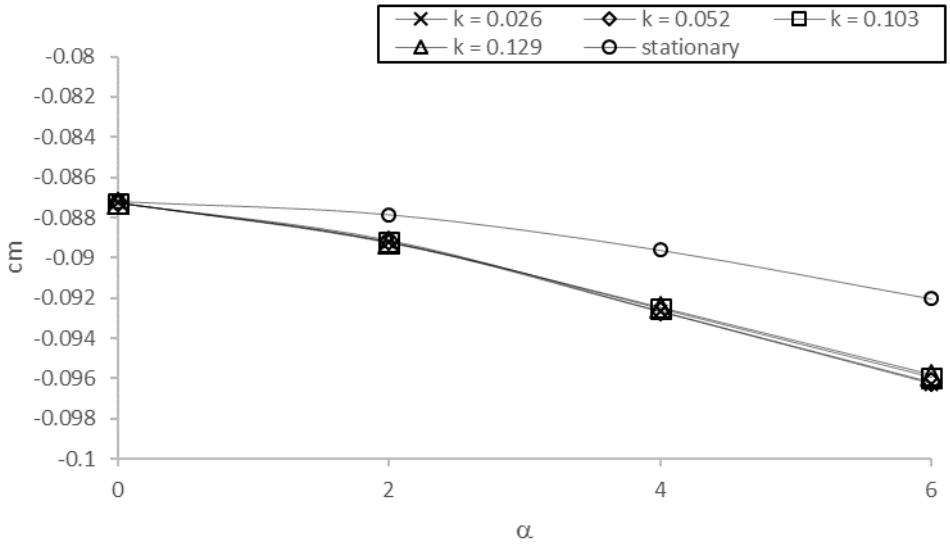

Figure 5-28 Time-averaged c_m at 25%c against α at h/c = 0.3 and A/c = 0.05

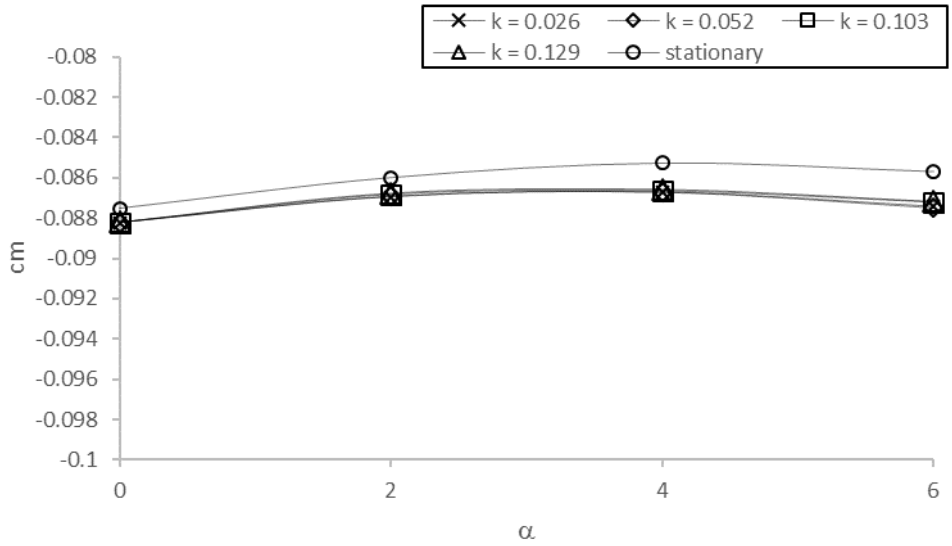

Figure 5-29 Time-averaged c_m at 25%c against α at h/c = 0.5 and A/c = 0.05

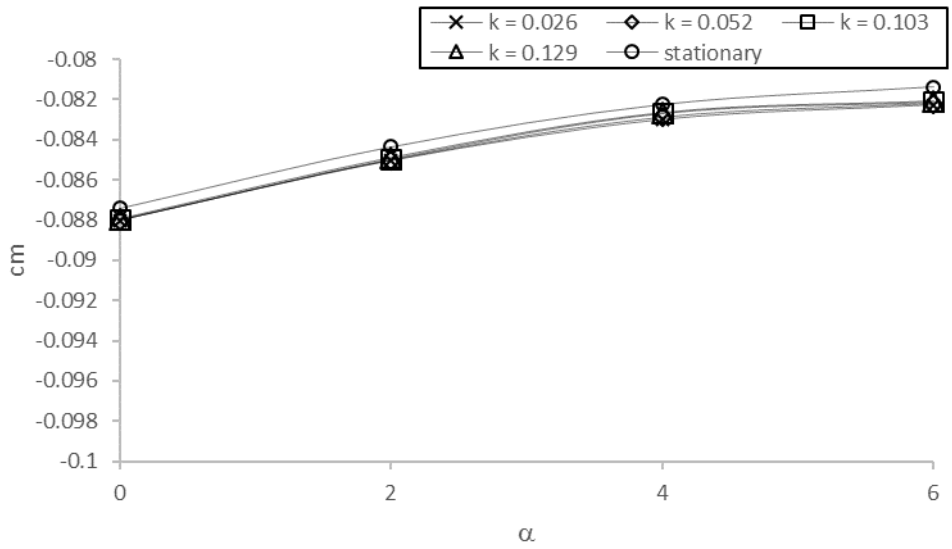

Figure 5-30 Time-averaged c_m at 25%c against α at h/c = 1.0 and A/c = 0.05

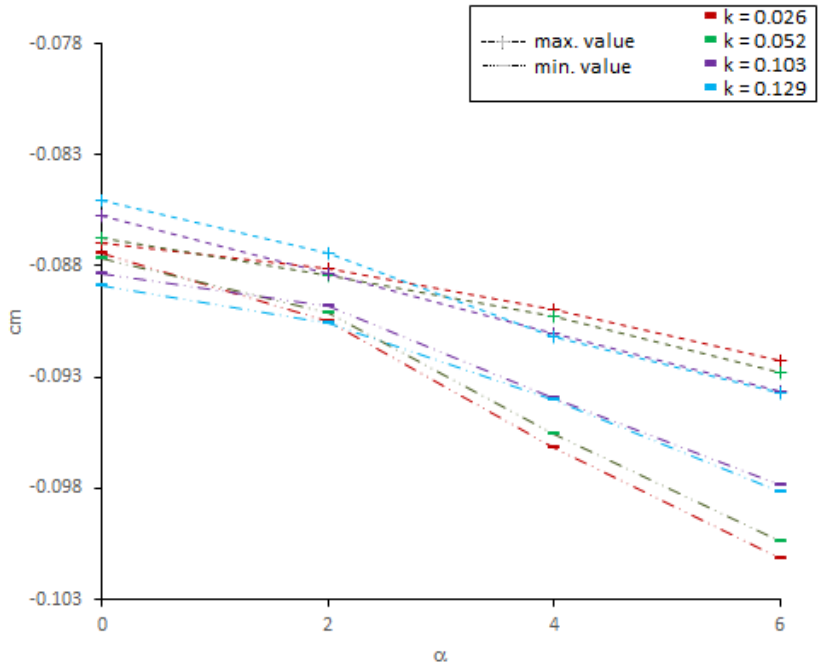

Figure 5-31 Maximum and minimum c_m at 25%c against α at h/c = 0.3 and A/c = 0.05

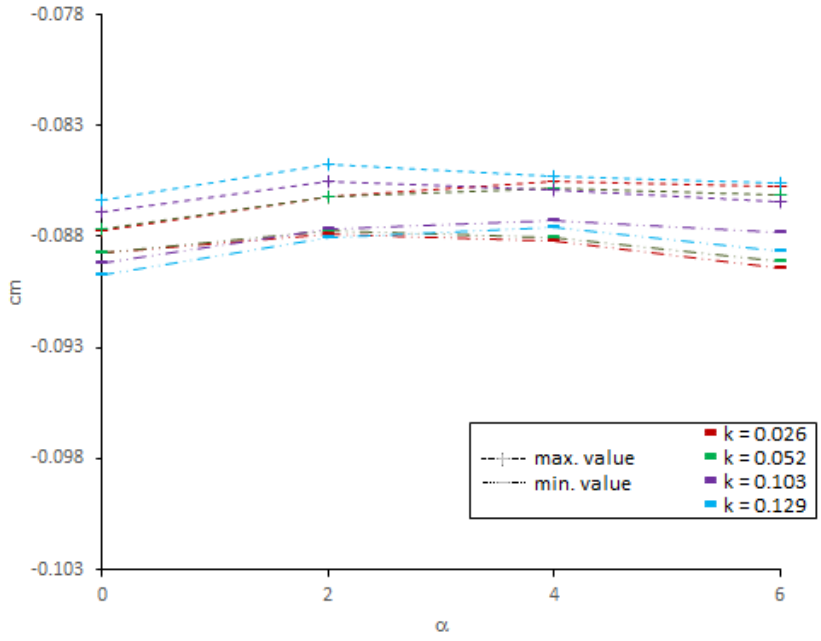

Figure 5-32 Maximum and minimum c_m at 25%c against α at h/c = 0.5 and A/c = 0.05

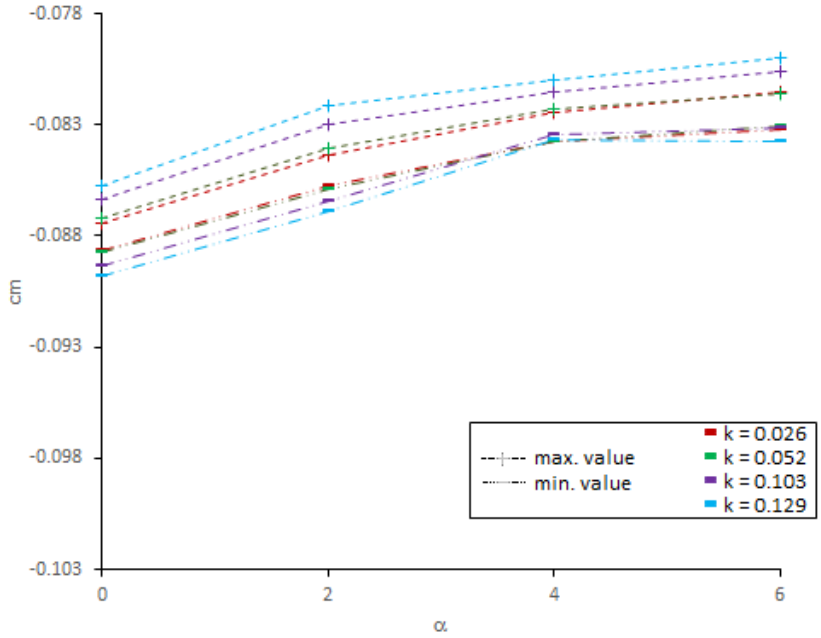

Figure 5-33 Maximum and minimum c_m at 25%c against α at h/c = 1.0 and A/c = 0.05

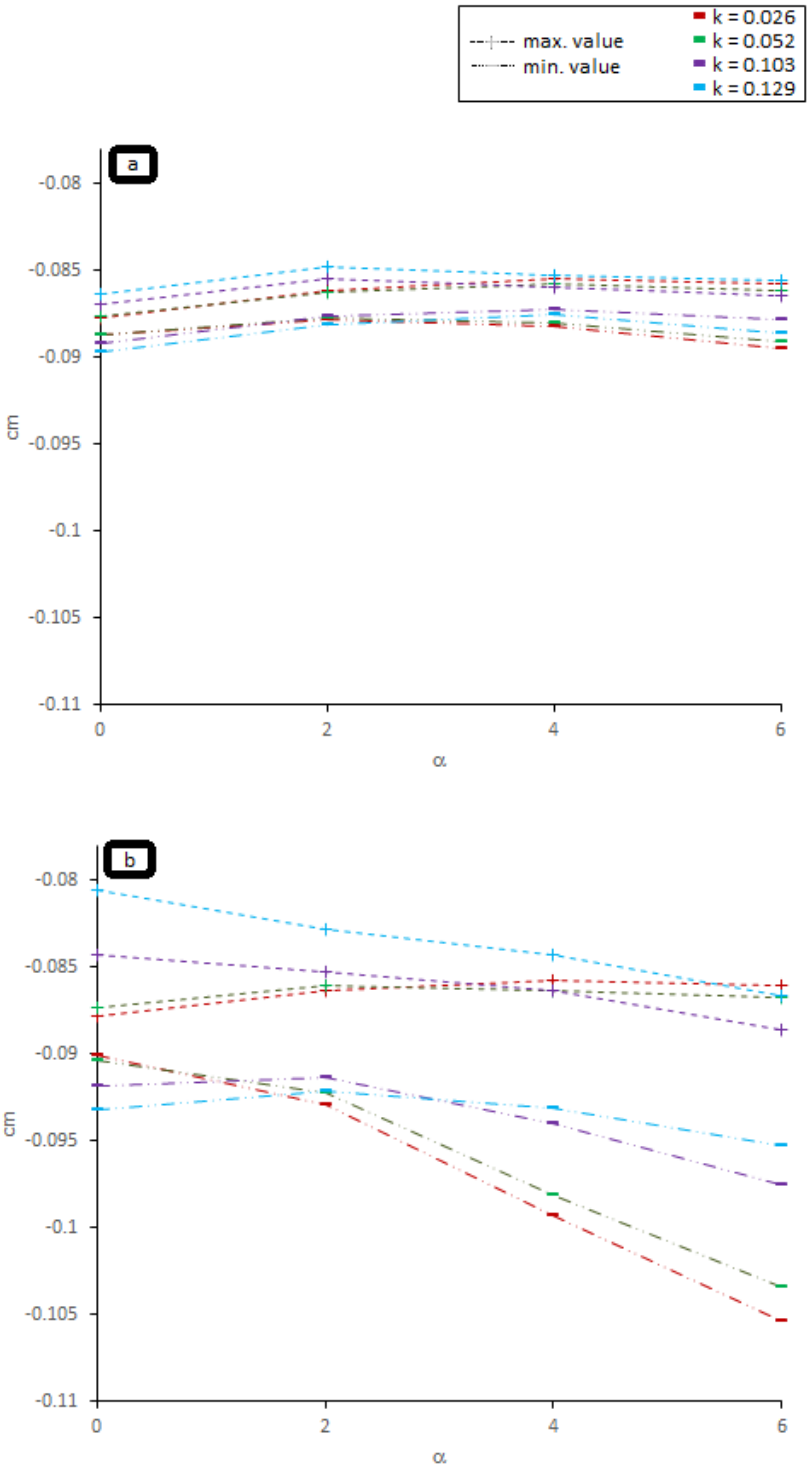

Figure 5-34 Maximum and minimum c_m at 25%c against α at h/c = 0.3 (a. A/c = 0.05; b. A/c = 0.15)

5.4 Main observations

The are several important points that can be drawn from the analysis of the aerodynamic data obtained with the CFD simulation. The main goal is that these data would be used to derive other sets of data including those for the full configuration of Ekranoplan 'Orlyonok' A-90 and eventually its stability derivatives, see Chapter 6. The observed trends are also useful to understand the behaviour of the full-configuration and its stability.

Another important aspect was also about the production of an academic article in the form of a conference paper (Adhynugraha et al., 2016), see Appendix B. The article was presented at the 2016 Applied Aerodynamics Conference in July 2016, in Bristol. Following the presentation, the article was accepted to be published in a journal, but the author decided to temporarily decline any offer to disseminate the results until the accomplishment of this thesis document.

5.5 Conclusion

The unsteady RANS CFD simulations that had been employed to produce the forces of an oscillating aerofoil in the ground effect showed interesting results. The angle of attack and height of the aerofoil, as well as the frequency and amplitude of the oscillatory motion, have noteworthy influences on the aerodynamic characteristics of the aerofoil in the ground effect.

In terms of the lift force, there is no significant difference between the time-averaged lift produced by an oscillating aerofoil and the lift generated by a non-oscillating one. However, the frequency and amplitude of oscillation affect the maximum and minimum lift forces monotonically. Differently, the oscillating aerofoil experiences a decrease in the time-averaged drag compared with the drag of a non-oscillating one. The effects of frequency and amplitude of oscillation on the drag are significant and nonlinear.

The effects of the lift and drag of an oscillating aerofoil are seen in its aerodynamic efficiency. A decrease in height and an increase in amplitude and frequency lead to a higher average efficiency.

The slope of the pitching moment coefficient against the angle of attack, which affects the aerofoil stability, changes with the height ride. The oscillation leads to a more negative pitching moment but without any clear link between the behaviour and the parameters of oscillation, i.e. frequency and amplitude of the oscillation.

6 STABILITY DERIVATIVES

This chapter discusses the estimation of stability derivatives of a WIGE craft configuration, considering the Ekranoplan 'Orlyonok' A90 as a case study. Before this step though, the procedure to estimate all the vehicle aerodynamic characteristics from the two-dimensional aerodynamic data previously obtained is also explained. The chapter encompasses four sections, namely: *(1) Aerodynamics of Ekranoplan in waves*; *(2) Stability derivatives method*; *(3) Stability derivatives analysis*; and *(4) Conclusion*.

6.1 Aerodynamics of Ekranoplan in waves

6.1.1 Some constraints

Following the CFD simulation to obtain aerodynamic data of the oscillating NACA 4412 profile in ground effect, the next attempt was to obtain the three-dimensional aerodynamic data. The three-dimensional aerodynamic data here means the aerodynamics of the wing, as well as the full configuration of a chosen vehicle.

There are two limitations that affect the method to attain the aerodynamics of a full WIGE craft configuration. The first challenge is to choose a configuration to be analysed. Apart from general configuration data, there is limited information publicly available for existing vehicles. The limitation includes the information on aerodynamics and the derivatives of forces and moments acting in the vehicles. A good series of investigations against the limitation is provided for Korea's twenty-passenger WIGE craft, both for aerodynamic (Chun et al., 2000) and stability analysis (Chun and Chang, 2002). However, later it was found that there is an issue in the definition of the height static stability criterion presented in the dynamic analysis. Earlier, a dynamic study was provided by Delhaye (1997). Despite it not being clearly presented in the thesis, Delhaye mentioned the method to obtain aerodynamic data from 2D aerofoil data.

The second issue is related to the method to obtain 3D aerodynamic data. To achieve high fidelity aerodynamic data, either from numerical or experimental

methods, requires a high commitment in time, infrastructures and costs. There are also various approaches that can be used to generate the 3D data. However, the discrepancy from actual condition should be expected. The technique that Delhaye used, as already mentioned in the previous paragraph, is one of the estimation approaches. Delhaye combined the preliminary aircraft design method in Roskam (1989, 1990) and Torenbeek (Torenbeek, 1982) to gain the aerodynamic data of the Ekranoplan 'Orlyonok' A90.

To mitigate the difficulties of both issues, the author decided to adopt the configuration and the approach used by Delhaye (1997). However, there are differences between the present study and Delhaye's in two matters. The first is the aerofoil employed for the study. Delhaye used the Clark-Y aerofoil, and the present study chose the NACA 4412. Both aerofoils are fortunately similar, see Figure 6-1. In the freestream condition, the two aerofoils show similarities in the trends of lift, drag and pitching moment, see Figure 6-2, Figure 6-3, and Figure 6-4. There are, indeed, differences in the values between the aerofoils, where the NACA 4412 is higher in magnitude of lift, drag and pitching moment. In the ground effect, the trends are also expected to be similar with the NACA 4412, being slightly more superior to the Clark-Y aerofoil.

The second difference is related to the source of the estimation method carried out between the two studies. As mentioned, Delhaye attained the data from a combination of semi-empirical formulation in Roskam and Torenbeek. The present study, however, adopted the semi-empirical formulation in Raymer (1999). Raymer proposes a simpler approach that is more straightforward.

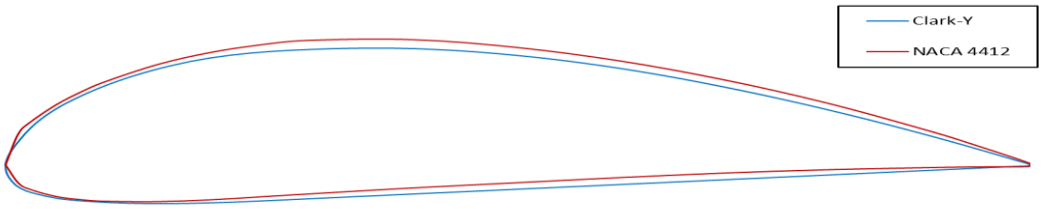

Figure 6-1 Clark-Y and NACA 4412 aerofoil

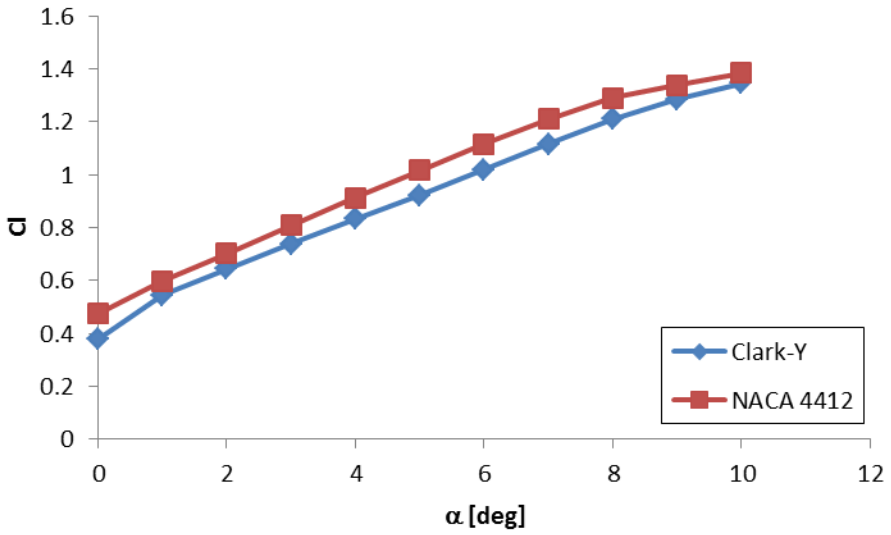

Figure 6-2 c_l against α at $Re = 500,000$ using Xfoil

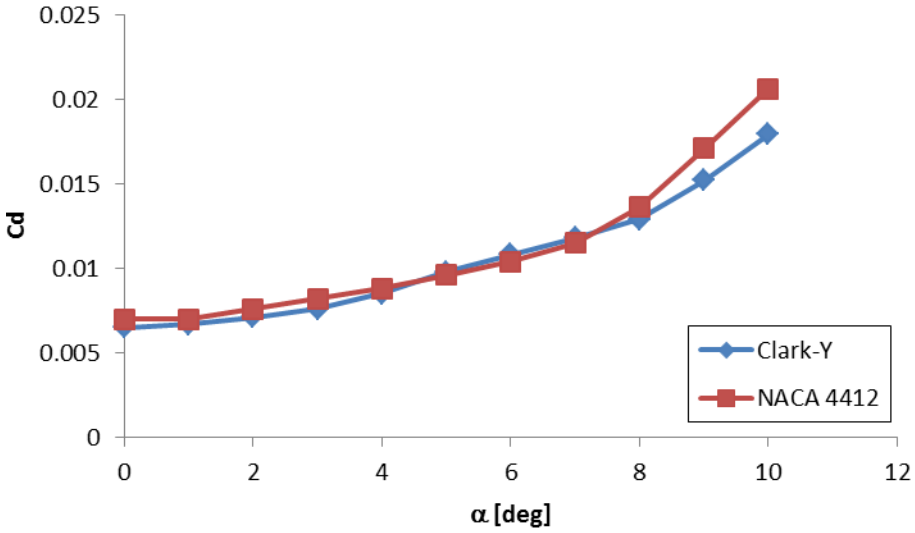

Figure 6-3 c_d against α at $Re = 500,000$ using Xfoil

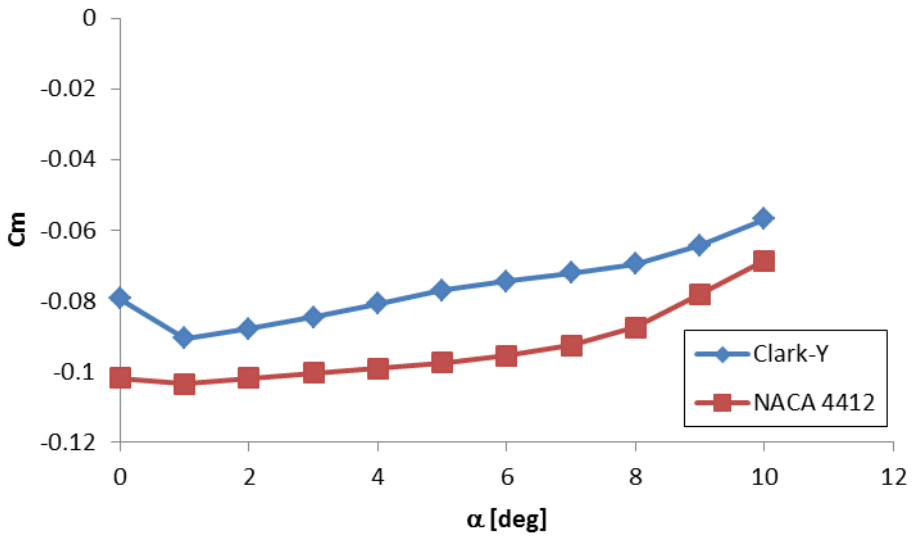

Figure 6-4 c_m against α at $Re = 500,000$ using Xfoil

6.1.2 The configuration

The configuration data of the Ekranoplan 'Orlyonok' A-90 are available in Delhaye (1997) and Yun et al. (2009), among others. However, there are some differences in some parameters in both sources. The first difference is in the weight that Delhaye stated as 130 tonnes and Yun et al. as 140 tonnes. The second difference is in the main wing span length, which Delhaye provided as 31 m, and Yun et al. as 31.5 m. The third difference is in the geometric aspect ratio, which in Delhaye was 3.1 and in Yun et al. it was 3.0.

Delhaye explained that the data correctness might be a concern in the investigation carried out. During the programme, Delhaye managed to communicate with the Central Hydrofoil Bureau to collect some data; however, not all required information was obtained. The difficulty had led Delhaye to estimate some parameters, referring to aerodynamic forces, by using the known information available at that moment. He added the challenging situation in determining the location of the centre of gravity (cg), the inertia and the stability derivatives.

To handle these differences, the author decided to use the data from Delhaye, despite the concern previously mentioned. It should be noted here that the configuration analysed in the present study is specific to the wing-fuselage-tail configuration without any involvement of high lift devices and control systems. The decision is due mainly to two reasons. The first is that Delhaye focused on the dynamic analysis of the Ekranoplan 'Orlyonok' A90, which can be utilised as a comparative study in a no wave condition. The second reason is the semi-empirical approach that Delhaye adopted is also suitable for this present work. As explained in the previous subsection and should be noted, there are some differences between the present study and Delhaye's (1997) work. The reasons for the difference are also presented in the previous section.

The following table gives the flight data of the Ekranoplan 'Orlyonok' A-90 based on Delhaye's (1997) thesis.

Table 6-1 WIGE craft configuration design

Parameter	Measurement	Unit
Mass, m	$130{,}000$	kg
Moment of inertia, I_y	$16{,}971{,}952$	$kg\ m^2$
Cruise speed, U_e	105	m/s
Mach number, Ma	0.31	-
Altitude, h	$sea\ level$	-
Air density, ρ	1.225	kg/m^3
Mean wing chord, mac	9.97	m
Wing area, S	306.4	m^2
Span, b	31	m
Aspect ratio, AR	3.1	-

6.1.3 The aerodynamics

A set of procedures in Raymer (1999) has been used to transform the aerodynamic data of the two-dimensional profile and the configuration data into full-configuration, three-dimensional, aerodynamic data. Obviously, the approach does not give high-fidelity aerodynamic data and can be treated as a rough prediction. However, in a preliminary design stage, the prediction is good enough to summarise the general behaviour of the configuration. Also, to produce high fidelity aerodynamic data of a vehicle was beyond the scope of the present study.

There were several steps to take before one can obtain the aerodynamic data of a full configuration. First, the two-dimensional aerodynamic data previously obtained was transformed into the aerodynamic data of the wing. The second step was to obtain the aerodynamic data for the wing-tail configuration. The tail was assumed to be placed on the ground effect since this is the normal condition of operation in the state considered (cruise). For the tail section, the NACA 0012 was adopted, and its aerodynamic characteristics were taken from Abbott and Doenhoff (1959). The last stage was to obtain the wing-tail-fuselage configuration. This configuration was considered as full setup and disregarded other details that might be available in the original configuration.

Regarding the effect of waves, the following parametric analysis was conducted. Two amplitudes were considered and four frequencies of oscillation for each amplitude. The amplitudes were $0.05c$ and $0.15c$, while the frequencies were $0.25\ rad/s$, $0.50\ rad/s$, $1.00\ rad/s$ and $1.25\ rad/s$. At the amplitude $0.05c$, the calculation was made for three different ride heights, i.e. $h/c = 0.3$, $h/c = 0.5$ and $h/c = 1$. At the amplitude $0.05c$, the calculation was made only for two different ride heights, i.e. $h/c = 0.5$ and $h/c = 1$.

The reason behind the choice of frequency of oscillation is based on the empirical data of typical waves available in WMO's (1998) *Guide to Wave Analysis and Forecasting*, 2nd edn. (2008). After travelling some distance, the typical wave periods are between 5 and 25 seconds which correspond to a particular range of wave frequencies (0.25 and $1.25\ rad/s$). Even though the value of 25 seconds is rather large, it is still considered to see the effect of higher values toward

aerodynamics especially when the system enters dynamic flow regime (examples of phenomena occur are Knoller-Betz / Katzmayr effect and squared sinusoidal drag force, see Subsection 5.3.2). As for the amplitude of motion, it was assumed small to assure that aerodynamic surface does not hit the ground during its oscillation. However, the most important reason for these assumptions is to ensure the applicability of the quasi-static approach of dynamic analysis proposed in Subsection 4.3.4. The ride height followed the set that was run in the CFD simulation.

The aerodynamic data for the Ekranoplan 'Orlyonok' A90 of the current study is available in Appendix G.

6.1.3.1 Lift

The wing of the Ekranoplan 'Orlyonok' A90 is rectangular. This configuration is convenient when applying the adopted semi-empirical formulation. The reason of the convenience mentioned is related to the simplification of involved formulae for rectangular wing. One clear example is the use of formula (6-5) below rather than (6-1) to determine C_{L_α}. Formula (6-5) is simpler due to no sweep angle involved.

The first step taken is to determine the lift-curve slope for the wing-fuselage configuration. Here, a subsonic assumption is adopted, and the slope is formulated as available in Raymer (1999, p.324):

$$C_{L_\alpha} = \frac{2\pi AR}{2 + \sqrt{4 + \frac{AR^2\beta^2}{\mathfrak{N}^2}\left(1 + \frac{\tan^2 \Lambda_{\max t}}{\beta^2}\right)}} \left(\frac{S_{Exp.}}{S_{Ref.}}\right)(FLF) \tag{6-1}$$

where,

$$\mathfrak{N} = \frac{c_{l_\alpha}}{2\pi/\beta} \tag{6-2}$$

$$\beta = \sqrt{1 - Ma^2} \tag{6-3}$$

$$FLF = 1.07(1 + d/b)^2 \tag{6-4}$$

with the components of the equations explained as follows:

- AR is the (effective) aspect ratio of the wing;
- $\Lambda_{\max t}$ is the sweep of the wing at the chord location where the aerofoil is the thickest;
- $S_{Exp.}$ is the exposed wing area, which is the wing reference area without the part being covered by the fuselage;
- $S_{Ref.}$ is the wing of the vehicle without any additional devices, such as endplates and winglets;
- $\Re$ is the aerofoil efficiency;
- c_{l_α} is the slope of aerofoil lift-curve;
- Ma is the Mach number;
- FLF is the lift factor of the fuselage;
- d is diameter of the fuselage; and
- b is the span of the wing.

Due to the rectangular wing of the Ekranoplan, equation (6-1) can be rewritten as:

$$C_{L_\alpha} = \frac{2\pi AR}{2 + \sqrt{4 + \frac{AR^2\beta^2}{\Re^2}}}\left(\frac{S_{Exp.}}{S_{Ref.}}\right)(FLF) \tag{6-5}$$

Knowing the angle of attack with C_L is equal to zero, one derives the curve function, that is:

$$C_L(\alpha) = C_{L_\alpha}\alpha + constant \tag{6-6}$$

Luckily, the angle of attack for $C_L = 0$ is the same for $c_l = 0$.

In the end, the lift is derived from the relationship, as follows:

$$L = \frac{1}{2}\rho_a U_e S_{Ref.} C_L \tag{6-7}$$

where L is lift force, C_L is its coefficient, ρ_a is air density, U_e is cruise speed, and $S_{Ref.}$ is the total surface area.

The same procedure is also applicable to determine the slope of lift-curve of the tail.

6.1.3.2 Drag

The estimation of drag comprises several details. The drag of the vehicle is a summing up of mainly two components, i.e. the parasite drag (C_{D_0}) and lift-induced drag (C_{D_i}). The formulation of the coefficient of drag in a general form is:

$$C_D = C_{D_0} + C_{D_i} \tag{6-8}$$

Both drag components are elaborated further in this part.

Once the drag coefficient is attained, conveniently the drag is derived as:

$$D = \frac{1}{2}\rho_a U_e S_{Ref.} C_D \tag{6-9}$$

where D is lift force, C_D is its coefficient, ρ_a is air density, U_e is cruise speed, and $S_{Ref.}$ is the total surface area.

Parasite drag

Starting with parasite drag, there are two ways to estimate the drag. The parasite drag itself is the drag that is attached to the configuration without induction from other factors due to the operation. Occasionally, it is also addressed as zero-lift drag, C_{D_0}.

The first method is to use an equivalent skin-friction method. The formulation (Raymer, 1999, p.340) is as follows:

$$C_{D_0} = C_{f_e} \frac{S_{Wet.}}{S_{Ref.}} \tag{6-10}$$

The component of C_{f_e} is described as equivalent skin friction coefficient, which, in this manner, includes both skin-friction and separation drag. The value of the coefficient varies, depending on the configuration. For WIGE craft, there is no particular value for this coefficient. However, several options are available that range from 0.0040 to 0.0065. This range (Raymer, 1999, p.341) is initially designated for light aircraft (0.0045 – twin propulsion; 0.0055 – single propulsion) and seaplanes (0.0040 – jet; 0.0065 – propeller). The component $S_{Wet.}$ explains the area exposure to the air, while $S_{Ref.}$ is about the total surface area of the vehicle.

The approach is impractical as there is no information available about the two components of the surface area mentioned above. This leads to the use of the second approach: the component build-up method.

The component build-up method does the estimation of the parasite drag of each component of the vehicle. The formulation for this technique (Raymer, 1999, p.342) is as follows:

$$C_{D_0} = \frac{\sum \left(C_{f_c} FF_c Q_c S_{Wet.c} \right)}{S_{Ref.}} + C_{D_{Misc.}} + C_{D_{L\&P}} \tag{6-11}$$

where

- C_{f_c} is the flat-plate skin-friction drag coefficient of a component. The subscript ‘c’ is replaceable with the components of the vehicle, e.g. wing, tail, fuselage, nacelle, and so on;
- FF_c is the form factor of a component that estimates the pressure drag due to the viscous separation;
- Q_c is the factor that calculates the interference effect on the component drag. The range of this parameter varies, depend on the component. For wing and fuselage, the value is equal to 1.0 in most cases;
- $S_{Wet.c}$ is the wetted area of a component;

- $S_{Ref.}$ is the total area of the craft;
- $C_{D_{Misc.}}$ is miscellaneous drag components for special features such as flaps, unretracted landing gear, and so on. In the present study, this part is negligible;
- $C_{D_{L\&P}}$ is the drag due to the contribution of leakages and protuberances. This part is also negligible for the present case.

The Reynolds number is the central factor in determining the friction coefficient, C_f. It should be noted that in calculating the coefficient of a component, the Reynolds number being used is the local Reynolds number, not the full configuration one. However, to be cautious, there is a difference between the estimation of the coefficient in laminar and turbulent flow.

The formulation for the laminar flow (Raymer, 1999, p.343) is as follows:

$$C_f = \frac{1.328}{\sqrt{Re}} \tag{6-12}$$

and for the turbulent flow (Raymer, 1999, p.343), it is as follows:

$$C_f = \frac{0.455}{(\log_{10} Re)^{2.58}(1 + 0.144Ma^2)^{0.65}} \tag{6-13}$$

The present study adopted the formulation for turbulent flow. However, due to the turbulent flow, the friction coefficient may be higher than what is produced by equation (6-13). Hence, an adjustment is needed by multiplying a factor to the Reynold's number. A more practical approach is available by using a 'fictitious' Reynold's number rather than the actual Reynolds number. In the case of the subsonic regime, the 'fictitious' Reynolds number as available in Raymer (1999, p.344), is given by:

$$Re_{cut} = 38.21\left(\frac{\ell}{SR}\right)^{1.053} \tag{6-14}$$

where,

- Re_{cut} is the fictitious cut-off Reynolds number of a component;
- ℓ is the reference length of the component being calculated, e.g. wing mac, tail mac, and the length of fuselage;
- SR is the skin roughness factor for which the value depends on the material or treatment toward the component being measured. The present study assumed all main components to be smoothly painted, thus the factor is 2.08×10^{-5}.

After determining the skin-friction coefficient, the form factor also needs to be defined. Unfortunately, the formulation may differ between one component and another (Raymer, 1999, p.344). For wing and tail, the formulation is as follows:

$$FF = \left[1 + \frac{0.6}{(x/c)_m}\left(\frac{t}{c}\right) + 100\left(\frac{t}{c}\right)^4\right][1.34Ma^{0.18}(\cos\Lambda_{\max t})^{0.28}] \qquad (6\text{-}15)$$

where,

- $(x/c)_m$ is the chord wise location of the aerofoil maximum thickness point. The parameter is given by $0.3c$ as the NACA 4412 is one of the low-speed aerofoils;
- (t/c) is the thickness ratio against chord length;
- Ma is Mach number;
- $\Lambda_{\max t}$ is the sweep of the wing at the chord location where the aerofoil is the thickest.

As the wing configuration in the Ekranoplan 'Orlyonok' A90 is considered rectangular, the equation (6-15) becomes:

$$FF = \left[1 + \frac{0.6}{(x/c)_m}\left(\frac{t}{c}\right) + 100\left(\frac{t}{c}\right)^4\right][1.34Ma^{0.18}] \qquad (6\text{-}16)$$

For the fuselage, the form factor is:

$$FF = 1 + \frac{60}{\cancel{\ell}^3} + \frac{\cancel{\ell}}{400} \qquad (6\text{-}17)$$

where,

$$f = \frac{\ell}{d} \tag{6-18}$$

with ℓ being the length of the fuselage and d is the diameter of the fuselage.

Lift-induced drag

Lift-induced drag, or simply called induced drag, is a component of the aerodynamic drag force that occurs due to the redirection of the airflow as the system moves within the airflow.

The formulation for induced drag is:

$$C_{D_i} = K{C_L}^2 \tag{6-19}$$

with C_{D_i} being the induced drag coefficient, C_L is lift coefficient, and K is the drag-due-to-lift factor.

The formulation for K in subsonic flow regime is as follows:

$$K = \frac{1}{\pi\, AR\, e} \tag{6-20}$$

With AR being the aspect ratio of the wing (or tail), and e is Oswald number.

The e for straight wing, like the Ekranoplan 'Orylonok', is given, as available in Raymer (1999, p.361), by:

$$e = 1.78(1 - 0.045\, AR^{0.68}) - 0.64 \tag{6-21}$$

In ground effect, the induced drag of a WIGE vehicle decreases by decreasing ride height. To determine the decrease, one needs to define the effective drag-due-to-lift factor, K_{eff}, to be used in equation (6-19). K_{eff} (Raymer, 1999, p.367) is given by:

$$K_{eff} = \frac{33(h/b)^{1.5}}{1 + 33(h/b)^{1.5}} K \quad (6\text{-}22)$$

with h being ride height and b is wing span.

6.1.3.3 Pitching moment

Static pitch stability of the vehicle is determined by the slope of the pitching moment curve against the angle of attack. The formulation of the criterion involves some detail, including the definition of the slope of wing lift curve and horizontal tail lift curve, pitching moment coefficient of the fuselage, and arms of lift forces relative to the centre of gravity. However, following the stability margin presented in Delhaye (1997), the formulation can be simplified as:

$$C_{m_\alpha} = C_{L_\alpha} SM \quad (6\text{-}23)$$

where, C_{m_α} is the slope of pitching moment coefficient against the angle of attack of the craft, C_{L_α} is the slope of lift coefficient against the angle of attack of the wing – available in the vehicle's lift force estimation, and SM is the static margin of the vehicle, given by a value of 0.15.

Delhaye set the static margin as a prediction rather than a measurement. This is understandable because further information of the vehicle was not available. Despite running three different static margins, the present study only takes one static margin, which Delhaye explained in detail in his thesis.

6.1.4 Further investigation on Delhaye's (1997) data

The initial expectation was there would be no significant difference in the aerodynamic and stability derivatives data in the present study from what Delhaye obtained. This expectation was due to the similarity of the two-dimensional profiles between the two studies (NACA 4412 against Clark-Y aerofoils). However, significant differences in some aspects of stability derivatives, especially the normal force due to the velocity, Z_u, were identified. To achieve the

same values of Z_u, the current work produced it at an angle of attack almost twice as what in Delhaye's work.

The differences led the author to conduct further study on Delhaye's work to investigate the main cause of the discrepancies, and it was found that the aerodynamic lift of the full Ekranoplan 'Orlyonok' A90 configuration gives a very high value. It is peculiar because usually the aerodynamic characteristics of a full vehicle configuration are less than its aerofoil aerodynamic characteristic, although may be slightly higher than its wing aerodynamic characteristic due to the contribution of the fuselage.

There is no exact data to validate against the Delhaye 3D vehicle data. However, a study carried out by Kumar (1968) illustrates that for a Clark-Y wing configuration with $AR = 2$ at $h/c = 0.5$ and $\alpha = 5$, the $C_L \approx 0.64$. The addition of endplates increases the lift significantly, and this proved by Kumar demonstrates the wing configuration with endplates gives $C_L \approx 1.04$ for the same condition. Comparing Kumar's investigation with full configuration with the full configuration adopted by Delhaye ($AR = 3.1$), the $C_L \approx 0.65$ and at the $h/c = 0.5$ is given by $\alpha = 1.8°$. Based on this, it is likely that Delhaye has considered the effect of endplates in the calculation. As the author tried to reformulate the Kumar case to get a lift slope similar to the vehicle configuration used by Delhaye, it turned out at $\alpha = 1.8°$ and $h/c = 0.5$, the $C_L \approx 0.64$.

With this piece of information, the author assumed that there are configuration differences between the present case and Delhaye's (1997) case. Therefore, it is incorrect to compare the present study and the case of Delhaye without noting these differences.

From this further investigation, one can also regard the effectiveness of endplates in producing higher aerodynamic lift for a vehicle.

6.2 Stability derivatives method

This study adopted the UK-style to derive the stability derivatives. The values of the stability derivatives, as shown in Appendix I, are influenced by both the ride height and the oscillation parameters, i.e. the frequency and the amplitude.

Due to the relatively low Mach number of the state of equilibrium at which the stability derivatives were evaluated, and the use of the 'quasi-static' dynamic analysis afterwards, the compressibility effects have been disregarded. This, however, may raise a concern when this disregard is applied for the case with high frequencies, as some literature has mentioned the effect of compressibility in the case of oscillation. Table 6-2 shows the stability derivatives based on the UK-style with some remarks about the setting for the present study.

Table 6-2 Longitudinal aerodynamic stability derivatives

Derivative	Expression		Remarks
X_u	$-2C_D - U_e\frac{\partial C_D}{\partial U} + \frac{2}{\rho_a U_e S}\frac{\partial \tau}{\partial U}$	(6-24)	The component $-U_e\frac{\partial C_D}{\partial U} + \frac{2}{\rho_a U_e S}\frac{\partial \tau}{\partial U}$ is set at zero due to the neglecting of compressibility
X_w	$C_L - \frac{\partial C_D}{\partial \alpha}$	(6-25)	
X_q	$-\overline{U}_{tail} - \frac{\partial C_{D\,tail}}{\partial \alpha_{tail}}$	(6-26)	Negligible
$X_{\dot{w}}$	$-\overline{U}_{tail} - \frac{\partial C_{D\,tail}}{\partial \alpha_{tail}}\frac{\partial \varepsilon}{\partial \alpha} \equiv X_q\frac{\partial \varepsilon}{\partial \alpha}$	(6-27)	Negligible
X_h	$-\frac{\partial C_D}{\partial (h/c)}$	(6-28)	
Z_u	$-2C_L - U_e\frac{\partial C_L}{\partial U}$	(6-29)	Made as a constant at 1.2943 (as set by Delhaye)

			The component $-U_e \frac{\partial C_L}{\partial U}$ is set at zero due to the neglecting of compressibility
Z_w	$-C_D - \frac{\partial C_L}{\partial \alpha}$	(6-30)	
Z_q	$-\bar{U}_{tail} a_1$	(6-31)	Made as a constant at -2.858 (as set by Delhaye)
$Z_{\dot{w}}$	$-\bar{U}_{tail} a_1 \frac{\partial \varepsilon}{\partial \alpha} \equiv Z_q \frac{\partial \varepsilon}{\partial \alpha}$	(6-32)	
Z_h	$-\frac{\partial C_L}{\partial (h/c)}$	(6-33)	
M_u	$U_e \frac{\partial C_m}{\partial U}$	(6-34)	Negligible
M_w	$\frac{dC_m}{d\alpha}$	(6-35)	Static pitch stability criteria
M_q	$-\bar{U}_{tail} a_1 \frac{\ell_{tail}}{\bar{\bar{c}}}$	(6-36)	Made as a constant at -6.14 (as set by Delhaye)
$M_{\dot{w}}$	$-\bar{U}_{tail} a_1 \frac{\ell_{tail}}{\bar{\bar{c}}} \equiv M_q \frac{\partial \varepsilon}{\partial \alpha}$	(6-37)	
M_h	$-\frac{\partial C_m}{\partial (h/c)}$	(6-38)	

6.3 Stability derivatives analysis

The impact of ride height on the stability derivatives was discussed by Delhaye (1997). This section will expand that analysis by including the oscillation parameters, i.e. the frequency and the amplitude of oscillation.

Figure 6-5 through to Figure 6-12 confirm what has been stated by Delhaye on the effect of ride height on the stability derivatives. However, in addition to this,

one can also identify the impact of oscillation on the stability derivatives; the value of the stability derivatives oscillates in a periodic manner, like the motion and the forces produced by the motion.

Figure 6-5 gives a depiction of the derivatives of axial force with respect to velocity, X_u. Its module decreases decreasing ride height; this is since the drag decreases by decreasing ride height. Also, the value of X_u is oscillatory as shown over one full wavelength.

The derivative of axial force with respect to the incidence, X_w, increases by the decrease in ride height. This phenomenon is depicted in Figure 6-6 and can be explained by the increase of lift by decreasing ground proximity.

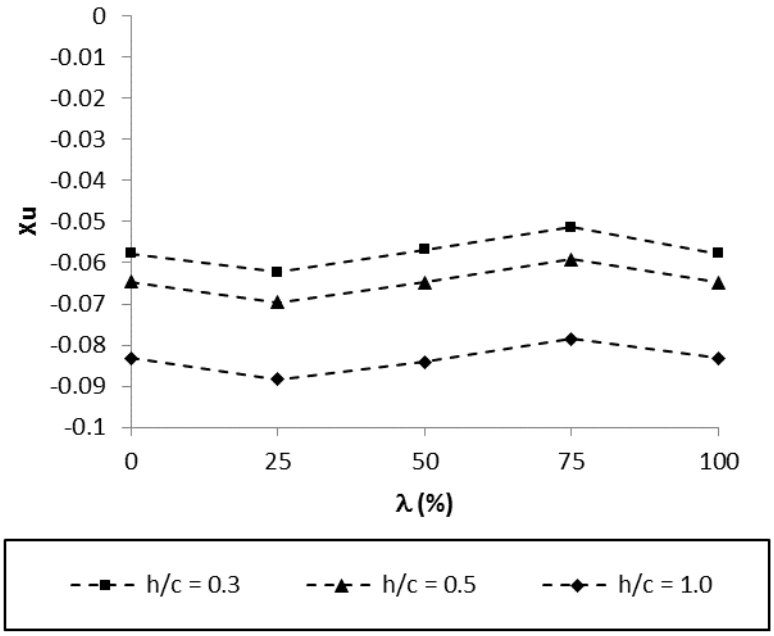

Figure 6-5 X_u for different ride heights ($\alpha = 4°$; $k = 0.026$; $A/c = 0.05$)

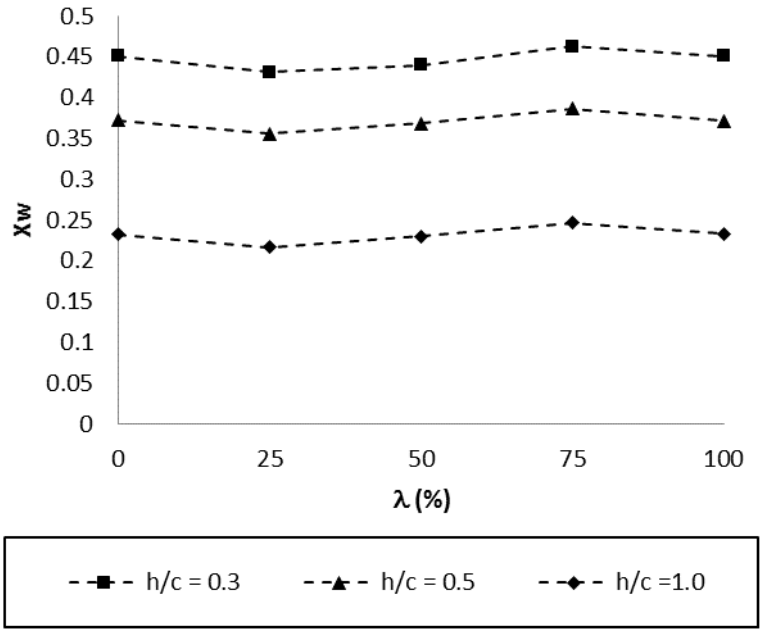

Figure 6-6 X_w for different ride heights ($\alpha = 4°$; $k = 0.026$; $A/c = 0.05$)

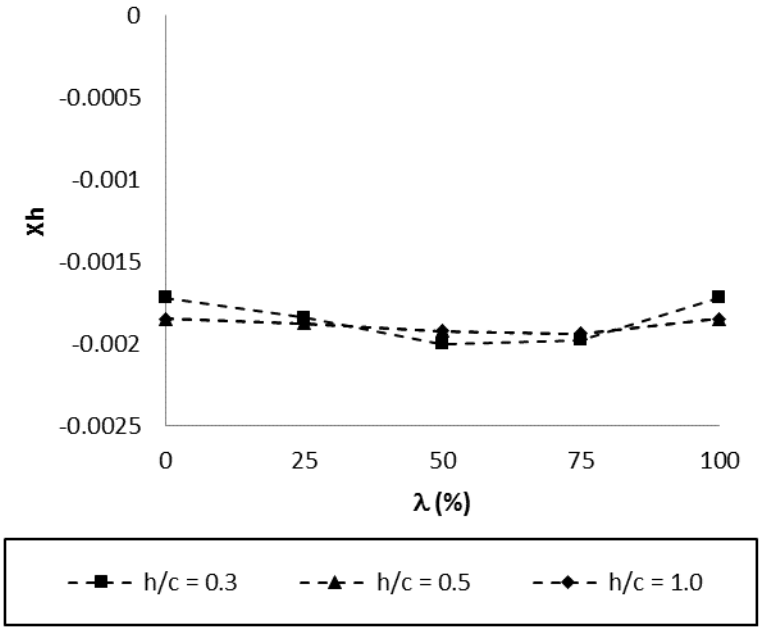

Figure 6-7 X_h for different ride heights ($\alpha = 4°$; $k = 0.026$; $A/c = 0.05$)

A slight fluctuation, Figure 6-7, is visible in the trend of the derivative of axial force with respect to the ride height, X_h, at the ride height of $0.3c$. On the contrary, if

the ride heights are $0.5c$ and c, it is rather constant along the wavelength, and this shows the effect of oscillation at these ride height is weak for this derivative. However, one may expect that the decreasing ride height amplifies the effect of oscillation on the derivatives, which can be identified with the fluctuation of the derivatives in the strong ground effect region (at $h/c = 0.3$ in this case).

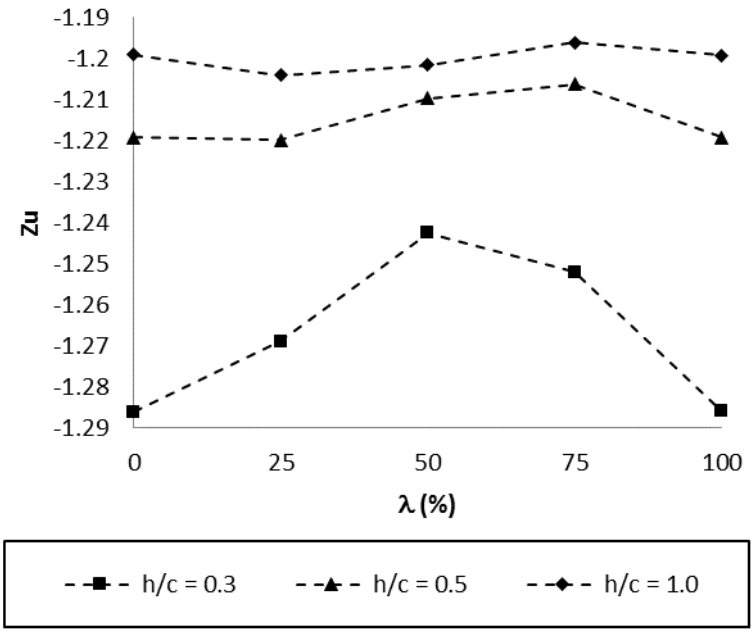

Figure 6-8 Z_u for different ride heights ($\alpha = 4°$; $k = 0.026$; $A/c = 0.05$)

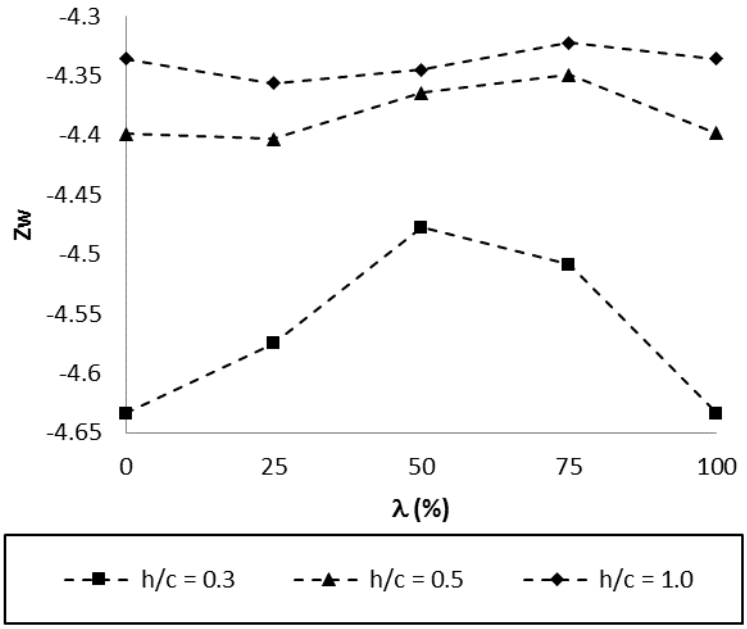

Figure 6-9 Z_w for different ride heights ($\alpha = 4°$; $k = 0.026$; $A/c = 0.05$)

The derivatives of the normal (vertical) force with respect to the horizontal velocity, Z_u, and with respect to the vertical velocity, Z_w, as depicted in Figure 6-8 and Figure 6-9, show a similar trend, i.e. their magnitudes increase by decreasing ride height. The trends are due to the increase in lift by decreasing height. For Z_w, when referring to the formulation of the derivatives, the drag also makes a contribution to the values. However, the impact of the slope of the lift coefficient against the angle of attack outweighs the contribution of the drag coefficient, thus the trend of the derivative seems more related to the trend of the lift. From both figures, one also can identify that there is a movement of the peak from 75% to 50% as the ride height decreases. This phenomenon can be traced back to the aerodynamic characteristics of the lift. Observing the phase lag of the lift coefficient of the vehicle, the trough of the coefficient occurs at 50% of the wavelength for 0.3 of ride height. However, by increasing height the trough shifts to 75% of the wavelength or moves to the right. It should be noted that the characteristic between the aerofoil and the full configuration in terms of the phase lags are not necessarily similar. In the aerofoil investigation, the phase lags tend to shift to the left by increasing height. The impact of phase lags of the

aerodynamic forces on the stability derivatives needs further investigation. The characteristics of drag force give no contribution to this phenomenon as the trend of it does not change by the alteration of the ride height. Interestingly, as depicted in Figure 6-11, the derivatives of pitching moment due to the incidence, M_w, also has a similar trend with the two derivatives just mentioned. If one traces back the aerodynamics of the Ekranoplan, the lift and the pitching moment has always the same trends. This similarity explains why these three derivatives have the same trends. Aside from the identification of the trends, one can straight away conclude that the oscillation has an amplifying effect on the derivatives by observing the figures.

The derivatives of normal force due to the ride height, Z_h, and the derivatives of pitching moment due to the ride height, M_h, show similar trends, see Figure 6-10 and Figure 6-12. The ride height clearly has nonlinear influence towards these derivatives. Unfortunately, the number of data produced by the present study is not sufficient to determine the trend of impact. Allegedly, the trend has an exponential-like relationship, as shown in the aerofoil, wing and full configuration aerodynamic data against ride height. This also can be concluded from the big leap between the case of $h/c = 0.3$ and $h/c = 0.5$. Also, the difference between $h/c = 0.5$ and $h/c = 1.0$ is small enough and almost overlap each other. All these circumstances exhibit a rapid decrease of the derivative value before it became relatively constant as the vehicle increases in its ride height.

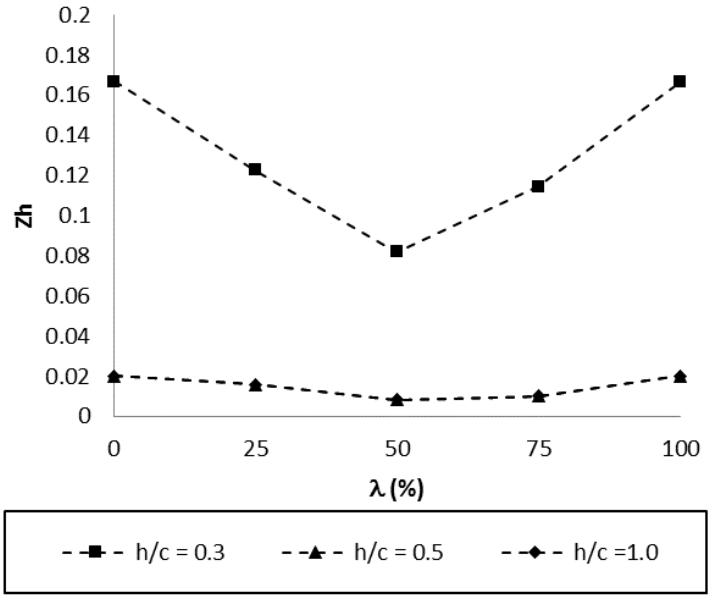

Figure 6-10 Z_h for different ride heights ($\alpha = 4°$; $k = 0.026$; $A/c = 0.05$)

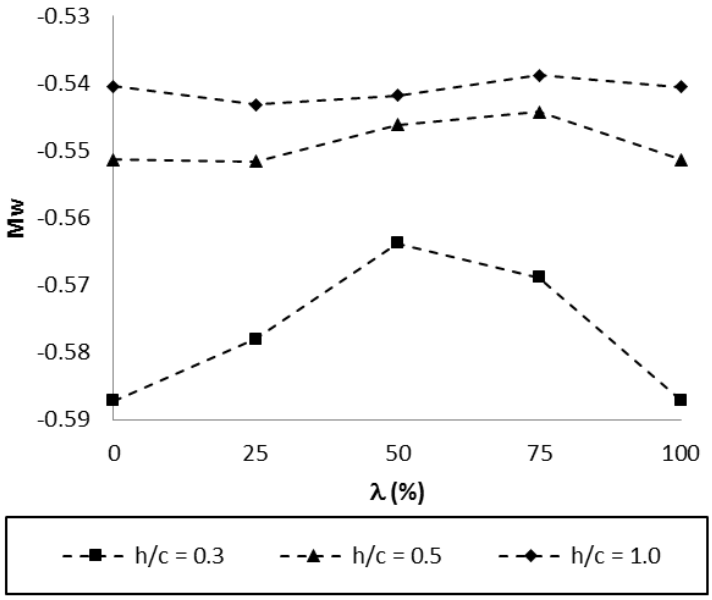

Figure 6-11 M_w for different ride heights ($\alpha = 4°$; $k = 0.026$; $A/c = 0.05$)

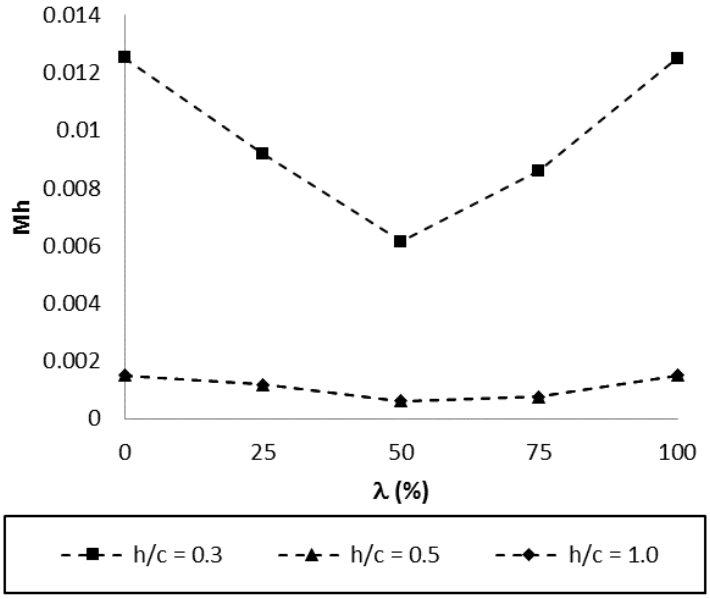

Figure 6-12 M_h for different ride heights ($\alpha = 4°$; $k = 0.026$; $A/c = 0.05$)

Regarding the phase lags, three main characteristics can be highlighted. Firstly, all the derivatives with respect to the ride height have phase lags of about $0\,rad/s$, and this means that there is no lag between the motion and the derivatives' value. Secondly, the derivatives of the axial force, i.e. X_u and X_w, have approximately $\pi/2\,rad/s$ phase lags. Thirdly, the derivatives of the normal force and of the pitching moment, i.e. Z_u, X_w and M_w, experience different phase lags depending on to the combination of the ride height and the oscillation.

The differences in the phase lag exhibit a variety of physical conditions of the characteristic of motion. In case of derivatives with respect to the ride height, no lag between the value of the derivatives and the motion is expected, due to the quasi-static method applied to determine the value of the derivatives. However, there is an exception in the derivative X_h, which by increasing reduced frequency, the derivative starts forming $\pi/2\,rad/s$ phase difference, see Figure 6-15. This means that the formation of the derivative is controlled by the ride height at low reduced frequencies, and by the oscillation at higher reduced frequencies. Differently, for Z_h and M_h, only the ride height controls the formation of the

derivatives. The second characteristic is about the $\pi/2\,rad/s$ phase difference indicated by X_u and X_w. The trend is similar to the phase lag of the drag forces during the motion. Lastly, the derivatives of the normal force and of the pitching moment exhibit more complexity, as parameters like ride height and reduced frequency affect the formation of the derivatives. Further investigation may be needed to determine the effect of each parameter separately.

Aside from the aforementioned derivatives, there are also other derivatives that are supposed to be considered. However, those derivatives were set at constant values following the dataset used by Delhaye. The constant values based on the nature of the derivatives are shown by the axial force derivative with respect to pitch rate, X_q, and the axial force derivative with respect to downwash lag, $X_{\dot{w}}$. The two derivatives demonstrate the effect of tailplane drag. However, the contribution of the drag is disregarded leading to the zero-value derivatives. Another derivative that was set as zero is the pitching moment derivative with respect to velocity, M_u. This derivative is Mach number dependent, but usually very low at low speed.

The illustration of the effect of frequency of oscillation towards stability derivatives can be seen in Figure 6-13 through to Figure 6-20.

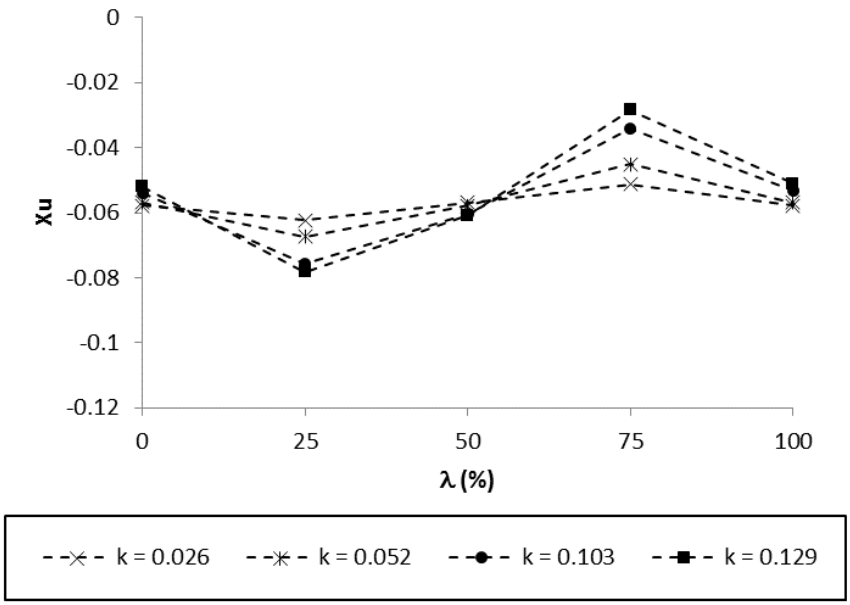

Figure 6-13 X_u for different reduced frequencies ($\alpha = 4°$; $h/c = 0.3$; $A/c = 0.05$)

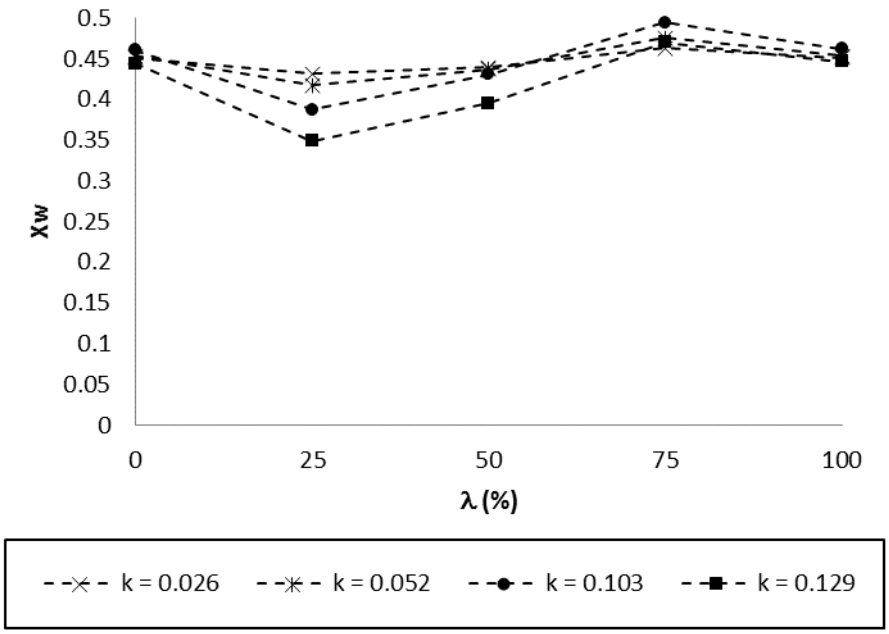

Figure 6-14 X_w for different reduced frequencies ($\alpha = 4°$; $h/c = 0.3$; $A/c = 0.05$)

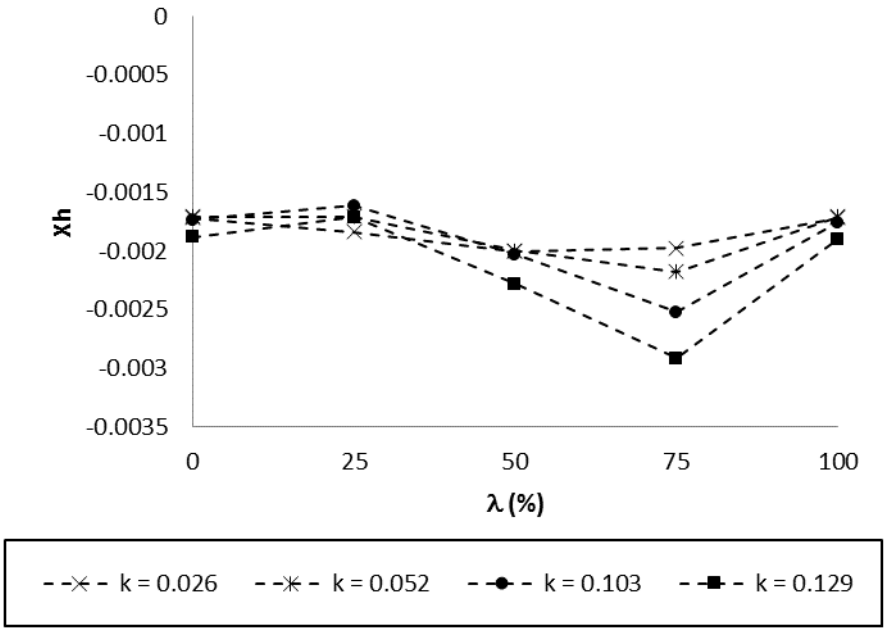

Figure 6-15 X_h for different reduced frequencies ($\alpha = 4°$; $h/c = 0.3$; $A/c = 0.05$)

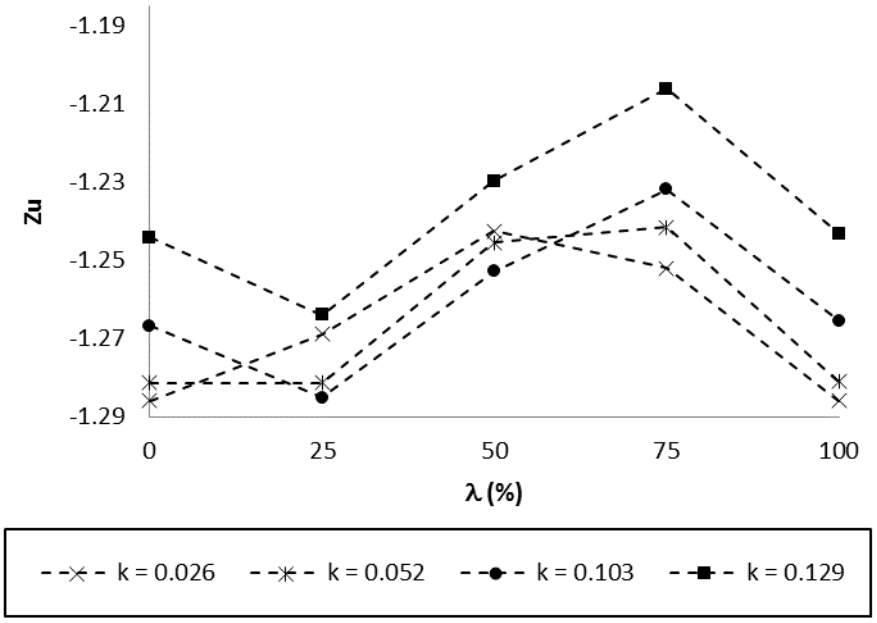

Figure 6-16 Z_u for different reduced frequencies ($\alpha = 4°$; $h/c = 0.3$; $A/c = 0.05$)

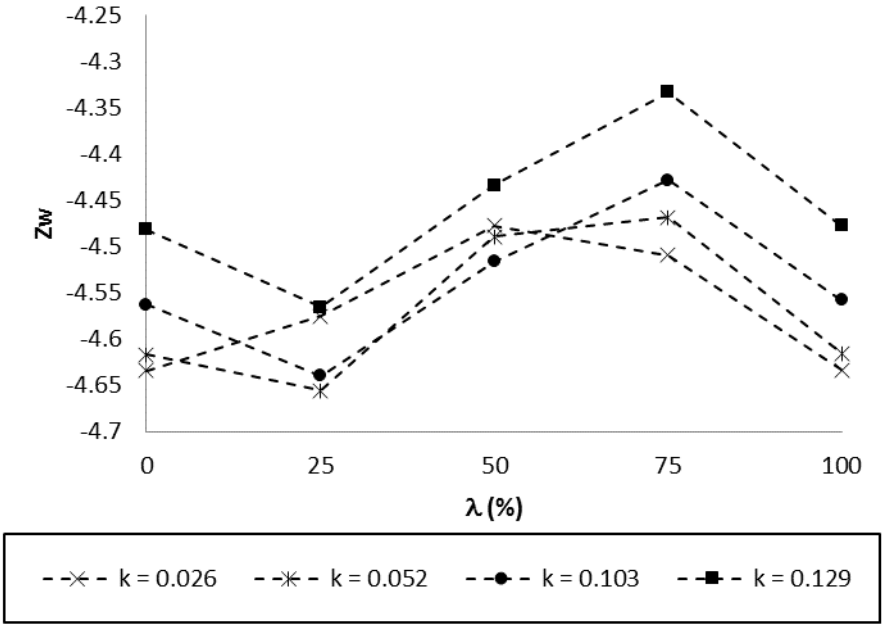

Figure 6-17 Z_w for different reduced frequencies ($\alpha = 4°$; $h/c = 0.3$; $A/c = 0.05$)

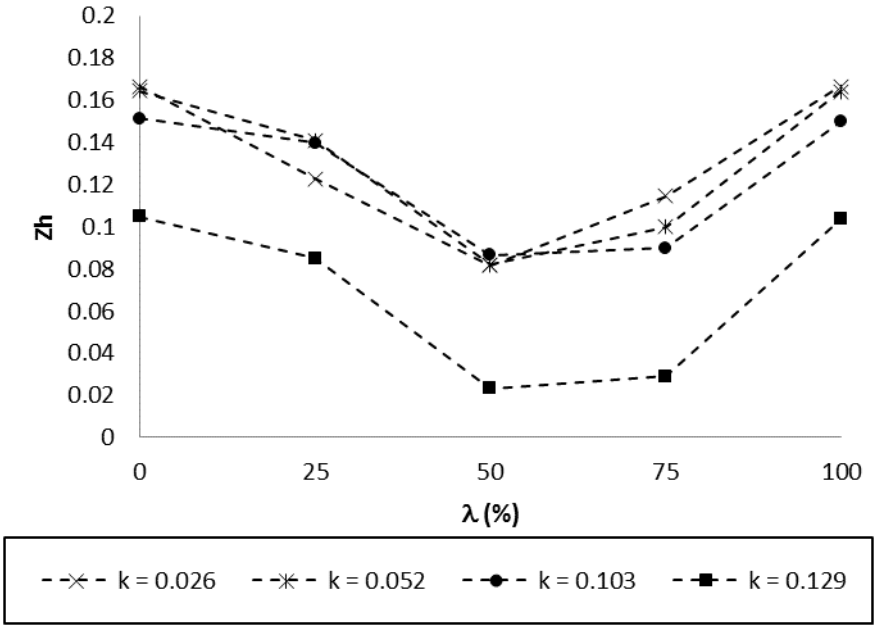

Figure 6-18 Z_h for different reduced frequencies ($\alpha = 4°$; $h/c = 0.3$; $A/c = 0.05$)

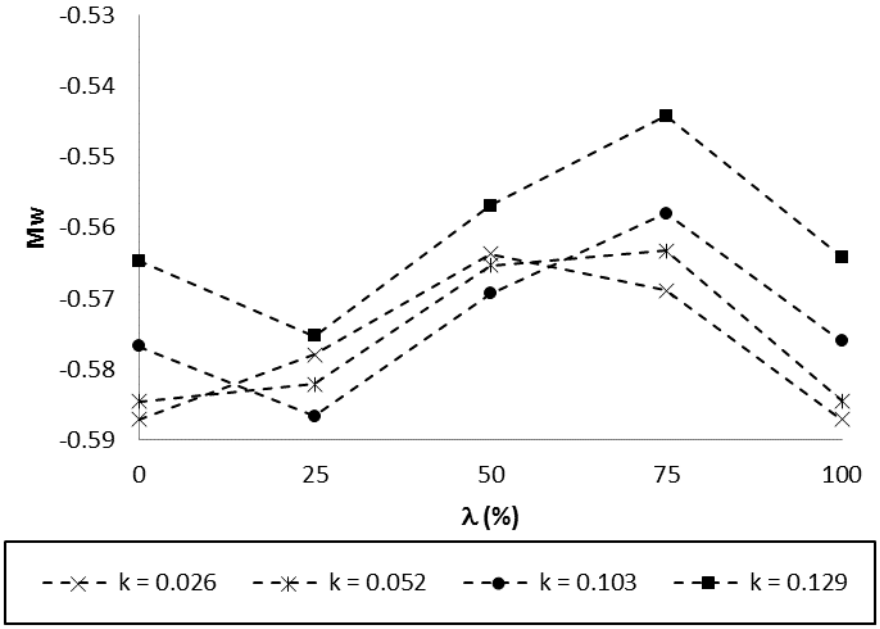

Figure 6-19 M_w for different reduced frequencies ($\alpha = 4°$; $h/c = 0.3$; $A/c = 0.05$)

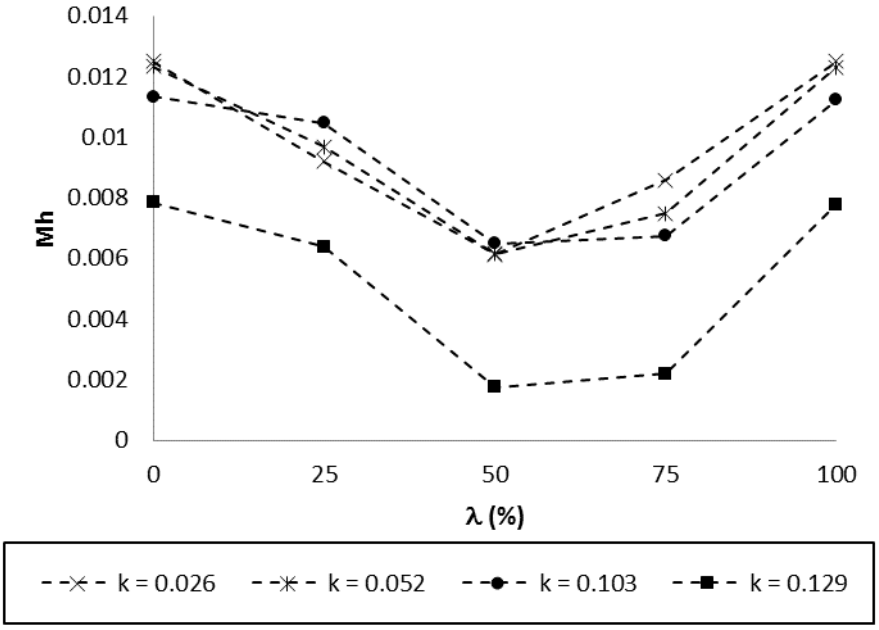

Figure 6-20 M_h for different reduced frequencies ($\alpha = 4°$; $h/c = 0.3$; $A/c = 0.05$)

Figure 6-13 depicts that the increase in frequency amplifies the amplitude of the oscillation of X_u. As discussed in Subsection 5.3.1, the frequency affects the vertical velocity due to the modification of the effective angle of attack. A very similar trend can be seen for X_w. However, its trough is steeper than the crest, as seen in Figure 6-14. This phenomenon identifies the effect of the lift force in X_w. The same trend seems to appear for X_h, especially for higher reduced frequencies, see Figure 6-15. At higher frequencies, the oscillation becomes more dominant over X_h than the ride height. The difference between X_w and X_h is the location of crests and troughs that contrasts by about $\pi/2\,rad/s$. This illustrates that the influence of ride height and the angle of attack for axial force derivatives is contradictory.

The behaviour of Z_u, Z_w and M_w as depicted in Figure 6-16, Figure 6-17, and Figure 6-19 shows the effect of frequency on the derivatives. The increase in frequency of motion leads to the increase in the amplitude of the derivatives. This is expected due to the same characteristics appearing in the aerodynamic analysis, both two-dimensional and three-dimensional.

There are differences in the peak of the amplitude of the curves; they can be identified by two categories. The first is the peak occurs at 50% wavelength, and it means the values of the derivatives move with no lags compared to the motion. This condition for the present study occurs only at one reduced frequency, $k = 0.026$. The second condition is peaked at 75% wavelength which delivers a sign of phase lags between the values of derivatives and the motion. This condition happens in reduced frequencies, $k = 0.052$, $k = 0.103$, and $k = 0.129$. In further detail, the derivatives' curves for $k = 0.052$ actually resemble a transition between the two conditions. This difference about the existence the phase lags can be explained by the concept of reduced frequency. As explained in Section 5.3, the low frequencies ($k = 0.026$ and $k = 0.052$) are considered to behave as a quasi-static motion and the higher frequencies ($k = 0.103$ and $k = 0.129$) are unsteady motion. The value $k = 0.05$ is often regarded as the transition between quasi-static and unsteady flow analysis. Thus, one can conclude that at $k = 0.026$, the effect of the ground still overshadows the effect of oscillation, and this

is depicted in the derivatives by showing no lags with the motion. At $k = 0.052$, the effect of oscillation starts to dominate before it completely overshadows the influence of ride height.

Another observation is also made about the values of the derivatives at high reduced frequencies ($k = 0.103$ and $k = 0.129$). For each derivative, rather than fluctuating at about the same average value as shown in low reduced frequencies, a jump of value is observed instead. This, again, shows the effect of oscillation towards the derivatives. In unsteady conditions, the mean value of the derivatives increases by increasing frequency.

The trend of reduced frequency on Z_h and M_h, as shown in Figure 5-18 and Figure 5-20, is predictable. The crests of the derivatives' curves appear at 50% wavelength. This means that no lag is expected compared to the motion. Regarding the values of the derivatives, the frequency may only have significant impact on these in unsteady motion (with $k = 0.103$ and $k = 0.129$). The increase in reduced frequency leads to the increase of derivatives' values.

The effect of the amplitude of oscillation is depicted in Figure 6-21 to Figure 6-28. In general, the increase in the amplitude of oscillation amplifies the values of derivatives, contributing to the range of maximum-minimum values' deviation. However, some details can be spotted, especially when they are combined with the effect of reduced frequencies.

In Figure 6-21, one can see the change in amplitude does not change the trend of X_u curve. It is noticeable that the increase in reduced frequency has a significant impact on the range of maximum and minimum values of the derivatives. At higher frequencies, the derivative may have positive values, shown as 75% of wavelength in Figure 6-21 [c, d]. This is due to the thrust generation due to Knoller (1909) - Betz (1912) or Katzmayr (1922) effect. The curve is expected to be following a sine function, linear with the fluctuation of the coefficient of drag force due to the oscillation. The behaviour of X_w, as depicted in Figure 6-22, shows more variety compared to X_u. In the first, one can see that at the lowest reduced frequency ($k = 0.026$), the amplitude only gives minor

impact on the values. The effect of amplitude is more noticeable with the increase in reduced frequency. When it is noticeable, one can also see that in some way, crest and trough have different amplification magnitude, see Figure 6-21 [c, d] and Figure 6-22 [c, d]. This state is possibly due to the condition squared periodic function of the drag occurring in the high reduced frequency as shown in the drag analysis of the aerofoil in Subsection 5.3.2. It is possible that the squared periodic motion also applies to the derivatives. Only due to a limited number of observation points, the possibility is only a hypothesis, thus further investigation in the future to prove the thought can be beneficial.

The derivative X_h also exhibits a range of variety of characteristics, see Figure 6-23. In part [a] of the figure, the increase in amplitude leads to more apparent fluctuation. This situation is getting more noticeable as the reduced frequency increases, see part [b] of the figure. When the flow condition is in a higher reduced frequency, see Figure 6-23 [c, d], the severity of fluctuation leads to the change in the function of the curve. The suggestion is also due to the formation of additional frequency as shown in the drag of the aerofoil at higher frequency. It is also likely that different amplitude leads to different phase lags in the range of high reduced frequency. A similar trend is shown by the derivatives, Z_h and M_h. However, the phenomenon in these two derivatives at the higher reduced frequencies is not likely to be related to the frequency development, as is X_h. The shift of crest and through between to curves with different amplitude may be related to the delay of lift force and pitching moment, to follow the motion of the vehicle, thus creating a phase difference in between, especially when the amplitude is getting larger. The difference is also translated into these two derivatives.

The characteristics of three derivatives, i.e. Z_u, Z_w, and M_w, exhibit strong similarities, see Figure 6-24, Figure 6-25, and Figure 6-27. At lower reduced frequencies ($k = 0.026$ and $k = 0.052$), the increase in amplitude significantly amplify the range of maximum and minimum values of the derivatives, see part [a, b] in each figure. Differently, at higher reduced frequencies ($k = 0.103$ and

$k = 0.129$), the change due to the change in amplitude of oscillation is not as strong as when it occurs in lower frequencies.

Ultimately, the stability derivative analysis of an oscillating WIGE craft configuration shows a wide range of phenomena that, from the present study, are beginning to be identified. The only concern of the present analysis is about the amount of data that can be generated to date. With all the data obtained, indeed some features can be determined. However, the features are still in rough trends and some further details may be needed. The complete behaviour of the stability derivatives will be revealed following more investigation. However, this proposition is for future research.

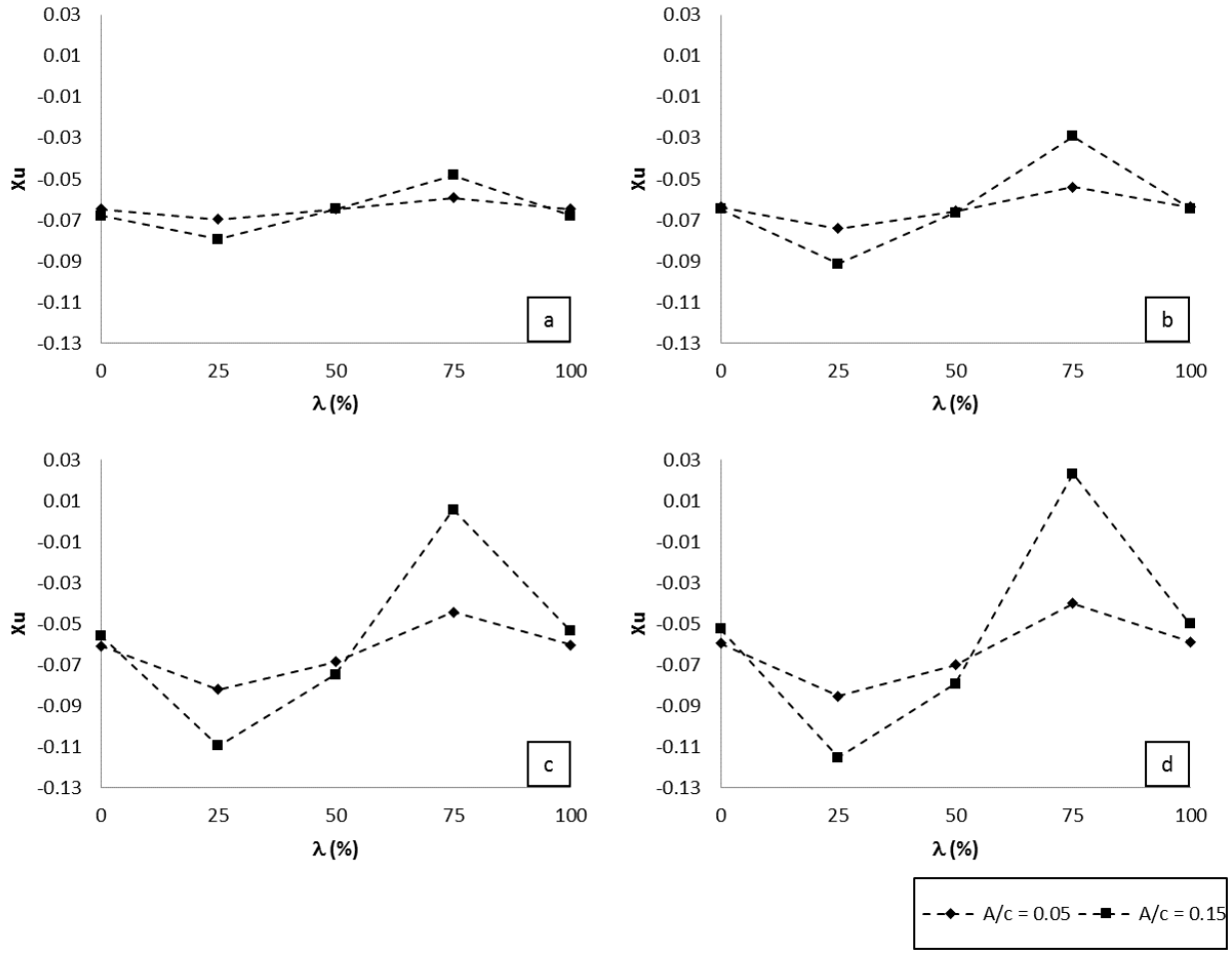

Figure 6-21 X_u for different amplitudes of oscillation ($\alpha = 4°$; $h/c = 0.5$; $k = 0.026$ [a], 0.052 [b], 0.103 [c], 0.129 [d])

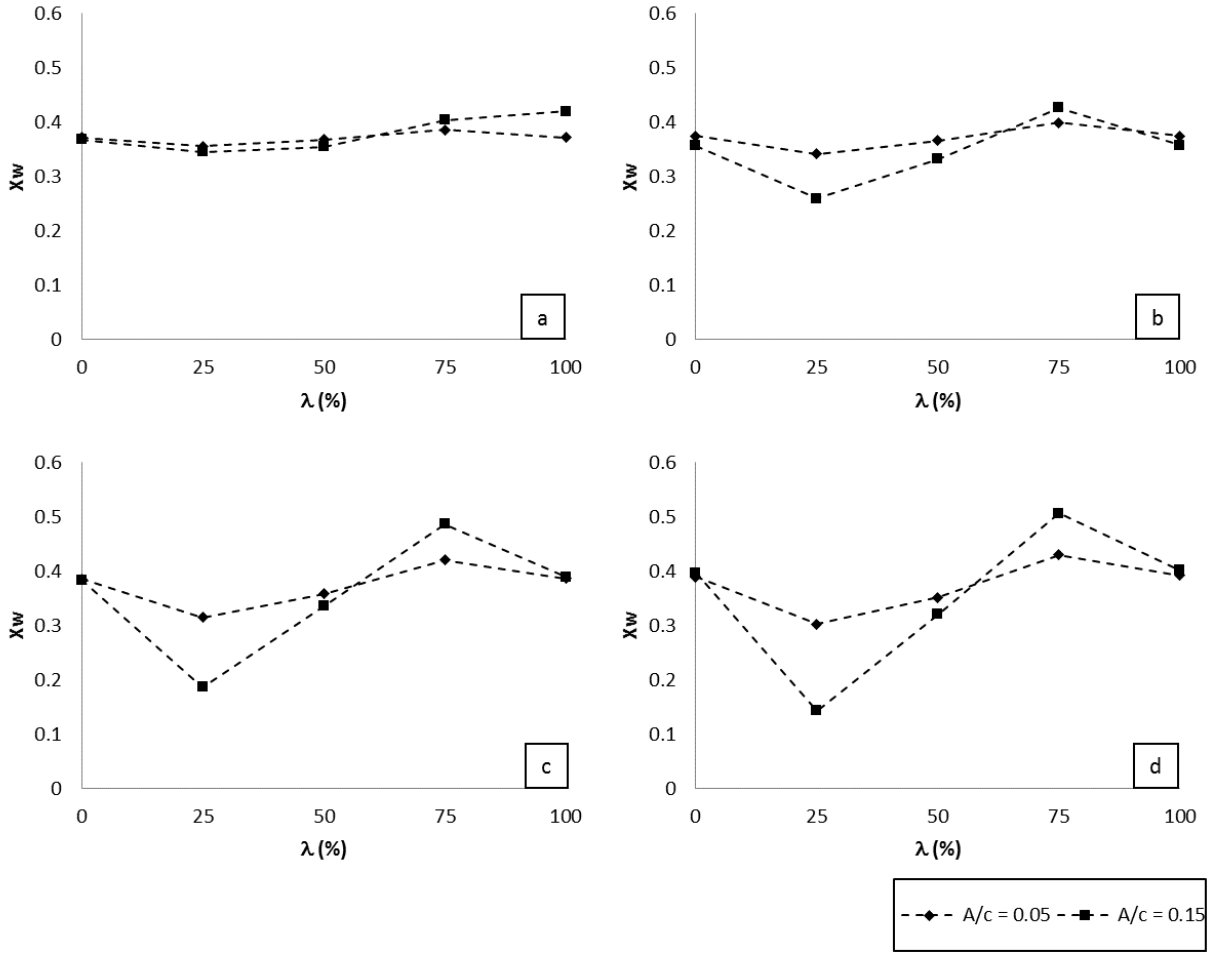

Figure 6-22 X_w for different amplitudes of oscillation ($\alpha = 4°$; $h/c = 0.5$; $k = 0.026$ [a], 0.052 [b], 0.103 [c], 0.129 [d])

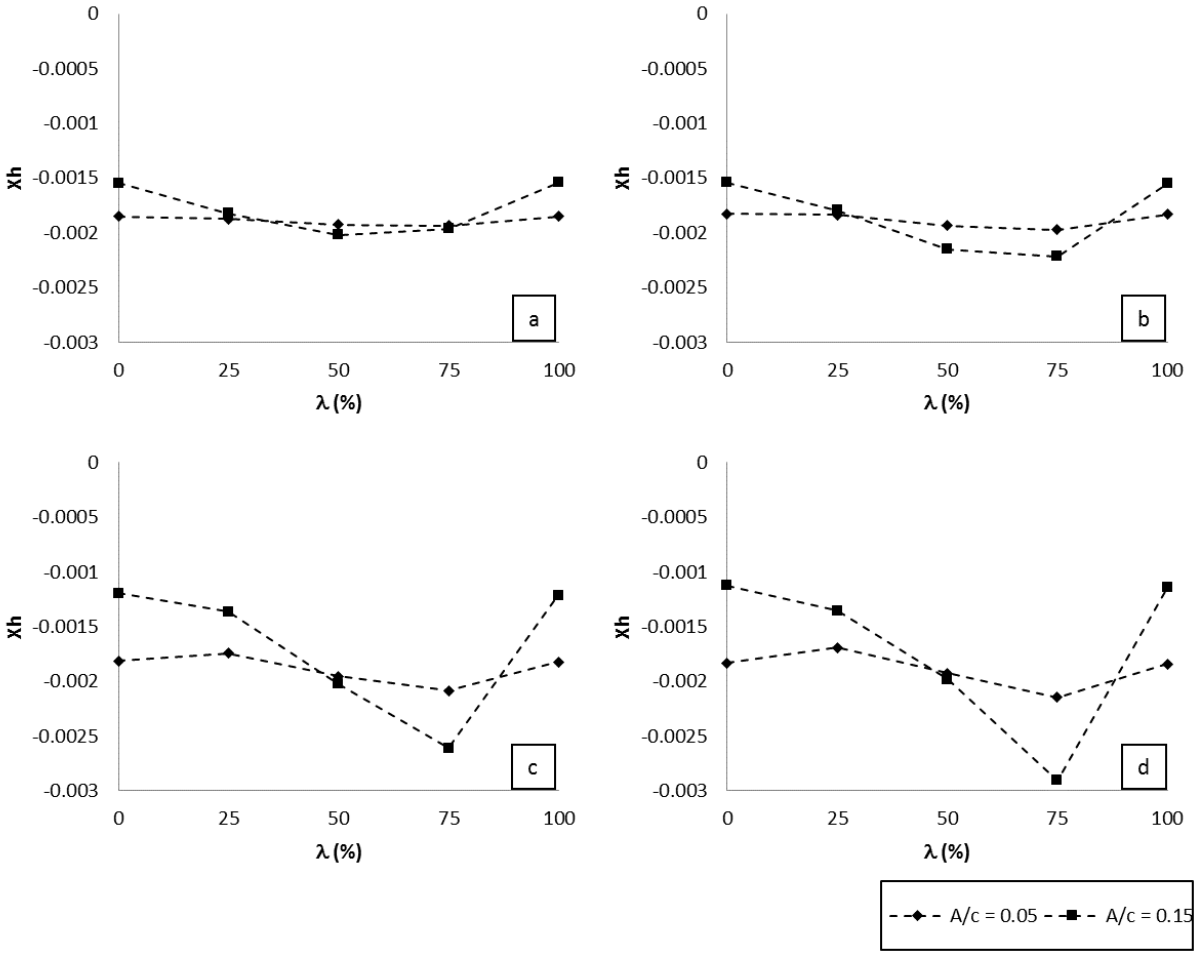

Figure 6-23 X_h for different amplitudes of oscillation ($\alpha = 4°$; $h/c = 0.5$; $k = 0.026$ [a], 0.052 [b], 0.103 [c], 0.129 [d])

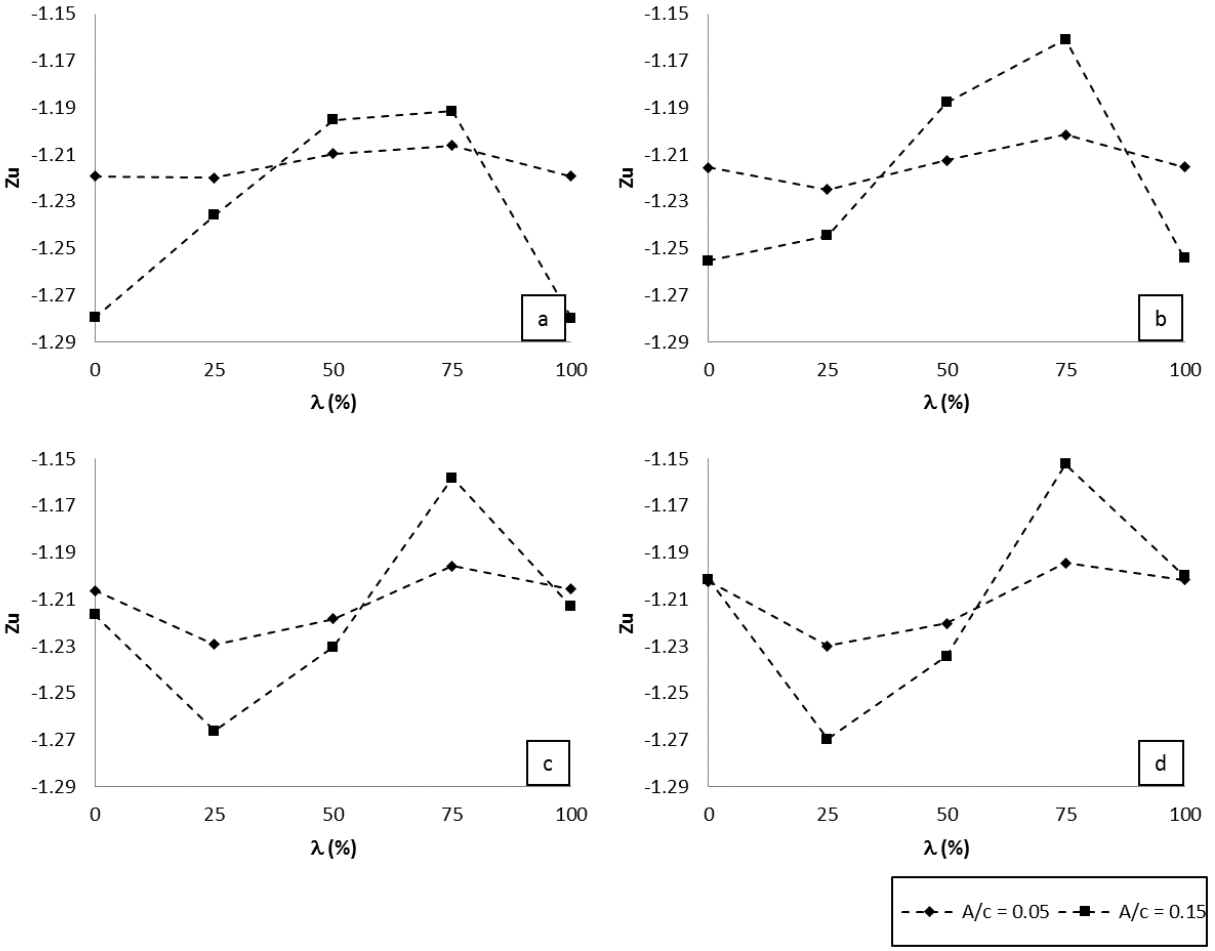

Figure 6-24 Z_u for different amplitudes of oscillation ($\alpha = 4°$; $h/c = 0.5$; $k = 0.026$ [a], 0.052 [b], 0.103 [c], 0.129 [d])

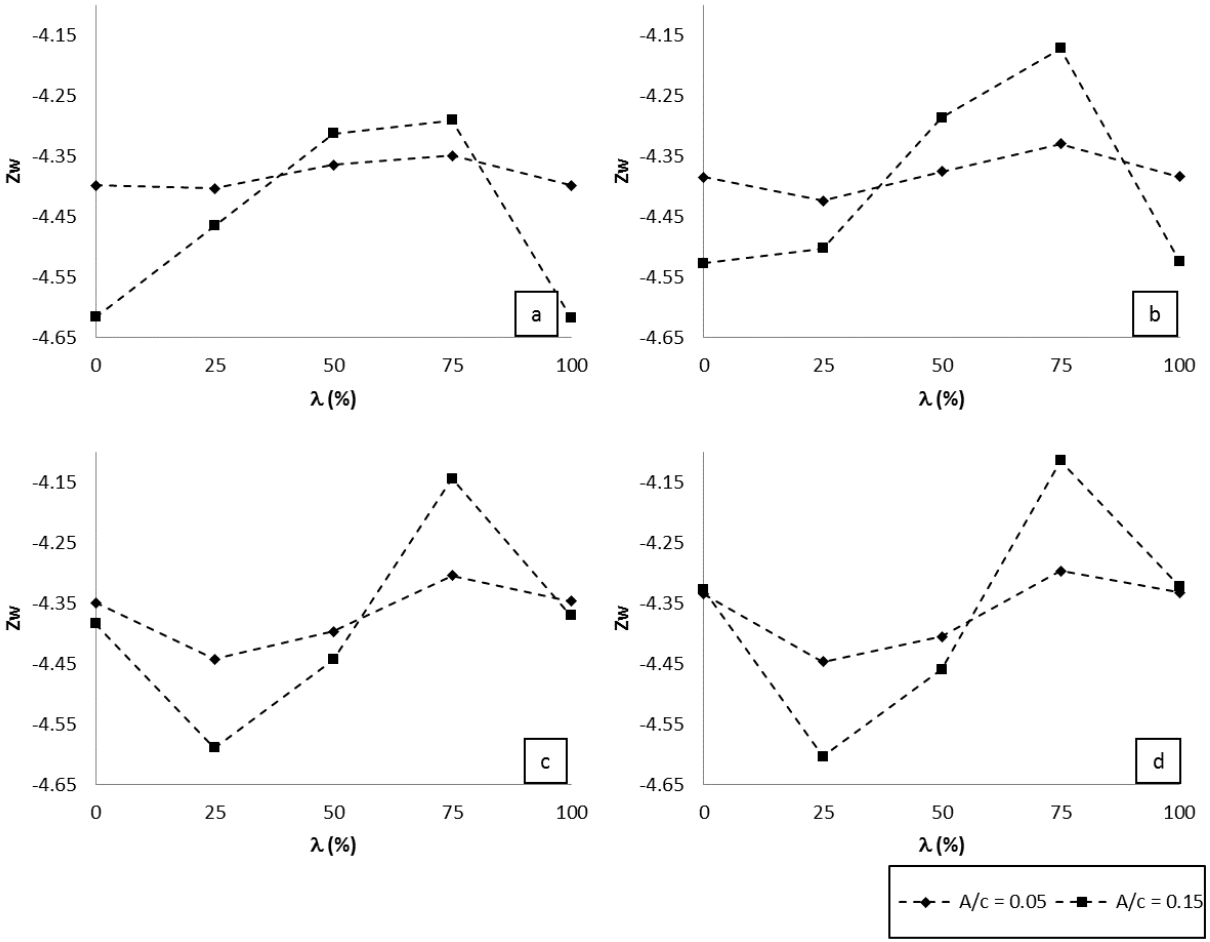

Figure 6-25 Z_w for different amplitudes of oscillation ($\alpha = 4°$; $h/c = 0.5$; $k = 0.026$ [a], 0.052 [b], 0.103 [c], 0.129 [d])

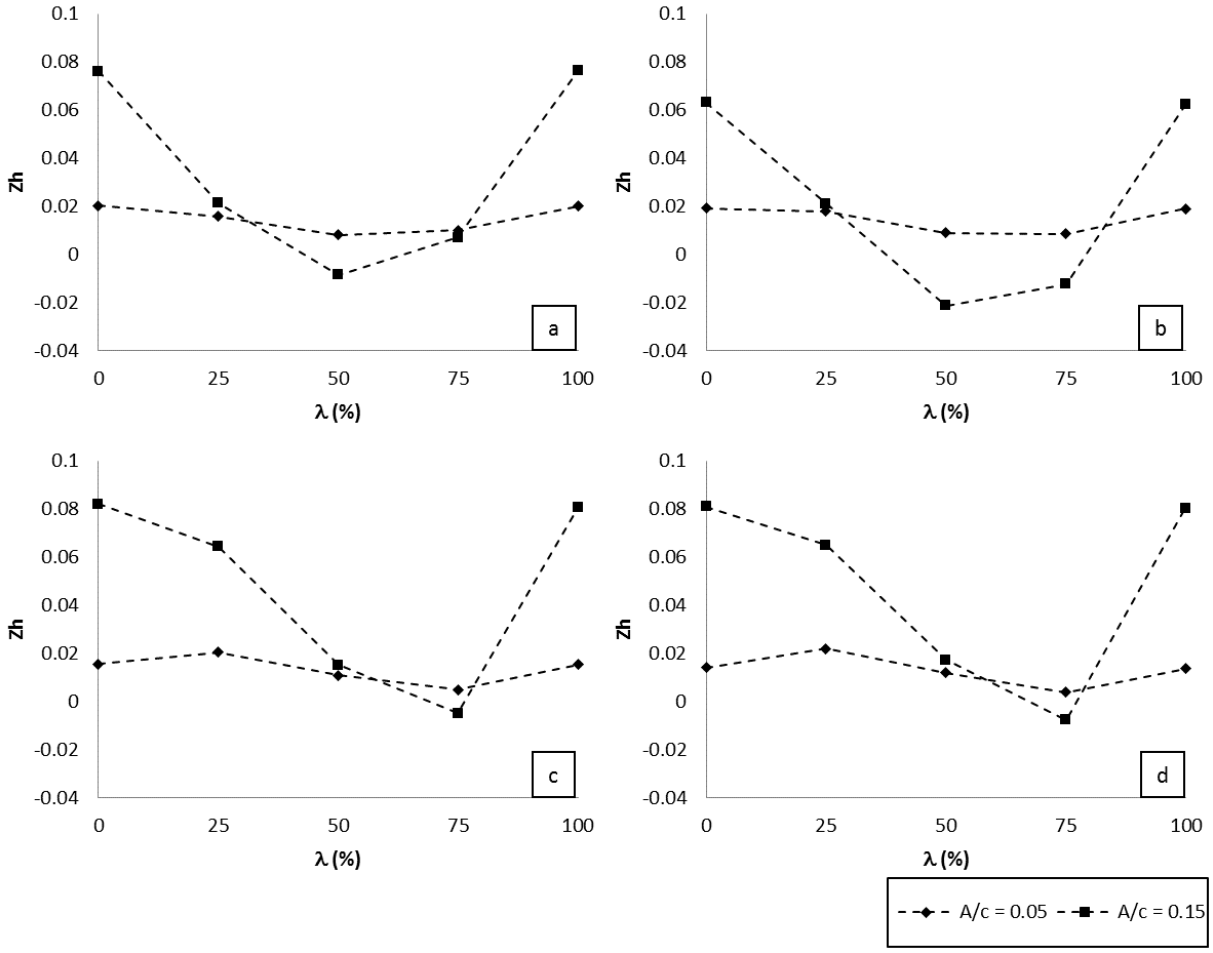

Figure 6-26 Z_h for different amplitudes of oscillation ($\alpha = 4°$; $h/c = 0.5$; $k = 0.026$ [a], 0.052 [b], 0.103 [c], 0.129 [d])

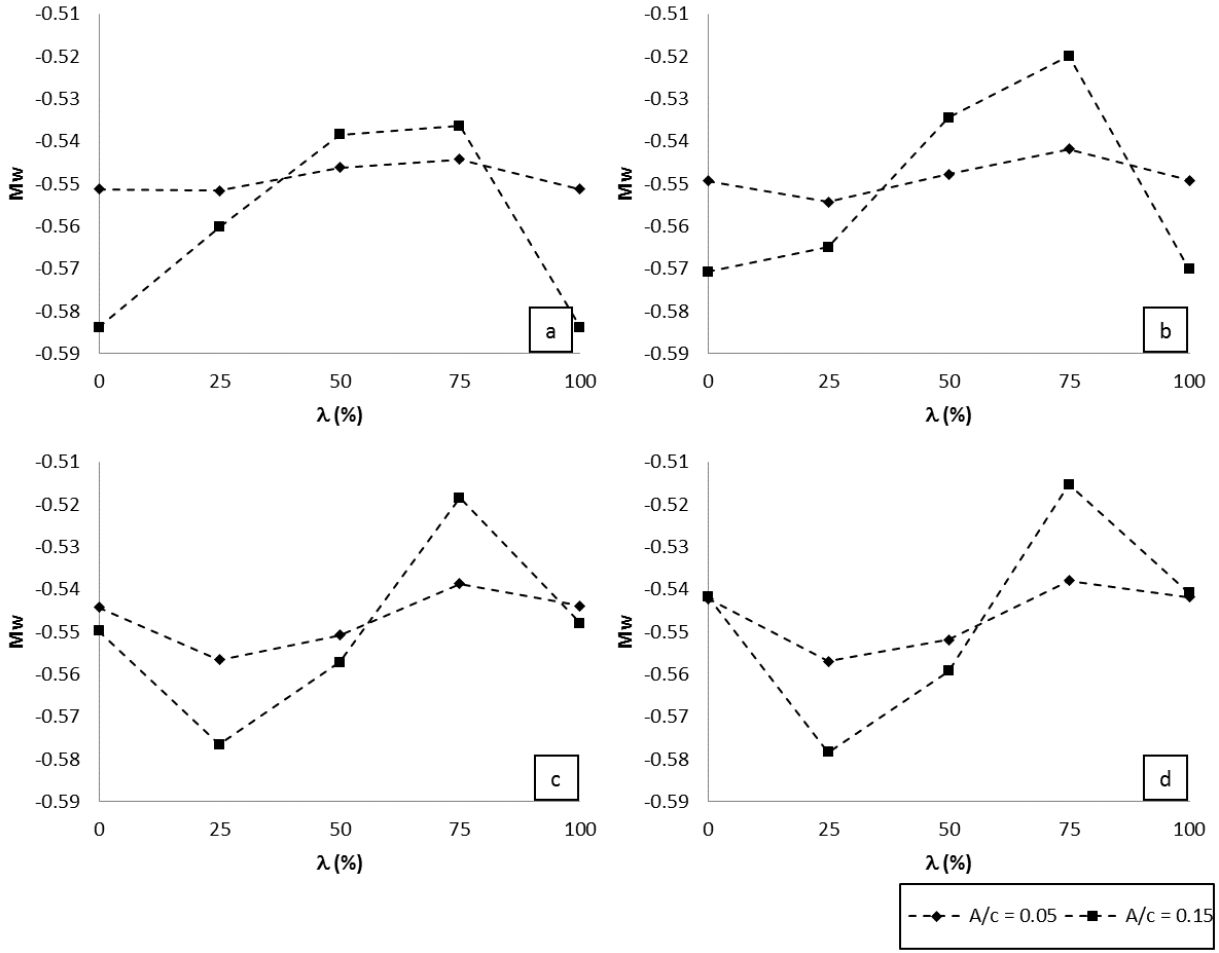

Figure 6-27 M_w for different amplitudes of oscillation ($\alpha = 4°$; $h/c = 0.5$; $k = 0.026$ [a], 0.052 [b], 0.103 [c], 0.129 [d])

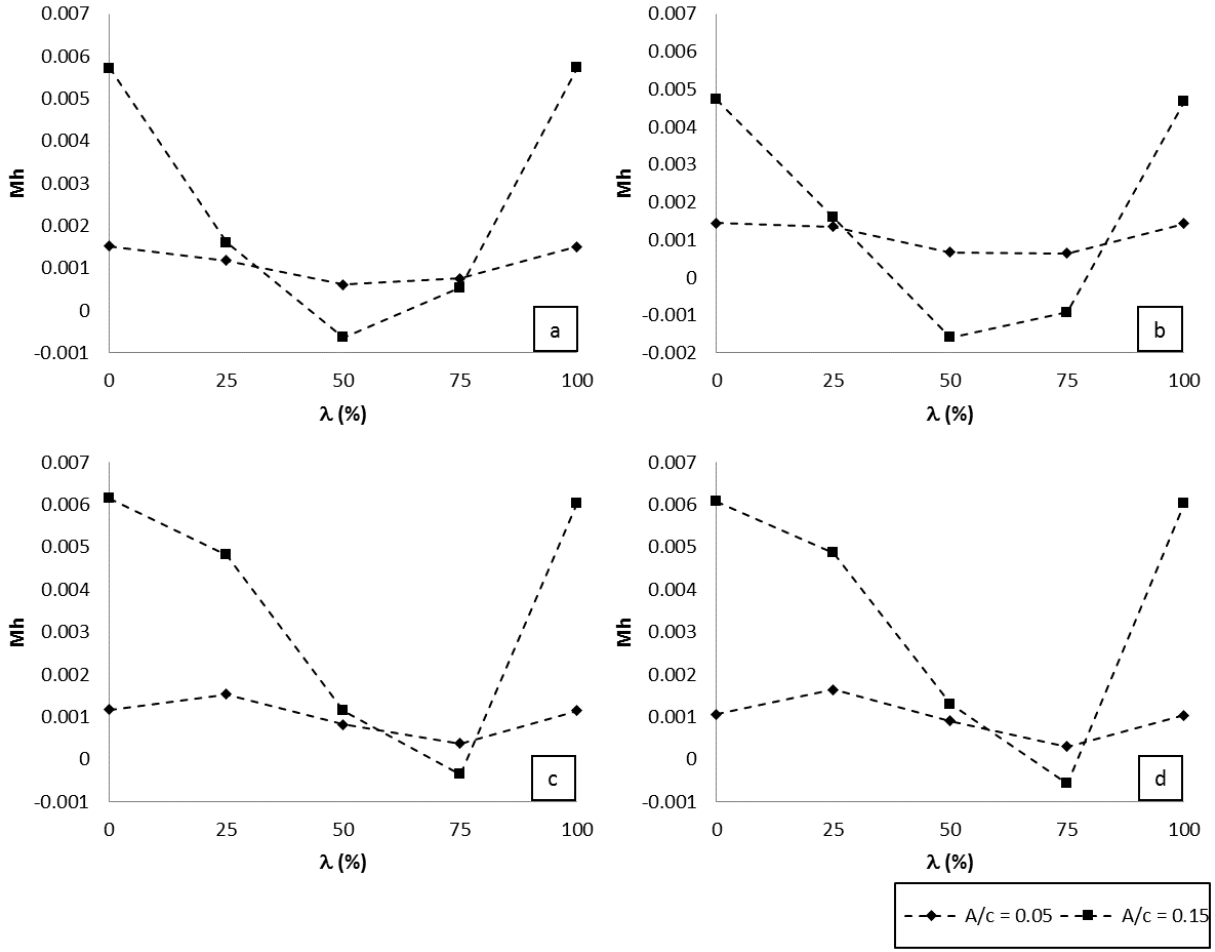

Figure 6-28 M_h for different amplitudes of oscillation ($\alpha = 4°$; $h/c = 0.5$; $k = 0.026$ [a], 0.052 [b], 0.103 [c], 0.129 [d])

6.4 Conclusion

The determination of the stability derivatives required substantial effort. Following the aerofoil data derived from the set of CFD simulations, as thoroughly explained in Chapter 5, two further steps were required. The first was to transform the 2D profile aerofoil data into the aerodynamic characteristics of the Ekranoplan ‘Orlyonok’ A-90 full configuration. The method used was a semi-empirical approach widely adopted for low-speed aircraft (Raymer, 1999). The second step consisted of obtaining the stability derivatives of the Ekranoplan. The stability derivatives were derived adopting the UK-style.

As expected, the derivation of aerofoil data resulted in data that also has the characteristics of oscillation. To summarise the discussion in this chapter, it can be said that the derivatives are the translation of manifestations which occurred in the aerodynamic analysis.

At lower reduced frequency, the effect of amplitude is not significant. However, the effect of amplitude at lower reduced frequencies is more significant for the normal force and pitching moment derivatives than at high reduced frequency. The quasi-static and unsteady aerodynamic reduced frequencies exhibited differences in amplitude of the derivatives, as well as the formation of phase lags. The explanation of the differences should be made case per case. In the axial force derivatives, for instance, the Knoller (1909) - Betz (1912) or Katzmayr (1922) effect is manifested in the values at higher reduced frequencies. A similar trend is shown in the normal force and pitching moment derivatives. The derivatives with respect to ride height are manifested more strongly in the ground effect region, and started diminishing with the increase in ride height.

7 STABILITY ANALYSES

This chapter demonstrates the use of the model of dynamics presented in Chapter 4 for a vehicle. The derivatives for the vehicle were discussed in Chapter 6. This chapter comprises five sections, and they are *(1) Introduction*; *(2) Verification of the implementation code using the Ekranoplan 'Orlyonok' A-90*; *(3) The effect of wing configuration*; *(4) Constant angle of attack versus constant coefficient of lift*; *(5) Effect of observation data points*; (*6) Effect of oscillation on the characteristic roots*; and *(7) Conclusion*.

7.1 Introduction

In Chapter 4, the model of dynamics is developed for the ground effect vehicle oscillating near the surface. As has been discussed, several methods may be applied to determine a solution for such a case. One of the approaches is the 'quasi-static' dynamic approach. To apply the methodology, several assumptions should be satisfied. It applies better in the condition of long wavelength and low frequencies.

The quasi-static approach is done by taking several observation points along, at least, one full wavelength, assuming that at those instantaneous points, the effect of oscillation is still observed as well as the ride height. The stability derivatives of each point are determined to be used in the homogeneous solution method. The homogeneous method is used for the system without the interference of external forces.

By applying this method to an oscillating system, one will have a set of homogeneous solutions rather than one exact solution. The set is expected to give hysteresis from its non-oscillating case, and from them, the stability behaviour of the system can be observed.

The Russian's Orlyonok A-90 has been adopted for the case study, with a modified wing section. The NACA 4412 aerofoil has been used as the section of the wing. This decision is due to plenty of studies that have analysed the characteristics of the aerofoil. This change results in different values of derivatives when compared to the

original reference (Delhaye, 1997). It is worthwhile noticing that this reference has excluded the effect control derivatives, which were also adopted in the present study.

7.2 Verification of the implementation code using the Ekranoplan 'Orlyonok' A-90

The model of dynamics proposed has been implemented in Matlab™ to perform a dynamic analysis of the WIGE vehicle. In the absence of experimental values, it is difficult to perform validation of the case. Therefore, a code-to-code comparison has been used to verify the present model, and comparing the results of the present model with those obtained by Delhaye (1997) was aimed to fulfil the objective of code verification and validation. The accuracy of the results from running the code determines whether the code is reliable enough to give adequate results. Figure 7-1 depict the flowchart of the code has been developed. The code is built as straightforward as possible to avoid confusion during the analysis. An example of the code is available in Appendix H.

The code developed in the present work gave satisfying results, as seen in

Table 7-1 and Figure 7-2, with the maximum differences being less than two percent. If the decimals of the present results are rounded to have the same decimals as Delhaye's (1997) data, both have the same values.

The high accuracy depicted by the present study gives the assurance that the code can be used for further analysis. As a reminder, the implementation in Matlab in the present study is based on a homogeneous solution with no interference from external forces. This is acceptable due for the oscillation case only because the assumption of 'quasi-static' approximation has been taken in the first place. This approach offers simplicity in reaching the solutions, although some of the dynamic effects may be disregarded. Yet, it supports the understanding of the oscillating phenomenon for the WIGE craft configuration. Considering the 'quasi-static' approximation, the fidelity of method to solve the problem may be challenged. However, for the present study, to

provide high fidelity results is beyond the scope of the research. Instead, this research is about capturing a general trend or behaviour of an oscillating ground effect vehicle.

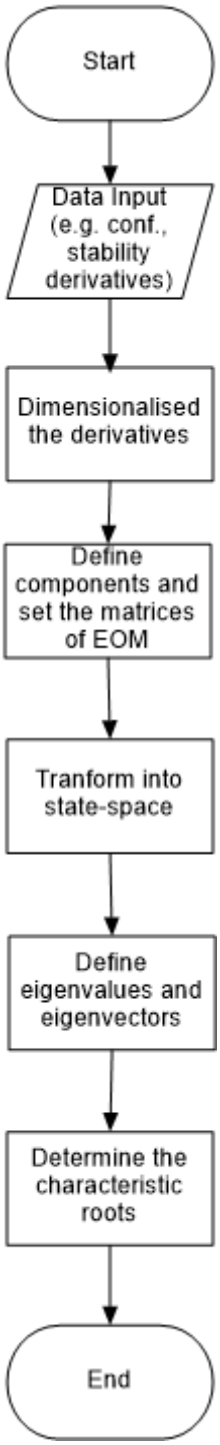

Figure 7-1 Flowchart of dynamic analysis

Table 7-1 Roots of oscillation of the Ekranoplan 'Orlyonok' A-90 with Clark-Y aerofoil

h/c	α	Delhaye's (1997) work	Present work
0.25	1.2	$r_{1,2} = -0.686 \pm 0.926i$ $r_{3,4} = -0.05 \pm 0.398i$ $r_5 = -0.026$	$r_{1,2} = -0.686 \pm 0.926i$ $r_{3,4} = -0.050 \pm 0.398i$ $r_5 = -0.0255$
0.375	1.5	$r_{1,2} = -0.686 \pm 0.95i$ $r_{3,4} = -0.025 \pm 0.418i$ $r_5 = -0.026$	$r_{1,2} = -0.686 \pm 0.951i$ $r_{3,4} = -0.025 \pm 0.418i$ $r_5 = -0.0260$
0.5	1.8	$r_{1,2} = -0.694 \pm 0.907i$ $r_{3,4} = -0.011 \pm 0.375i$ $r_5 = -0.028$	$r_{1,2} = -0.694 \pm 0.907i$ $r_{3,4} = -0.011 \pm 0.375i$ $r_5 = -0.0284$
0.625	2.0	$r_{1,2} = -0.708 \pm 0.856i$ $r_{3,4} = 0.0076 \pm 0.294i$ $r_5 = -0.031$	$r_{1,2} = -0.708 \pm 0.856i$ $r_{3,4} = 0.0076 \pm 0.294i$ $r_5 = -0.0311$
OGE	2.8	$r_{1,2} = -0.721 \pm 0.672i$ $r_{3,4} = -0.0047 \pm 0.108i$	

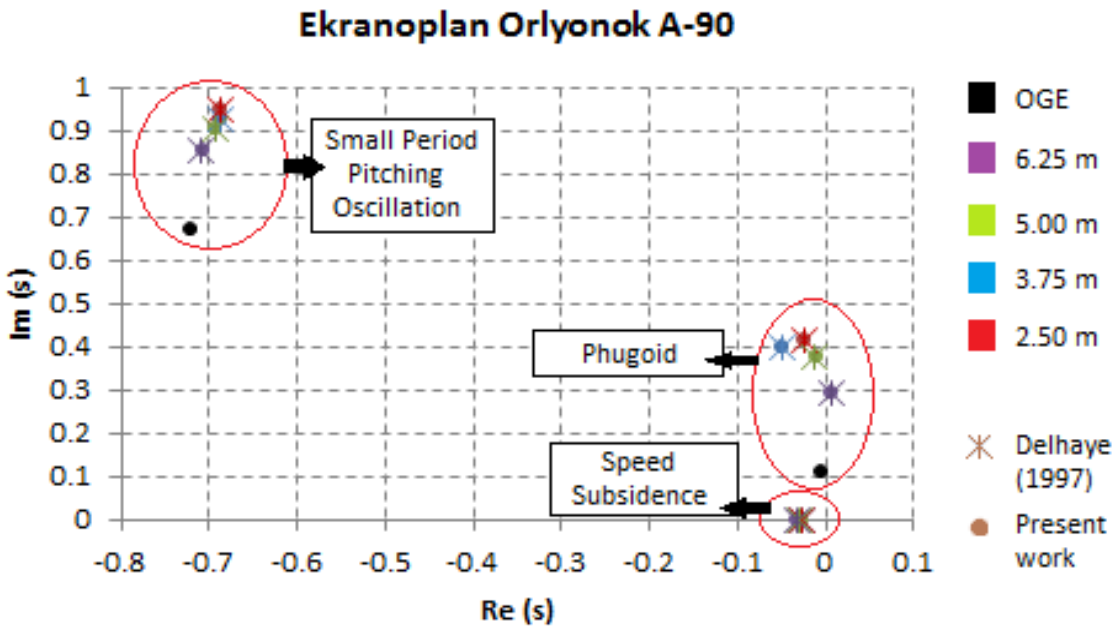

Figure 7-2 Characteristic roots of the Ekranoplan 'Orlyonok' A-90

7.3 The effect of wing configuration

The question is: “to what extent does the effect of wing configuration affect the dynamic stability of a full vehicle?” This section is about to answer this very question.

First of all, the aerofoil adopted and analysed with a CFD approach in the present study (see Chapter 5), i.e. NACA 4412, was incorporated in the configuration for stability analyses with several preliminary steps, as explained in Chapter 6. However, the aerofoil used by Delhaye is different, i.e. Clark-Y. Due to the difference in the aerofoil profiles, the author tried to compare the stability analyses from both pieces of work. NACA 4412 and Clark-Y are known for their good performance in the ground effect condition and have a similar shape. The good performance is due to their relatively flat lower surface.

Before proceeding, it is worthwhile mentioning that some concerns were raised about the comparison between the present study (using the NACA 4412 wing section) and Delhaye’s (1997) work (using the Clark Y wing section). Initial expectation is that similarities will be produced because the aerofoil profiles are alike. However, the comparison shows substantial differences that are, in the beginning, assumed due to the different aerofoils. However, the discrepancies are too wide if taking only a two-

dimensional profile into account. With further investigation, as mentioned in Subsection 6.1.4, it is likely that Delhaye had considered the use of endplates in the calculation. This is despite there being no mention in Delhaye's thesis about the use of these configuration features. The inclusion of endplates gives significant increases in the aerodynamic characteristics. On the other hand, the present study only considered the basic wing-fuselage-tail configuration, and therefore the aerodynamic characteristics of it are lower than Delhaye's configuration.

Delhaye (1997), indeed, pointed out that the aerodynamic data was not validated against any experimental data. The same situation also applies to the present study.

7.3.1 Aerodynamics and stability derivatives

The aerodynamic data from Delhaye's work present some unexpected characteristics. The aerodynamic characteristics of the full configuration surprisingly give higher lift than the two-dimensional profile. This fact contrasts the common understanding that the ground effect lift weakens in the vehicle form by up to 65 percent. It has been previously mentioned that Delhaye may have considered the use of endplates despite no clear statement about this matter.

These data have, therefore, assumed to be not suitable for a direct comparison. Nonetheless, a qualitative comparison was made to gain any physical insight of the stability behaviour in the ground effect.

Figure 7-3 depicts the relationship between the X_u derivative and ride height h/c. As the effect of propulsion was neglected in the analysis, the derivative represents only the drag forces, neglecting the effect of compressibility that led to X_u being $[-2C_D]$. A discussion of longitudinal motion of WIGE vehicles by Staufenbiel and Kleineidam (1980) derived the same expression.

The figure shows that X_u becomes less negative by decreasing h/c. This characteristic applies to both configurations: Delhaye's (1997) work and the present study. The curves illustrate that the drag of the vehicle decreases by the decrease in ride height. The illustration presents the implication of the ground effect phenomenon towards drag. The ground effect alters the flow field around the body and affects the decrease

in the downwash angle. The decline in the downwash angle leads to the increase in an effective angle of attack. These changes cause the change in lift and drag. A reduction in induced drag is the main reason for the change in drag in the ground effect (Carter, 1961; Holloran and O'Meara, 1999).

Unfortunately, the author could not go further to compare the differences between the NACA 4412 and Clark-Y for this aspect. Figure 7-3 implies that the magnitude of X_u produced by Delhaye with the Clark-Y wing section is larger in magnitude than the present study with the NACA 4412 wing section. However, instead of the wing sections, the variance in the three-dimensional configuration can explain more the occurrence of differences between the present study and Delhaye's work.

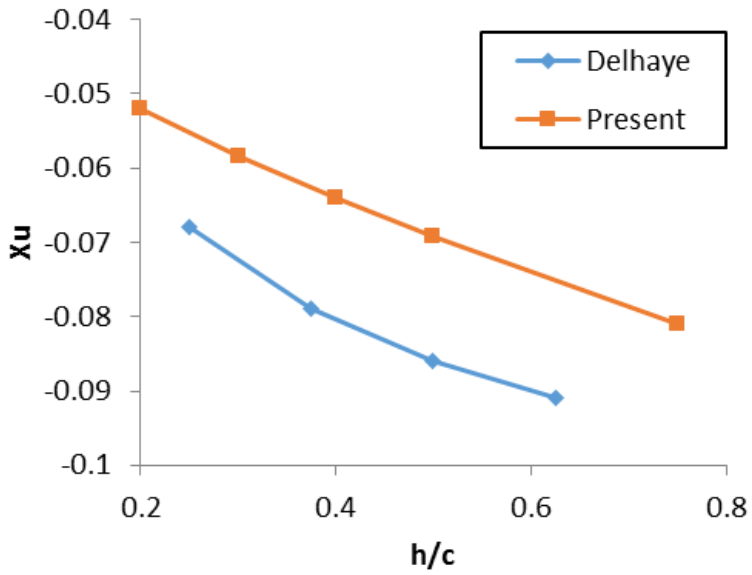

Figure 7-3 The derivative of X_u

As explained in Cook (2013, pt.6.2.2), the phugoid mode is a low-frequency oscillation in speed u, coupled into pitch altitude θ and height h. The change in X_u correlates with the change in the phugoid mode. A reduced-order equation shown in Cook (2013, p.162) demonstrates this relationship. The equation without contribution from the control system is as follows:

$$\begin{bmatrix}\dot{u}\\ \dot{\theta}\end{bmatrix} = \begin{bmatrix} x_u - x_w\left(\dfrac{m_u U_e - m_q z_u}{m_w U_e - m_q z_w}\right) & g \\ \dfrac{m_u z_w - m_w z_u}{m_w U_e - m_q z_w} & 0 \end{bmatrix}\begin{bmatrix}u\\ \theta\end{bmatrix} \tag{7-1}$$

or in simpler form

$$\dot{\mathbf{x}} = \boldsymbol{A}_p \mathbf{x} \tag{7-2}$$

The equation above may be solved algebraically. However, the characteristic equation is more conveniently shown as:

$$\boldsymbol{\Delta}(s) = \det\left[s\boldsymbol{I} - \boldsymbol{A}_p\right] = 0 \tag{7-3}$$

whence,

$$\begin{gathered}\boldsymbol{\Delta}(s) = s^2 + 2\varsigma_p\omega_p s + {\omega_p}^2 \\ \boldsymbol{\Delta}(s) = s^2 - \left(x_u - x_w\left(\frac{m_u U_e - m_q z_u}{m_w U_e - m_q z_w}\right)\right)s + g\left(\frac{m_u z_w - m_w z_u}{m_w U_e - m_q z_w}\right)\end{gathered} \tag{7-4}$$

With the assumption $m_u \to 0$, $|m_u z_w| \ll |m_w z_u|$, and $|m_w U_e| \gg |m_w z_w|$, the expression for the damping and natural frequency is as follows:

$$\begin{gathered}2\varsigma_p\omega_p = -x_u \\ \omega_p = \sqrt{\frac{-g z_u}{U_e}}\end{gathered} \tag{7-5}$$

The relationship above shows that z_u affects the phugoid natural frequency and x_u relates to the phugoid damping and natural frequency. It is known that the nondimensionalised form of x_u and z_u are X_u and Z_u, and both related to the magnitude of C_D and C_L respectively.

The expression of x_u in equation (7-5) gives a piece of information that it affects the real value of the phugoid mode. The decrease in the drag decreases the magnitude of X_u, thus the real value of phugoid also decreases. With the decrease in drag with decreasing ride height, as shown in Figure 7-3, one may expect that the real value of phugoid becomes more negative from zero with decreasing ride height, both for Delhaye's (1997) case and the present case.

Figure 7-4 illustrates the relationship between X_w and h/c. In the ground proximity, the trend is that X_w becomes higher by decreasing height for both cases, which is expected following the relationship, $[C_L - \partial C_D/\partial\, \alpha]$. This derivative explains the lift and drag effect due to incidences' perturbation. The derivative X_w also contributes to the characteristic of the phugoid mode, the relationship of which is shown in equation (7-4).

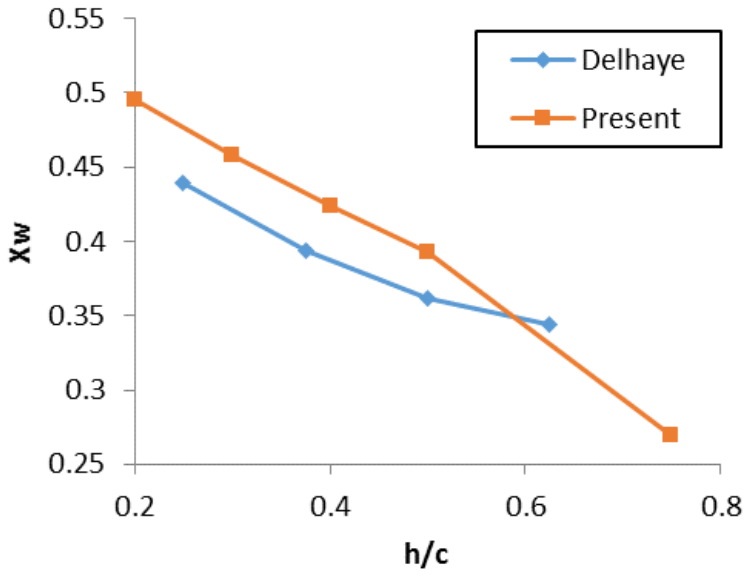

Figure 7-4 The derivative of X_w

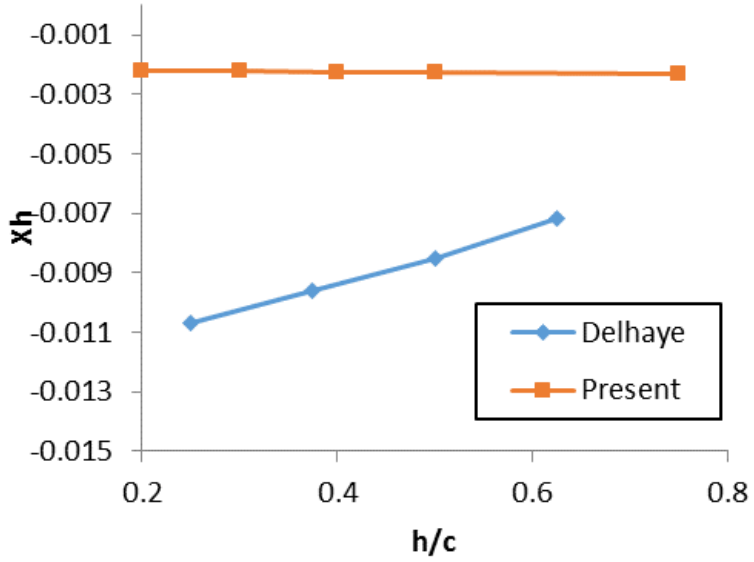

Figure 7-5 The derivative of X_h

The two different configurations showed a very significant difference in the change of drag due to decreasing ride height. Considering the depiction of the axial force derivative due to height, X_h in Figure 7-5, the present case shows almost no changes in the coefficient of drag, C_D, by decreasing ride height. On the contrary, Delhaye's result has more negative X_h. Different configurations are responsible for the difference in the aerodynamic characteristics between the two cases. One can conclude that the endplates significantly affect the value of these derivatives.

As mentioned in Subsection 6.1.4, it is assumed that Delhaye has considered the endplates in the analysis and they have significantly improved the aerodynamic lift. Although Delhaye did not particularly mention this, there is another support from an investigation into this matter (Kumar, 1968), and by deploying the case similar to the configuration adopted by Delhaye, it gives similar results. The changes not only happen for lift but also contribute to the increase of drag from two factors, i.e. the profile drag and the induced-lift drag. This is the reason for a higher magnitude of X_u, X_w, and X_h in Delhaye's (1997) case compared to the present study.

The details of aerodynamic differences due to the differences in configuration, both 2D and 3D, need further study in the future. For this present stage, as it is beyond the scope of the research, general logic is a sufficient explanation.

One can approximate with $\partial C_L/\partial \alpha$, the normal force derivative with respect to incidence, Z_w, as the contribution of drag may be ignored. Figure 7-6 illustrates that Z_w of the configuration adopted for the present study has a larger absolute value than the configuration adopted by Delhaye. However, the curve also depicts that the change of the derivatives in the present study is more moderate than in the Delhaye case. These two pieces of information provide a conclusion that the difference in $\partial C_L/\partial \alpha$ will affect the slope of the derivative against h/c (it is worth reminding the reader that the contribution of lift is constant in Z_w).

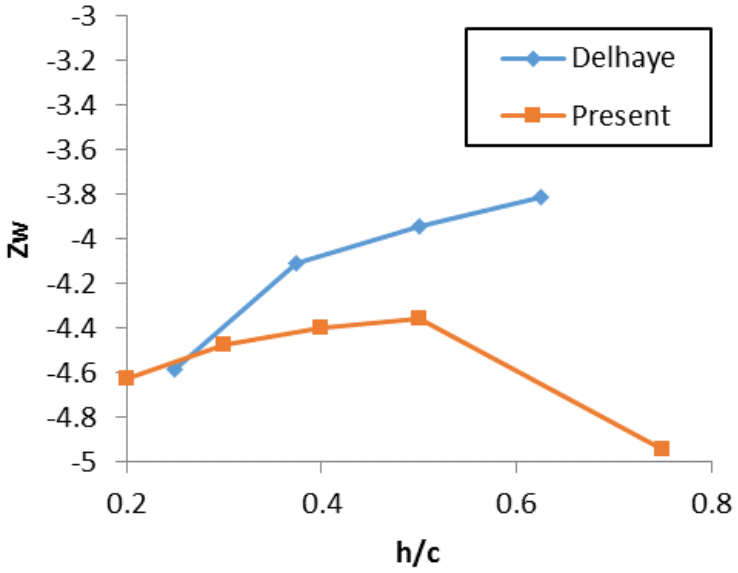

Figure 7-6 The derivative of Z_w

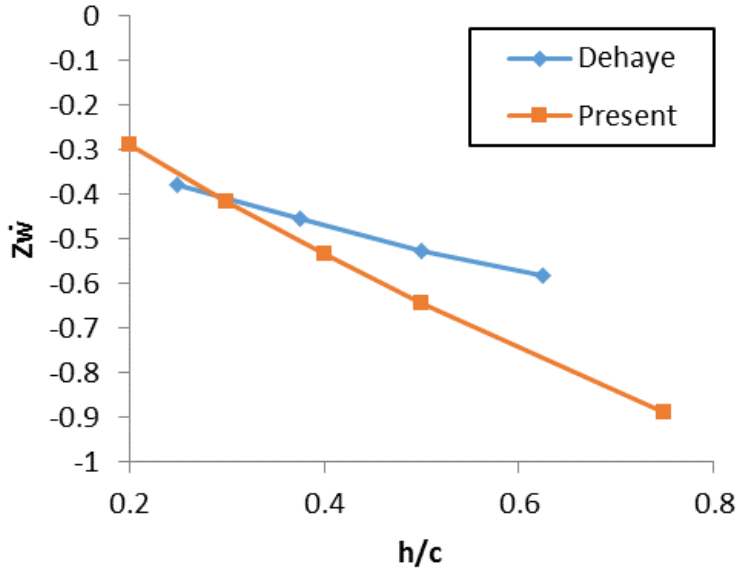

Figure 7-7 The derivative of $Z_{\dot{w}}$

It is known that Z_w is related to dynamic characteristics of the short period pitching oscillation (SPPO) mode. Therefore, one may expect that the configuration in the present study will have a wider range of short period values but, on the other hand, are lower than in Delhaye's case. Further explanation will be discussed later in the thesis.

Figure 7-7 depicts the derivative $Z_{\dot{w}}$. This derivative is taken into account in the studies by UK researchers but is ignored by Russian researchers and Staufenbiel's study (1980). This derivative assumes a smaller absolute value by decreasing the ride height. The values given in Delhaye's case are mostly higher but the value range is more limited. The difference in values shown by the curves again confirms the interdependence between the effective angle of attack and downwash angle. Having learned from previous discussion that the effective angle of attack in Delhaye's case is lower than in the present study, the downwash will also be lower, leading to higher $Z_{\dot{w}}$.

The significance of h/c is identified by the ratio of coefficient of lift to the ride height ratio, $\partial C_L/\partial\,(h/c)$, linked to the derivative Z_h, as shown in Figure 7-8. As expected, this parameter increases by decreasing height, although the two configurations show a substantially different behaviour. The present study shows an exponential trend

while Delhaye's (1997) work presents a different function. Here, one may deduce that the configuration has a significant implication for the behaviour of the derivatives. The present study shows the trend is similar to the trend of the lift of its 2D wing section in the ground effect; the similarities are expected. Differently, the configuration in Delhaye's work gives a different tendency than the trend of the 2D aerodynamics' case. This is possibly due to the endplates' contribution but other investigation may be needed. At the current stage, the author has only found that the endplates augment the lift production (Rozhdestvensky, 2006) but no further explanation is available about the trend of the augmentation itself.

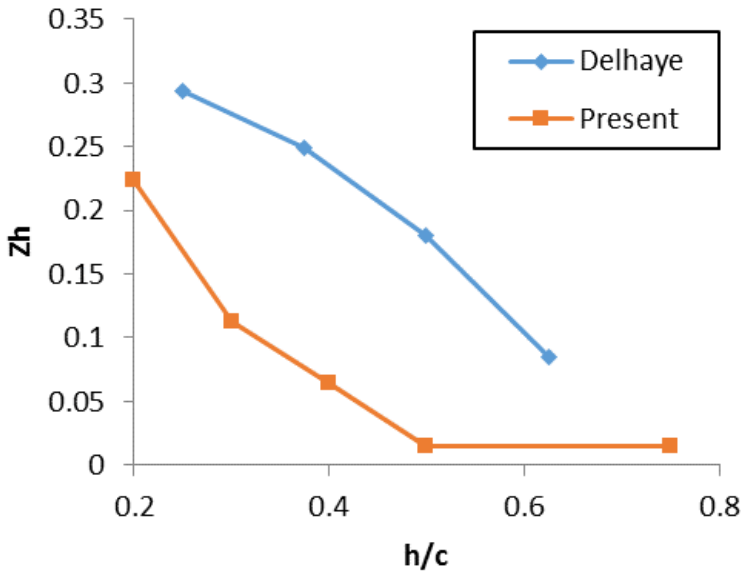

Figure 7-8 The derivative of Z_h

The ratio of pitching moment against the angle of attack, $\partial C_m/\partial \alpha$ is linked to the M_w, depicted in Figure 7-9. These curves demonstrate that M_w is more negative by decreasing height, except for one case of configuration, in Delhaye's case, at 0.2*c* of ride height. There is a sudden increase in M_w compared to other heights; this is probably an error in Delhaye's calculation. The configuration in the present study has a less negative M_w than in Delhaye's study. The negative values shown by the curves in Figure 7-9 inform that both are statically stable from the pitch point of view. The more negative M_w values by decreasing ride height are related to the surge of lift as

the vehicle approaches the ground. Moreover, the decreasing height increases the effective angle of attack due to the downwash intensification. Both conditions require larger moments to keep the system stable.

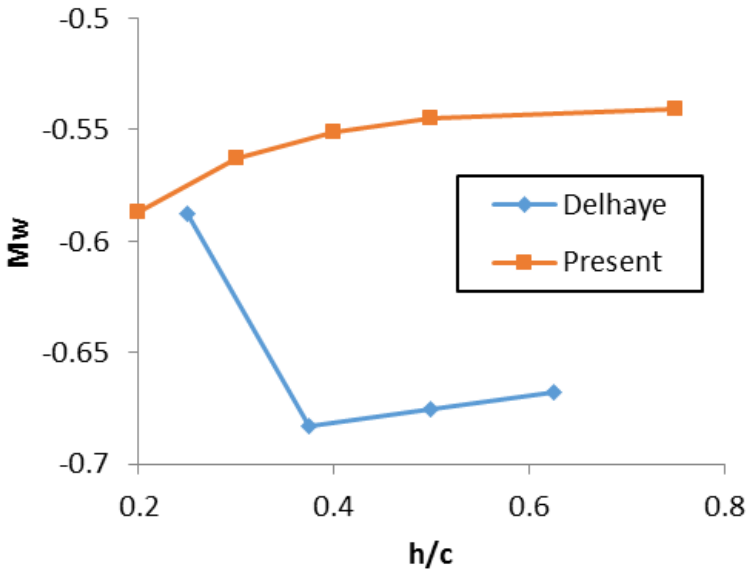

Figure 7-9 The derivative of M_w

Figure 7-10 depicted the derivative $M_{\dot{w}}$. The derivative explains the pitching moment with respect to the rate of change of normal velocity. Both curves in the figure show a similar trend that is getting less negative in value by decreasing ride height. Cook (2013, pt.13.2.6) mentioned that this derivative makes a substantial contribution to the damping of the SPPO mode. Figure 7-10 demonstrates that the decrease in ride height decreases the damping in the SPPO mode of the vehicle.

It should be noted that $\partial C_m/\partial\,\alpha$ is not the only parameter that influences WIGE craft static stability; ride height also plays an important role. The derivative of the pitching moment with respect to ride height, $\partial C_m/\partial(h/c)$, is linked to M_h, depicted in Figure 7-11. It shows a similar trend to Z_h, i.e. M_h of the configuration of the present study decreases exponentially with the ride height, while the configuration in Delhaye's (1997) study shows a particular function.

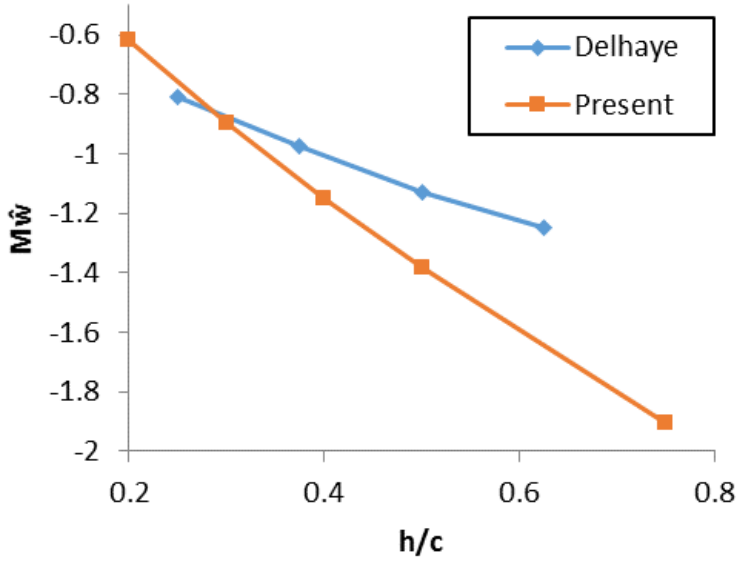

Figure 7-10 The derivative of $M_{\hat{w}}$

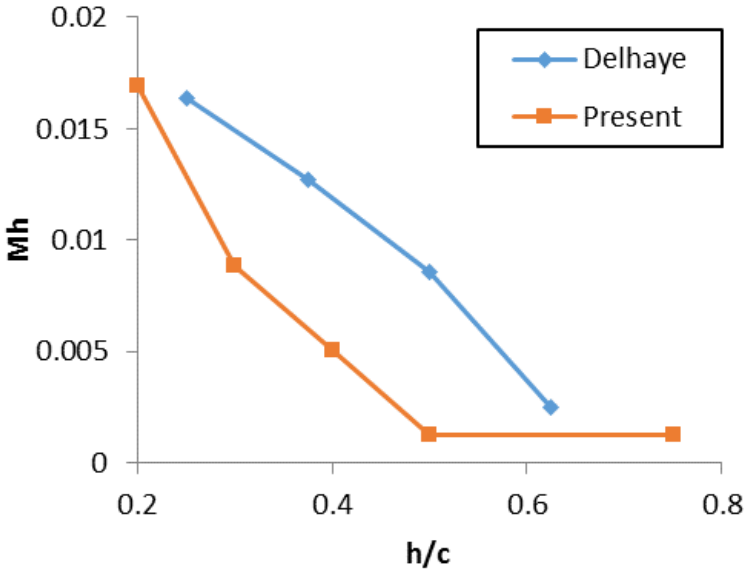

Figure 7-11 The derivative of M_h

Cook (2013, pt.6.2.1) explains that the SPPO mode is excited and manifests as a second order oscillation for which the principal variables are incidence, pitch rate and pitch attitude. These are linked to several aerodynamic derivatives, i.e. Z_w, Z_q, M_w and M_q. In the present study, the expressions for Z_q and M_q are not available, but both are linked to other derivatives, i.e. $Z_{\dot{w}}$ and $M_{\dot{w}}$.

A reduced-order equation shown in Cook (2013, p.156) indicates the relationship in the SPPO mode. The equation without contribution from the control system is as follows:

$$\begin{bmatrix} \dot{w} \\ \dot{q} \\ \dot{\theta} \end{bmatrix} = \begin{bmatrix} z_w & z_q & z_\theta \\ m_w & m_q & m_\theta \\ 0 & 1 & 0 \end{bmatrix} \begin{bmatrix} w \\ q \\ \theta \end{bmatrix} \tag{7-6}$$

In its simplest form the equation becomes:

$$\begin{bmatrix} \dot{w} \\ \dot{q} \end{bmatrix} = \begin{bmatrix} z_w & z_q \\ m_w & m_q \end{bmatrix} \begin{bmatrix} w \\ q \end{bmatrix} \tag{7-7}$$

which is possible when the assumption of $z_\theta = m_\theta = 0$ is taken into account.

The set of solutions is given by:

$$\begin{aligned} \boldsymbol{\Delta}(s) &= s^2 + 2\varsigma_s \omega_s s + {\omega_s}^2 \\ \boldsymbol{\Delta}(s) &= s^2 - \left(m_q + z_w\right)s + \left(m_q z_w - m_w U_e\right) \end{aligned} \tag{7-8}$$

The approximation of the damping and natural frequency is expressed as follows:

$$\begin{aligned} 2\varsigma_s \omega_s &= -\left(m_q + z_w\right) \\ \omega_s &= \sqrt{m_q z_w - m_w U_e} \end{aligned} \tag{7-9}$$

The relationship above shows that z_w, m_q and m_w affect the damping and natural frequency of the SPPO mode. As mentioned in Cook (2013, p.158), the solutions are a little bit complex as they involve several aerodynamic derivatives, and various contributions of these derivatives may not always be advantageous.

7.3.2 Dynamic Stability

Table 7-2 lists the roots of oscillation for the Ekranoplan 'Orlyonok' A-90 configuration adopted by the present study for the range of ride height between 0.2 and 0.75, keeping the coefficient of lift constant. Figure 7-12, Figure 7-13, and Figure 7-14 graphically depict the roots of the SPPO, phugoid, and speed subsidence mode of oscillation, as presented in Delhaye's work (the Clark Y wing section, endplates assumed) and in the present study (the NACA 4412 wing section, regular wingtip).

Table 7-2 Roots of oscillation of the Ekranoplan 'Orlyonok' A-90 (present study)

h/c	α [deg]	Roots of oscillation
0.2	4.1	$r_{1,2} = -0.6773 \pm 0.9141i$
		$r_{3,4} = -0.0563 \pm 0.2909i$
		$r_5 = -0.0183$
0.3	4.3	$r_{1,2} = -0.7058 \pm 0.8227i$
		$r_{3,4} = -0.0268 \pm 0.2197i$
		$r_5 = -0.0246$
0.4	4.5	$r_{1,2} = -0.7278 \pm 0.7737i$
		$r_{3,4} = -0.010 \pm 0.1791i$
		$r_5 = -0.0296$
0.5	4.6	$r_{1,2} = -0.7541 \pm 0.7307i$
		$r_{3,4} = -0.0085 \pm 0.1289i$
		$r_5 = -0.0341$
0.75	4.6	$r_{1,2} = -0.8248 \pm 0.6874i$
		$r_{3,4} = -0.0100 \pm 0.1210i$
		$r_5 = -0.0399$

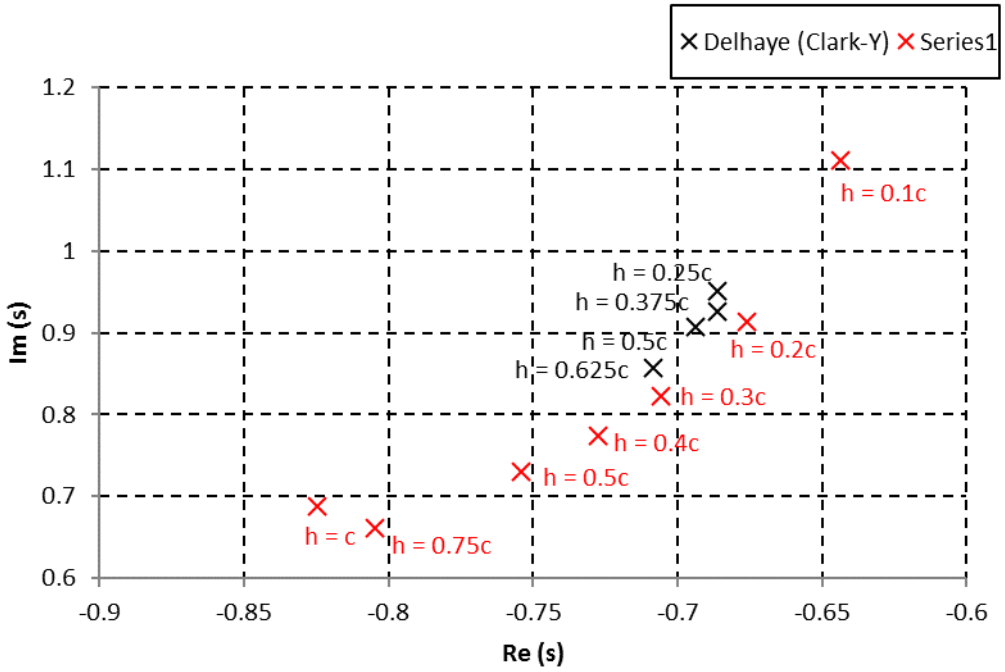

Figure 7-12 Characteristic roots of the SPPO mode of the Ekranoplan 'Orlyonok' A-90

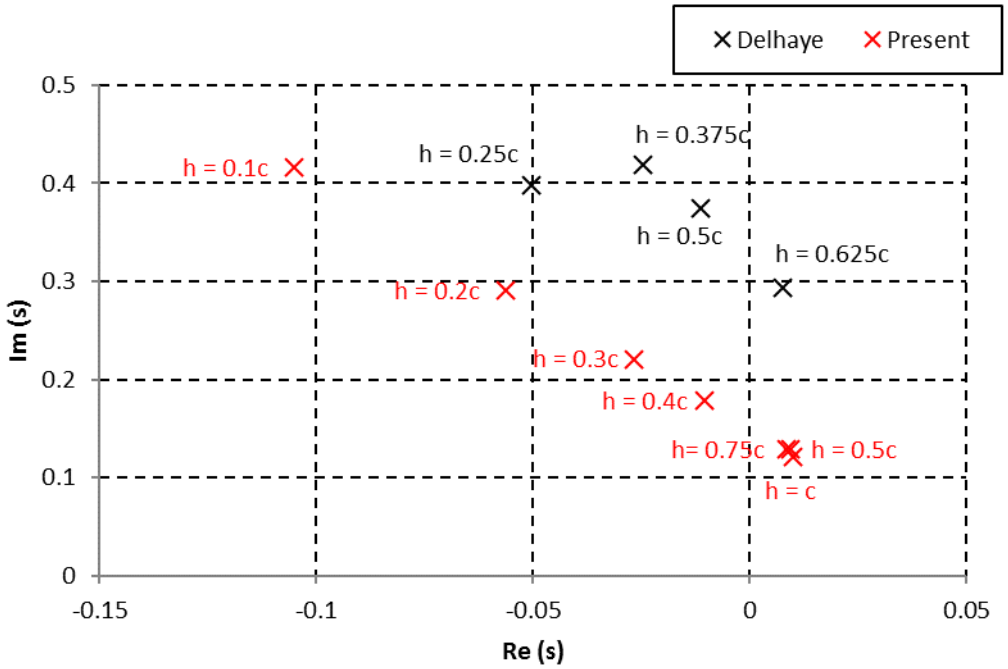

Figure 7-13 Characteristic roots of the phugoid mode of the Ekranoplan 'Orlyonok' A-90

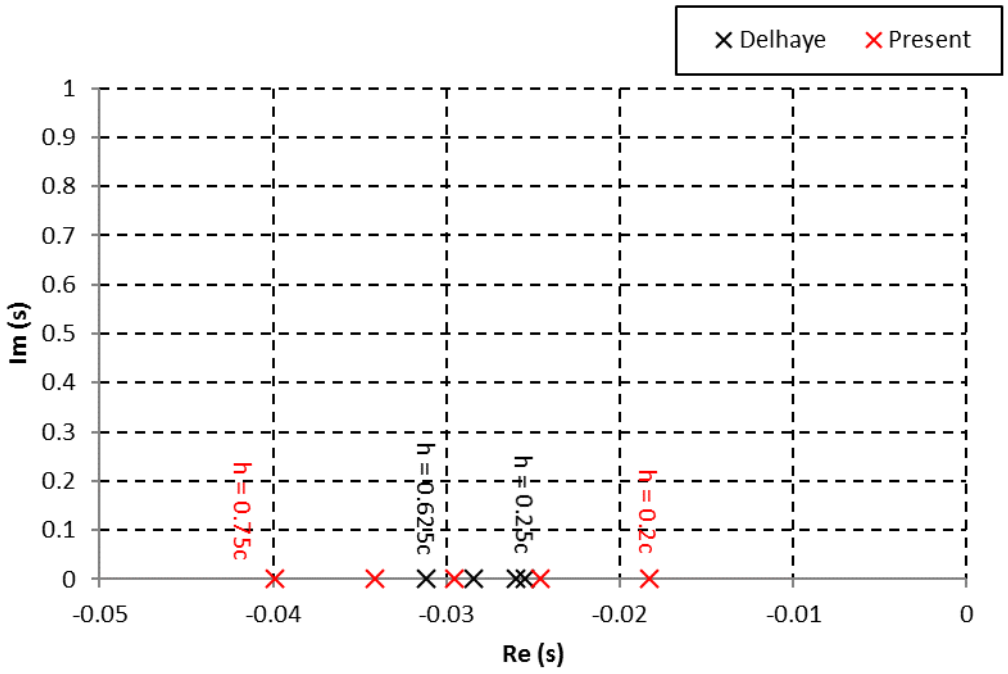

Figure 7-14 Characteristic roots of the subsidence mode of the Ekranoplan 'Orlyonok' A-90

The SPPO roots represented in Figure 7-12 show that the ride height has a much stronger influence for the configuration adopted for the present study than for the Delhaye (1997) case. For instance, in Delhaye's case, the imaginary values vary between ± 0.8 and ± 0.9 for a ride height between $0.25c$ and $0.625c$, while for the present case, the same variation occurs at ride heights between $0.2c$ and $0.3c$. The present case shows a wider range of roots of the SPPO mode. This indicates that the configuration adopted by Delhaye is more unresponsive toward the change in the ride height. From the design point of view, this is a good feature as the design range would not be too wide.

Also from Figure 7-12, one can recognise that the imaginary component of the roots for Delhaye's case is slightly larger than for the present study. The disparity in imaginary values between both configurations is expected due to the absolute values of the aerodynamic derivatives Z_w, M_w and $M_{\dot{w}}$. The configuration adopted by Delhaye

has larger values than the configuration adopted in the present study for these derivatives; see Figure 7-6, Figure 7-9, and Figure 7-10.

It is known that the SPPO mode is influenced mainly by the time response of *w* and *q* (Cook, 2013, pp.156–159). In the analyses, the variance of *q* in the calculation is neglected as all derivatives due to the pitch rate are made constant. This simplification leads to the conclusion that the difference is due to the time response of *w* only and it is interchangeable with the angle of attack, *α*. From this relationship, it can be concluded that the difference in the imaginary part of the roots is related to the difference in the angle of attack or, more precisely, in the gradient of pitching moment against the angle of attack. The configuration adopted by Delhaye has a larger gradient that leads to larger imaginary part of the roots, and also leads to larger natural frequencies than the configuration adopted in the present study for the same ride height.

With regard to the difference in the real components, it can be seen that for the present case, the real values cover a wide range by changing ride height. This phenomenon is likely to be caused by the derivative of normal force with respect to the ride height. The increment of the value by decreasing the ride height in the present study is more substantial than for Delhaye's (1997) case.

The phugoid mode of oscillation characteristics, as shown in Figure 7-13, also shows some discrepancies between the configuration adopted by Delhaye and that in the present work. In the present case, there are lower imaginary values than in Delhaye's work. It indicates that in the configuration adopted by Delhaye is higher in X_u than the configuration adopted in the present case. This is related to the differences in drag force, as has explained in Subsection 7.3.1 which, in Delhaye's case, demonstrates larger values at each height. The configuration adopted by Delhaye shows instability occurring at the ride height $0.625c$, while for the present case, it comes earlier, at the ride height $0.5c$. This may indicate that the addition of endplates, as assumed in the Delhaye case, improve the stability of the vehicle.

The phugoid mode of oscillation characteristics for the configuration adopted in the present study can be separated into three regions. The first region, where the effect of ride height is minimal, is for a ride height towards the freestream (in this study for ride heights $\geq 0.5c$). The second region, where the height moderately influences the

phugoid mode characteristics, occurs in an intermediate ride height range (in this study for ride heights between $0.3c$ and $0.5c$). The third region, where the height has a substantial effect, occurs for conditions closer to the extreme ground effect regime (in this case for ride heights $\leq 0.2c$).

The characteristics of the phugoid mode are linked to the time variation of u and θ (Cook, 2013, pp.159–163). In both analysis cases, u only affects the axial force (drag). The θ gives information about the downwash angle ε. The ratio of downwash angle to the angle of attack $\partial\varepsilon/\partial\alpha$ in Delhaye's case is smaller than in the present study. This is because the effective angle of attack in the present case is larger than in Delhaye's work in order to obtain a similar aerodynamic characteristic.

For the speed subsidence mode, as shown in Figure 7-14, there is a significant difference between configurations adopted in Delhaye's (1997) case and the present study. In the present study, the roots of the speed subsidence mode have a wider range of value than in Delhaye's case with a similar range of ride height. This shows that the configuration adopted by Delhaye has more rigidity in operation, which is expected due to the assumed endplates in the configuration.

All the findings from the previous investigations confirm the importance of careful choice of wing configuration since it has a substantial impact on the stability of the WIGE craft. Further, Rozhdestvensky (2006) comments on the importance of the profile choice from the aerodynamic efficiency point of view. It conveys the effect of the choice of the aerofoil on the stability of the craft.

7.4 Constant angle of attack versus constant coefficient of lift

This section compares and contrasts two approaches that can be used to perform the stability analysis of a vehicle in the ground effect condition. The first approach is to present the results keeping the lift constant, varying the angle of attack. The approach that was used by Delhaye (1997) had a coefficient of lift maintained at 0.616. The results presented in the two previous sections have also adopted this approach. Another perspective is given by keeping a constant the angle of attack, as in Chun and Chang (2002).

Table 7-3 and Table 7-4 show the roots of characteristic polynomial along with the natural frequencies and damping ratios using both approaches ($C_L = 0.616$ and $\alpha = 4°$) for the configuration of the Ekranoplan 'Orlyonok' A-90 adopted in the present study. The natural frequency and damping ratio of both SPPO and phugoid modes is not substantially affected by the choice: they are different to the speed subsidence mode; see Figure 7-15, Figure 7-16, and Figure 7-17. In the speed subsidence mode, the difference between the two options diminishes by reducing ride height. The effect of the constant angle of attack to speed subsidence, as depicted in Figure 7-17, is less significant by increasing height than the constant lift.

The difference in the speed subsidence mode is linked with the w and θ, as shown in the relationship for the h derivative from the equations of motion below:

$$\dot{H} = -w + \theta U_e \tag{7-10}$$

In the case of constant lift, the increase of effective angle of attack with the increase in the ride height is expected. The increase of effective angle of attack is linked with the effective pitch position of the vehicle. As the pitch angle increases, the derivatives with respect to ride heights increase. Contrarily, in the case of a constant angle of attack, one may expect, relatively, the same pitch position but, at the same time, it has a decreasing lift by increasing ride height. This is the reason that the constant lift curve tends to have larger absolute values with the increase in ride height compared to the constant angle of attack curve in Figure 7-17.

Table 7-3 Roots of oscillation, natural frequency and damping ratio of the Ekranoplan 'Orlyonok' A-90 at constant C_L = 0.616

h/c	α [deg.]	Mode		Speed subsidence
		Short period	Phugoid	
0.1	3.4	$-0.6436 \pm 1.1107i$	$-0.1053 \pm 0.4166i$	0.0046
		$\omega_s = 1.2837$	$\omega_p = 0.4297$	
		$\zeta_s = 0.5014$	$\zeta_p = 0.2450$	
0.2	4.1	$-0.6762 \pm 0.9132i$	$-0.0563 \pm 0.2909i$	0.0199
		$\omega_s = 1.1363$	$\omega_p = 0.2963$	
		$\zeta_s = 0.5951$	$\zeta_p = 0.1899$	
0.3	4.3	$-0.7058 \pm 0.8227i$	$-0.0268 \pm 0.2197i$	−0.0246
		$\omega_s = 1.0840$	$\omega_p = 0.2214$	
		$\zeta_s = 0.6511$	$\zeta_p = 0.1210$	
0.4	4.5	$-0.7278 \pm 0.7737i$	$-0.0104 \pm 0.1791i$	−0.0296
		$\omega_s = 1.0622$	$\omega_p = 0.1795$	
		$\zeta_s = 0.6851$	$\zeta_p = 0.0580$	
0.5	4.6	$-0.7541 \pm 0.7307i$	$0.0085 \pm 0.1289i$	−0.0341
		$\omega_s = 1.0500$	$\omega_p = 0.1292$	
		$\zeta_s = 0.7181$	$\zeta_p = -0.0657$	
0.75	4.6	$-0.8248 \pm 0.6874i$	$0.0100 \pm 0.1210i$	−0.0399
		$\omega_s = 1.0737$	$\omega_p = 0.1215$	
		$\zeta_s = 0.7725$	$\zeta_p = -0.0827$	
1.0	4.6	$-0.8046 \pm 0.6614i$	$0.0092 \pm 0.1294i$	−0.0391
		$\omega_s = 1.0415$	$\omega_p = 0.1297$	
		$\zeta_s = 0.7725$	$\zeta_p = -0.0709$	

Table 7-4 Roots of oscillation, natural frequency and damping ratio of the Ekranoplan 'Orlyonok' A-90 at constant α = 4º

h/c	C_L	Mode		Speed subsidence
		Short period	Phugoid	
0.1	0.6971	$-0.6290 \pm 1.1348i$ $\omega_s = 1.2975$ $\zeta_s = 0.4848$	-0.1224 ± 0.4020i $\omega_p = 0.4202$ $\zeta_p = 0.2913$	-0.0110
0.2	0.6426	$-0.6768 \pm 0.9126i$ $\omega_s = 1.1362$ $\zeta_s = 0.5957$	$-0.0554 \pm 0.2915i$ $\omega_p = 0.2967$ $\zeta_p = 0.1866$	-0.0181
0.3	0.6204	$-0.7061 \pm 0.8234i$ $\omega_s = 1.0847$ $\zeta_s = 0.6510$	$-0.0239 \pm 0.2212i$ $\omega_p = 0.2225$ $\zeta_p = 0.1074$	-0.0230
0.4	0.6096	$-0.7251 \pm 0.7779i$ $\omega_s = 1.063$ $\zeta_s = 0.6818$	$-0.0086 \pm 0.1796i$ $\omega_p = 0.1798$ $\zeta_p = 0.0480$	-0.0264
0.5	0.6036	$-0.7471 \pm 0.7388i$ $\omega_s = 1.0507$ $\zeta_s = 0.7110$	$0.0078 \pm 0.1264i$ $\omega_p = 0.1266$ $\zeta_p = -0.613$	-0.0300
0.75	0.6000	$-0.8106 \pm 0.7029i$ $\omega_s = 1.0729$ $\zeta_s = 0.7555$	$0.0081 \pm 0.1191i$ $\omega_p = 0.1194$ $\zeta_p = -0.0678$	-0.0333
1.0	0.6002	$-0.7912 \pm 0.6798i$ $\omega_s = 1.0431$ $\zeta_s = 0.7585$	$0.0083 \pm 0.1265i$ $\omega_p = 0.1268$ $\zeta_p = -0.0656$	-0.0338

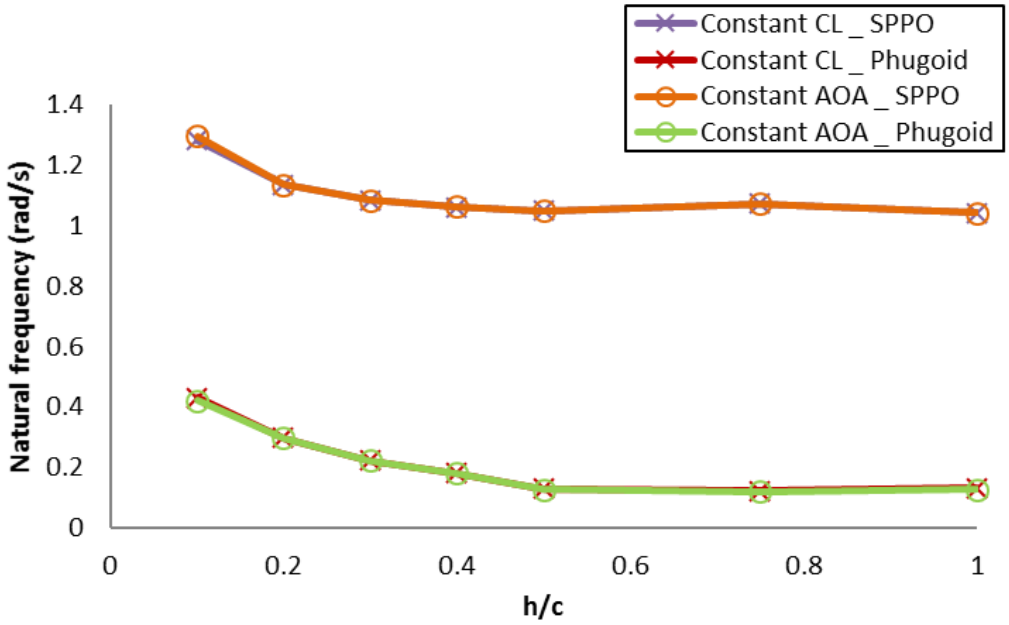

Figure 7-15 Natural frequencies of the Ekranoplan 'Orlyonok' A-90

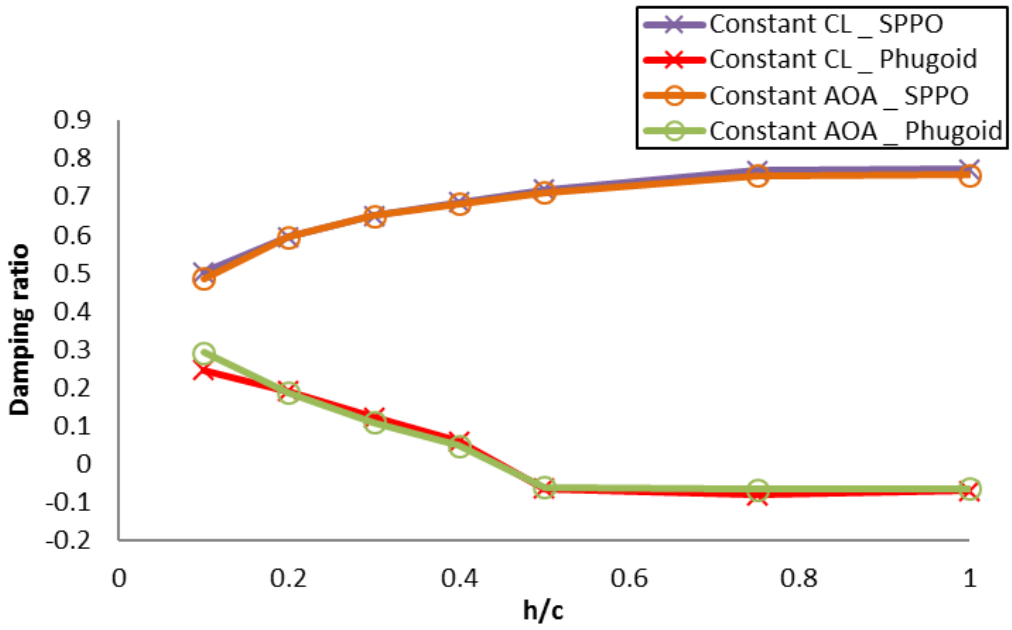

Figure 7-16 Damping ratio of the Ekranoplan 'Orlyonok' A-90

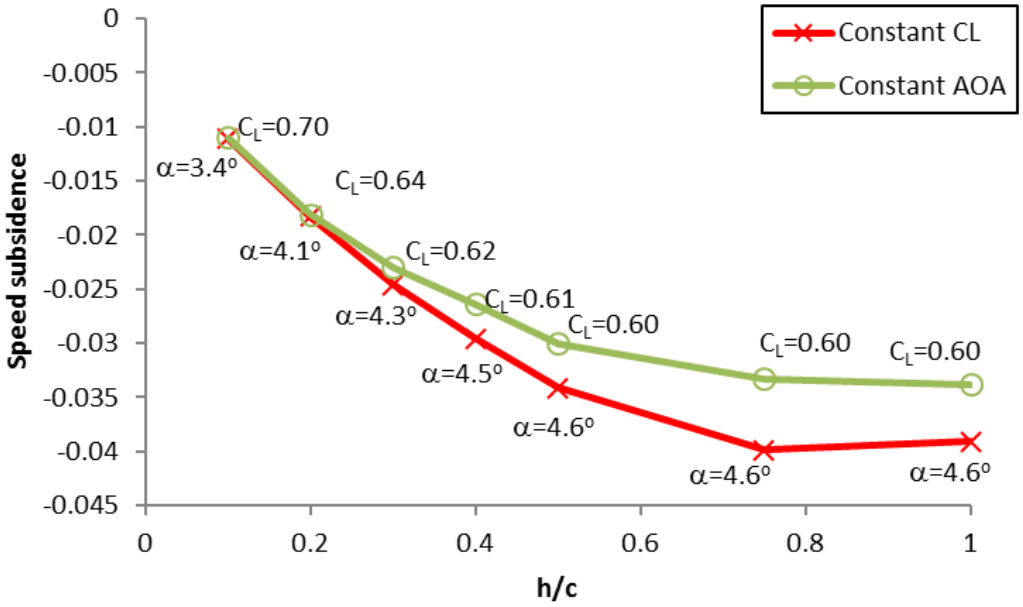

Figure 7-17 Speed subsidence of the Ekranoplan 'Orlyonok' A-90

From the vantage point of controllability, it is more challenging to keep lift constant than to maintain the angle of attack constant considering the oscillation of the system. Nonetheless, the stability analyses the present case are undertaken with the approach of a steady lift, following the approach by Delhaye (1997). This decision is taken from the fact that the preceding comparison explained in Sections 7.2 and 7.3 refers to the Delhaye work. The second reason is related to reducing the level complexity; this is because with constant lift one can reduce at least one free variable, i.e. Z_w becomes constant. The third reason relates to the effect to the overall characteristic of the natural frequency and damping ratio. As just explained, there are no significant differences by keeping the lift constant or the angle of attack constant.

7.5 Effect of observation data points

The CFD simulations performed using the oscillating NACA 4412 aerofoil in the ground effect covered three ride heights ($h = 0.3c$, $0.5c$ and c), four frequencies ($\omega = 0.25$, 0.50, 1.00, and $1.25\ rad/s$), and two amplitudes ($A = 0.05c$ and $0.15c$).

This has been considered a good compromise between the time and resources available, the accuracy of the results, and the range of parameters investigated. Following the calculation of the stability derivatives (see Section 6.2), the author used linear interpolation for most of the data and nearest neighbour interpolation for the last data point. It has been observed that a larger number of ride heights, frequencies, and amplitudes would have allowed a better estimation of the stability derivatives.

To test the accuracy of stability derivatives with three heights' data, the author has compared the characteristic roots for the non-oscillating case, approximated from three ride heights' and seven ride heights' datasets.

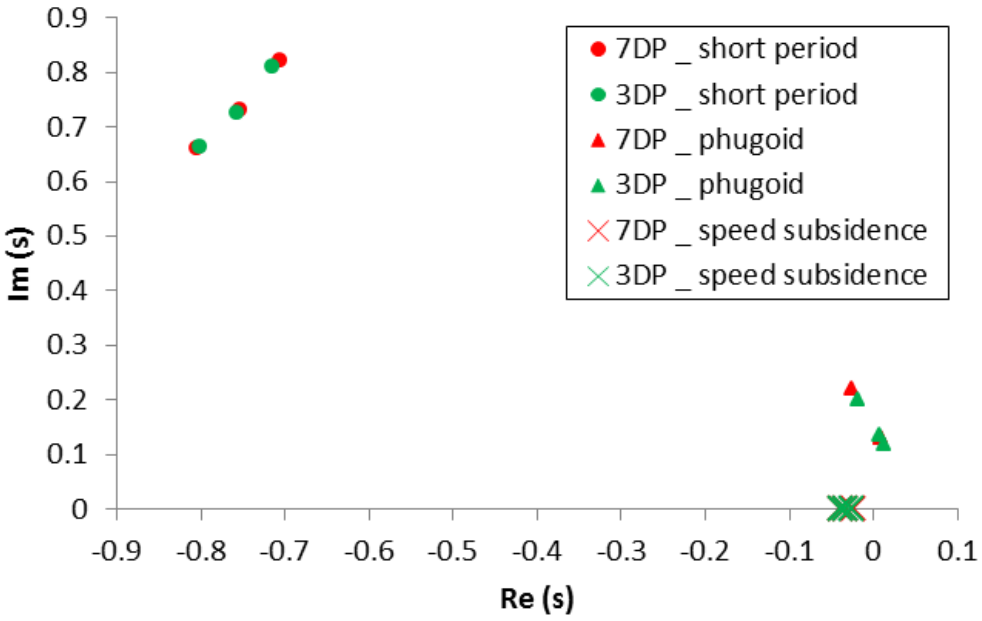

Figure 7-18 Effect of different data points on characteristic roots of the Ekranoplan 'Orlyonok' A-90 (at $h/c = 0.3$, 0.5, and 1.0)

Figure 7-18 shows that at $h/c = 0.3$, $h/c = 0.5$ and $h/c = 1.0$, the trend of the derivatives' values estimated with seven data points and three data points; as can be observed, they are very similar. The discrepancies are small for the SPPO and speed subsidence with less than two percent difference. A concern may

occur to the phugoid mode, as its real values are around 30% different between the analyses using three data points and seven data points. However, the percentage is obtained from small denominator numbers. In absolute terms, the difference in numbers does not exceed one thousandth.

The results give a reasonable level of confidence to proceed to the next step with the oscillating case with the three heights' dataset.

7.6 Effect of oscillation on the characteristic roots

Following the results described in Chapter 5, it has been observed that for small angles of attack and ride heights towards extreme ground effect, the lift coefficient drops substantially due to the Venturi effect. Thus, the range of angles of attack that creates such a phenomenon is excluded from the following stability analysis.

In Chapter 6, the impact of the oscillation on the aerodynamics of the vehicle has been shown. A substantial impact on the dynamic stability characteristics is, therefore, expected. The initial hypothesis is that the characteristic roots of the oscillating case would go through a hysteresis path. It is worth being reminded that the vehicle experiences periodic changes in both motion and forces, and the hysteresis here means the characteristic disparity from the relative position of the vehicle over the surface in non-oscillating conditions. The illustration of how oscillation affects the characteristic roots is depicted in Figure 7-19, Figure 7-20, and Figure 7-21 for the SPPO, Phugoid, and speed subsidence modes, respectively; the hypothesis has been confirmed.

Figure 7-19 shows the hysteresis of the SPPO mode for the oscillation with $A = 0.05c$ and $\omega = 0.25\, rad/s$ (or $k = 0.026$), compared to the non-oscillating case. The root values change in a loop form. A general observation from the figure is that, with decreasing height, the natural frequency of the mode increases, and the damping decreases. This observation on the mode's natural frequency behaviour is deduce from the increase in the length between the roots and the point of origin of root locus by the decrease in ride height. On the other hand, the slopes of the roots from the point of origin of root locus also increases by the

decrease in ride height which indicates the behaviour of damping ratio. It is known that the length between the point of origin and a root value indicates the magnitude of the natural frequency. On the other hand, the slope is linked to the damping ratio; the larger the slope, the smaller the damping ratio becomes.

Here, one can also distinguish three types of loop form. The first type is a horizontally flattened loop, occurring at $h/c = 1.0$ (represented in green in the figure). The second type is a moderate loop, occurring at $h/c = 0.5$ (represented in blue in the figure). The third type is a leaning oval loop, occurring at $h/c = 0.3$ (represented in red in the figure). These differences are expected to be influenced by several parameters, i.e. ride height, frequency, amplitude, and effective angle of attack.

At $h/c = 1.0$, the damping property of the SPPO mode changes periodically, as can be seen in the real component of green loop curve in Figure 7-19. Interestingly, the imaginary component is relatively stable, which indicates the change in damping is compensated almost by the natural frequency of the mode following the relationship $\omega_s\sqrt{1-{\zeta_s}^2} = constant$.

In Cook (2013, p.158), the damping of a conventional aeroplane is linearly linked to the derivative M_q. However, in the ground effect case, the effect of ride height also contributes to the damping, especially by the derivative M_h. Thus, even though the derivative is made constant (following Delhaye's setting), one should not expect that the damping in SPPO mode remains constant.

The effect of ride height also affects the natural frequency of the SPPO mode which is linked to the M_w (Cook, 2013, p.158). From stability derivatives analysis in section 6.3, the value of M_w changes periodically due to the oscillation of the vehicle.

It worth reminding that at $h/c = 1.0$ the effect of ride height is considerably small to damping ratio and natural frequency of the SPPO mode. From the observation has been made, at this ride height the deviation of the crest and trough is very

small with only about 0.004 difference which apply for both the natural frequency and damping ratio of the SPPO mode.

At $h/c = 0.5$, the characteristic roots move into more a squared loop shown by the blue curve in Figure 7-19. In addition, one can see that the curve is higher in both imaginary and real values compared to the curve produced at $h/c = 1.0$.

The shift of curve position showing that the increase in the natural frequency of the mode and the decrease in damping ratio. The decrease in damping ratio is more progressive than the increase in the natural frequency. On the other hand, the curve loop indicates that the effect of oscillation toward the SPPO mode. The oscillation has slightly more impact on the natural frequency than the damping ratio. The deviation of the crest and trough of the natural frequency at $h/c = 0.5$ is 0.008, while the damping ratio only gives 0.005 for value discrepancy.

The effect of ride height is stronger in closer proximity, as shown by the red curve in Figure 7-19 for $h/c = 0.3$. Here both the natural frequency and damping ratio is strongly affected by the ride height. This can be determined from the longer range of real and imaginary components of the root values, which are contributed by the derivative M_w and M_h. From the analysis of stability derivatives, it is known that there is a significant range for both derivatives at this ride height compared to the other higher heights. At this ride height, the deviation of the crest and trough of the natural frequency is multiplied by almost tenfold compared to what occurred at $h/c = 1.0$. For the damping ratio, the deviation between $h/c = 1.0$ and $h/c = 0.3$ increases by eightfold.

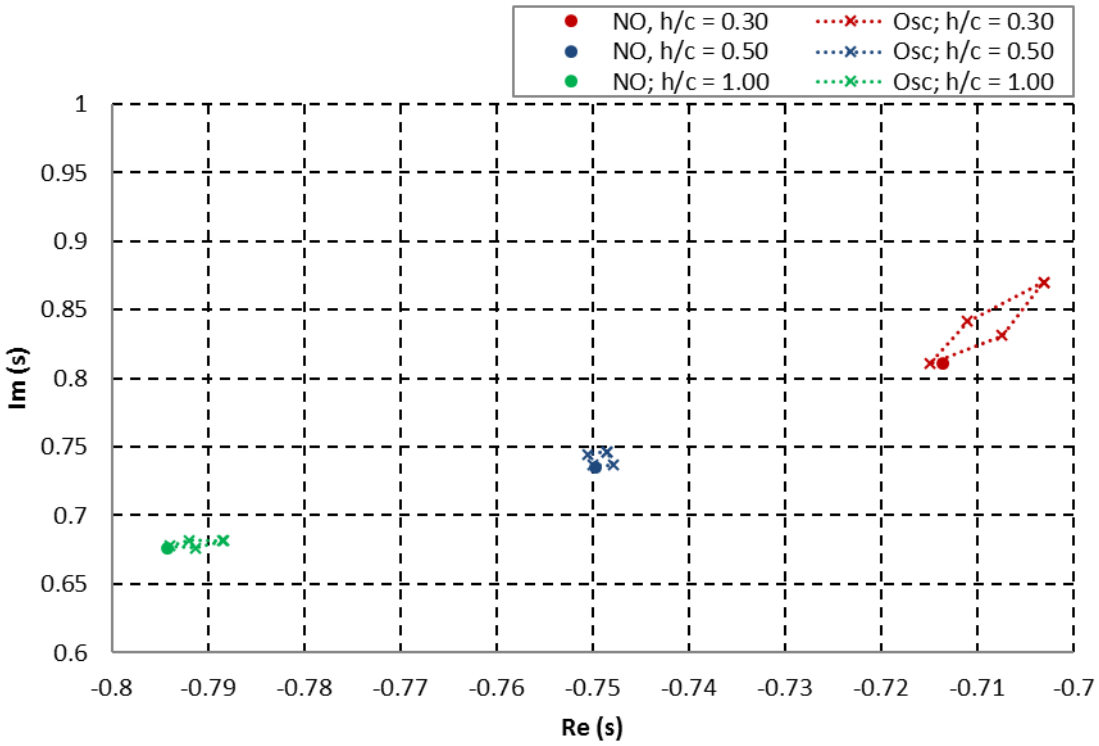

Figure 7-19 Characteristic roots of the SPPO mode of the Ekranoplan 'Orlyonok' A-90 for non-oscillating and oscillating cases ($k = 0.026$; $A/c = 0.05$)

It worth mentioning that at all heights, the curves loop in a clockwise manner and the crest of amplitudes occurs at 50% of the wavelength. This indicates that the root at these heights has about $\pi\, rad/s$ phase difference from the motion. Interestingly, it also informs that the maximum damping occurs in 50% of the wavelength for all ride heights.

From the three curves, one can also see that the crest of amplitude occurs near the root value when the craft is in a non-oscillation condition. From this, the author expects that the periodic changes of the root in SPPO mode for a given condition are similar to the function of the motion but with $\pi\, rad/s$ phase. It is also expected that the mean value of the characteristic root of the oscillating vehicle is near to the characteristic root of the vehicle without oscillation.

Figure 7-20 depicts the behaviour of the phugoid mode. Just like the SPPO mode, the phugoid roots for the oscillating case change from time to time, creating a

loop. However, the loop is so thin thus looks like a line instead of a ring. This happens for all ride heights.

The explanation of the hysteresis behaviour can be traced back to the derivative Z_u of the present configuration. In Cook (2013, p.162) it is explained that the natural frequency of the phugoid mode for conventional aircraft is linked with this derivative. However, it known that for the configuration adopted for the present study, the derivative was set as a constant. Without considering the effect of height for now, one may say the effect of natural frequency is constant to the natural frequency of the root. However, the case shows a difference with the occurrence of the range of root values. This shows the effect of height exists in the mode.

The difference in the range shown by the three heights is expected to be exponential, and it can be explained by the logic of the ground effect phenomenon. In Figure 7-20 at $h/c = 1.0$ (depicted in the green curve) and $h/c = 0.5$ (depicted in the blue curve), the range of the root values is almost similar, but the range becomes strikingly wider at $h/c = 0.3$. This is expected as it follows the trend in the derivative Z_h. It is also observed that the decrease in ride height allows the vehicle to be more stable in the phugoid mode, which also behaves exponentially. At $h/c = 0.5$, the values only decrease a little compared to the $h/c = 1.0$. When at $h/c = 0.3$, a significant decrease occurs bringing the curve in the negative area of the real component. This phenomenon shows the constraints of the vehicle regarding the operational ride height.

Also, one may observe the change of the damping ratio, where the smallest damping occurs in 50% of the wavelength.

Another observation about the curves in Figure 7-20 is the position of the amplitude and the looping behaviour. All the curves have the trough of amplitude at 50% of the wavelength, and the values change in a clockwise manner. This shows that the phugoid mode behaves in about $\pi\, rad/s$ phase difference from the motion, or in other words the mode is negating the motion.

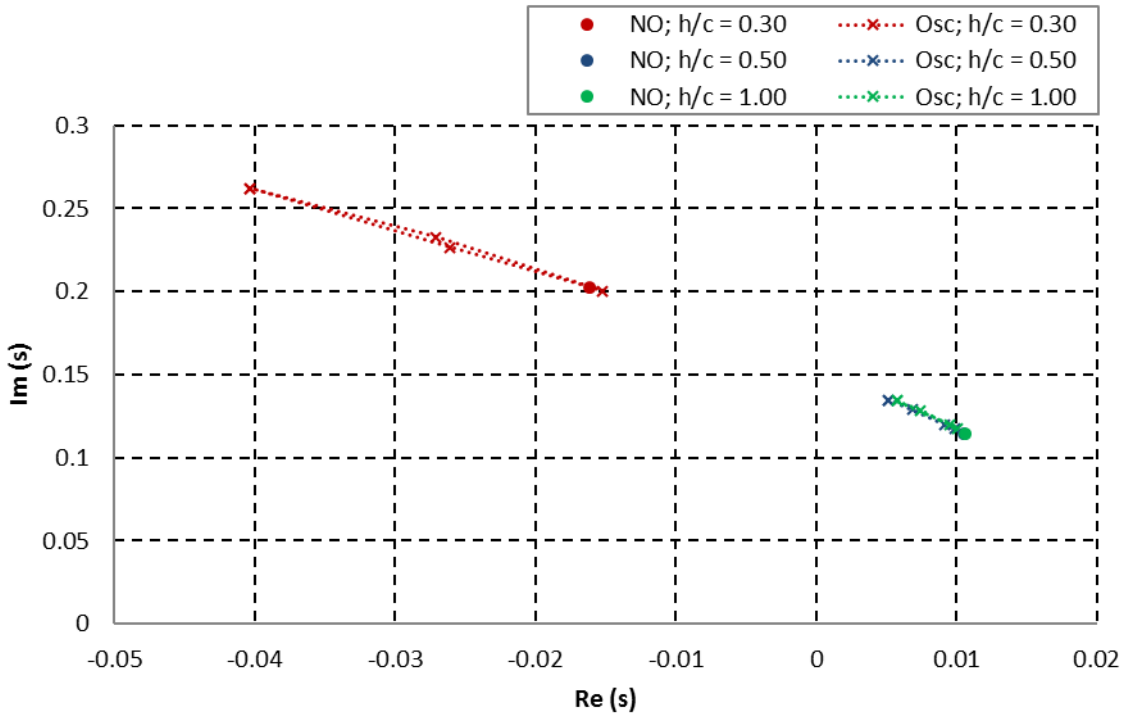

Figure 7-20 Characteristic roots of the phugoid mode of the Ekranoplan 'Orlyonok' A-90 for non-oscillating and oscillating cases ($k = 0.026$; $A/c = 0.05$)

The hysteresis behaviour is also linked to the characteristics of the natural frequency and damping ratio of the mode. It has been observed that in the phugoid mode for the case as shown in Figure 7-20, the natural frequency and damping ratio oscillate in a similar manner. It means there is no phase difference between the natural frequency and damping ratio.

Figure 7-21 depicts the behaviour of the speed subsidence mode, which also shows the fluctuation of values due to the oscillation indicating the hysteresis from the non-oscillating case. It has a similarity to the other two modes from the point of view that the range of its values depends on the ride height. This behaviour is reasonable as the subsidence mode relates to the ride height dynamic stability. In the figure, it can be seen that the decreasing ride height widens the range of the root values. However, it worth reminding that the speed

subsidence mode is a non-oscillatory root. It has a different explanation why the alteration of the range of root values due to the change in ride height.

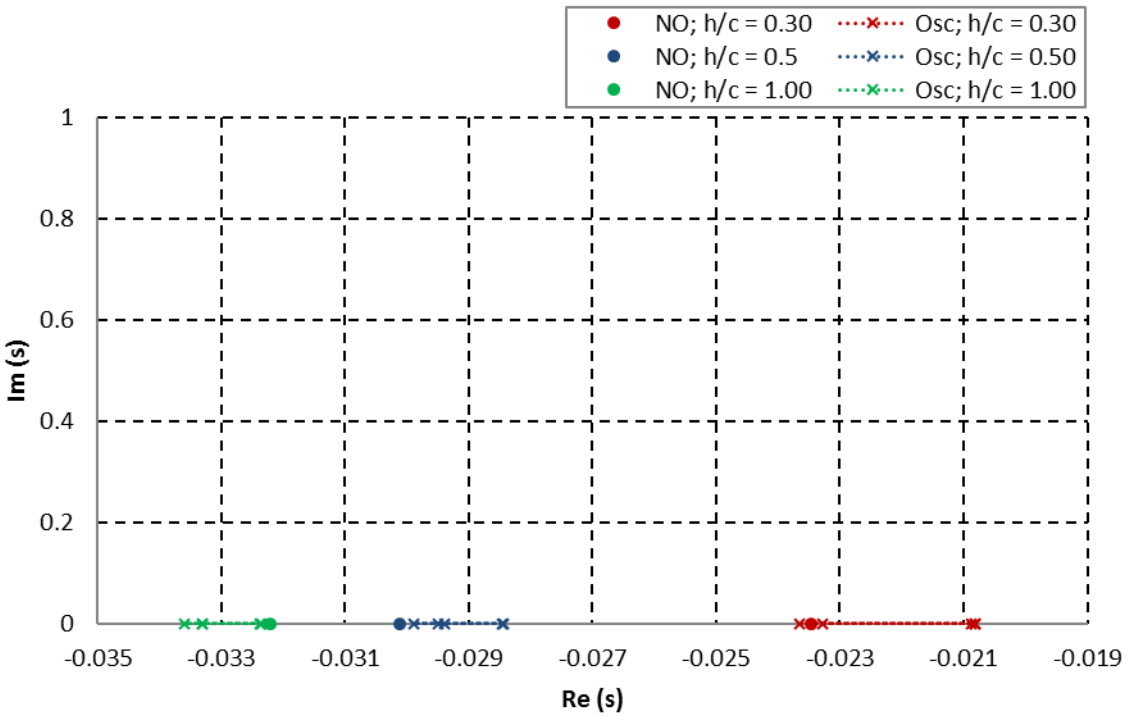

Figure 7-21 Characteristic roots of the speed subsidence mode of the Ekranoplan 'Orlyonok' A-90 for non-oscillating and oscillating cases ($k = 0.026$; $A/c = 0.05$)

From the system of equations of motion, the speed subsidence mode is linked with the normal component of velocity and pitch angle; that is $\partial h/\partial t = -w + U_e\theta$. The oscillation of the vehicle affects the values of vertical velocity w, as has been explained in Section 5.3. Moreover, the oscillation also affects the effective angle of attack which is linked with θ. The value of the root in each position along the wavelength is determined by the instantaneous value of w and θ at that position.

It is also observed that as the decrease in ride height increases the root becomes closer to zero. This is related to θ that determines the attitude of the vehicle. To

reach the same lift force as required in this case, the pitch angle needed is smaller for closer proximity. This leads to higher speed subsidence.

The effect of frequency of oscillation is depicted in Figure 7-22 for the SPPO mode, Figure 7-23 for the phugoid mode, and Figure 7-24 for the speed subsidence mode.

In the case of the SPPO mode, one can see the evolution of hysteresis. With the increase in frequency, the loop curves show significant changes at $h/c = 0.3$ compared to the higher ride heights. However, further detail can be attained for each height regarding the effect of the frequency of oscillation.

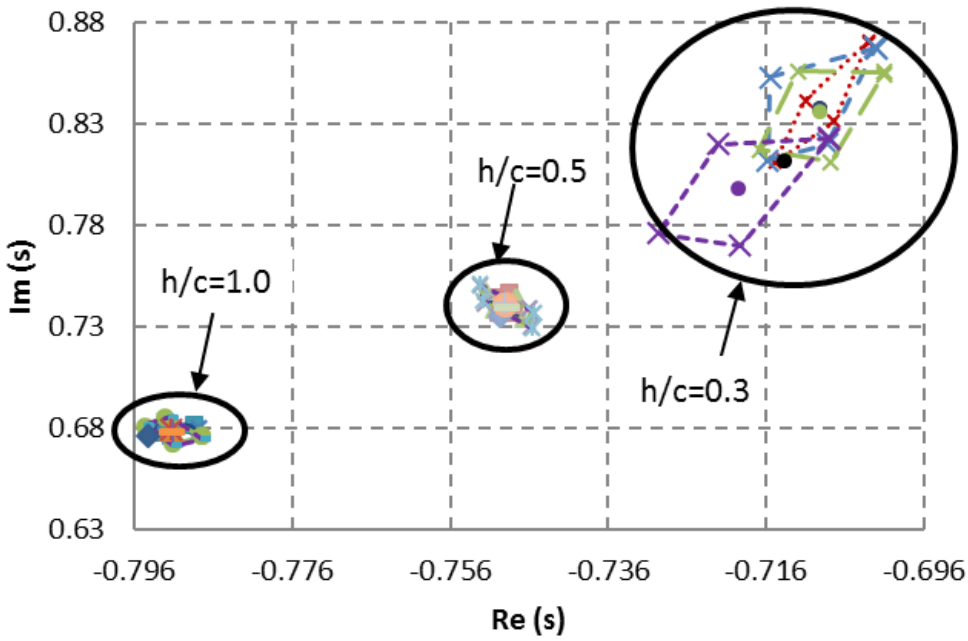

Figure 7-22 Roots of the SPPO mode at various k and h/c with $A/c = 0.05$

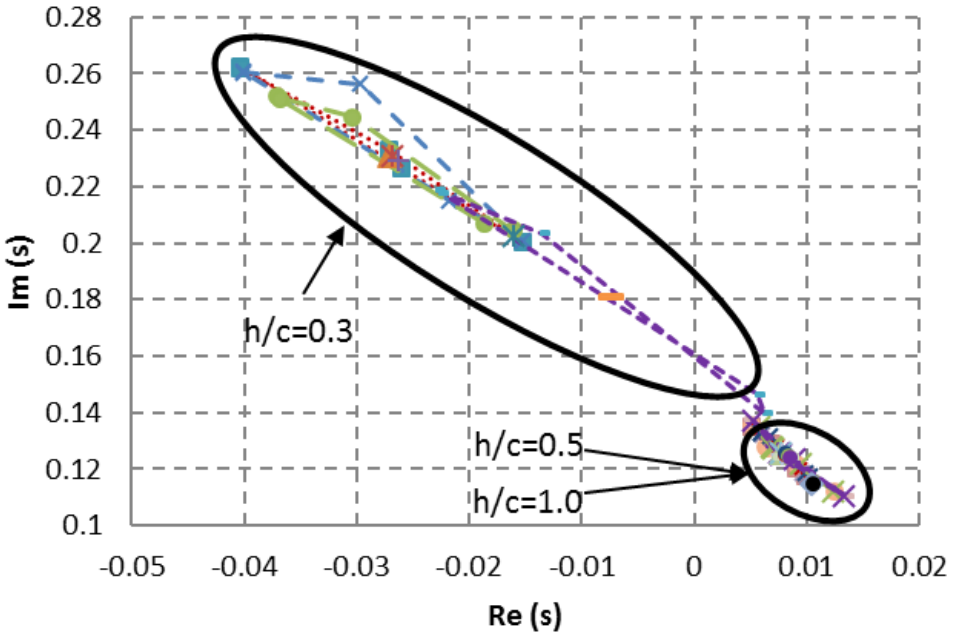

Figure 7-23 Roots of the phugoid mode at various k and h/c with $A/c = 0.05$

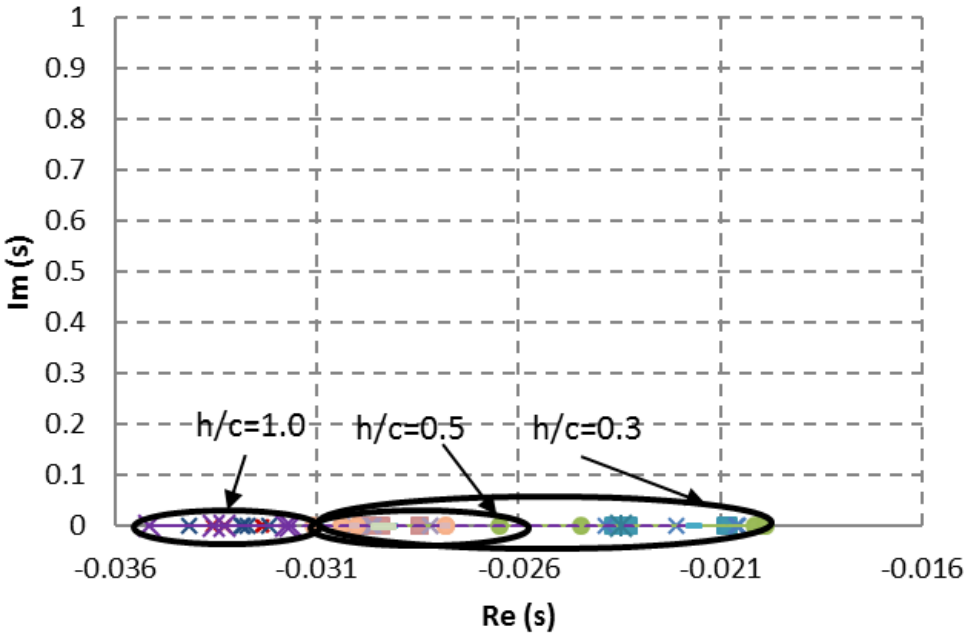

Figure 7-24 Roots of the subsidence mode at different k and h/c with $A/c = 0.05$

Figure 7-25 depicts the roots of the SPPO mode for $h/c = 1.0$. Here one can see that no significant difference applies to the range of real components, but an increase occurs for the range of imaginary components. In addition, with five observation points through a wavelength, it can be seen the curve has a more squared form (or with more points, expectedly, to be more rounded). This indicates that at this height the increase of frequency of oscillation dominantly affects the natural frequency of the mode than its damping behaviour.

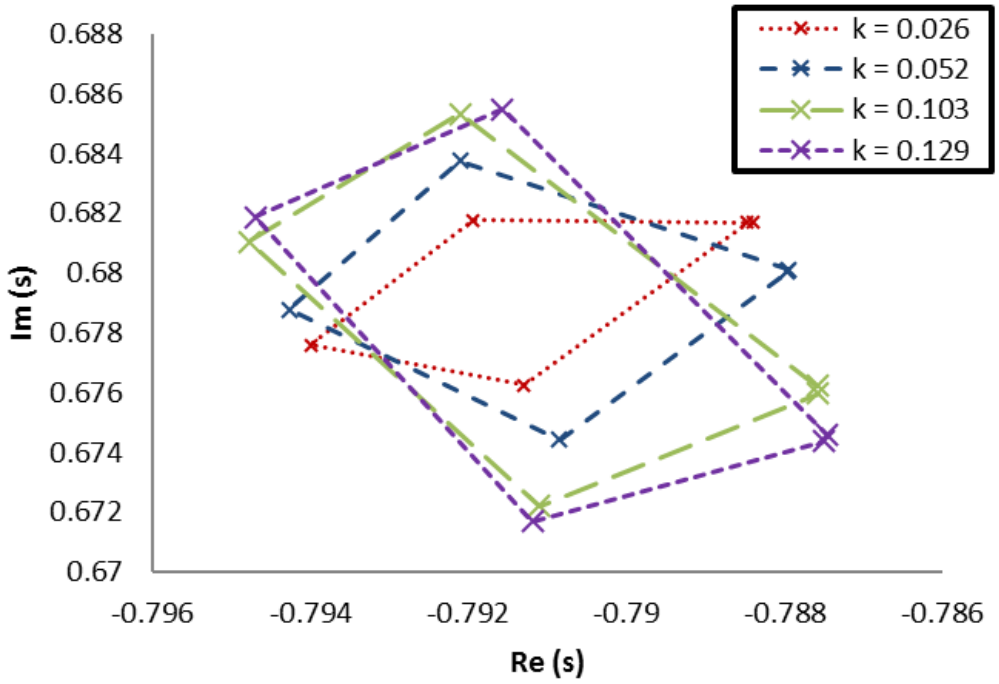

Figure 7-25 Roots of the SPPO mode at different k, $h/c = 1.0$, and $A/c = 0.05$

It is also observed that the peak of amplitude experiences a shift to 25% of the wavelength for $k = 0.052 - 0.129$, from before the peak occur at 0% of the wavelength for $k = 0.026$. From this, one may conclude the increase in frequency of oscillation that not only the range of natural frequency of the SPPO mode get wider but also there is also positive phase lag to the characteristic roots for this height.

At $h/c = 0.5$, an immediate identification regarding the effect of the alteration of frequency of oscillation is about the shape of the loop, see Figure 7-26. At this height, not only does the range of imaginary components of the roots become wider due to the increase of frequency of oscillation, but also the range of real components of the roots stretch. Here, one may expect the change occurs due to the deviation of both natural frequency and damping properties of the SPPO mode. The increase in frequency of oscillation leads to a wider range of natural frequency and damping ratio.

The shift of the location of the amplitude is also observed in this ride height. At $k = 0.026$, the peak happens at 0% of the wave length, while at $k = 0.052 - 0.129$, it happens at 25% of the wave length. Interestingly, there is a variety of where the maximum damping ratio occurs during one complete periodic motion, depending on the frequency of oscillation. At lower frequencies ($k = 0.026 - 0.052$), the maximum damping occurs at 50% of the wave length. At larger frequencies ($k = 0.103 - 0.129$), it happens at 75% of the wave length. The shift is determined from the slope of the characteristic root values to the point of origin of the root locus.

Despite the effect of frequency of oscillation being identified as $h/c = 1.0$ and $h/c = 0.5$, the impact is trivial. Referring to Figure 7-22, the change is very small causing the root values to look like a mass of points. The most significant impact occurs at $h/c = 0.3$.

In Figure 7-27, an expansion of the loop from $k = 0.026$ to $k = 0.103$ for $h/c = 0.3$ is identified, especially the change in the range of the real components of the roots for the SPPO mode. The expansion of the range of the natural frequency of the mode, due to the increasing frequency of oscillation, is responsible for this phenomenon.

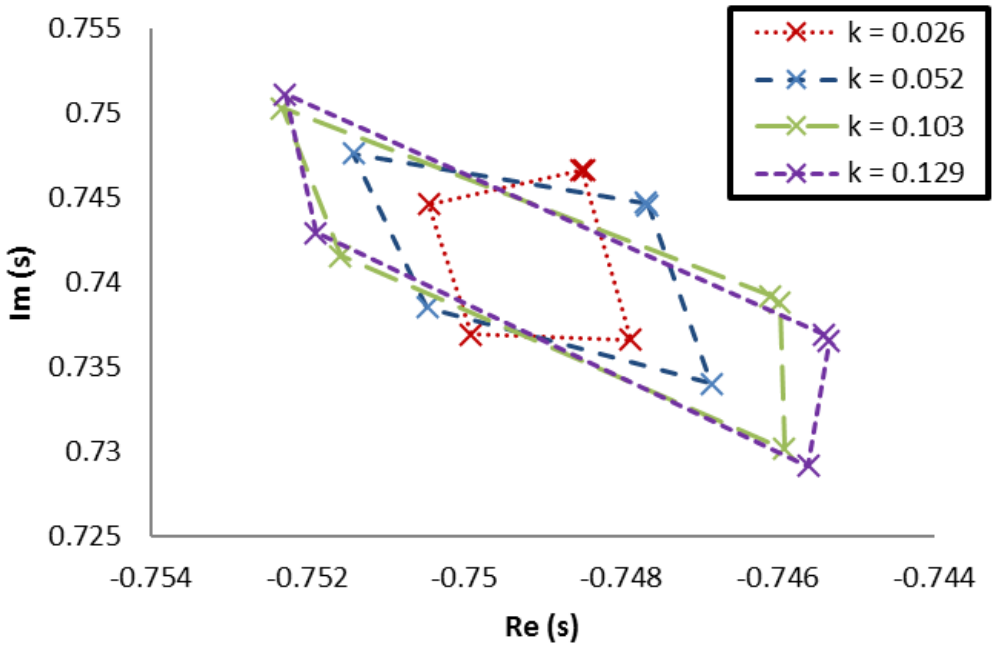

Figure 7-26 Roots of the SPPO mode at different k, $h/c = 0.5$, and $A/c = 0.05$

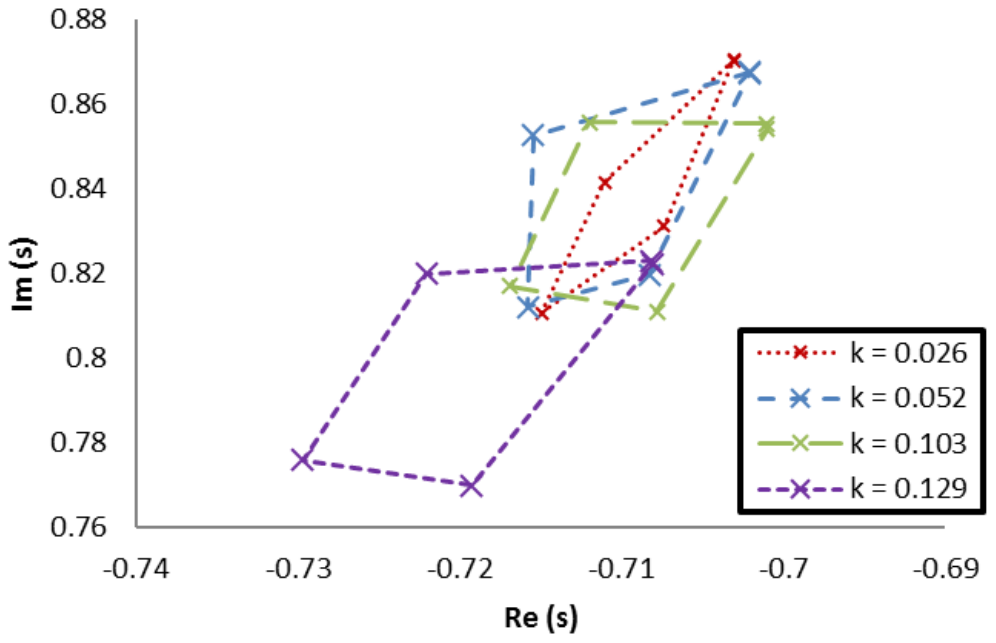

Figure 7-27 Roots of the SPPO mode at different k, $h/c = 0.3$, and $A/c = 0.05$

A peculiarity occurs at $k = 0.129$, where the loop curve shifts quite significantly. Here, one may identify that the change in the damping property is responsible for the shift. The peculiarity can be explained from what occurs at the aerodynamic level for a given frequency of oscillation, i.e. the occurrence of the Knoller (1909) – Betz (1912) or Katzmayr (1922) effect; see Subsection 5.3.2. It is known that the phenomenon is indicated with the production of positive drag force. With the condition, one can expect the change in the derivative Z_w which is linked to the damping of the vehicle, most dominantly. It is expected to have a decreasing Z_w at certain points of observation, which decreases the damping ratio for this mode quite significantly.

In the case of the phugoid mode, there are no significant characteristic differences between $h/c = 1.0$ and $h/c = 0.5$, see Figure 7-28 and Figure 7-29. The increase in the frequency of oscillation leads to a wider range of the values of the mode. The effect of oscillation manifests in the natural frequency and damping ratio of the mode with the increasing frequency of oscillation.

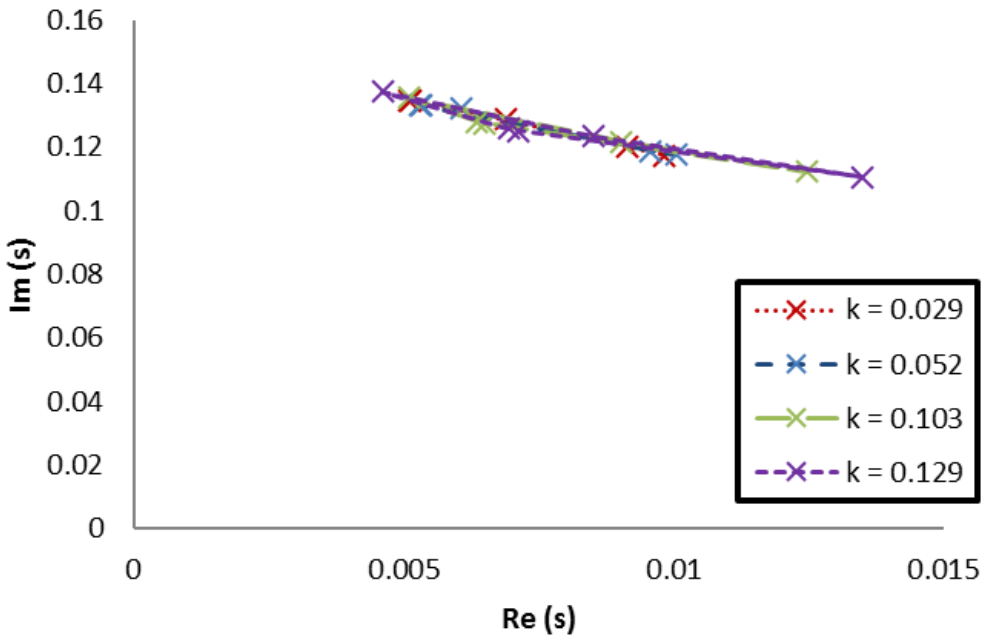

Figure 7-28 Roots of the phugoid mode at different k, $h/c = 1.0$, and $A/c = 0.05$

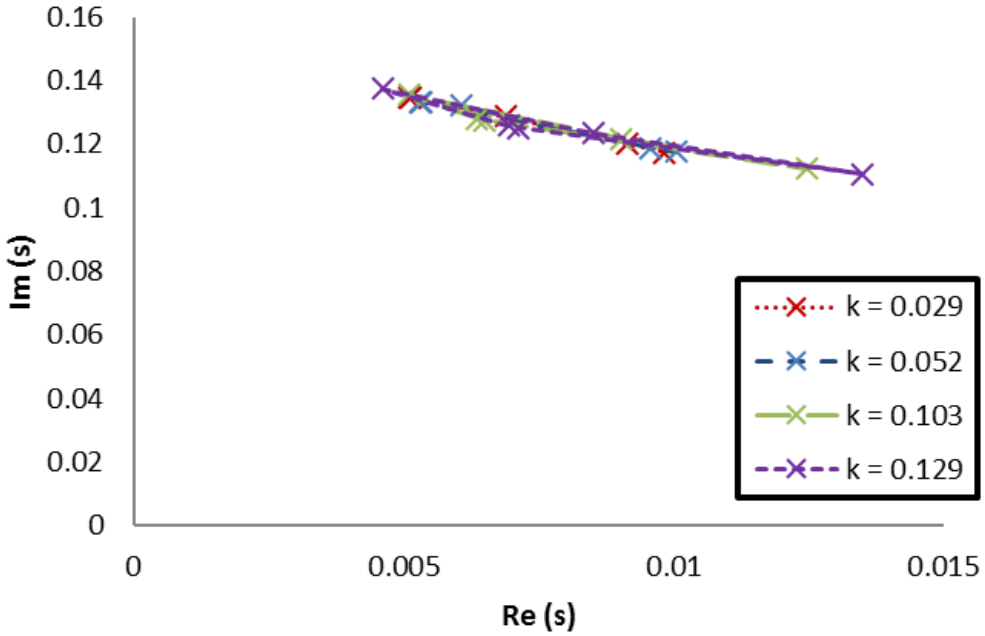

Figure 7-29 Roots of the phugoid mode at different k, $h/c = 0.5$, and $A/c = 0.05$

In the CFD analysis on drag force in Subsection 5.3.2, it is known that the increase in frequency leads to a wider deviation between the maximum and minimum drag force. The deviation carries on for the drag of craft configuration (see Subsection 6.1.3) and the derivative X_u (see Section 6.3). As the damping ratio is linked to the derivative X_u, the behaviour of the curve shown in both figures is affected by the characteristics of the derivative.

The most important observation regarding the effect of frequency of oscillation on the phugoid mode should be given for the case of the strong ground effect region; in this analysis, it is shown by $h/c = 0.3$, see Figure 7-30.

The general behaviour of the mode at this ride height is quite similar to the other two heights. The difference is only in the range of the root values; the wider range is expected. As previously discussed in this section, the range of values is about the contribution ride heights in the form of Z_h.

It is also observed that a significant shift occurs at $k = 0.129$, similar to what happens in the SPPO mode. However, even though it is still related to the Knoller

(1909) – Betz (1912) or Katzmayr (1922) effect, the explanation is a little bit different to the SPPO mode. One may expect the change in the derivative X_u, which is linked to the phugoid damping ratio of the vehicle, most dominantly. It is expected to have a decreasing or even positive X_u at certain points of observation, which decrease the phugoid mode damping ratio.

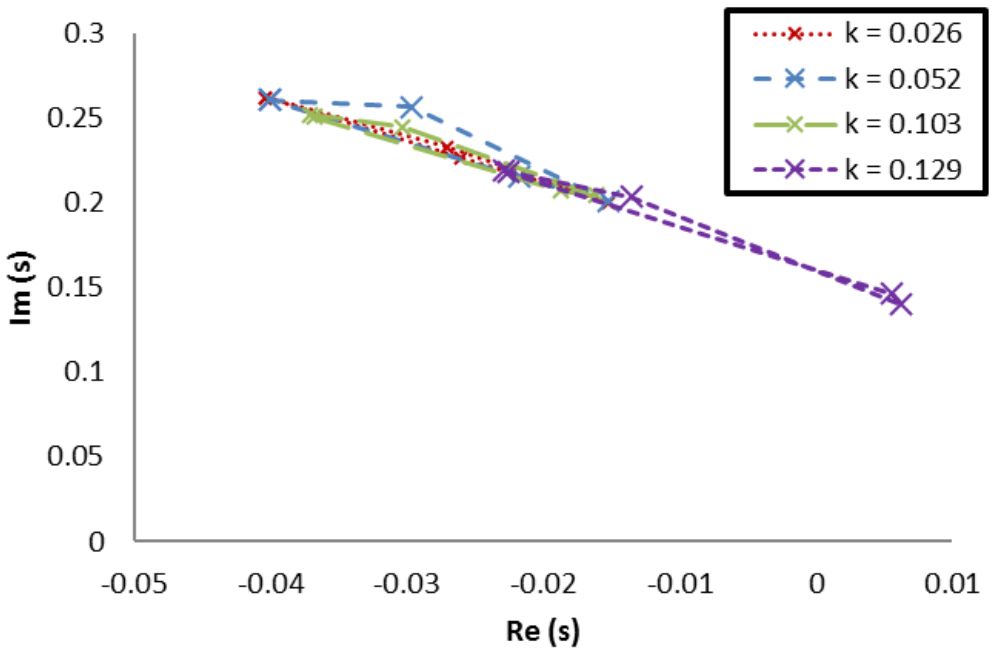

Figure 7-30 Roots of the phugoid mode at different k, $h/c = 0.3$, and $A/c = 0.05$

In the speed subsidence mode, as shown in Figure 7-24, one can expect the expansion of the roots by the increase in the frequency of oscillation. The expansion is due to the fluctuation of w that is contributing to the value of the root. The higher the frequency of oscillation, the wider the w range of value becomes.

Figure 7-31, Figure 7-32, and Figure 7-33 demonstrate the influence of amplitude of oscillation to the characteristic roots of the SPPO, phugoid, and subsidence modes. All the modes have widened-hysteresis, due to the larger amplitude of oscillation. The enlargement is expected since it happens in the aerodynamic and the stability derivative level.

For the SPPO mode, the increase in amplitude also enlarges the values of natural frequency and damping ratio; see Figure 7-31. However, there is a significant difference between lower frequencies ($k = 0.026 - 0.052$) and larger frequencies ($k = 0.103 - 0.129$). The expansion occurring at lower frequencies is an enlargement of the loops, while in higher frequencies it is not only the enlargement of the loops, but also the shift of loop location is identified. The explanation of this difference is likely to be related to the range of frequency. As explained in Section 5.3, the first two frequencies are considered as quasi-static movement where the effect of ride height exists. Differently, at the latter frequency, which is higher, the motion is considered unsteady where the effect of oscillation overshadows the impact from ride height.

The phugoid also experiences enlargement of natural frequency and damping ratio, marked with a longer range of the root values (see Figure 7-32). The expansion of the range is quite linear, giving six to seven times' wider range of root values by a threefold increase of the amplitude of oscillation.

The lengthening of the range of the speed subsidence mode is also linear by six to seven times by tripling the amplitude of oscillation, see Figure 7-33. In Delhaye (1997, p.51), it is stated that the phugoid mode is tied to the speed subsidence mode. Here, the relationship is manifested by the same magnitude of amplification due to the change in the amplitude of oscillation.

To conclude this discussion, the author wants to underline that all the phenomena captured in the present study have shown the importance of a thorough design for a lifting system flying in a curved ground effect. Some validation approaches may be useful to enrich the understanding of this discussion.

7.7 Conclusion

This chapter is about the verification of a dynamic model that has been proposed in this thesis. It also provides several insights about the stability behaviour of a configuration regarding flying over curved surfaces or simply oscillating in a ground effect.

With regard to behaviour, the oscillation of the system affected the characteristic roots where hysteresis is found in every mode. The ride height, frequency and amplitude of motion give an effect on the wider range of values of the modes. They also have an impact on the natural frequency and damping ratio.

In the SPPO mode, the hysteresis forms a ring curve. The decrease in ride height, in general, leads to an increase in the natural frequency and a decrease in the damping ratio. The frequency of oscillation affected the mode from the range of the root hysteresis as well as the shift of the peak of hysteresis relative to the motion of the vehicle. The effect of amplitude is also related to the expansion of the range of the root hysteresis. However, the analysis of the effect of amplitude should be coupled with the reduced frequency of the system.

The phugoid mode provides hysteresis in a line form. The effect of ride height is exponential where the decrease of ride height leads to the increase of the range of the root hysteresis. The increase in amplitude and frequency of oscillation is also responsible for the increase in the range of the root hysteresis.

The non-oscillatory speed subsidence mode is greatly affected by the change in parameters w and θ. When oscillation occurs, the values of both vary from time to time and influence the range of hysteresis of the root.

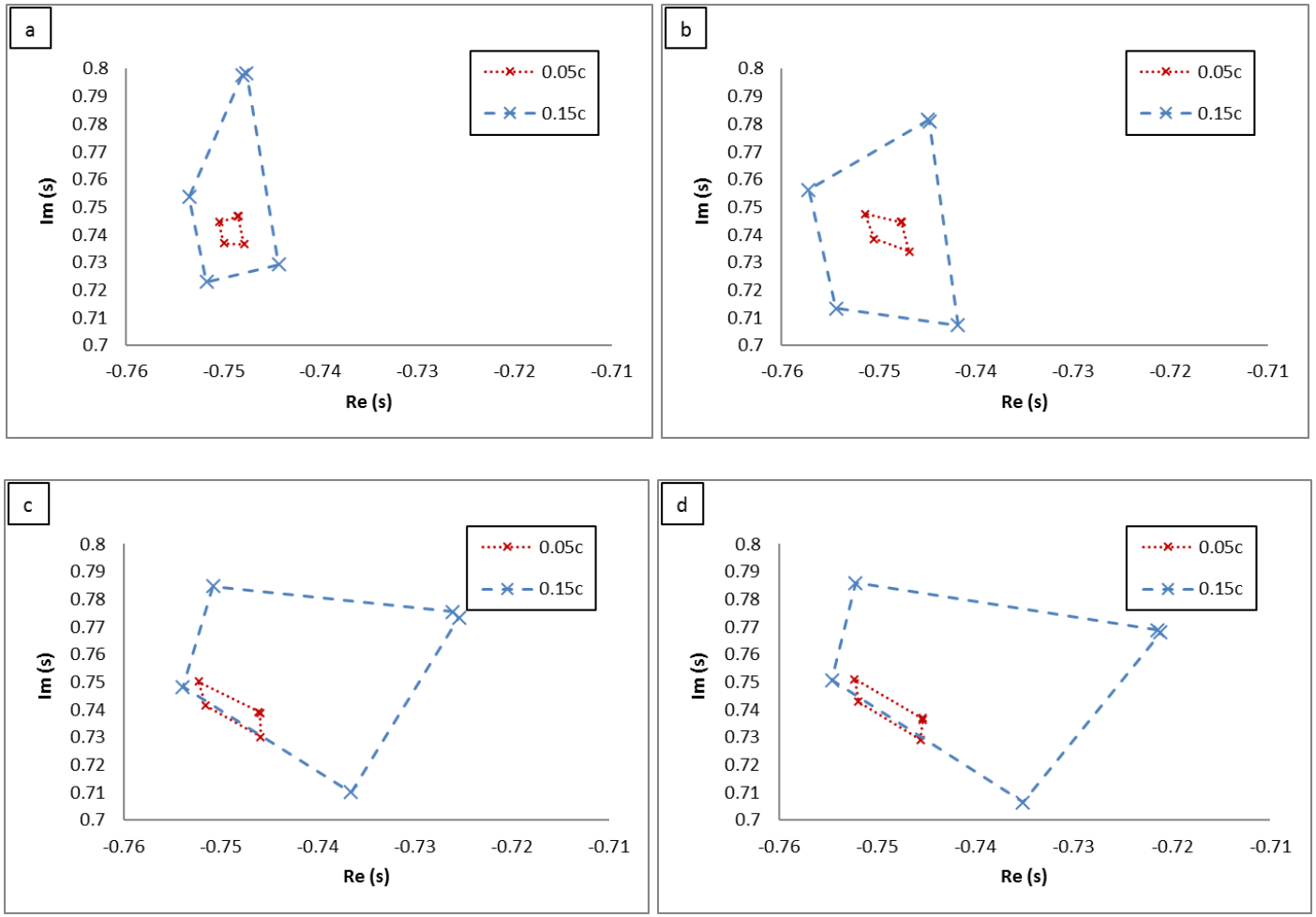

Figure 7-31 Roots of the SPPO mode at different A/c and $h/c = 0.5$ (a. $k = 0.026$; b. $k = 0.052$; c. $k = 0.103$; d. $k = 0.129$)

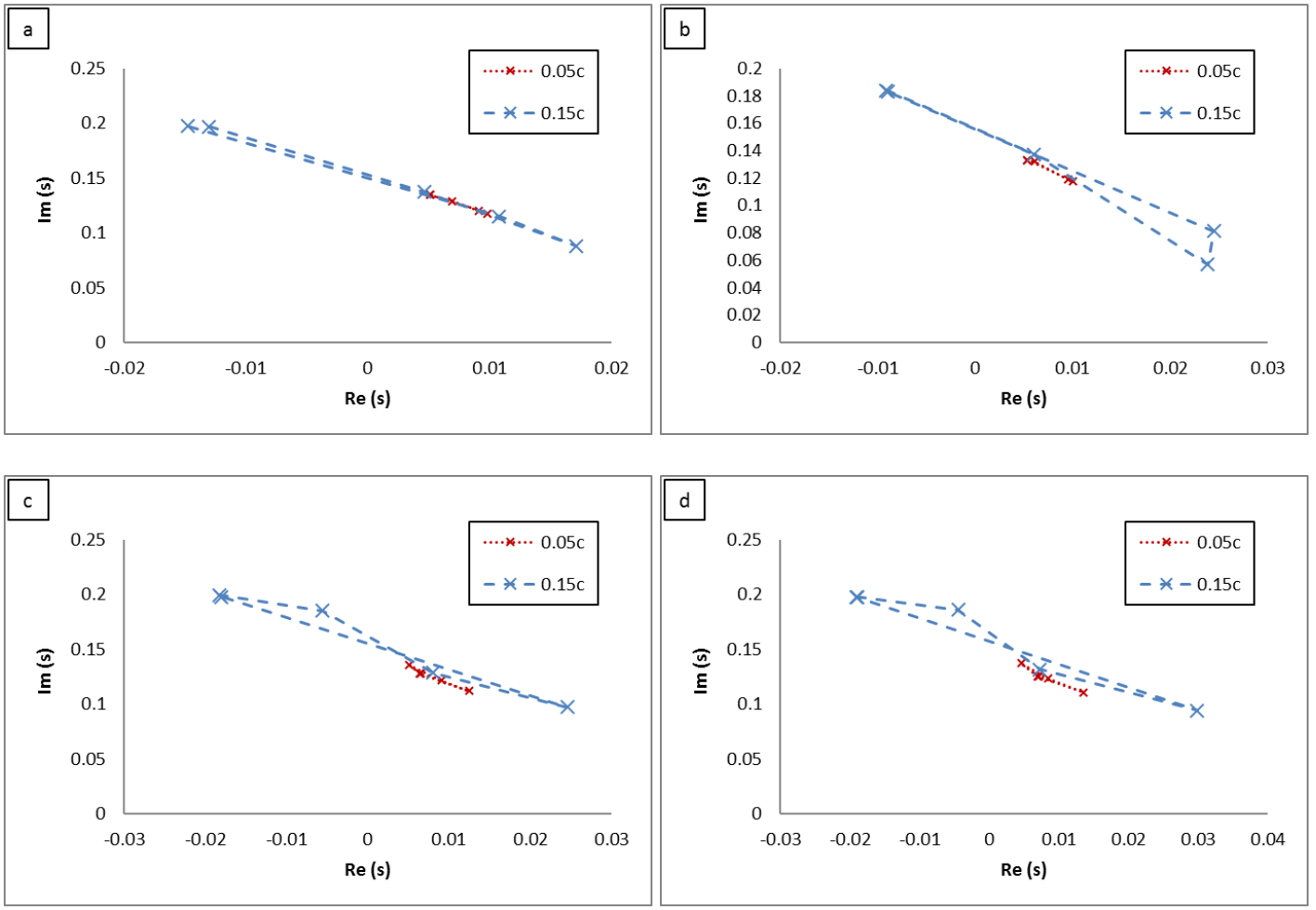

Figure 7-32 Roots of the phugoid mode at different A/c and $h/c = 0.5$ (a. $k = 0.026$; b. $k = 0.052$; c. $k = 0.103$; d. $k = 0.129$)

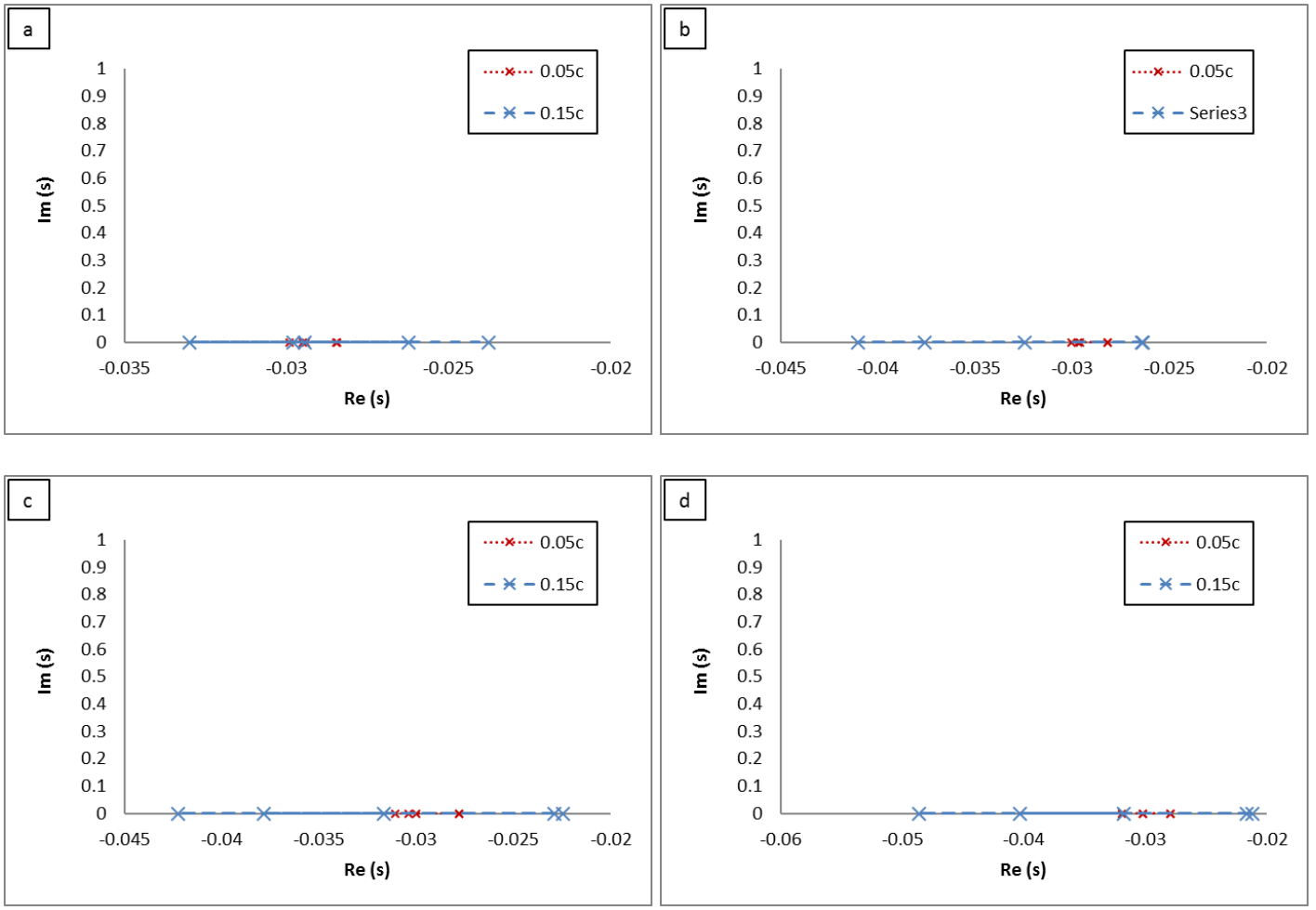

Figure 7-33 Roots of the subsidence mode at different A/c and $h/c = 0.5$ (a. $k = 0.026$; b. $k = 0.052$; c. $k = 0.103$; d. $k = 0.129$)

8 RESEARCH CONCLUSIONS AND FUTURE DEVELOPMENT

This chapter concludes the discussion of this thesis. It has three sections, and they are *(1) Introduction*; *(2) Research conclusio*n; and *(3) Future development*.

8.1 Introduction

The proposal of new configuration concepts is based on some evidence that the demand for more reliable high-speed marine vehicles (HSMVs) is growing. The main advantages are a higher speed combined with an excellent payload. One of the new concepts in the HSMV realm is the aerodynamically alleviated marine vehicle (AAMV). The concept can be described as the use of aerodynamics and hydrodynamics to lift the weight of the vehicle thus aerodynamic surfaces are a part of the configuration.

The concept promotes several advantages, i.e., among others, smaller total drag and higher speed than the conventional HSMV. It also bridges the speed and payload gap between the traditional HSMV and aircraft. However, as a new concept, there are many areas to be further investigated. So far, very little research has been conducted on AAMVs and, therefore, one needs to refer to the HSMV and WIGE craft literature constantly.

The present study focuses on the modelling and analysis of the longitudinal stability of AAMVs in the presence of waves. This work is the continuation of a previous investigation (Collu, 2008), where the effect of waves were not taken into account.

8.2 Research conclusions

The main results of the present work can be summarised in the following points:

- Problem identification in several related disciplines, to give an idea of the knowledge gaps for AAMVs. It also encourages researchers to conduct investigations in those areas.
- Development of a system of equations of motion of AAMVs, specifically in the longitudinal motion with the influence of waves.
- Assessment of the aerodynamic coefficient of a profile, in ground effect and wavy conditions, using computational fluid dynamics (CFD).
- Stability derivatives derivation for a configuration of WIGE craft operating in ground effect and the presence of waves.
- Stability analyses based on the proposed solution of the system of equations of motion using acquired derivatives.

8.2.1 Research problems' identification

A thorough literature survey has been performed to identify the problems that may occur in AAMVs. One can see from this study that there were plenty of options available to conduct in-depth research.

The physical problems in AAMVs can be categorised into two main areas. The first category is the problems related to the system itself, for instance, the aerodynamics, structural integrity, and stability. The second category is the problems related to external factors that eventually affect the system of the vehicle, for example, the presence of waves or gusts. There is also another problem that is not related to the physical domain but has a major impact on the development of the technology, i.e. economics, where costs are the main concern.

Despite the problems that may be encountered, the AAMV also highlights a potential advantage, i.e. the fulfilment of the gap in the speed and payload between traditional HSMVs and aircraft. The investigation on this matters has contributed to the discussion of a conference paper where the author is one of the co-authors (James et al., 2014).

Concerning the research, the author decided to continue the work of Collu (2008) on the dynamics of the vehicle. This current study adds the effect of waves to the previously developed system of equations of motion, only to find that the concept is not well established for vehicles adopting ground effect. Therefore, to obtain a good comprehension of what happens in the vehicle with ground effect, the focus is narrowed down into WIGE craft.

8.2.2 System of equations of motion and the solution

In Chapter 4, the expansion of the system of equations for WIGE vehicles due to the presence waves is presented. Starting from the general systems of equations of motion, the discussion continues to a preferred solution of the system of equations for WIGE craft with the influence of waves is presented.

The preferred solution can be considered a ‘quasi-static’ dynamic solution. The term ‘quasi-static’ means that the assumption of the whole system is in equilibrium at any given point that is considered. For this situation, a no dynamics effect is taken into account.

The approach of ‘quasi-static’ is applicable under certain conditions, i.e. the waves are fully developed with a wavelength more than the characteristic length (in this case the chord length of an aerofoil), and the frequency of motion is small enough in order not to exhibit the dynamic effect.

To verify the proposed solution, a case study was suggested using a particular configuration. Unfortunately, there are inadequate data available on the derivatives of the chosen configuration in the circumstance of occurrences of waves. Hence the author conducted data acquisition.

The data were obtained in three stages. The first stage focused on deriving two-dimensional aerodynamic data through a series of CFD simulations. The second stage transformed the obtained data into three-dimensional aerodynamic data, using a widely established (in the aerospace industry) empirical design approach. The last part focused on estimating the stability derivatives.

Once the stability derivatives were available to observe from several points, i.e. variations in ride height, frequency and amplitude of oscillation, the author managed to conduct a stability analysis considering the influence of waves.

8.2.3 Aerodynamic data

The series of CFD simulations that were carried out to produce the aerodynamic data of the NACA 4412 aerofoil have revealed some noteworthy findings.

The first finding confirms the previously conducted study on the same aerofoil, exclusively on the lift generation. At small angles of attack, i.e. 0° in this study, the NACA 4412 produced a decreasing lift for a decrease in ride height. The reduction in the lift is due to the formation of a Venturi channel between the lower part of the leading edge of the aerofoil and the ground, leading to a pressure drop.

The second finding is the fact that the lift and drag forces, as well as the pitching moment, oscillate periodically following wave elevation. Even though not always, the lift and pitch moment have similar phase lags while drag differs by almost $\pi/2\ rad$.

The results show no significant difference between the time-averaged lift of the oscillating NACA 4412 profile and the constant lift generated by the non-oscillating case. On the contrary, the time-averaged drag of an oscillating NACA 4412 profile experiences a decrease compared to the drag of the aerofoil in stationary conditions. The decline of the time-averaged drag effect is enhanced by the increase in frequency and amplitude of oscillation.

Consequently, the averaged aerodynamic efficiency of the oscillating profile is higher than the static one. Interestingly, the time-averaged pitching moment also shows the alteration with the oscillation but without an explicit relationship towards the frequency and amplitude of oscillation. The fact is that the coefficient of moment, c_m, against the angle of attack, α, of the oscillating NACA 4412 profile shows similar characteristics, without a clear dependency on the frequency and

amplitude of oscillation. The slope of the oscillating aerofoil is more negative than the stationary one.

There are differences with regard to the maximum and minimum values of lift, drag, and pitching moment. In the case of lift, the frequency and amplitude of oscillation affect the maximum and minimum lift forces monotonically, i.e. augmenting the frequency and amplitude leads to linear increments of the range size of the maximum and minimum lift. The effects of the frequency and amplitude of oscillation on the maximum and minimum coefficient of drag are nonlinearly significant. In the pitching moment, there are only irregularities shown by the maximum and minimum values.

The discussion of aerodynamic data and how it was obtained has been disseminated in a conference paper titled, ‘A numerical investigation on the aerodynamics of an oscillating aerofoil in ground effect’ (Adhynugraha et al., 2016).

8.2.4 Stability derivatives

8.2.4.1 Aerodynamics of the Ekranoplan ‘Orlyonok’ A90

The aerodynamic characteristics of the adopted Ekranoplan ‘Orlyonok’ A90 have been obtained using a semi-empirical approach widely employed in a preliminary design of aircraft using the aerodynamic data for the NACA 4412.

Following the characteristics of the two-dimensional aerodynamic data, the periodic changing of the Ekranoplan’s aerodynamic characteristics is obtained. It occurs as expected, resembling the aerodynamic trend in a 2D case with respect to the change in ride height, except for the drag. The difference is in drag characteristics due to the contribution of induced drag which decreases by the decreasing ride height.

8.2.4.2 Stability derivatives

Between the two approaches adopted in the literature, it was decided to perform the analysis of the stability derivatives at constant lift coefficient rather than in the

angle of attack. This approach has been chosen following Delhaye's (1997) arrangement as it is the reference for a code-to-code validation for the initial analysis for the non-oscillating case. The parameters are ride height, frequency, and amplitude of oscillation. The UK-style to form stability derivatives was used. It was observed that the derivatives cover a range of values.

8.2.5 Characteristic roots

Understanding the dynamic behaviour of a system can be done by determining the characteristic roots. From the analysis carried out, it can be identified that the ride height, frequency and amplitude of oscillation have a great impact towards the stability modes.

In the SPPO mode, hysteresis occurs due to the oscillation of the vehicle, shown in ring loops. The underpinning parameters, i.e. ride height, amplitude and frequency of oscillation, affect the range of hysteresis substantially. The wide-ranging phenomena that occur in this mode are linked to the 2D aerodynamic behaviour. This shows the importance of aerodynamic design to provide stability of the vehicle. Regarding the ride height, the general trend is the decrease in the damping ratio as the vehicle gets closer to surface. The effect of frequency of oscillation is more obvious in the strong ground effect region ($h/c = 0.3$) due to the change of the derivative M_w and M_h. At the highest frequency of oscillation for this ride height, a peculiarity appears as the hysteresis loop shift. The shift has the consequences of the decrease in damping ratio and the increase of natural frequency of the mode. This phenomenon is due to the Knoller (1909) – Betz (1912) or Katzmayr (1922) effect. The effect of amplitude is quite straightforward with the expansion of the loop size by its increase. The expansion means a larger range of the natural frequency of the mode.

The phugoid mode also provides hysteresis but in a line form. The characteristics for this mode are dominantly affected by the derivatives X_u and Z_w. The effect of ride height is exponential to the range of root hysteresis. The increase in amplitude and frequency of oscillation is also responsible for the increase in the

range of the root hysteresis. The phenomena that occur here also resemble that of behaviours at the aerodynamic level. The effect of the damping ratio can be classed as minimal in the phugoid mode. Thus, it is concluded there is no significant change to the hysteresis line. Another phenomenon is also observed regarding the shift of the location of the roots for $k = 0.129$ at $h/c = 0.3$. The shift has the consequence of the decrease in natural frequency of the mode. This phenomenon is again due to the Knoller (1909) – Betz (1912) or Katzmayr (1922) effect. The effect of amplitude is quite straightforward with the linear expansion of the length of the hysteresis line by its increase.

The non-oscillatory speed subsidence mode is significantly affected by the change in parameters w and θ, which vary from time to time due to the oscillation of the vehicle.

8.3 Future Development

As a relatively recent concept, the AAMV configuration needs further analytical and experimental investigations. Following the initial study on longitudinal dynamics of the vehicle, this research expanded the previous understanding considering the effect on the aerodynamics and, consequently, on the stability of the AAMV in the presence of waves. The research has opened a new insight that has hardly been discussed in the realm of WIGE craft.

Suggestions for future work are listed in the following subsections.

8.3.1 Experimental investigation

The CFD work has been of great value to the aerodynamic ground effect. It gives a set of data, even though not much, that helps in the understanding of the effect of wave motion on the aerodynamics. Some studies have been carried out in the field; however, the spectrums have been too narrow, which make it difficult to expand the discussion into stability analysis.

As the set of data has not been produced in any other study before, concern about the fidelity of the data may arise. This concern opens an opportunity to conduct an experimental investigation to validate the existing data produced in the present study or even create a new set of data. This will be beneficial for the assurance of theoretical understanding of ground effect aerodynamics.

8.3.2 Validation of stability analysis

The verification of this study adopted an existing configuration, but some modification was made due to limited information available. This situation made apparent one of the shortcomings of this study as no validation was carried out.

For the next stage of the investigation, it is essential to have a ready-to-validate configuration, so the results of the stability analysis will have meaningful results. This idea is also an opportunity for some parties to conduct collaborative research between research institutions and manufacturers (e.g. a shipbuilder).

8.3.3 Lateral-directional analysis

At this point, the studies on the dynamics of the AAMV are always focused on its longitudinal motion. Expanding the analysis to the lateral-directional motion is important. From the literature review that has been carried out in this research, the lateral-directional analysis also offers challenges to be solved.

The analysis in lateral-directional motion may not always be about the operability but also the ergonomics (other than safety – which is a must), especially if the vehicle is aimed at transporting passengers. The instability may occur in the lateral-directional plane for many reasons, and the investigation in the field may anticipate the hazard and find the solution to avoid it.

8.3.4 Preliminary design

So far, to the knowledge of the author, the only recent development of AAMV technology for a commercial purpose is the French A2V. However, there is still big commercial potential to commercialise the concept.

The small number of such vehicles that are available at the current stage provides the opportunity to propose ideas how the vehicle should be designed. No fixed regulation is set and it opens many options for the development of AAMVs.

The methods adopted may incorporate several different approaches and perspectives. One ambitious goal to propose is to have a vehicle that can be manufactured and operated with the costs of a high-speed marine vehicle, but with the performance of an aircraft / high-speed helicopter. The work will be very challenging considering all the related aspects, such as aerodynamics, hydrodynamics, stability, structure analysis, material science, and much more.

REFERENCES

Abbott, I.H. and Doenhoff, A.E.V. (1959) *Theory of wing sections, including a summary of airfoil data*. NY: Dover Publications, Inc.

Abramson, H.N. (1974) 'Structural Dynamics of Advanced Marine Vehicles', *International Symposium on the Dynamics of Marine Vehicles and Structures in Waves*. University College London, England, 1-5 April 1974. San Antonio, Texas, USA: Southwest Research Institute. Available at: https://trid.trb.org/view.aspx?id=43234 (Accessed: 12 May 2017).

Adhynugraha, M.I. (2014) *Development and validation of a dynamics model for an AAMV configuration with water waves consideration*. Cranfield, UK: Cranfield University.

Adhynugraha, M.I. (2015) *Development of a dynamic model for a wing in ground effect vehicle in waves*. Cranfield, UK: Cranfield University.

Adhynugraha, M.I., Nishino, T. and Collu, M. (2016) 'A numerical investigation on aerodynamics of an oscillating aerofoil in ground effect'. *2016 RAeS Applied Aerodynamics Conference*. Bristol, 19-21 July 2016.

Ahmed, M.R. and Sharma, S.D. (2005) 'An investigation on the aerodynamics of a symmetrical airfoil in ground effect', *Experimental Thermal and Fluid Science*, 29(6), pp. 633–647.

Ahmed, M.R., Takasaki, T. and Kohama, Y. (2007) 'Aerodynamics of a NACA4412 airfoil in ground effect', *AIAA Journal*, 45(1), pp. 37–47.

Art Anderson Associates (2004) *Rich passage research - passenger only fast ferry project*. Bremerton, WA: Art Anderson Associates.

Baird, N. (1998) *The world fast ferry market*. Melbourne, Australia: Baird Publications.

Betz, A. (1912) 'Ein beitrag zur erklaerung des segelfluges', *Zeitschrift für Flugtechnik und Motorluftschiffahrt*, 3(21), pp. 269–272.

Blount, D.L. and Codega, L.T. (1992) ‘Dynamic stability of planing boats’, *Marine Technology*, 29(1), pp. 4–12.

Boschetti, P. and Cardenas, E. (2012) ‘Ground effect on the longitudinal stability of an unmanned airplane’. *50th AIAA Aerospace Sciences Meeting including the New Horizons Forum and Aerospace Exposition*. Nashville, Tennessee, USA, 09 - 12 January 2012. USA: AIAA. Available at: 10.2514/6.2012-1051 (Accessed: 4 June 2014).

Carter, A.W. (1961) NASA-TN-D-970, L-1693: *Effect of ground proximity on the aerodynamic characteristics of aspect-ratio-1 airfoils with and without end plates*. Washington, DC, USA: NASA Langley Research Center. Available at: https://ntrs.nasa.gov/search.jsp?R=19980228064 (Accessed: 30 November 2016).

Casson, L. (1991) *The ancient mariners: seafarers and sea fighters of the Mediterranean in ancient times*. Princeton, New Jersey, USA: Princeton University Press.

Chen, Y.-S. and Schweikhard, W.G. (1985) ‘Dynamic ground effects on a two-dimensional flat plate’, *Journal of Aircraft*, 22(7), pp. 638–640.

Chun, H.H. and Chang, C.H. (2002) ‘Longitudinal stability and dynamic motions of a small passenger WIG craft’, *Ocean Engineering*, 29(10), pp. 1145–1162.

Chun, H.H., Chang, J.H., Paik, K.J. and Shin, M.S. (2000) ‘Wind Tunnel Test on the Aerodynamic Characteristics of a PARWIG Craft’, *Journal of the Society of Naval Architects of Korea*, 37(3), pp. 57–68.

Collu, M. (2008) *Dynamics of marine vehicles with aerodynamic surfaces*. PhD Thesis. Cranfield, UK: Cranfield University.

Collu, M., Patel, M.H. and Trarieux, F. (2007) ‘A unified mathematical model for high speed hybrid (air and water-borne) vehicles’, *2nd International Conference on Marine Research and Transportation*. Ischia, Naples, Italy, 28-30 June, 2007.

Collu, M., Patel, M.H. and Trarieux, F. (2008a) ‘High speed marine vehicles with aerodynamic surfaces: development of a dynamic model for a novel configuration’, *Cranfield Multi Strand Conference*. Cranfield, Bedfordshire, UK, 6-7 May 2008.

Collu, M., Patel, M.H. and Trarieux, F. (2008b) ‘A mathematical model to analyze the static stability of hybrid (aero-hydrodynamically supported) vehicles’, *8th Symposium on High Speed Marine Vehicle*. Naples, Italy, 21-23 May 2008.

Collu, M., Patel, M.H. and Trarieux, F. (2010) ‘The longitudinal static stability of an aerodynamically alleviated marine vehicle, a mathematical model’, *Proceedings of the Royal Society of London A: Mathematical, Physical and Engineering Sciences*, 466(2116), pp. 1055–1075.

Cook, M.V. (2013) *Flight dynamics principles: a linear systems approach to aircraft stability and control*. 3rd edn. Waltham, Massachusetts, USA: Butterworth-Heinemann.

Delhaye, H. (1997) *An investigation into the longitudinal stability of wing in ground effect vehicles*. PhD Thesis. Cranfield, UK: Cranfield University.

Doctors, L.J. (1985) *Hydrodynamics of high-speed small craft*. Michigan, USA: University of Michigan.

Doctors, L.J. (1997) ‘Analysis of the efficiency of an Ekranocat: a very high speed catamaran with aerodynamic alleviation’, *International Conference on Wing in Ground Effect Craft (WIGs 97)*. London, UK, 4-5 December 1997. London: Royal Institution of Naval Architects, Vol.4.

Durand, E. (1998) *Time domain modeling of unsteady aerodynamic forces on a flapping airfoil*. Thesis. USA: Massachusetts Institute of Technology. Available at: http://dspace.mit.edu/handle/1721.1/47668 (Accessed: 21 March 2017).

Etkin, B. (2012) *Dynamics of atmospheric flight*. NY: Dover Publications, Inc.

Faltinsen, O.M. (2005) *Hydrodynamics of high-speed marine vehicles*. Cambridge, England: Cambridge University Press.

Fernández Soto, C. (2013) *Investigation of an oscillating single-element wing in ground effect*. MSc Thesis. Cranfield, UK: Cranfield University. Available at: http://cclibweb-3.central.cranfield.ac.uk/handle/1826.1/8496 (Accessed: 12 July 2015).

Foshag, W.F. (1966) R-2179: *Literature search and comprehensive bibliography of wings in ground effect and related phenomena*. USA: Aerodynamic Laboratory, Department of the Navy.

Fridsma, G. (1969) R-1275: *A systematic study of the rough-water performance of planing boats*. Hoboken, New Jersey, USA: Davidson Lab., Stevens Institute of Technology.

Gabrielli, G. and von Karman, T. (1950) 'What price speed? Specific power required for propulsion of vehicles', *Mechanical Engineering*, 72(10), pp. 775–781.

Garrick, I.E. (1936) NACA-TR-567: *Propulsion of a flapping and oscillating aerofoil*. Langley Field: NASA Langley Aeronautical Lab.

Gera, J. (1995) 'Stability and control of wing-in-ground effect vehicles or wing ships', *Proceedings of the 33rd Aerospace Sciences Meeting and Exhibit*. Reno, Nevada, 9-12 January 1995. USA: AIAA. Available at: http://arc.aiaa.org/doi/abs/10.2514/6.1995-339 (Accessed: 6 June 2014).

Hall, I.A. (1994) *An investigation into the flight dynamics of wing in ground effect aircraft operating in aerodynamic flight*. MSc Thesis. Cranfield, UK: Cranfield University. Available at: http://cclibweb-3.central.cranfield.ac.uk/handle/1826.1/3109 (Accessed: 6 July 2015).

Halloran, M. and O'Meara, S. (1999) *Wing in ground effect craft review*. Melbourne, Australia: DSTO Aeronautical and Maritime Research Laboratory.

Hsien, C.-M. and Chen, C.-K. (1996) 'Aerodynamic characteristics of a two-dimensional airfoil with ground effect', *Journal of Aircraft*, 33(2), pp. 386–392.

Husa, B. (2000) *Stepped hull development for amphibious aircraft*. Snohomish, Washington, USA: Orion Technologies, Aerospace Design and Engineering. Available at: http://www.homebuiltairplanes.com/forums/attachments/aircraft-design-aerodynamics-new-technology/13538d1312777085-articles-hull.pdf (Accessed: 6 June 2014).

Ichikawa, M. and Ando, S. (1991) 'Aerodynamic Response of a Thin Airfoil Flying over and in Proximity to a Wavy Wall Surface-Lifting Surface Theory', *Journal of the Japan Society for Aeronautical and Space Sciences*, 39(451), pp. 395–402.

Im, Y.-H. and Chang, K.-S. (2000) 'Unsteady Aerodynamics of a Wing-in-Ground-Effect Airfoil Flying over a Wavy Wall', *Journal of Aircraft*, 37(4), pp. 690–696.

Iosilevskii, G. (2008) 'Asymptotic theory of an oscillating wing section in weak ground effect', *European Journal of Mechanics - B/Fluids*, 27(4), pp. 477–490.

Irodov, R.D. (1974) *Criteria of the longitudinal stability of the Ekranoplan*. Ohio, USA: Foreign Technology Division Wright-Patterson AFB.

Ito, Y. and Iwashita, H. (2016) 'Characteristics of Unsteady Aerodynamics and Pressure Fields of Wings Flying with Heave Motion in the Ground Effect', *Journal of the Japan Society of Naval Architects and Ocean Engineers*, 24, pp. 69–83.

James, D., Adhynugraha, M.I., Collu, M. and Trarieux, F. (2014) 'Aerodynamically Alleviated Marine Vehicles (AAMV): a review of the main challenges and considerations about the hydrodynamic aspects', *HSMV 2014: 10th Symposium in High Speed Marine Vehicle*. Naples, Italy, 15-17 October 2014.

Jane, F.T., Jackson, P., Munson, K. and Peacock, L. (2009) *Jane's All the World's Aircraft*. USA: McGraw-Hill.

Johnston, R.J. (1985) 'Hydrofoils', *Naval Engineers Journal*, 97(2), pp. 142–199.

Jones, K.D., Dohring, C.M. and Platzer, M.F. (1998) 'Experimental and computational investigation of the Knoller-Betz effect', *AIAA Journal*, 36(7), pp. 1240–1246.

Journeé, J.M.J. and Pinkster, J. (2002) *Introduction in ship hydro-mechanics*. The Netherlands: Delft University of Technology.

Kaario, T.J. (1959) 'The principles of ground effect vehicles', in *Symposium on Ground Effect Phenomena*. Princeton, New Jersey, USA: Princeton University.

Kallio, J.A. (1978) DTNSRDC/SPD-0847-01: *Results of full scale trials on two high speed planing craft (KUDU 2 and KAAMA)*. Bethesda, Maryland, USA: David W. Taylor Naval Ship Research and Development Center.

Katayama, T., Hinami, K. and Ikeda, Y. (2000) 'Longitudinal motion of a super high-speed planing craft in regular head waves', *Proceedings of the 4th Osaka Colloquium on Seakeeping Performance of Ships*. Osaka, Japan, 17-21 October 2000. Ōsaka, Japan: Cosmosquare International Education and Training Center, pp. 214–220. Available at: http://www.marine.osakafu-u.ac.jp/~lab07/kata-laboHP/katayama_PP/OC2000.pdf (Accessed: 6 June 2014).

Katz, J. (1985) 'Calculation of the Aerodynamic Forces on Automotive Lifting Surfaces', *Journal of Fluids Engineering*, 107(4), pp. 438–443.

Katzmayr, R. (1922) NACA-TM-147: *Effect of periodic changes of angle of attack on behavior of airfoils*. Washington, DC, USA: NACA. Available at: http://ntrs.nasa.gov/search.jsp?R=19930083152 (Accessed: 12 January 2016).

Kikuchi, M., Hirano, K., Yuge, T., Iseri, K. and Kohama, Y. (2002) 'Measurement of aerofoil characteristics by method of towing model', *Transactions of the Japan Society of Mechanical Engineers Series B*, 68(676), pp. 3378–3385.

Kirillovykh, V. and Privalov, E.I. (1996) 'Transport amphibious platforms: a new type of high-speed craft', *Proceedings of Workshop on Ekranoplans and Very Fast Craft*. Sydney, Australia, 5-6 December 1996. Sydney, NSW, Australia: Institute of Marine Engineers, pp. 121–133.

Knoller, R. (1909) *Die gesetze des luftwiderstandes*. Vienna: Verlag des Österreichischer Flugtechnischen Vereines.

Koochesfahani, M.M. (1989) ‘Vortical patterns in the wake of an oscillating airfoil’, *AIAA Journal*, 27(9), pp. 1200–1205.

Kosari, A. and Chamanpara, H. (2016) ‘Investigation of longitudinal dynamics of a small WIG craft in flight over sea Waves’, *Ocean Engineering*, 127, pp. 23–31.

Kumar, P.E. (1967) CoA Report Aero No. 196: *Stability of ground effect wings: a preliminary survey of theoretical and experimental techniques*. Cranfield, UK: College of Aeronautics, Cranfield University. Available at: http://repository.tudelft.nl/assets/uuid:c3bdc1e4-f5b3-4fc4-9142-ff11f173c251/CoA%20Report%20No.196.pdf (Accessed: 6 June 2014).

Kumar, P.E. (1968) CoA Report Aero No. 201: *An experimental investigation into the aerodynamic characteristics of a wing, with and without endplates, in ground effect*. Cranfield, UK: College of Aeronautics, Cranfield University. Available at: http://resolver.tudelft.nl/uuid:4e6deeb2-649a-4dd1-a551-a6eb223d8883 (Accessed: 22 May 2017).

Ladson, C.L. (1988) NASA-TM-4074, L-16472, NAS 1.15:4074: *Effects of independent variation of Mach and Reynolds numbers on the low-speed aerodynamic characteristics of the NACA 0012 airfoil section*. Hampton, Virginia, USA: NASA Langley Research Center. Available at: http://ntrs.nasa.gov/archive/nasa/casi.ntrs.nasa.gov/19880019495.pdf (Accessed: 14 January 2016).

Lai, J.C.S. and Platzer, M.F. (1999) ‘Jet Characteristics of a Plunging Airfoil’, *AIAA Journal*, 37(12), pp. 1529–1537.

Liang, H., Wang, X., Zou, L. and Zong, Z. (2014) ‘Numerical study of two-dimensional heaving airfoils in ground effect’, *Journal of Fluids and Structures*, 48, pp. 188–202.

Liang, H., Zong, Z. and Zou, L. (2013a) ‘Nonlinear lifting theory for unsteady WIG in proximity to incident water waves. Part 1: Two-dimension’, *Applied Ocean Research*, 43, pp. 99–111.

Liang, H., Zong, Z. and Zou, L. (2013b) ‘Nonlinear lifting theory for unsteady WIG in proximity to incident water waves. Part 2: Three-dimension’, *Applied Ocean Research*, 43, pp. 88–98.

Mahon, S. and Zhang, X. (2004) ‘Computational analysis of pressure and wake characteristics of an aerofoil in ground effect’, *Journal of Fluids Engineering*, 127(2), pp. 290–298.

Martin, M. (1976) Report 76-0068: *Theoretical determination of porpoising instability of high-speed planing boats*. Bethesda, Maryland, USA: David W. Taylor Naval Ship Research and Development Center.

Maskalik, A.I., Kolizaw, B. and Zhukov, V. (2000) *Ekranoplans: peculiarity of the theory and design*. St. Petersburg, Russia: Sudostroyeniye.

Matsuzaki, T., Yoshioka, S., Kato, T. and Kohama, Y. (2008) ‘Unsteady aerodynamic characteristics of wings in ground effect’, *Proceedings of the 40th JAXA Workshop on ‘Investigation and Control of Boundary-Layer Transition’*. Mimitsu-ken, Hyuga City, Miyazaki, 14-16 March 2007. Japan: JAXA, pp. 53–56. Available at: https://repository.exst.jaxa.jp/dspace/handle/a-is/38290 (Accessed: 7 May 2017).

McCroskey, W.J. (1987) NASA-TM-100019: *A critical assessment of wind tunnel results for the NACA 0012 airfoil*. Moffet Field, California, USA: NASA Ames Research Center.

McCroskey, W.J. and Philippe, J.J. (1975) ‘Unsteady Viscous Flow on Oscillating Airfoils’, *AIAA Journal*, 13(1), pp. 71–79.

Menter, F.R. (1993) ‘Zonal Two Equation Kappa-Omega Turbulence Models for Aerodynamic Flows’, *24th AIAA Fluid Dynamics Conference*. Orlando, Florida, USA, 6-9 July 1993. Moffet Field, California, USA: NASA Ames Research Center. Available at: https://ntrs.nasa.gov/search.jsp?R=19960044572 (Accessed: 5 May 2017).

Menter, F.R. (1994) ‘Two-equation eddy-viscosity turbulence models for engineering applications’, *AIAA Journal*, 32(8), pp. 1598–1605.

Mistry, R. (2012) *An investigation into the effect on the wake of an oscillating wing in ground proximity*. MSc Thesis. Cranfield, UK: Cranfield University. Available at: http://cclibweb-3.central.cranfield.ac.uk/handle/1826.1/5784 (Accessed: 12 July 2015).

Molina, J. and Zhang, X. (2010) 'Aerodynamics of an oscillating wing in ground effect', in *48th AIAA Aerospace Sciences Meeting Including the New Horizons Forum and Aerospace Exposition*. Reston, Virginia, USA: AIAA. Available at: http://arc.aiaa.org/doi/abs/10.2514/6.2010-318 (Accessed: 24 February 2016).

Molina, J. and Zhang, X. (2011) 'Aerodynamics of a Heaving Airfoil in Ground Effect', *AIAA Journal*, 49(6), pp. 1168–1179.

Molina, J., Zhang, X. and Alomar, A. (2016) 'Aerodynamics of a Pitching and Heaving Airfoil in Ground Effect', *AIAA Journal*, 54(4), pp. 1158–1171.

Molina, J., Zhang, X. and Angland, D. (2011) 'On the unsteady motion and stability of a heaving airfoil in ground effect', *Acta Mechanica Sinica*, 27(2), pp. 164–178.

Mook, D.T. and Nuhait, A.O. (1989) 'Numerical simulation of wings in steady and unsteady ground effects', *Journal of Aircraft*, 26(12), pp. 1081–1089.

Moore, N.J. (2004) *An experimental investigation into wing in ground effect over flat and wavy surfaces*. PhD Thesis. Southampton, UK: University of Southampton. Available at: http://ethos.bl.uk/OrderDetails.do?uin=uk.bl.ethos.419402 (Accessed: 12 July 2015).

Moryossef, Y. and Levy, Y. (2004) 'Effect of oscillations on airfoils in close proximity to the ground', *AIAA Journal*, 42(9), pp. 1755–1764.

Nebylov, A.V. and Wilson, P.A. (2002) *Ekranoplanes: controlled flight close to the sea*. Southampton, UK: WIT Press.

Nelson, H.C. (1951) *Lift and moment on oscillating triangular and related wings with supersonic edges*. Washington, DC: National Aeronautics and Space Administration.

Neumark, S. (1956) *Analysis of short period longitudinal oscillations of an aircraft - interpretation of flight test*. London, UK: HM Stationery Office.

Newman, J.N. (1977) *Marine Hydrodynamics*. Cambridge, Mass.: MIT Press.

Nishino, T. (2016) 'Turbulence Modelling' [3-hour introductory course], *CFD for Renewable Energy and CFD for Industrial Processes*. Cranfield University.

Nitta, K. (1994) 'Analysis of aerodynamics of airfoils moving over a wavy wall', *Journal of Aircraft*, 31(2), pp. 387–395.

Ollila, R.G. (1980) 'Historical review of WIG vehicles', *Journal of Hydronautics*, 14(3), pp. 65–76.

Paek, C.S. (2006) *The viability of commercializing wing-in-ground (WIG) craft in connection with technical, economic and safety aspects followed by IMO legislation*. PhD Thesis. Malmö, Sweden: World Maritime University. Available at: http://www.maica.or.kr/reference/files/WIG%EB%85%BC%EB%AC%B8(%EC%98%81%EB%AC%B8%ED%8C%90).pdf (Accessed: 9 June 2014).

Papanikolaou, A. (2002) 'Developments and potential of advanced marine vehicles concepts', *Bulletin of the KANSAI Society of Naval Architects*, 55, pp. 50–54.

Patankar, S.V. and Spalding, D.B. (1972) 'A calculation procedure for heat, mass and momentum transfer in three-dimensional parabolic flows', *International Journal of Heat and Mass Transfer*, 15(10), pp.1787-1806.

Pietrzak, P. (2013) *Investigation of an oscillating double-element wing in ground effect*. MSc Thesis. Cranfield, UK: Cranfield University. Available at: http://cclibweb-3.central.cranfield.ac.uk/handle/1826.1/8033 (Accessed: 12 July 2015).

Pinkerton, R.M. (1963) *Report No. 563: Calculated and Measured Pressure Distributions over the Midspan Section of the NACA 4412 Airfoil*. Hampton, Virginia, USA: NASA Langley Memorial Aeronautical Lab. Available at: http://ntrs.nasa.gov/archive/nasa/casi.ntrs.nasa.gov/19930091638.pdf (Accessed: 6 July 2015).

Plensky, V.-E. (2012) *Investigation of an oscillating double-element wing in ground effect*. MSc Thesis. Cranfield, UK: Cranfield University. Available at: http://cclibweb-3.central.cranfield.ac.uk/handle/1826.1/6718 (Accessed: 12 July 2015).

Pope, S.B. (2001) *Turbulent flows*. Cambridge: Cambridge University Press.

Qu, Q., Jia, X., Wang, W., Liu, P. and Agarwal, R.K. (2014a) 'Numerical simulation of the flowfield of an airfoil in dynamic ground effect', *Journal of Aircraft*, 51(5), pp. 1659–1662.

Qu, Q., Jia, X., Wang, W., Liu, P. and Agarwal, R.K. (2014b) 'Numerical study of the aerodynamics of a NACA 4412 airfoil in dynamic ground effect', *Aerospace Science and Technology*, 38, pp. 56–63.

Raymer, D.P. (1999) *Aircraft design: a conceptual approach*. USA: AIAA.

Raymond, A.E. (1921) NACA-TN-67: *Ground influence on airfoils*. Washington, DC, USA: NACA. Available at: http://ntrs.nasa.gov/search.jsp?R=19930080862 (Accessed: 2 June 2016).

Reeves, J.M. (1993) 'The case for surface effect research, platform applications and development opportunities', *Proceedings of the NATO-AGARD Fluid Mechanics Panel Symposium in Long Range and Long Range Endurance Operation of Aircraft (FMP'93)*. Kijkduin (The Hague), The Netherlands, 24th-27th May 1993. The Netherland: NATO, pp. 24–27.

Roskam, J. (1989) *Airplane Design, Part V: component Weight Estimation*. Kansas, USA: The University of Kansas.

Roskam, J. (1990) *Airplane Design, Part VI: Preliminary Calculation of Aerodynamic, Thrust and Power Characteristics*. Kansas, USA: The University of Kansas.

Rozhdestvensky, K.V. (2006) 'Wing-in-ground effect vehicles', *Progress in Aerospace Sciences*, 42(3), pp. 211–283.

Rumsey, C. (2014) *2D NACA 0012 airfoil validation*. Available at: http://turbmodels.larc.nasa.gov/naca0012_val.html (Accessed: 12 July 2015).

Runyan, H.L., Woolston, D.S. and Rainey, G.A. (1955) *NACA-TR-1262: Theoretical and experimental investigation of the effect of tunnel walls on the forces on an oscillating airfoil in two-dimensional subsonic compressible flow*. Langley Field, Virginia, USA: NACA Langley Aeronautical Lab..

Savitsky, D. (1964) 'Hydrodynamic design of planing hulls', *Marine Technology*, 1(1). Available at: http://ci.nii.ac.jp/naid/10007199074/ (Accessed: 9 June 2014).

Savitsky, D. (1992) 'Overview of planning hull developments', *Proceedings of Intersociety High Performance Marine Vehicles Conference*. Arlington, Virginia, USA, 24-27 June 1992. Arlington, VA, USA: American Society of Naval Engineers.

Savitsky, D. and Brown, P.W. (1976) 'Procedures for hydrodynamic evaluation of planing hulls in smooth and rough water', *Marine Technology*, 13(4), pp. 381–400.

Sears, W.R. (1976) 'Unsteady motion of airfoils with boundary-layer separation', *AIAA Journal*, 14(2), pp. 216–220.

Shipps, P. (1976) 'Hybrid ram-wing/planing craft - today's raceboats, tomorrow's outlook', *AIAA/SNAME Advanced Marine Vehicles Conference*. Arlington, Virginia, USA, 20-22 September 1976. New York, USA: AIAA, pp. 1–8. Available at: http://arc.aiaa.org/doi/abs/10.2514/6.1976-877 (Accessed: 10 June 2014).

Staufenbiel, R. and Kleineidam, G. (1980) ‘Longitudinal motion of low-flying vehicles in nonlinear flowfields’, *Proceedings of the Congress of the International Council of the Aeronautical Sciences*. Munich: ICAS, pp. 293–308.

Staufenbiel, R.W. and Yeh, B.-T. (1977) *Stability and control of ground effect aircraft in longitudinal motion (Flugeigenschaften in der Laengsbewegung von Bodeneffekt-Fluggeraeten)*. Bethesda, Maryland, USA: David W. Taylor Naval Ship Research and Development Center.

Steinbach, D. (1997) ‘Comment on “Aerodynamic Characteristics of a Two-Dimensional Airfoil with Ground Effect”’, *Journal of Aircraft*, 34(3), pp. 455–456.

Stokes, G.G. (1851) *On the effect of the internal friction of fluids on the motion of pendulums (Vol. 9)*. Cambridge: Pitt Press.

Torenbeek, E. (1982) *Synthesis of subsonic airplane design*. The Netherlands: Delft University Press.

Troesch, A.W. (1992) ‘On the hydrodynamics of vertically oscillating planing hulls’, *Journal of Ship Research*, 36(4), pp. 317–331.

Troesch, A.W. and Falzarano, J.M. (1993) ‘Modern nonlinear dynamical analysis of vertical plane motion of planing hulls’, *Journal of Ship Research*, 37(3), pp. 189–199.

Truscott, S., Parkinson, J.B., Ebert, J.W. and Valentine, E.F. (1938) *NACA-TN-668: Hydrodynamic and Aerodynamic Tests of Models of Flying Boat Hulls Designed For Low Aerodynamic Drag*. Langley Field, Virginia, USA: NACA Langley Aeronautical Lab.

Tuncer, I.H. and Platzer, M.F. (1996) ‘Thrust generation due to airfoil flapping’, *AIAA Journal*, 34(2), pp. 324–331.

Ward, T.M., Goelzer, H.F. and Cook, P.M. (1978) ‘Design and performance of the ram wing planing craft-KUDU II’, *AIAA/SNAME Advanced Marine Vehicles Conference*. San Diego, California, USA, 17-19 April 1978. New York, USA: AIAA, pp. 17–19.

WMO (1998) *Guide to Wave Analysis and Forecasting*. 2nd edn. Geneva, Switzerland: Secretariat of World Meteorological Organization, 702. Available at: https://www.wmo.int/pages/prog/amp/mmop/documents/WMO%20No%20702/WMO702.pdf (Accessed: 14 July 2015).

Wu, J. and Zhao, N. (2013) 'Ground effect on flapping wing'. *Procedia Engineering*, *67*, pp.295-302.

www.lemarin.fr (2015) *A2V présente son prototype de navire rapide et économe en énergie*. France: Le Marin. Available at: http://www.lemarin.fr/secteurs-activites/shipping/21446-a2v-presente-son-prototype-de-navire-rapide-et-econome-en-energie (Accessed: 5 February 2016).

www.meretmarine.com (2015) *A2V: Des bateaux ultra-rapides à portance aérodynamique*. France: Mer et Marine. Available at: http://www.meretmarine.com/fr/content/a2v-des-bateaux-ultra-rapides-portance-aerodynamique (Accessed: 5 February 2016).

Yang, W., Ying, C.-J. and Yang, Z. (2010) 'Aerodynamic study of WIG craft near curved ground', *Journal of Hydrodynamics*, Ser. B, 22(5, Supplement 1), pp. 371–376.

Yong, J., Smith, R., Hatano, L. and Hillmansen, S. (2005) 'What price speed-revisited', *Ingenia*, 22, pp. 46–51.

Young, J. and Lai, J.C.S. (2004) 'Oscillation Frequency and Amplitude Effects on the Wake of a Plunging Airfoil', *AIAA Journal*, 42(10), pp. 2042–2052.

Yun, L., Bliault, A. and Doo, J. (2009) *WIG craft and Ekranoplan: ground effect craft technology*. New York, USA: Springer.

Zarnick, E.E. (1978) *A nonlinear mathematical model of motions of a planing boat in regular waves*. Bethesda, Maryland, USA.: David W. Taylor Naval Ship Research and Development Center.

APPENDICES

The following pages include the appendices that are composed with the objectives to provide some information that may complement the discussion in the main body of this thesis.

There are nine appendices, as follows:

- Appendix A demonstrates the two front pages (abstract, introduction and main challenges) of a conference paper where the author has made a contribution in its dissemination;
- Appendix B shows the front page (abstract and introduction) of another conference paper where the author is the first author;
- Appendix C briefly discusses the kinematics;
- Appendix D talks about the frequency of encounter;
- Appendix E provides the calculation results of the frequency of encounter of a system undergoing waves load with certain parameters involved (speed, course angle, and frequency of motion);
- Appendix F contains aerodynamic data attained from CFD simulations;
- Appendix G presents aerodynamic data for a WIGE craft configuration based on the Ekranoplan ‘Orlyonok’ A-90;
- Appendix H shows the sample of MATLABTM code for dynamic analysis
- Appendix I shows the stability derivatives of the configuration; and
- Appendix J provides the results of the calculation of characteristic roots.

Appendix A **Abstract of conference paper for the 10th Symposium on High Speed Marine Vehicles in Naples, Italy (October 2014)**

Aerodynamically Alleviated Marine Vehicles (AAMV): a review of the main challenges and considerations about the hydrodynamic aspects

D. James, M.I. Adhynugraha, M. Collu, F. Trarieux
Ocean Systems Test Laboratory, Cranfield University, Cranfield, UK

Several new high speed marine vehicle configurations have been developed during the last two decades, due to an increasing demand for such vehicles for civil and military transportation. At the upper end of the speed range, a vessel can be equipped with aerodynamic lifting surfaces in order to alleviate the weight of the vehicle, leading to a lower effective displacement, with lower hydrodynamic drag and required power.

A general review of the latest research on wing-in-ground effect (WIG) vehicles has been undertaken, highlighting some of the main technological challenges. From the earliest stages of development longitudinal stability has been one of the main challenges to be resolved. Additionally, the promise of increased aerodynamic efficiencies demonstrated at the theoretical level has not been easily achieved, often due to matters of stability, hydrodynamics, structural design and operational practicalities. Hydrodynamically, overcoming hump drag has proven problematic, often requiring significantly higher power during the take-off phase than at any other time in the operational profile. Whilst several general methods have evolved to address this issue, the limitations imposed by various configurations remain impediments to more efficient and effective designs.

The present work includes specific considerations for the preliminary design of a hullform with more favourable waterborne characteristics than existing WIGs. Initial tank testing was carried out to assess resistance performance for a representative operational profile during a take-off phase.

INTRODUCTION

1.1 Context

Various high speed marine vehicle configurations have been developed during the last several decades, due to an increasing demand for such vehicles in civil and military marine transportation (Clark et al. 2004). Yong (Yong et al. 2005), has recently updated a study initially conducted by Von Karman and Gabrielli (Gabrielli & Von Karman 1950), showing the relative speed and transport efficiency of current modes of transportation. Marine vehicles have maintained a permanent place in the global economy for several reasons, such as their efficiency in transporting a high volume of goods over large distances, and their effectiveness and efficiency in smaller and more localised routes and applications.

There are a number of options in the field of high speed marine vehicles, most notably planing monohulls, slender hulled catamarans and trimarans, hydrofoils, surface effect ships, air cushion vehicles and wing in ground effect (WIG) craft. Although WIG craft employ aerodynamic surfaces to bodily rise free of the water surface, this category of vehicle is internationally recognised as a marine vessel first and foremost. One of the reasons for this classification is that operation is necessarily near the water surface in order to exploit the favourable ground effect. Vehicles that can operate both in and out of ground effect are possible, although once a critical operational

altitude is reached further civil aviation regulations are applied (Rozhdestvensky 2006).

Therefore, there seems to be a clear case to maximise the potential of a near surface marine vehicle, able to achieve speeds typical of aircraft whilst exploiting aerodynamic, regulatory and ultimately cost efficiencies to operate in a similar manner to traditional marine vehicles (Paek, 2006). This paper will document some of the primary technical impediments to WIG development, and to the realisation of a true hybrid marine craft.

Historically, WIG have physically resembled low flying aircraft, with their associated geometrical features. However, these characteristics have often proved unfavourable in a marine environment. Attention is now focussed on the development of a hybrid class of vessel, able to comfortably operate on the water surface yet still deliver the speed of aircraft during an airborne cruise mode. This has been termed an Aerodynamically Alleviated Marine Vehicle (AAMV), as it employs aerodynamic lifting surfaces to counteract the gravitational weight of the vehicle, resulting in a lower effective displacement, wetted surface, and ultimately resistance for a given speed. The resulting increase in transport efficiency using this type of configuration promises the ability to move people and cargo over water with much greater comfort, speed and efficiency than is currently achievable by any other method.

The AAMV can operate successfully in a number of modes: low speed displacement and so-called semi-displacement waterborne modes; a transient condition defined by hydrodynamic and aerodynamic forces of the same order of magnitude (Collu, 2008); and finally completely free of the water surface for high speed transit, fully airborne although not beyond the influence of the ground effect zone.

2 MAIN CHALLENGES

2.1 Stability & control

Longitudinal pitch stability has been identified as one of the key design parameters that are critical for success of WIG craft. The necessary proximity of the ground plane that offers the promise of increased aerodynamic efficiencies at flying heights not more than 10% of the wing chord, measured from the horizontal ground to the trailing edge of the foil, demands sufficient stability and control to avoid unintended physical contact with the ground surface (Korolyov, 1998).

This proximity also complicates the equilibrium states necessary for stable operation, introducing the concept of an aerodynamic centre in height in addition to the more recognised and understood aerodynamic centre in pitch.

The mathematical approach for the determination of pitch and height stability for ground effect wings was begun by Kumar (1967) in his research at Cranfield College of Aeronautics, where the basic problem was framed and investigated. Independently, Irodov in U.S.S.R. and Staufenbiel and Kleinedam in Germany (Irodov 1974; Staufenbiel 1980) further developed the mathematical framework to investigate the longitudinal stability of WIG vehicles. It was shown that there is a change of pitching moment about the vessel centre of gravity with a change of height above ground, and what is termed a change in the position of the aerodynamic centre with height above ground.

Figure 1 shows a graphical representation of the necessary positions of the aerodynamic centres in pitch and height, and body centre of gravity for airborne stability near the ground. The implications of these relationships permeate every aspect of the WIG craft and must be thoroughly understood before any meaningful progress can be made toward its development.

Appendix B **Abstract of conference paper for 2016 Applied Aerodynamics Conference in Bristol, UK (July 2016)**

A numerical investigation on aerodynamics of an oscillating aerofoil in ground effect

Muhammad Ilham Adhynugraha
Cranfield University, UK
Badan Pengkajian dan Penerapan Teknologi, Indonesia
m.adhynugraha@cranfield.ac.uk

Takafumi Nishino
Cranfield University, UK
t.nishino@cranfield.ac.uk

Maurizio Collu
Cranfield University, UK
maurizio.collu@cranfield.ac.uk

***Abstract* – Numerical simulations are carried out to study the aerodynamic characteristics of an oscillating asymmetric aerofoil in close proximity to a flat surface. The final aim is to develop a database of aerodynamic coefficients to be used for the preliminary design of Wing in Ground (WIG) effect vehicles. The flow simulations are conducted using the 2D unsteady Reynolds Averaged Navier-Stokes (URANS) equations and the SST k-ω turbulence model. The aerodynamics of the profile has been parametrically analysed, considering ranges of the main parameters influencing the underlying physics, i.e. angle of attack, ride height, frequency and amplitude of oscillation. It is shown that the average lift of oscillating aerofoil has no difference from the lift of non-oscillating aerofoil. However, the maximum and minimum lift coefficients of the oscillating aerofoil are affected by the frequency and amplitude of the oscillation. Both average and maximum-minimum drag coefficients of the oscillating aerofoil are strongly influenced by the frequency and amplitude of oscillation. More negative values of the average pitching moment are obtained in oscillatory environment. Also, the gradient of the moment against the angle of attack changes with the ride height. These results demonstrate that all parameters considered in this study contribute to the nonlinear behaviour of the aerofoil.**

***Keywords* – ground effect; oscillating aerofoil; lift and drag; pitching moment**

Introduction

Aerodynamic characteristics of a wing flying near the ground have been discussed for nearly one century. The special behaviour of a wing near the ground was recognized at the beginning of the history of machinery flight (Rozhdestvensky, 2006), but comprehensive investigations of this phenomenon were started later in 1920s. A technical note by Raymond (1921) was one of the first studies on the topic. Although the research in this field is extensive, the details of the phenomenon have not been fully understood.

The basic understanding of a wing flying near the ground is that it will experience an enhancement of lift and a reduction of induced drag. These advantages have been employed in the design of a new concept of high speed marine vehicles, namely the wing-in-ground (WIG) effect craft. One of the successful examples of the implementation of this WIG technology was demonstrated by Russian Navy's 'Ekranoplan' project (Rozhdestvensky, 2006).

On the other hand, the aerodynamics of an oscillating wing has been extensively investigated in the fields of insect-inspired robotics and micro air vehicles. The flow regimes examined in these fields of research are characterised by low Reynolds numbers and high oscillation frequencies.

Combining the ground effect and the effect of wing oscillation is an interesting research topic. This combination has not been discussed much in

Appendix C **Review on kinematics**

When a mathematical model is developed to explain the motion of an AAMV or WIGE craft, the influence of the ride height above the surface on aerodynamic forces and moments is taken into account.

In pure longitudinal motions, it requires three approximations and assumptions (Etkin, 2012, p.161) as follows:

1. The flat earth approximation;
2. The existence of a plane symmetry; and
3. The absence of rotor gyroscopic effect.

The first assumption is the most important part as it determines the framework of a moving vehicle, understood as a kinematic study.

The study of kinematics requires coordinates' systems to represent the vehicle in space and also a technique for a transformation between one coordinate system to another coordinate system (basically between moving and fixed frames).

In the motion of an AAMV or WIGE craft and the forces and moments acting on it, there are three axis systems involved, i.e. an earth-axis system ($O_Ex_Ey_Ez_E$) and two body-axis systems. The two body-axis systems are body-fixed axes ($O_Bx_By_Bz_B$) and air-trajectory axes ($O_Wx_Wy_Wz_W$). These systems were utilised in some past studies for both AAMV and WIGE craft analysis (Collu, 2008; Delhaye, 1997; Gera, 1995; Irodov, 1974; Staufenbiel and Yeh, 1977). There is another set of body-axes so-called stability axes ($O_Sx_Sy_Sz_S$). This frame rotates about the y-axis (O_Sy_S) of an angle of effective angle of attack to keep aligned the x-axis (O_Sx_S) with the cruising speed. At equilibrium condition, the wind axes and stability axes overlap each other.

The directions of the component earth-axis system ($O_Ex_Ey_Ez_E$) are fixed. The *z*-axis (O_Ez_E) is directed vertically downwards, and the *x*-axis (O_Ex_E) is directed forwards and parallel to the surface (when operating over water surfaces, the O_Ex_E would be parallel to the undisturbed waterline).

The body-fixed axes ($O_Bx_By_Bz_B$) have some characteristics. The first characteristic is that the centre of gravity in the longitudinal reference axis acts as the point of origin.

The following feature is the direction of each axis. The x-axis (O_Bx_B) is directed towards the nose of the vehicle. The z-axis (O_Bz_B) is normal to the x-axis and located in the symmetry plane of the vehicle pointing downwards. The y-axis (O_By_B) is normal to the other two axes and oriented to starboard.

The air-trajectory axes ($O_Wx_Wy_Wz_W$) have origin fixed to the vehicle, usually the centre of gravity. The direction of the x-axis (O_Wx_W) is parallel to the velocity vector of the vehicle relative to the atmosphere. The z-axis (O_Wz_W) lies in the plane of symmetry of the vehicle.

The ride height, h, is the distance taken vertically from the vehicle's point of origin (centre of gravity) to the surface. It supposed not to be confused with the height measured vertically from the centre of gravity of the vehicle to the earth reference, z.

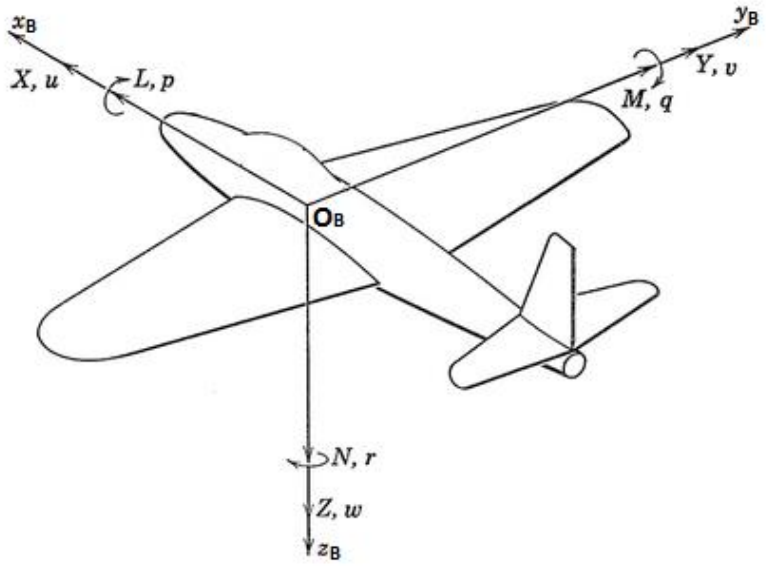

L = rolling moment p = rate of roll
M = pitching moment q = rate of pitch
N = yawing moment r = rate of yaw

$[X, Y, Z]$ = components of resultant force
$[u, v, w]$ = components of velocity

Figure C-1 Notation for body axes

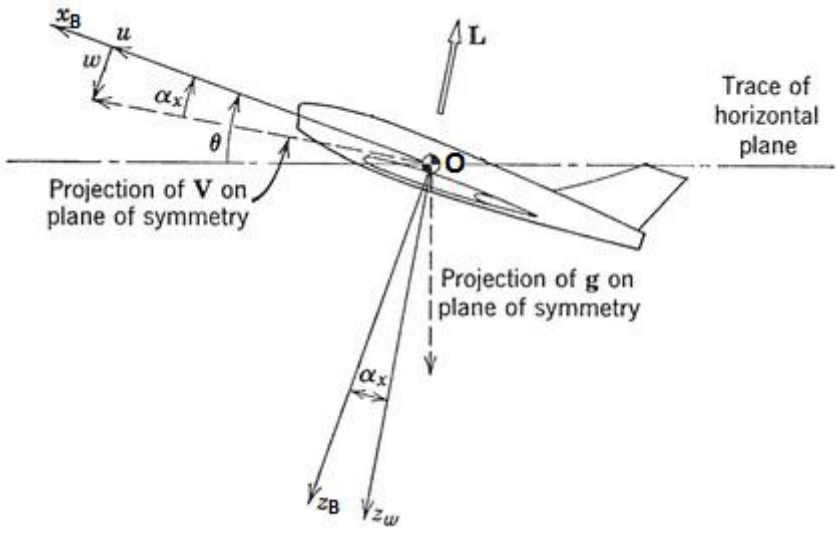

Figure C-2 Plane of symmetry

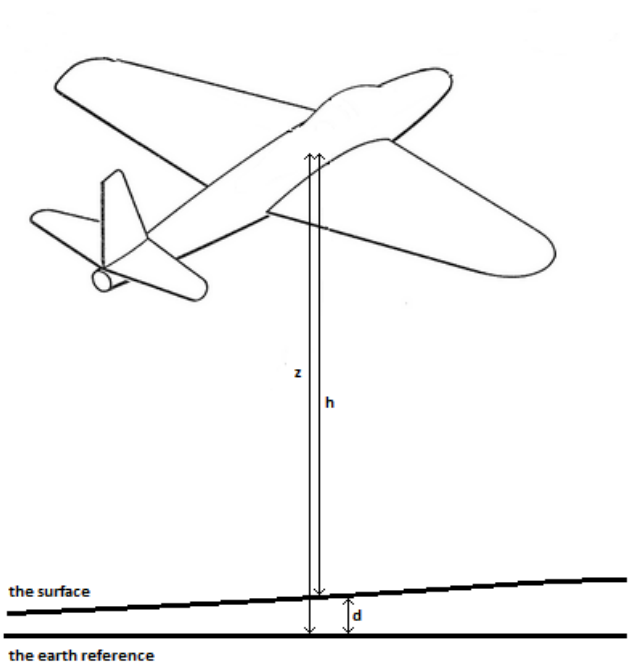

Figure C-3 Height parameter convention

Appendix D **Concept of frequency of encounter**

In ship hydromechanics, it is necessary to take the frequency of encounter into account. The frequency of encounter is the apparent frequency experienced by a marine vehicle when it moves with a forward speed.

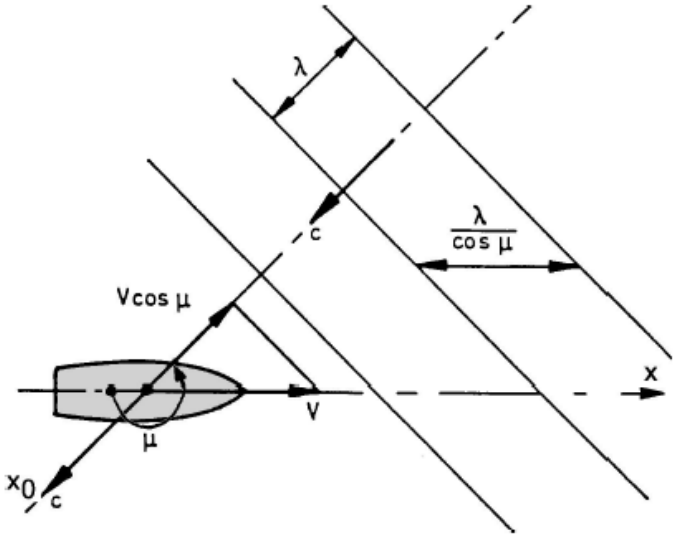

Figure D-1 Frequency of encounter (Journeé and Pinkster, 2002)

The wave speed c, defined in a direction with an angle μ relative to the vehicle's speed vector V, follows this formulation:

$$c = \frac{\varpi}{k} = \frac{\lambda}{T} \tag{D-1}$$

However, in the case of waves in a head sea, there is a change in defining the parameters. Here, as formulated in Journeé and Pinkster (2002), the period of encounter becomes:

$$T_e = \frac{\lambda}{c + V\cos(\mu - \pi)} = \frac{\lambda}{c - V\cos\mu} \tag{D-2}$$

Thus, the frequency of encounter respectively becomes:

$$\omega_e = \frac{2\pi}{T_e} = \frac{2\pi(c - V\cos\mu)}{\lambda}$$
$$\omega_e = k(c - V\cos\mu) \quad \text{(D-3)}$$

Using the relationship of $k \cdot c = \varpi$, the formulation of the frequency of encounter becomes:

$$\omega_e = \omega - kV\cos\mu \quad \text{(D-4)}$$

Information about the frequency of encounter is beneficial to the implementation of the model being developed. A range of reasonable frequencies can be inputted to the program and CFD simulation. In this particular instance, a calculation of the frequency of encounter has been done for several target configurations. The target configurations here were adopted from several WIGE craft.

From the conducted literature survey, it has been found that the typical cruise speed of WIG craft is between 20 and 60 m/s. There are also craft with much higher speeds, but the number is few. In airborne phase, the speeds that will be used are the take-off speeds, which at this point are assumed to be half of the cruise speed of the craft.

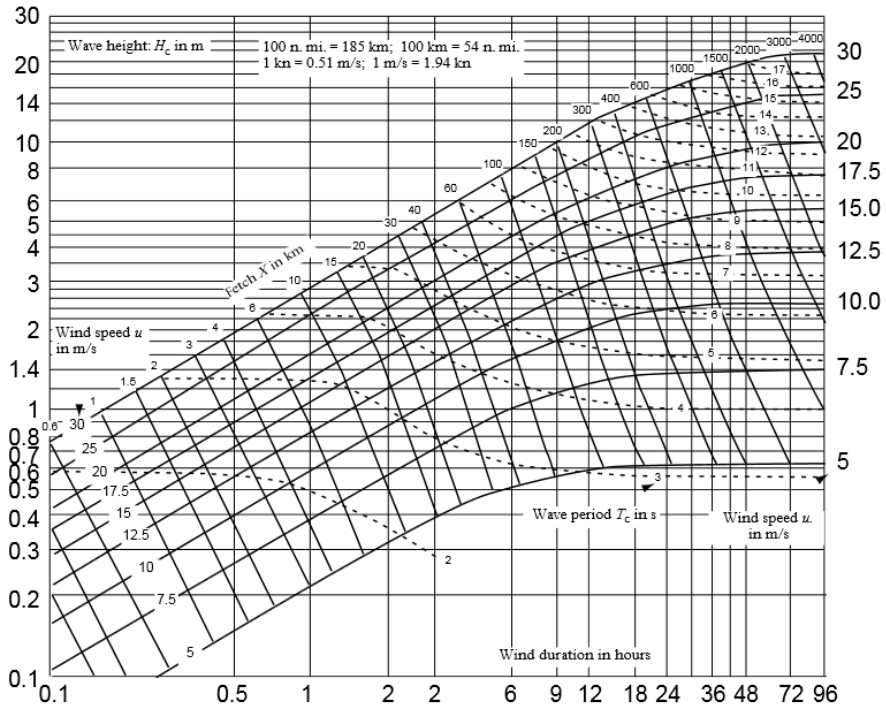

Figure D-2 Manual wave forecasting diagram (WMO, 2008)

One way to forecast and analyse wave elevation is by using the diagram as shown above (WMO, 2008). From this graph, the typical wave speeds are between 5 and 30 m/s and wave periods are between 2 and 17 seconds. However, the waves that are created locally can then travel a thousand miles and become swells, that yields to slightly higher periods. In this case the wave frequency is limited between 0.25 and 1.25 rad/s. Based on this information and following the set of formula above, it is found that WIGE craft have the frequency of encounter ω_e between 0 and 20 rad/s.

Appendix E **Calculation of frequency of encounter**

Table E-1 Frequency of encounter for ω = 0.25 rad/s

ω=0.25												
	k at wave speed=5 m/s				k at wave speed=17.5 m/s				k at wave speed=30 m/s			
μ	0.008				0.014				0.05			
0	0.17	0.07	0.01	-0.35	0.11	-0.065	-0.17	-0.8	-0.25	-0.875	-1.25	-3.5
30	0.181	0.094	0.042	-0.27	0.129	-0.023	-0.114	-0.659	-0.183	-0.724	-1.049	-2.998
60	0.21	0.16	0.13	-0.05	0.18	0.0925	0.04	-0.275	0	-0.3125	-0.5	-1.625
90	0.25	0.25	0.25	0.25	0.25	0.25	0.25	0.25	0.25	0.25	0.25	0.25
120	0.29	0.34	0.37	0.55	0.32	0.408	0.46	0.775	0.5	0.813	1	2.125
150	0.319	0.406	0.458	0.77	0.371	0.523	0.614	1.159	0.683	1.224	1.549	3.498
180	0.33	0.43	0.49	0.85	0.39	0.565	0.67	1.3	0.75	1.375	1.75	4
210	0.319	0.406	0.458	0.77	0.371	0.523	0.614	1.159	0.683	1.224	1.549	3.498
240	0.29	0.34	0.37	0.55	0.32	0.408	0.46	0.775	0.5	0.813	1	2.125
270	0.25	0.25	0.25	0.25	0.25	0.25	0.25	0.25	0.25	0.25	0.25	0.25
300	0.21	0.16	0.13	-0.05	0.18	0.0925	0.04	-0.275	0	-0.3125	-0.5	-1.625
330	0.181	0.094	0.042	-0.27	0.129	-0.023	-0.114	-0.659	-0.183	-0.724	-1.049	-2.998
360	0.17	0.07	0.01	-0.35	0.11	-0.065	-0.17	-0.8	-0.25	-0.875	-1.25	-3.5
T/O speed	10 m/s	22.5 m/s	30 m/s	75 m/s	10 m/s	22.5 m/s	30 m/s	75 m/s	10 m/s	22.5 m/s	30 m/s	75 m/s

Table E-2 Frequency of encounter for ω = 0.375 rad/s

ω=0.375												
	k at wave speed=5 m/s				k at wave speed=17.5 m/s				k at wave speed=30 m/s			
μ	0.013				0.021				0.075			
0	0.245	0.083	-0.015	-0.6	0.165	-0.098	-0.255	-1.2	-0.375	-1.313	-1.875	-5.25
30	0.262	0.122	0.037	-0.469	0.193	-0.034	-0.171	-0.990	-0.275	-1.086	-1.574	-4.496
60	0.31	0.229	0.18	-0.113	0.27	0.139	0.06	-0.413	0	-0.469	-0.75	-2.438
90	0.375	0.375	0.375	0.375	0.375	0.375	0.375	0.375	0.375	0.375	0.375	0.375
120	0.44	0.521	0.57	0.863	0.48	0.611	0.69	1.163	0.75	1.219	1.5	3.188
150	0.488	0.6288	0.713	1.219	0.557	0.784	0.921	1.739	1.025	1.836	2.324	5.246
180	0.505	0.6675	0.765	1.35	0.585	0.8475	1.005	1.95	1.125	2.0625	2.625	6
210	0.488	0.6288	0.713	1.219	0.557	0.784	0.921	1.739	1.025	1.836	2.324	5.246
240	0.44	0.521	0.57	0.863	0.48	0.611	0.69	1.163	0.75	1.219	1.5	3.188
270	0.375	0.375	0.375	0.375	0.375	0.375	0.375	0.375	0.375	0.375	0.375	0.375
300	0.31	0.229	0.18	-0.113	0.27	0.139	0.06	-0.413	0	-0.469	-0.75	-2.438
330	0.262	0.122	0.037	-0.469	0.193	-0.034	-0.171	-0.990	-0.275	-1.086	-1.574	-4.496
360	0.245	0.083	-0.015	-0.6	0.165	-0.098	-0.255	-1.2	-0.375	-1.313	-1.875	-5.25
T/O speed	10 m/s	22.5 m/s	30 m/s	75 m/s	10 m/s	22.5 m/s	30 m/s	75 m/s	10 m/s	22.5 m/s	30 m/s	75 m/s

Table E-3 Frequency of encounter for ω = 0.5 rad/s

ω=0.5												
	k at wave speed=5 m/s				k at wave speed=17.5 m/s				k at wave speed=30 m/s			
μ	0.017				0.029				0.1			
0	0.33	0.1175	-0.01	-0.775	0.21	-0.153	-0.37	-1.675	-0.5	-1.75	-2.5	-7
30	0.353	0.169	0.058	-0.604	0.249	-0.065	-0.253	-1.384	-0.366	-1.449	-2.098	-5.995
60	0.415	0.309	0.245	-0.138	0.355	0.174	0.065	-0.588	0	-0.625	-1	-3.25
90	0.5	0.5	0.5	0.5	0.5	0.5	0.5	0.5	0.5	0.5	0.5	0.5
120	0.585	0.691	0.755	1.138	0.645	0.826	0.935	1.588	1	1.625	2	4.25
150	0.647	0.831	0.942	1.604	0.751	1.065	1.253	2.384	1.366	2.449	3.098	6.995
180	0.67	0.8825	1.01	1.775	0.79	1.1525	1.37	2.675	1.5	2.75	3.5	8
210	0.647	0.831	0.942	1.604	0.751	1.065	1.253	2.384	1.366	2.449	3.098	6.995
240	0.585	0.691	0.755	1.138	0.645	0.826	0.935	1.588	1	1.625	2	4.25
270	0.5	0.5	0.5	0.5	0.5	0.5	0.5	0.5	0.5	0.5	0.5	0.5
300	0.415	0.309	0.245	-0.138	0.355	0.174	0.065	-0.588	0	-0.625	-1	-3.25
330	0.353	0.169	0.058	-0.604	0.249	-0.065	-0.253	-1.384	-0.366	-1.449	-2.098	-5.995
360	0.33	0.1175	-0.01	-0.775	0.21	-0.153	-0.37	-1.675	-0.5	-1.75	-2.5	-7
T/O speed	10 m/s	22.5 m/s	30 m/s	75 m/s	10 m/s	22.5 m/s	30 m/s	75 m/s	10 m/s	22.5 m/s	30 m/s	75 m/s

Table E-4 Frequency of encounter for ω = 0.625 rad/s

ω=0.625												
	k at wave speed=5 m/s				k at wave speed=17.5 m/s				k at wave speed=30 m/s			
μ	0.021				0.036				0.125			
0	0.415	0.153	-0.005	-0.95	0.265	-0.185	-0.455	-2.075	-0.625	-2.188	-3.125	-8.75
30	0.443	0.216	0.079	-0.739	0.313	-0.076	-0.310	-1.713	-0.458	-1.811	-2.623	-7.494
60	0.52	0.389	0.31	-0.163	0.445	0.22	0.085	-0.725	0	-0.781	-1.25	-4.063
90	0.625	0.625	0.625	0.625	0.625	0.625	0.625	0.625	0.625	0.625	0.625	0.625
120	0.73	0.861	0.94	1.413	0.805	1.03	1.165	1.975	1.25	2.031	2.5	5.313
150	0.807	1.034	1.171	1.989	0.937	1.326	1.560	2.963	1.708	3.061	3.873	8.744
180	0.835	1.0975	1.255	2.2	0.985	1.435	1.705	3.325	1.875	3.4375	4.375	10
210	0.807	1.034	1.171	1.989	0.937	1.326	1.560	2.963	1.708	3.061	3.873	8.744
240	0.73	0.861	0.94	1.413	0.805	1.03	1.165	1.975	1.25	2.031	2.5	5.313
270	0.625	0.625	0.625	0.625	0.625	0.625	0.625	0.625	0.625	0.625	0.625	0.625
300	0.52	0.389	0.31	-0.163	0.445	0.22	0.085	-0.725	0	-0.781	-1.25	-4.063
330	0.443	0.216	0.079	-0.739	0.313	-0.076	-0.310	-1.713	-0.458	-1.811	-2.623	-7.494
360	0.415	0.153	-0.005	-0.95	0.265	-0.185	-0.455	-2.075	-0.625	-2.188	-3.125	-8.75
T/O speed	10 m/s	22.5 m/s	30 m/s	75 m/s	10 m/s	22.5 m/s	30 m/s	75 m/s	10 m/s	22.5 m/s	30 m/s	75 m/s

Table E-5 Frequency of encounter for ω = 0.75 rad/s

ω=0.75												
	k at wave speed=5 m/s				k at wave speed=17.5 m/s				k at wave speed=30 m/s			
μ	0.025				0.043				0.15			
0	0.5	0.1875	0	-1.125	0.32	-0.218	-0.54	-2.475	-0.75	-2.633	-3.75	-10.5
30	0.533	0.263	0.100	-0.874	0.378	-0.088	-0.367	-2.043	-0.549	-2.179	-3.147	-8.993
60	0.625	0.469	0.375	-0.188	0.535	0.266	0.105	-0.863	0	-0.941	-1.5	-4.875
90	0.75	0.75	0.75	0.75	0.75	0.75	0.75	0.75	0.75	0.75	0.75	0.75
120	0.875	1.031	1.125	1.688	0.965	1.234	1.395	2.363	1.5	2.441	3	6.375
150	0.967	1.237	1.4	2.374	1.122	1.588	1.867	3.543	2.049	3.679	4.647	10.493
180	1	1.3125	1.5	2.625	1.18	1.7175	2.04	3.975	2.25	4.1325	5.25	12
210	0.967	1.237	1.4	2.374	1.122	1.588	1.867	3.543	2.049	3.679	4.647	10.493
240	0.875	1.031	1.125	1.688	0.965	1.234	1.395	2.363	1.5	2.441	3	6.375
270	0.75	0.75	0.75	0.75	0.75	0.75	0.75	0.75	0.75	0.75	0.75	0.75
300	0.625	0.469	0.375	-0.188	0.535	0.266	0.105	-0.863	0	-0.941	-1.5	-4.875
330	0.533	0.263	0.100	-0.874	0.378	-0.088	-0.367	-2.043	-0.549	-2.179	-3.147	-8.993
360	0.5	0.1875	0	-1.125	0.32	-0.218	-0.54	-2.475	-0.75	-2.633	-3.75	-10.5
T/O speed	10 m/s	22.5 m/s	30 m/s	75 m/s	10 m/s	22.5 m/s	30 m/s	75 m/s	10 m/s	22.5 m/s	30 m/s	75 m/s

Table E-6 Frequency of encounter for ω = 0.875 rad/s

ω=0.875												
	k at wave speed=5 m/s				k at wave speed=17.5 m/s				k at wave speed=30 m/s			
μ	0.029				0.05				0.175			
0	0.585	0.223	0.005	-1.3	0.375	-0.25	-0.625	-7.875	-0.875	-3.063	-4.375	-12.25
30	0.624	0.310	0.122	-1.009	0.442	-0.099	-0.424	-6.703	-0.641	-2.535	-3.672	-10.492
60	0.73	0.549	0.44	-0.213	0.625	0.3125	0.125	-3.5	0	-1.094	-1.75	-5.688
90	0.875	0.875	0.875	0.875	0.875	0.875	0.875	0.875	0.875	0.875	0.875	0.875
120	1.02	1.201	1.31	1.963	1.125	1.4375	1.625	5.25	1.75	2.844	3.5	7.438
150	1.126	1.440	1.628	2.759	1.308	1.849	2.174	8.453	2.391	4.285	5.422	12.242
180	1.165	1.528	1.745	3.05	1.375	2	2.375	9.625	2.625	4.813	6.125	14
210	1.126	1.440	1.628	2.759	1.308	1.849	2.174	8.453	2.391	4.285	5.422	12.242
240	1.02	1.201	1.31	1.963	1.125	1.438	1.625	5.25	1.75	2.844	3.5	7.438
270	0.875	0.875	0.875	0.875	0.875	0.875	0.875	0.875	0.875	0.875	0.875	0.875
300	0.73	0.549	0.44	-0.213	0.625	0.3125	0.125	-3.5	0	-1.094	-1.75	-5.688
330	0.624	0.310	0.122	-1.009	0.442	-0.099	-0.424	-6.703	-0.641	-2.535	-3.672	-10.492
360	0.585	0.223	0.005	-1.3	0.375	-0.25	-0.625	-7.875	-0.875	-3.063	-4.375	-12.25
T/O speed	10 m/s	22.5 m/s	30 m/s	75 m/s	10 m/s	22.5 m/s	30 m/s	75 m/s	10 m/s	22.5 m/s	30 m/s	75 m/s

Table E-7 Frequency of encounter for ω = 1 rad/s

ω=1												
	k at wave speed=5 m/s				k at wave speed=17.5 m/s				k at wave speed=30 m/s			
μ	0.033				0.057				0.2			
0	0.67	0.2575	0.01	-1.475	0.43	-0.283	-0.71	-3.275	-1	-3.5	-5	-14
30	0.714	0.357	0.143	-1.143	0.506	-0.111	-0.481	-2.702	-0.732	-2.897	-4.196	-11.99
60	0.835	0.629	0.505	-0.238	0.715	0.359	0.145	-1.138	0	-1.25	-2	-6.5
90	1	1	1	1	1	1	1	1	1	1	1	1
120	1.165	1.371	1.495	2.238	1.285	1.641	1.855	3.138	2	3.25	4	8.5
150	1.286	1.643	1.857	3.143	1.494	2.111	2.481	4.702	2.732	4.897	6.196	13.99
180	1.33	1.743	1.99	3.475	1.57	2.2825	2.71	5.275	3	5.5	7	16
210	1.286	1.643	1.857	3.143	1.494	2.111	2.481	4.702	2.732	4.897	6.196	13.99
240	1.165	1.371	1.495	2.238	1.285	1.641	1.855	3.138	2	3.25	4	8.5
270	1	1	1	1	1	1	1	1	1	1	1	1
300	0.835	0.629	0.505	-0.238	0.715	0.359	0.145	-1.138	0	-1.25	-2	-6.5
330	0.714	0.357	0.143	-1.143	0.506	-0.111	-0.481	-2.702	-0.732	-2.897	-4.196	-11.99
360	0.67	0.2575	0.01	-1.475	0.43	-0.283	-0.71	-3.275	-1	-3.5	-5	-14
T/O speed	10 m/s	22.5 m/s	30 m/s	75 m/s	10 m/s	22.5 m/s	30 m/s	75 m/s	10 m/s	22.5 m/s	30 m/s	75 m/s

Table E-8 Frequency of encounter for ω = 1.125 rad/s

ω=1.125												
	k at wave speed=5 m/s				k at wave speed=17.5 m/s				k at wave speed=30 m/s			
μ	0.038				0.064				0.225			
0	0.745	0.27	-0.015	-1.725	0.485	-0.315	-0.795	-3.675	-1.125	-3.938	-5.625	-15.75
30	0.796	0.385	0.138	-1.343	0.571	-0.122	-0.534	-3.032	-0.824	-3.259	-4.721	-13.489
60	0.935	0.6975	0.555	-0.3	0.805	0.405	0.165	-1.275	0	-1.406	-2.25	-7.313
90	1.125	1.125	1.125	1.125	1.125	1.125	1.125	1.125	1.125	1.125	1.125	1.125
120	1.315	1.553	1.695	2.55	1.445	1.845	2.085	3.525	2.25	3.656	4.5	9.563
150	1.454	1.865	2.112	3.593	1.679	2.372	2.788	5.282	3.074	5.509	6.971	15.739
180	1.505	1.98	2.265	3.975	1.765	2.565	3.045	5.925	3.375	6.1875	7.875	18
210	1.454	1.865	2.112	3.593	1.679	2.372	2.788	5.282	3.074	5.509	6.971	15.739
240	1.315	1.553	1.695	2.55	1.445	1.845	2.085	3.525	2.25	3.656	4.5	9.563
270	1.125	1.125	1.125	1.125	1.125	1.125	1.125	1.125	1.125	1.125	1.125	1.125
300	0.935	0.6975	0.555	-0.3	0.805	0.405	0.165	-1.275	0	-1.406	-2.25	-7.313
330	0.796	0.385	0.138	-1.343	0.571	-0.122	-0.534	-3.032	-0.824	-3.259	-4.721	-13.489
360	0.745	0.27	-0.015	-1.725	0.485	-0.315	-0.795	-3.675	-1.125	-3.938	-5.625	-15.75
T/O speed	10 m/s	22.5 m/s	30 m/s	75 m/s	10 m/s	22.5 m/s	30 m/s	75 m/s	10 m/s	22.5 m/s	30 m/s	75 m/s

Table E-9 Frequency of encounter for ω = 1.25 rad/s

ω=1.25												
	k at wave speed=5 m/s				k at wave speed=17.5 m/s				k at wave speed=30 m/s			
μ	0.042				0.071				0.25			
0	0.83	0.305	-0.01	-1.9	0.54	-0.3475	-0.88	-4.075	-1.25	-4.375	-6.25	-17.5
30	0.886	0.432	0.159	-1.478	0.635	-0.133	-0.594	-3.362	-0.915	-3.621	-5.245	-14.988
60	1.04	0.778	0.62	-0.325	0.895	0.451	0.185	-1.413	0	-1.563	-2.5	-8.125
90	1.25	1.25	1.25	1.25	1.25	1.25	1.25	1.25	1.25	1.25	1.25	1.25
120	1.46	1.723	1.88	2.825	1.605	2.049	2.315	3.913	2.5	4.063	5	10.625
150	1.614	2.068	2.341	3.978	1.865	2.633	3.095	5.862	3.415	6.121	7.745	17.488
180	1.67	2.195	2.51	4.4	1.96	2.8475	3.38	6.575	3.75	6.875	8.75	20
210	1.614	2.068	2.341	3.978	1.865	2.633	3.095	5.862	3.415	6.121	7.745	17.488
240	1.46	1.723	1.88	2.825	1.605	2.049	2.315	3.913	2.5	4.063	5	10.625
270	1.25	1.25	1.25	1.25	1.25	1.25	1.25	1.25	1.25	1.25	1.25	1.25
300	1.04	0.778	0.62	-0.325	0.895	0.451	0.185	-1.413	0	-1.563	-2.5	-8.125
330	0.886	0.432	0.159	-1.478	0.635	-0.133	-0.594	-3.362	-0.915	-3.621	-5.245	-14.988
360	0.83	0.305	-0.01	-1.9	0.54	-0.3475	-0.88	-4.075	-1.25	-4.375	-6.25	-17.5
T/O speed	10 m/s	22.5 m/s	30 m/s	75 m/s	10 m/s	22.5 m/s	30 m/s	75 m/s	10 m/s	22.5 m/s	30 m/s	75 m/s

Appendix F **Aerodynamic data of the NACA 4412**

F.1 Aerodynamic data at α = 0º and h/c = 0.3

Table F-1 (F.1) at A = 0.05c and ω = 0.25 rad/s

	cd	cl	cm total	cm ac
Max	0.010	0.408	0.189	-0.0870
Mean	0.009	0.378	0.182	-0.0872
Min	0.008	0.350	0.175	-0.0874
Crest phase lag (rad)	1.550	-1.200	-1.200	3.050
Trough phase lag (rad)	1.638	-0.913	-0.850	2.838

Table F-2 (F.1) at A = 0.05c and ω = 0.50 rad/s

	Cd	cl	cm total	cm ac
Max	0.011	0.430	0.195	-0.0867
Mean	0.009	0.378	0.182	-0.0873
Min	0.006	0.328	0.169	-0.0877
Crest phase lag (rad)	1.475	-1.450	-1.450	3.025
Trough phase lag (rad)	1.550	-1.225	-1.200	2.525

Table F-3 (F.1) at A = 0.05c and ω = 1.00 rad/s

	cd	cl	cm total	cm ac
Max	0.013	0.474	0.206	-0.0858
Mean	0.009	0.378	0.182	-0.0873
Min	0.003	0.284	0.158	-0.0884
Crest phase lag (rad)	1.350	-1.600	-1.500	-3.100
Trough phase lag (rad)	1.400	-1.450	-1.350	2.600

Table F-4 (F.1) at A = 0.05c and ω = 1.25 rad/s

	cd	cl	cm total	cm ac
Max	0.013	0.494	0.211	-0.0851
Mean	0.008	0.378	0.182	-0.0873
Min	0.002	0.265	0.154	-0.0889
Crest phase lag (rad)	1.250	-1.625	-1.563	3.063
Trough phase lag (rad)	1.375	-1.438	-1.375	3.000

F.2 Aerodynamic data at α = 0º and h/c = 0.5

Table F-5 (F.2) at A = 0.05c and ω = 0.25 rad/s

	cd	cl	cm total	cm ac
Max	0.010	0.422	0.194	-0.0878
Mean	0.009	0.403	0.189	-0.0882
Min	0.008	0.383	0.184	-0.0887
Crest phase lag (rad)	1.413	-1.500	-1.713	-0.888
Trough phase lag (rad)	1.613	-1.488	-1.600	-0.475

Table F-6 (F.2) at A = 0.05c and ω = 0.50 rad/s

	cd	cl	cm total	cm ac
Max	0.011	0.441	0.198	-0.0876
Mean	0.009	0.402	0.189	-0.0882
Min	0.006	0.364	0.180	-0.0887
Crest phase lag (rad)	1.400	-1.550	-1.550	-1.575
Trough phase lag (rad)	1.550	-1.575	-1.575	-0.850

Table F-7 (F.2) at A = 0.05c and ω = 1.00 rad/s

	cd	cl	cm total	cm ac
Max	0.013	0.476	0.206	-0.0869
Mean	0.009	0.403	0.189	-0.0882
Min	0.003	0.330	0.172	-0.0892
Crest phase lag (rad)	1.400	-1.650	-1.550	-2.000
Trough phase lag (rad)	1.350	-1.650	-1.600	-1.850

Table F-8 (F.2) at A = 0.05c and ω = 1.25 rad/s

	cd	cl	cm total	cm ac
Max	0.014	0.491	0.210	-0.0863
Mean	0.009	0.402	0.189	-0.0882
Min	0.002	0.315	0.168	-0.0897
Crest phase lag (rad)	1.375	-1.688	-1.625	-2.313
Trough phase lag (rad)	1.375	-1.625	-1.625	-2.438

Table F-9 (F.2) at A = 0.15c and ω = 0.25 rad/s

	cd	cl	cm total	cm ac
Max	0.012	0.461	0.204	-0.0878
Mean	0.009	0.391	0.187	-0.0889
Min	0.005	0.327	0.172	-0.0901
Crest phase lag (rad)	1.500	-1.538	-1.650	-0.575
Trough phase lag (rad)	1.600	-1.013	-1.013	-1.125

Table F-10 (F.2) at A = 0.15c and ω = 0.50 rad/s

	cd	cl	cm total	cm ac
Max	0.014	0.521	0.218	-0.0873
Mean	0.008	0.390	0.186	-0.0888
Min	-0.0003	0.265	0.156	-0.0903
Crest phase lag (rad)	1.375	-1.675	-1.675	-1.225
Trough phase lag (rad)	1.475	-1.300	-1.275	-1.425

Table F-11 (F.2) at A = 0.15c and ω = 1.00 rad/s

	cd	cl	cm total	cm ac
Max	0.016	0.631	0.243	-0.0842
Mean	0.005	0.388	0.185	-0.0885
Min	-0.013	0.149	0.128	-0.0918
Crest phase lag (rad)	0.850	-1.750	-1.700	-2.300
Trough phase lag (rad)	1.350	-1.450	-1.450	-2.050

Table F-12 (F.2) at A = 0.15c and ω = 1.25 rad/s

	cd	cl	cm total	cm ac
Max	0.016	0.684	0.256	-0.0805
Mean	0.004	0.387	0.185	-0.0881
Min	-0.019	0.098	0.116	-0.0932
Crest phase lag (rad)	0.687	-1.750	-1.688	-2.500
Trough phase lag (rad)	1.313	-1.438	-1.438	-2.188

F.3 Aerodynamic data at α = 0º and h/c = 1.0

Table F-13 (F.3) at A = 0.05c and ω = 0.25 rad/s

	Cd	cl	cm total	cm ac
Max	0.010	0.423	0.193	-0.0874
Mean	0.009	0.406	0.190	-0.0880
Min	0.008	0.389	0.186	-0.0886
Crest phase lag (rad)	1.513	-1.625	-1.738	-0.938
Trough phase lag (rad)	1.525	-1.625	-1.750	-0.650

Table F-14 (F.3) at A = 0.05c and ω = 0.50 rad/s

	cd	cl	cm total	cm ac
Max	0.011	0.439	0.197	-0.0872
Mean	0.009	0.406	0.190	-0.0880
Min	0.007	0.373	0.182	-0.0888
Crest phase lag (rad)	1.475	-1.650	-1.700	-1.375
Trough phase lag (rad)	1.475	-1.650	-1.700	-1.025

Table F-15 (F.3) at A = 0.05c and ω = 1.00 rad/s

	cd	cl	cm total	cm ac
Max	0.013	0.467	0.203	-0.0863
Mean	0.009	0.406	0.189	-0.0880
Min	0.004	0.344	0.175	-0.0894
Crest phase lag (rad)	1.350	-1.700	-1.650	-1.950
Trough phase lag (rad)	1.350	-1.700	-1.700	-1.750

Table F-16 (F.3) at A = 0.05c and ω = 1.25 rad/s

	cd	cl	cm total	cm ac
Max	0.014	0.479	0.206	-0.0857
Mean	0.009	0.406	0.189	-0.0880
Min	0.003	0.332	0.173	-0.0898
Crest phase lag (rad)	1.313	-1.688	-1.625	-2.188
Trough phase lag (rad)	1.313	-1.688	-1.688	-2.063

Table F-17 (F.3) at A = 0.15c and ω = 0.25 rad/s

	cd	cl	cm total	cm ac
Max	0.012	0.458	0.202	-0.0874
Mean	0.009	0.406	0.190	-0.0890
Min	0.005	0.354	0.178	-0.0909
Crest phase lag (rad)	1.513	-1.638	-1.713	-0.763
Trough phase lag (rad)	1.513	-1.600	-1.750	-0.738

Table F-18 (F.3) at A = 0.15c and ω = 0.50 rad/s

	cd	cl	cm total	cm ac
Max	0.015	0.508	0.213	-0.0862
Mean	0.008	0.406	0.190	-0.0888
Min	0.0004	0.304	0.167	-0.0916
Crest phase lag (rad)	1.450	-1.675	-1.650	-1.775
Trough phase lag (rad)	1.425	-1.650	-1.700	-1.125

Table F-19 (F.3) at A = 0.15c and ω = 1.00 rad/s

	cd	cl	cm total	cm ac
Max	0.017	0.593	0.231	-0.0821
Mean	0.006	0.405	0.190	-0.0884
Min	-0.010	0.215	0.147	-0.0929
Crest phase lag (rad)	1.400	-1.700	-1.600	-2.100
Trough phase lag (rad)	1.350	-1.700	-1.700	-1.550

Table F-20 (F.3) at A = 0.15c and ω = 1.25 rad/s

	cd	cl	cm total	cm ac
Max	0.017	0.629	0.239	-0.0794
Mean	0.005	0.405	0.189	-0.0881
Min	-0.015	0.179	0.138	-0.0938
Crest phase lag (rad)	1.563	-1.750	-1.563	-2.188
Trough phase lag (rad)	1.313	-1.688	-1.688	-1.625

F.4 Aerodynamic data at α = 2º and h/c = 0.3

Table F-21 (F.4) at A = 0.05c and ω = 0.25 rad/s

	cd	cl	cm total	cm ac
Max	0.011	0.669	0.257	-0.0881
Mean	0.009	0.646	0.251	-0.0892
Min	0.007	0.624	0.245	-0.0905
Crest phase lag (rad)	1.513	-2.038	-2.288	-0.050
Trough phase lag (rad)	1.550	-1.925	-2.050	-0.025

Table F-22 (F.4) at A = 0.05c and ω = 0.50 rad/s

	cd	cl	cm total	cm ac
Max	0.012	0.687	0.261	-0.0884
Mean	0.009	0.646	0.251	-0.0891
Min	0.005	0.604	0.240	-0.0901
Crest phase lag (rad)	1.475	-1.850	-1.950	0.225
Trough phase lag (rad)	1.500	-1.750	-1.825	-0.100

Table F-23 (F.4) at A = 0.05c and ω = 1.00 rad/s

	cd	cl	cm total	cm ac
Max	0.015	0.728	0.272	-0.0884
Mean	0.008	0.646	0.251	-0.0892
Min	0.0002	0.564	0.230	-0.0898
Crest phase lag (rad)	1.400	-1.800	-1.850	3.000
Trough phase lag (rad)	1.400	-1.650	-1.650	2.350

Table F-24 (F.4) at A = 0.05c and ω = 1.25 rad/s

	cd	cl	cm total	cm ac
Max	0.017	0.746	0.276	-0.0874
Mean	0.008	0.646	0.251	-0.0893
Min	-0.002	0.546	0.225	-0.0905
Crest phase lag (rad)	1.375	-1.750	-1.750	2.813
Trough phase lag (rad)	1.375	-1.625	-1.563	2.438

F.5 Aerodynamic data at α = 2º and h/c = 0.5

Table F-25 (F.5) at A = 0.05c and ω = 0.25 rad/s

	cd	cl	cm total	cm ac
Max	0.011	0.643	0.248	-0.0861
Mean	0.009	0.625	0.243	-0.0869
Min	0.007	0.607	0.239	-0.0879
Crest phase lag (rad)	1.500	-1.788	-2.025	-0.425
Trough phase lag (rad)	1.525	-1.788	-1.900	-0.375

Table F-26 (F.5) at A = 0.05c and ω = 0.50 rad/s

	cd	cl	cm total	cm ac
Max	0.012	0.660	0.251	-0.0862
Mean	0.009	0.625	0.243	-0.0869
Min	0.005	0.590	0.235	-0.0877
Crest phase lag (rad)	1.475	-1.725	-1.800	-1.225
Trough phase lag (rad)	1.475	-1.700	-1.775	-0.625

Table F-27 (F.5) at A = 0.05c and ω = 1.00 rad/s

	cd	cl	cm total	cm ac
Max	0.015	0.691	0.259	-0.0855
Mean	0.009	0.624	0.243	-0.0868
Min	0.001	0.557	0.227	-0.0876
Crest phase lag (rad)	1.400	-1.700	-1.600	-2.250
Trough phase lag (rad)	1.350	-1.700	-1.700	-1.450

Table F-28 (F.5) at A = 0.05c and ω = 1.25 rad/s

	cd	cl	cm total	cm ac
Max	0.016	0.705	0.262	-0.0847
Mean	0.008	0.624	0.243	-0.0868
Min	-0.0007	0.543	0.224	-0.0881
Crest phase lag (rad)	1.375	-1.688	-1.563	-2.500
Trough phase lag (rad)	1.375	-1.625	-1.625	-2.250

Table F-29 (F.5) at A = 0.15c and ω = 0.25 rad/s

	cd	cl	cm total	cm ac
Max	0.014	0.695	0.264	-0.0863
Mean	0.009	0.636	0.248	-0.0892
Min	0.003	0.576	0.233	-0.0929
Crest phase lag (rad)	1.563	-2.088	-2.375	-0.613
Trough phase lag (rad)	1.463	-1.775	-1.963	-0.238

Table F-30 (F.5) at A = 0.15c and ω = 0.50 rad/s

	cd	cl	cm total	cm ac
Max	0.018	0.749	0.276	-0.0860
Mean	0.008	0.635	0.248	-0.0891
Min	-0.004	0.519	0.220	-0.0922
Crest phase lag (rad)	1.475	-1.925	-2.100	-1.150
Trough phase lag (rad)	1.425	-1.675	-1.800	-0.400

Table F-31 (F.5) at A = 0.15c and ω = 1.00 rad/s

	cd	cl	cm total	cm ac
Max	0.023	0.850	0.298	-0.0852
Mean	0.006	0.631	0.246	-0.0887
Min	-0.020	0.411	0.194	-0.0914
Crest phase lag (rad)	1.300	-1.800	-1.750	-2.050
Trough phase lag (rad)	1.300	-1.600	-1.600	-1.350

Table F-32 (F.5) at A = 0.15c and ω = 1.25 rad/s

	cd	cl	cm total	cm ac
Max	0.024	0.894	0.308	-0.0828
Mean	0.004	0.629	0.246	-0.0886
Min	-0.028	0.363	0.183	-0.0921
Crest phase lag (rad)	1.188	-1.813	-1.688	-2.313
Trough phase lag (rad)	1.313	-1.563	-1.563	-1.750

F.6 Aerodynamic data at α = 2º and h/c = 1.0

Table F-33 (F.6) at A = 0.05c and ω = 0.25 rad/s

	cd	cl	cm total	cm ac
Max	0.011	0.626	0.241	-0.0844
Mean	0.009	0.610	0.238	-0.0851
Min	0.007	0.594	0.234	-0.0858
Crest phase lag (rad)	1.500	-1.675	-1.913	-0.763
Trough phase lag (rad)	1.550	-1.638	-1.800	-0.575

Table F-34 (F.6) at A = 0.05c and ω = 0.50 rad/s

	cd	cl	cm total	cm ac
Max	0.013	0.641	0.244	-0.0840
Mean	0.009	0.610	0.238	-0.0850
Min	0.006	0.579	0.230	-0.0859
Crest phase lag (rad)	1.425	-1.625	-1.625	-1.650
Trough phase lag (rad)	1.475	-1.650	-1.675	-0.800

Table F-35 (F.6) at A = 0.05c and ω = 1.00 rad/s

	cd	cl	cm total	cm ac
Max	0.015	0.668	0.250	-0.0830
Mean	0.009	0.610	0.237	-0.0850
Min	0.002	0.551	0.224	-0.0864
Crest phase lag (rad)	1.400	-1.650	-1.550	-2.100
Trough phase lag (rad)	1.400	-1.700	-1.700	-1.850

Table F-36 (F.6) at A = 0.05c and ω = 1.25 rad/s

	cd	cl	cm total	cm ac
Max	0.016	0.679	0.253	-0.0822
Mean	0.009	0.609	0.237	-0.0849
Min	0.0004	0.539	0.222	-0.0869
Crest phase lag (rad)	1.313	-1.688	-1.563	-2.188
Trough phase lag (rad)	1.313	-1.688	-1.625	-2.063

Table F-37 (F.6) at A = 0.15c and ω = 0.25 rad/s

	cd	cl	cm total	cm ac
Max	0.014	0.661	0.250	-0.0841
Mean	0.009	0.613	0.240	-0.0865
Min	0.004	0.563	0.228	-0.0892
Crest phase lag (rad)	1.525	-1.713	-1.900	-0.925
Trough phase lag (rad)	1.513	-1.700	-1.863	-0.613

Table F-38 (F.6) at A = 0.15c and ω = 0.50 rad/s

	cd	cl	cm total	cm ac
Max	0.018	0.706	0.259	-0.0828
Mean	0.009	0.612	0.239	-0.0863
Min	-0.003	0.515	0.218	-0.0900
Crest phase lag (rad)	1.450	-1.700	-1.750	-1.600
Trough phase lag (rad)	1.475	-1.675	-1.800	-0.875

Table F-39 (F.6) at A = 0.15c and ω = 1.00 rad/s

	cd	Cl	cm total	cm ac
Max	0.023	0.786	0.275	-0.0784
Mean	0.007	0.610	0.238	-0.0858
Min	-0.016	0.429	0.198	-0.0913
Crest phase lag (rad)	1.400	-1.750	-1.700	-2.000
Trough phase lag (rad)	1.350	-1.700	-1.750	-1.250

Table F-40 (F.6) at A = 0.15c and ω = 1.25 rad/s

	cd	Cl	cm total	cm ac
Max	0.024	0.821	0.282	-0.0749
Mean	0.005	0.609	0.238	-0.0855
Min	-0.023	0.393	0.191	-0.0921
Crest phase lag (rad)	1.250	-1.750	-1.625	-2.250
Trough phase lag (rad)	1.313	-1.688	-1.688	-1.500

F.7 Aerodynamic data at α = 4º and h/c = 0.3

Table F-41 (F.7) at A = 0.05c and ω = 0.25 rad/s

	cd	Cl	cm total	cm ac
Max	0.012	0.897	0.319	-0.0900
Mean	0.010	0.870	0.310	-0.0927
Min	0.007	0.844	0.301	-0.0962
Crest phase lag (rad)	1.538	-2.538	-2.738	0.050
Trough phase lag (rad)	1.650	-2.313	-2.513	-0.025

Table F-42 (F.7) at A = 0.05c and ω = 0.50 rad/s

	cd	Cl	cm total	cm ac
Max	0.014	0.909	0.321	-0.0902
Mean	0.010	0.869	0.310	-0.0926
Min	0.004	0.829	0.298	-0.0956
Crest phase lag (rad)	1.500	-2.175	-2.425	0.450
Trough phase lag (rad)	1.525	-2.000	-2.175	0.100

Table F-43 (F.7) at A = 0.05c and ω = 1.00 rad/s

	cd	Cl	cm total	cm ac
Max	0.019	0.940	0.328	-0.0910
Mean	0.009	0.868	0.309	-0.0925
Min	-0.001	0.796	0.290	-0.0939
Crest phase lag (rad)	1.400	-1.850	-1.900	0.650
Trough phase lag (rad)	1.350	-1.800	-1.800	0.550

Table F-44 (F.7) at A = 0.05c and ω = 1.25 rad/s

	cd	cl	cm total	cm ac
Max	0.020	0.955	0.332	-0.0912
Mean	0.009	0.868	0.309	-0.0925
Min	-0.004	0.780	0.286	-0.0940
Crest phase lag (rad)	1.375	-1.813	-1.750	1.125
Trough phase lag (rad)	1.313	-1.688	-1.750	1.813

F.8 Aerodynamic data at α = 4º and h/c = 0.5

Table F-45 (F.8) at A = 0.05c and ω = 0.25 rad/s

	cd	cl	cm total	cm ac
Max	0.012	0.842	0.298	-0.0855
Mean	0.010	0.826	0.293	-0.0867
Min	0.007	0.808	0.288	-0.0882
Crest phase lag (rad)	1.400	-2.038	-2.588	-0.175
Trough phase lag (rad)	1.613	-1.963	-2.163	-0.113

Table F-46 (F.8) at A = 0.05c and ω = 0.50 rad/s

	cd	cl	cm total	cm ac
Max	0.014	0.857	0.300	-0.0858
Mean	0.010	0.826	0.293	-0.0867
Min	0.005	0.794	0.285	-0.0880
Crest phase lag (rad)	1.475	-1.775	-1.875	0.300
Trough phase lag (rad)	1.475	-1.775	-1.925	-0.100

Table F-47 (F.8) at A = 0.05c and ω = 1.00 rad/s

	cd	cl	cm total	cm ac
Max	0.018	0.886	0.307	-0.0859
Mean	0.010	0.825	0.293	-0.0866
Min	-0.00009	0.764	0.278	-0.0872
Crest phase lag (rad)	1.400	-1.700	-1.600	-2.300
Trough phase lag (rad)	1.350	-1.700	-1.750	-1.150

Table F-48 (F.8) at A = 0.05c and ω = 1.25 rad/s

	cd	cl	cm total	cm ac
Max	0.020	0.900	0.311	-0.0853
Mean	0.009	0.825	0.292	-0.0866
Min	-0.002	0.750	0.274	-0.0876
Crest phase lag (rad)	1.375	-1.688	-1.563	-2.813
Trough phase lag (rad)	1.313	-1.688	-1.688	2.750

Table F-49 (F.8) at A = 0.15c and ω = 0.25 rad/s

	cd	cl	cm total	cm ac
Max	0.017	0.914	0.326	-0.0858
Mean	0.010	0.850	0.303	-0.0913
Min	0.002	0.787	0.284	-0.0992
Crest phase lag (rad)	1.550	-2.500	-2.763	-0.525
Trough phase lag (rad)	1.538	-1.988	-2.263	-0.150

Table F-50 (F.8) at A = 0.15c and ω = 0.50 rad/s

	cd	cl	cm total	cm ac
Max	0.022	0.950	0.331	-0.0864
Mean	0.009	0.848	0.303	-0.0910
Min	-0.007	0.738	0.274	-0.0981
Crest phase lag (rad)	1.475	-2.150	-2.550	-0.150
Trough phase lag (rad)	1.475	-1.850	-2.000	-0.025

Table F-51 (F.8) at A = 0.15c and ω = 1.00 rad/s

	cd	cl	cm total	cm ac
Max	0.031	1.032	0.343	-0.0863
Mean	0.007	0.841	0.300	-0.0900
Min	-0.025	0.640	0.252	-0.0940
Crest phase lag (rad)	1.400	-1.900	-1.750	-2.050
Trough phase lag (rad)	1.300	-1.700	-1.750	-0.700

Table F-52 (F.8) at A = 0.15c and ω = 1.25 rad/s

	cd	cl	cm total	cm ac
Max	0.034	1.075	0.354	-0.0843
Mean	0.005	0.839	0.299	-0.0899
Min	-0.034	0.596	0.241	-0.0931
Crest phase lag (rad)	1.313	-1.813	-1.625	-2.250
Trough phase lag (rad)	1.313	-1.688	-1.688	-1.063

F.9 Aerodynamic data at α = 4º and h/c = 1.0

Table F-53 (F.9) at A = 0.05c and ω = 0.25 rad/s

	cd	cl	cm total	cm ac
Max	0.012	0.818	0.287	-0.0824
Mean	0.010	0.803	0.283	-0.0830
Min	0.008	0.787	0.280	-0.0838
Crest phase lag (rad)	1.513	-1.663	-1.838	-0.400
Trough phase lag (rad)	1.513	-1.663	-1.850	-0.488

Table F-54 (F.9) at A = 0.05c and ω = 0.50 rad/s

	cd	cl	cm total	cm ac
Max	0.014	0.832	0.290	-0.0823
Mean	0.010	0.802	0.283	-0.0829
Min	0.005	0.772	0.276	-0.0837
Crest phase lag (rad)	1.425	-1.650	-1.700	-0.925
Trough phase lag (rad)	1.450	-1.700	-1.800	-0.725

Table F-55 (F.9) at A = 0.05c and ω = 1.00 rad/s

	cd	cl	cm total	cm ac
Max	0.018	0.859	0.296	-0.0815
Mean	0.010	0.801	0.283	-0.0827
Min	0.001	0.743	0.269	-0.0835
Crest phase lag (rad)	1.350	-1.650	-1.550	-2.250
Trough phase lag (rad)	1.300	-1.700	-1.700	-1.100

Table F-56 (F.9) at A = 0.05c and ω = 1.25 rad/s

	cd	cl	cm total	cm ac
Max	0.019	0.870	0.299	-0.0809
Mean	0.010	0.801	0.283	-0.0827
Min	-0.0009	0.732	0.266	-0.0837
Crest phase lag (rad)	1.313	-1.625	-1.563	-2.438
Trough phase lag (rad)	1.313	-1.688	-1.625	2.750

Table F-57 (F.9) at A = 0.15c and ω = 0.25 rad/s

	cd	cl	cm total	cm ac
Max	0.017	0.851	0.296	-0.0824
Mean	0.010	0.806	0.286	-0.0846
Min	0.003	0.757	0.274	-0.0879
Crest phase lag (rad)	1.525	-1.750	-2.000	-0.538
Trough phase lag (rad)	1.550	-1.713	-1.913	-0.725

Table F-58 (F.9) at A = 0.15c and ω = 0.50 rad/s

	cd	cl	cm total	cm ac
Max	0.022	0.8924	0.3036	-0.0810
Mean	0.009	0.8041	0.2850	-0.0843
Min	-0.005	0.7116	0.2640	-0.0883
Crest phase lag (rad)	1.475	-1.675	-1.750	-1.650
Trough phase lag (rad)	1.475	-1.700	-1.775	-0.925

Table F-59 (F.9) at A = 0.15c and ω = 1.00 rad/s

	cd	cl	cm total	cm ac
Max	0.030	0.970	0.320	-0.0755
Mean	0.008	0.801	0.284	-0.0837
Min	-0.021	0.630	0.246	-0.0892
Crest phase lag (rad)	1.350	-1.600	-1.400	-2.300
Trough phase lag (rad)	1.300	-1.700	-1.750	-1.300

Table F-60 (F.9) at A = 0.15c and ω = 1.25 rad/s

	cd	cl	cm total	cm ac
Max	0.033	1.003	0.328	-0.0723
Mean	0.006	0.800	0.283	-0.0834
Min	-0.028	0.595	0.239	-0.0901
Crest phase lag (rad)	1.313	-1.625	-1.375	-2.313
Trough phase lag (rad)	1.313	-1.688	-1.688	-1.563

F.10 Aerodynamic data at α = 6º and h/c = 0.3

Table F-61 (F.10) at A = 0.05c and ω = 0.25 rad/s

	cd	cl	cm total	cm ac
Max	0.014	1.084	0.371	-0.0922
Mean	0.011	1.055	0.359	-0.0963
Min	0.008	1.029	0.349	-0.1011
Crest phase lag (rad)	1.475	-2.725	-2.888	0.087
Trough phase lag (rad)	1.838	-2.438	-2.738	0.000

Table F-62 (F.10) at A = 0.05c and ω = 0.50 rad/s

	cd	cl	cm total	cm ac
Max	0.017	1.090	0.370	-0.0928
Mean	0.011	1.054	0.359	-0.0962
Min	0.005	1.017	0.347	-0.1004
Crest phase lag (rad)	1.475	-2.350	-2.625	0.175
Trough phase lag (rad)	1.575	-2.075	-2.375	-0.125

Table F-63 (F.10) at A = 0.05c and ω = 1.00 rad/s

	cd	cl	cm total	cm ac
Max	0.023	1.115	0.375	-0.0937
Mean	0.011	1.053	0.358	-0.0959
Min	-0.002	0.990	0.341	-0.0979
Crest phase lag (rad)	1.400	-1.900	-1.950	0.700
Trough phase lag (rad)	1.350	-1.800	-2.000	0.550

Table F-64 (F.10) at A = 0.05c and ω = 1.25 rad/s

	cd	cl	cm total	cm ac
Max	0.025	1.129	0.379	-0.0937
Mean	0.011	1.052	0.358	-0.0958
Min	-0.005	0.975	0.337	-0.0982
Crest phase lag (rad)	1.375	-1.813	-1.813	1.063
Trough phase lag (rad)	1.375	-1.688	-1.688	1.750

F.11 Aerodynamic data at α = 6º and h/c = 0.5

Table F-65 (F.11) at A = 0.05c and ω = 0.25 rad/s

	cd	cl	cm total	cm ac
Max	0.014	1.019	0.342	-0.0857
Mean	0.011	1.004	0.337	-0.0874
Min	0.008	0.988	0.333	-0.0894
Crest phase lag (rad)	1.525	-2.200	-2.638	-0.250
Trough phase lag (rad)	1.613	-1.988	-2.388	-0.138

Table F-66 (F.11) at A = 0.05c and ω = 0.50 rad/s

	cd	cl	cm total	cm ac
Max	0.017	1.031	0.344	-0.0861
Mean	0.011	1.004	0.338	-0.0875
Min	0.005	0.976	0.330	-0.0891
Crest phase lag (rad)	1.575	-1.775	-2.050	0.050
Trough phase lag (rad)	1.475	-1.825	-1.925	-0.250

Table F-67 (F.11) at A = 0.05c and ω = 1.00 rad/s

	cd	cl	cm total	cm ac
Max	0.022	1.058	0.350	-0.0864
Mean	0.011	1.003	0.337	-0.0872
Min	-0.0004	0.947	0.323	-0.0878
Crest phase lag (rad)	1.400	-1.650	-1.550	-2.650
Trough phase lag (rad)	1.250	-1.700	-1.800	2.100

Table F-68 (F.11) at A = 0.05c and ω = 1.25 rad/s

	cd	cl	cm total	cm ac
Max	0.024	1.071	0.354	-0.0856
Mean	0.011	1.002	0.337	-0.0872
Min	-0.003	0.934	0.320	-0.0886
Crest phase lag (rad)	1.375	-1.625	-1.563	-3.000
Trough phase lag (rad)	1.250	-1.563	-1.563	2.375

Table F-69 (F.11) at A = 0.15c and ω = 0.25 rad/s

	cd	cl	cm total	cm ac
Max	0.020	1.099	0.378	-0.0861
Mean	0.011	1.033	0.351	-0.0939
Min	0.002	0.972	0.330	-0.1054
Crest phase lag (rad)	1.563	-2.688	-2.913	-0.213
Trough phase lag (rad)	1.600	-2.113	-2.488	-0.075

Table F-70 (F.11) at A = 0.15c and ω = 0.50 rad/s

	cd	cl	cm total	cm ac
Max	0.027	1.119	0.377	-0.0868
Mean	0.011	1.030	0.350	-0.0933
Min	-0.008	0.931	0.322	-0.1034
Crest phase lag (rad)	1.575	-2.325	-2.750	-0.025
Trough phase lag (rad)	1.425	-1.875	-2.075	-0.125

Table F-71 (F.11) at A = 0.15c and ω = 1.00 rad/s

	cd	cl	cm total	cm ac
Max	0.039	1.188	0.384	-0.0886
Mean	0.009	1.022	0.347	-0.0922
Min	-0.028	0.844	0.303	-0.0975
Crest phase lag (rad)	1.400	-1.700	-1.600	-2.000
Trough phase lag (rad)	1.350	-1.700	-1.850	-0.700

Table F-72 (F.11) at A = 0.15c and ω = 1.25 rad/s

	cd	cl	cm total	cm ac
Max	0.044	1.228	0.395	-0.0867
Mean	0.008	1.018	0.345	-0.0917
Min	-0.038	0.802	0.294	-0.0953
Crest phase lag (rad)	1.313	-1.563	-1.375	-3.063
Trough phase lag (rad)	1.250	-1.563	-1.313	2.563

F.12 Aerodynamic data at α = 6º and h/c = 1.0

Table F-73 (F.12) at A = 0.05c and ω = 0.25 rad/s

	cd	cl	cm total	cm ac
Max	0.015	0.995	0.330	-0.0815
Mean	0.012	0.982	0.327	-0.0823
Min	0.009	0.968	0.323	-0.0832
Crest phase lag (rad)	1.500	-1.650	-1.913	-0.400
Trough phase lag (rad)	1.525	-1.638	-1.875	-0.425

Table F-74 (F.12) at A = 0.05c and ω = 0.50 rad/s

	cd	cl	cm total	cm ac
Max	0.017	1.008	0.332	-0.0816
Mean	0.012	0.981	0.326	-0.0822
Min	0.006	0.954	0.320	-0.0830
Crest phase lag (rad)	1.425	-1.575	-1.575	-1.825
Trough phase lag (rad)	1.450	-1.625	-1.700	-0.725

Table F-75 (F.12) at A = 0.05c and ω = 1.00 rad/s

	cd	cl	cm total	cm ac
Max	0.0215024	1.03303	0.33844	-0.08058084
Mean	0.011482869	0.980766802	0.326278722	-0.082130136
Min	0.000793829	0.928514	0.314298	-0.083099237
Crest phase lag (rad)	1.350	-1.600	-1.550	-2.450
Trough phase lag (rad)	1.300	-1.650	-1.700	-3.150

Table F-76 (F.12) at A = 0.05c and ω = 1.25 rad/s

	cd	cl	cm total	cm ac
Max	0.023	1.044	0.341	-0.0800
Mean	0.011	0.981	0.326	-0.0821
Min	-0.002	0.917	0.311	-0.0837
Crest phase lag (rad)	1.313	-1.625	-1.375	-2.625
Trough phase lag (rad)	1.250	-1.625	-1.438	2.875

Table F-77 (F.12) at A = 0.15c and ω = 0.25 rad/s

	cd	cl	cm total	cm ac
Max	0.020	1.024	0.338	-0.0816
Mean	0.012	0.985	0.330	-0.0845
Min	0.003	0.943	0.320	-0.0885
Crest phase lag (rad)	1.538	-1.738	-2.450	-0.513
Trough phase lag (rad)	1.550	-1.738	-2.113	-0.438

Table F-78 (F.12) at A = 0.15c and ω = 0.50 rad/s

	cd	cl	cm total	cm ac
Max	0.027	1.060	0.344	-0.0799
Mean	0.011	0.984	0.329	-0.0841
Min	-0.006	0.902	0.311	-0.0890
Crest phase lag (rad)	1.475	-1.625	-1.550	-1.825
Trough phase lag (rad)	1.450	-1.700	-1.875	-0.900

Table F-79 (F.12) at A = 0.15c and ω = 1.00 rad/s

	cd	cl	cm total	cm ac
Max	0.038	1.134	0.361	-0.0734
Mean	0.009	0.979	0.327	-0.0832
Min	-0.024	0.824	0.294	-0.0898
Crest phase lag (rad)	1.400	-1.550	-1.300	-2.350
Trough phase lag (rad)	1.350	-1.700	-1.800	-1.200

Table F-80 (F.12) at A = 0.15c and ω = 1.25 rad/s

	cd	cl	cm total	cm ac
Max	0.042	1.165	0.368	-0.0690
Mean	0.008	0.975	0.325	-0.0823
Min	-0.033	0.787	0.286	-0.0899
Crest phase lag (rad)	1.375	-1.563	-1.313	-2.375
Trough phase lag (rad)	1.313	-1.625	-1.625	-1.313

F.13 Aerodynamic data at α = 8º and h/c = 0.3

Table F-81 (F.13) at A = 0.05c and ω = 0.25 rad/s

	cd	cl	cm total	cm ac
Max	0.018	1.228	0.409	-0.0943
Mean	0.014	1.204	0.397	-0.0990
Min	0.010	1.181	0.388	-0.1046
Crest phase lag (rad)	1.525	-2.838	-3.000	0.050
Trough phase lag (rad)	1.600	-2.513	-2.813	-0.037

Table F-82 (F.13) at A = 0.05c and ω = 0.50 rad/s

	cd	cl	cm total	cm ac
Max	0.021	1.229	0.407	-0.0949
Mean	0.014	1.203	0.397	-0.0988
Min	0.007	1.174	0.387	-0.1032
Crest phase lag (rad)	1.450	-2.375	-2.750	0.100
Trough phase lag (rad)	1.425	-2.150	-2.375	-0.025

Table F-83 (F.13) at A = 0.05c and ω = 1.00 rad/s

	cd	cl	cm total	cm ac
Max	0.027	1.255	0.412	-0.1001
Mean	0.014	1.200	0.396	-0.0983
Min	0.0003	1.147	0.381	-0.1010
Crest phase lag (rad)	1.350	-1.700	-1.700	0.900
Trough phase lag (rad)	1.300	-1.700	-1.700	1.400

Table F-84 (F.13) at A = 0.05c and ω = 1.25 rad/s

	cd	cl	cm total	cm ac
Max	0.033	1.233	0.402	-0.0880
Mean	0.018	1.157	0.379	-0.0920
Min	0.002	1.084	0.358	-0.0973
Crest phase lag (rad)	1.313	-1.750	-1.750	1.125
Trough phase lag (rad)	1.188	-1.625	-1.688	1.375

F.14 Aerodynamic data at α = 8º and h/c = 0.5

Table F-85 (F.14) at A = 0.05c and ω = 0.25 rad/s

	cd	cl	cm total	cm ac
Max	0.017	1.167	0.379	-0.0864
Mean	0.014	1.157	0.375	-0.0884
Min	0.010	1.144	0.371	-0.0907
Crest phase lag (rad)	1.488	-2.200	-2.813	-0.063
Trough phase lag (rad)	1.550	-2.075	-2.450	-0.238

Table F-86 (F.14) at A = 0.05c and ω = 0.50 rad/s

	cd	cl	cm total	cm ac
Max	0.021	1.178	0.380	-0.0871
Mean	0.014	1.156	0.375	-0.0883
Min	0.007	1.133	0.370	-0.0898
Crest phase lag (rad)	1.475	-1.500	-1.600	0.150
Trough phase lag (rad)	1.400	-1.700	-1.825	-0.725

Table F-87 (F.14) at A = 0.05c and ω = 1.00 rad/s

	cd	Cl	cm total	cm ac
Max	0.026	1.205	0.387	-0.0867
Mean	0.014	1.154	0.374	-0.0880
Min	0.0009	1.105	0.362	-0.0895
Crest phase lag (rad)	1.300	-1.500	-1.450	0.000
Trough phase lag (rad)	1.250	-1.600	-1.600	1.950

Table F-88 (F.14) at A = 0.05c and ω = 1.25 rad/s

	cd	Cl	cm total	cm ac
Max	0.029	1.220	0.391	-0.0853
Mean	0.014	1.153	0.374	-0.0878
Min	-0.002	1.0900	0.358	-0.0904
Crest phase lag (rad)	1.313	-1.500	-1.375	2.813
Trough phase lag (rad)	1.313	-1.500	-1.313	2.313

Table F-89 (F.14) at A = 0.15c and ω = 0.25 rad/s

	Cd	cl	cm total	cm ac
Max	0.025	1.223	0.409	-0.0824
Mean	0.016	1.159	0.379	-0.0919
Min	0.005	1.102	0.358	-0.1065
Crest phase lag (rad)	1.550	-2.800	-2.988	0.063
Trough phase lag (rad)	1.625	-2.100	-2.463	-0.050

Table F-90 (F.14) at A = 0.15c and ω = 0.50 rad/s

	Cd	cl	cm total	cm ac
Max	0.036	1.202	0.395	-0.0811
Mean	0.018	1.135	0.371	-0.0894
Min	-0.003	1.053	0.347	-0.1010
Crest phase lag (rad)	1.450	-2.475	-2.900	0.050
Trough phase lag (rad)	1.400	-1.925	-2.175	-0.175

Table F-91 (F.14) at A = 0.15c and ω = 1.00 rad/s

	Cd	cl	cm total	cm ac
Max	0.047	1.312	0.420	-0.0868
Mean	0.014	1.145	0.375	-0.0909
Min	-0.025	0.970	0.329	-0.0966
Crest phase lag (rad)	1.200	-1.450	-1.500	1.600
Trough phase lag (rad)	1.300	-1.550	-1.550	1.550

Table F-92 (F.14) at A = 0.15c and ω = 1.25 rad/s

	Cd	cl	cm total	cm ac
Max	0.053	1.353	0.434	-0.0834
Mean	0.013	1.139	0.373	-0.0903
Min	-0.034	0.923	0.315	-0.1001
Crest phase lag (rad)	1.313	-1.563	-1.563	2.938
Trough phase lag (rad)	1.250	-1.500	-1.500	1.500

F.15 Aerodynamic data at α = 8º and h/c = 1.0

Table F-93 (F.15) at A = 0.05c and ω = 0.25 rad/s

	cd	cl	cm total	cm ac
Max	0.017	1.152	0.367	-0.0815
Mean	0.014	1.141	0.365	-0.0822
Min	0.011	1.129	0.363	-0.0832
Crest phase lag (rad)	1.500	-1.500	-1.600	-0.500
Trough phase lag (rad)	1.488	-1.488	-1.888	-0.463

Table F-94 (F.15) at A = 0.05c and ω = 0.50 rad/s

	cd	cl	cm total	cm ac
Max	0.020	1.164	0.370	-0.0817
Mean	0.014	1.140	0.365	-0.0822
Min	0.008	1.117	0.360	-0.0827
Crest phase lag (rad)	1.450	-1.425	-1.300	-1.975
Trough phase lag (rad)	1.400	-1.525	-1.575	-0.775

Table F-95 (F.15) at A = 0.05c and ω = 1.00 rad/s

	cd	cl	cm total	cm ac
Max	0.026	1.189	0.377	-0.0804
Mean	0.014	1.139	0.365	-0.0820
Min	0.002	1.091	0.353	-0.0834
Crest phase lag (rad)	1.350	-1.450	-1.350	-2.700
Trough phase lag (rad)	1.300	-1.500	-1.500	2.800

Table F-96 (F.15) at A = 0.05c and ω = 1.25 rad/s

	cd	cl	cm total	cm ac
Max	0.029	1.200	0.380	-0.0793
Mean	0.014	1.139	0.364	-0.0819
Min	-0.002	1.078	0.349	-0.0841
Crest phase lag (rad)	1.313	-1.563	-1.375	-3.063
Trough phase lag (rad)	1.250	-1.563	-1.313	2.563

Table F-97 (F.15) at A = 0.15c and ω = 0.25 rad/s

	cd	cl	cm total	cm ac
Max	0.024	1.174	0.374	-0.0818
Mean	0.014	1.143	0.368	-0.0847
Min	0.003	1.108	0.360	-0.0893
Crest phase lag (rad)	1.50	-1.45	-2.4875	-1.60
Trough phase lag (rad)	1.4875	-1.575	-2.125	-0.5125

Table F-98 (F.15) at A = 0.15c and ω = 0.50 rad/s

	cd	cl	cm total	cm ac
Max	0.032	1.208	0.381	-0.0792
Mean	0.014	1.139	0.367	-0.0841
Min	-0.006	1.070	0.353	-0.0892
Crest phase lag (rad)	1.45	-1.4	-1.25	-2.05
Trough phase lag (rad)	1.475	-1.6	-1.925	-0.95

Table F-99 (F.15) at A = 0.15c and ω = 1.00 rad/s

	Cd	cl	cm total	cm ac
Max	0.046	1.279	0.399	-0.0695
Mean	0.014	1.106	0.354	-0.0799
Min	-0.022	0.939	0.313	-0.0868
Crest phase lag (rad)	1.15	-1.40	-1.25	-2.60
Trough phase lag (rad)	1.40	-1.45	-1.45	2.55

Table F-100 (F.15) at A = 0.15c and ω = 1.25 rad/s

	cd	cl	cm total	cm ac
Max	0.051	1.310	0.408	-0.0654
Mean	0.013	1.103	0.353	-0.0794
Min	-0.031	0.905	0.304	-0.0888
Crest phase lag (rad)	1.1875	-1.375	-1.3125	-2.875
Trough phase lag (rad)	1.375	-1.3125	-1.25	2.5

Appendix G **Aerodynamic data of the Ekranoplan ‘Orlyonok’ A-90**

G.1 Freestream condition

Table G-1 Aerodynamic data at freestream condition

h/c	α	CD	CL	Cmac
0.1	0.00	0.0202	0.3486	0.0930
	2.00	0.0200	0.5228	0.0705
	3.43	0.0224	0.6472	0.0544
	4.00	0.0236	0.6971	0.0478
	6.00	0.0286	0.8714	0.0254
	8.00	0.0363	1.0457	0.0029
0.2	0.00	0.0196	0.3213	0.0930
	2.00	0.0216	0.4820	0.0725
	4.00	0.0260	0.6426	0.0520
	4.06	0.0260	0.6472	0.0515
	6.00	0.0321	0.8033	0.0316
	8.00	0.0405	0.9639	0.0111
0.3	0.00	0.0200	0.3102	0.0930
	2.00	0.0229	0.4653	0.0734
	4.00	0.0281	0.6204	0.0537
	4.34	0.0292	0.6472	0.0503
	6.00	0.0354	0.7755	0.0341
	8.00	0.0449	0.9306	0.0144
0.4	0.00	0.0205	0.3048	0.0930
	2.00	0.0241	0.4572	0.0738
	4.00	0.0302	0.6096	0.0545
	4.49	0.0320	0.6472	0.0498
	6.00	0.0385	0.7620	0.0353
	8.00	0.0493	0.9144	0.0160
0.5	0.00	0.0210	0.3018	0.0930
	2.00	0.0253	0.4527	0.0740
	4.00	0.0321	0.6036	0.0550
	4.58	0.0346	0.6472	0.0495
	6.00	0.0416	0.7545	0.0360
	8.00	0.0536	0.9053	0.0169
….				

....				
0.75	0.00	0.0222	0.3000	0.0930
	2.00	0.0282	0.4500	0.0741
	4.00	0.0371	0.6000	0.0552
	4.63	0.0405	0.6472	0.0493
	6.00	0.0492	0.7500	0.0364
	8.00	0.0645	0.9000	0.0175
1.0	0.00	0.0234	0.3001	0.0930
	2.00	0.0309	0.4502	0.0741
	4.00	0.0418	0.6003	0.0552
	4.62	0.0460	0.6472	0.0493
	6.00	0.0565	0.7504	0.0363
	8.00	0.0750	0.9004	0.0174

G.2 Oscillating condition

Table G-2 Aerodynamic data at A = 0.05c and ω = 0.25 rad/s

λ	h/c	0.3			0.5			1.0		
	α	C_D	C_L	C_mac	C_D	C_L	C_mac	C_D	C_L	C_mac
0	0.00	0.0203	0.3215	0.0930	0.0210	0.3048	0.0930	0.0233	0.2998	0.0930
	2.00	0.0232	0.4822	0.0725	0.0253	0.4572	0.0738	0.0307	0.4497	0.0741
	4.00	0.0289	0.6430	0.0520	0.0323	0.6096	0.0545	0.0416	0.5995	0.0553
	6.00	0.0367	0.8037	0.0315	0.0419	0.7621	0.0353	0.0562	0.7494	0.0364
	8.00	0.0471	0.9645	0.0110	0.0542	0.9145	0.0160	0.0746	0.8993	0.0175
25%	0.00	0.0213	0.3172	0.0930	0.0222	0.3050	0.0930	0.0247	0.3010	0.0930
	2.00	0.0250	0.4758	0.0728	0.0272	0.4575	0.0738	0.0326	0.4516	0.0740
	4.00	0.0311	0.6345	0.0527	0.0348	0.6099	0.0545	0.0442	0.6021	0.0551
	6.00	0.0393	0.7931	0.0325	0.0449	0.7624	0.0352	0.0595	0.7526	0.0361
	8.00	0.0497	0.9517	0.0123	0.0577	0.9149	0.0160	0.0785	0.9031	0.0172
50%	0.00	0.0201	0.3106	0.0930	0.0211	0.3024	0.0930	0.0235	0.3004	0.0930
	2.00	0.0231	0.4659	0.0733	0.0255	0.4537	0.0739	0.0310	0.4506	0.0741
	4.00	0.0284	0.6212	0.0536	0.0324	0.6049	0.0549	0.0420	0.6008	0.0552
	6.00	0.0358	0.7765	0.0340	0.0419	0.7561	0.0358	0.0568	0.7510	0.0363
	8.00	0.0455	0.9318	0.0143	0.0541	0.9073	0.0167	0.0754	0.9012	0.0174
75%	0.00	0.0187	0.3130	0.0930	0.0196	0.3016	0.0930	0.0221	0.2990	0.0930
	2.00	0.0209	0.4695	0.0731	0.0233	0.4523	0.0740	0.0288	0.4485	0.0742
	4.00	0.0256	0.6260	0.0533	0.0296	0.6031	0.0550	0.0393	0.5980	0.0554
	6.00	0.0324	0.7825	0.0334	0.0384	0.7539	0.0360	0.0533	0.7475	0.0366
	8.00	0.0415	0.9390	0.0136	0.0499	0.9047	0.0170	0.0713	0.8971	0.0178
100%	0.00	0.0203	0.3215	0.0930	0.0210	0.3048	0.0930	0.0234	0.2998	0.0930
	2.00	0.0232	0.4822	0.0725	0.0253	0.4572	0.0738	0.0307	0.4497	0.0741
	4.00	0.0289	0.6430	0.0520	0.0323	0.6096	0.0545	0.0416	0.5996	0.0553
	6.00	0.0367	0.8037	0.0315	0.0419	0.7621	0.0353	0.0562	0.7495	0.0364
	8.00	0.0471	0.9644	0.0110	0.0542	0.9145	0.0160	0.0746	0.8994	0.0175

Table G-3 Aerodynamic data at A = 0.05c and ω = 0.50 rad/s

λ	h/c	0.3			0.5			1.0		
	α	C_D	C_L	C_mac	C_D	C_L	C_mac	C_D	C_L	C_mac
0	0.00	0.0201	0.3203	0.0930	0.0208	0.3039	0.0930	0.0231	0.2991	0.0930
	2.00	0.0229	0.4805	0.0726	0.0250	0.4558	0.0738	0.0303	0.4486	0.0742
	4.00	0.0285	0.6407	0.0522	0.0319	0.6078	0.0547	0.0410	0.5982	0.0554
	6.00	0.0361	0.8008	0.0318	0.0413	0.7597	0.0355	0.0555	0.7477	0.0366
	8.00	0.0462	0.9610	0.0114	0.0534	0.9116	0.0163	0.0737	0.8972	0.0178
25%	0.00	0.0224	0.3192	0.0930	0.0233	0.3062	0.0930	0.0257	0.3017	0.0930
	2.00	0.0269	0.4805	0.0727	0.0289	0.4593	0.0737	0.0343	0.4526	0.0740
	4.00	0.0337	0.6407	0.0524	0.0371	0.6125	0.0543	0.0463	0.6035	0.0550
	6.00	0.0425	0.8008	0.0320	0.0479	0.7656	0.0350	0.0622	0.7543	0.0360
	8.00	0.0535	0.9610	0.0117	0.0611	0.9187	0.0156	0.0817	0.9052	0.0170
50%	0.00	0.0203	0.3114	0.0930	0.0213	0.3032	0.0930	0.0238	0.3009	0.0930
	2.00	0.0234	0.4671	0.0733	0.0258	0.4547	0.0739	0.0314	0.4514	0.0741
	4.00	0.0289	0.6228	0.0535	0.0329	0.6063	0.0548	0.0426	0.6018	0.0551
	6.00	0.0364	0.7784	0.0338	0.0425	0.7579	0.0356	0.0575	0.7523	0.0362
	8.00	0.0462	0.9341	0.0141	0.0549	0.9095	0.0165	0.0762	0.9027	0.0172
75%	0.00	0.0172	0.3104	0.0930	0.0181	0.3004	0.0930	0.0207	0.2983	0.0930
	2.00	0.0186	0.4656	0.0733	0.0212	0.4506	0.0741	0.0269	0.4474	0.0743
	4.00	0.0226	0.6208	0.0537	0.0269	0.6008	0.0552	0.0368	0.5966	0.0555
	6.00	0.0286	0.7760	0.0340	0.0350	0.7510	0.0363	0.0503	0.7457	0.0367
	8.00	0.0375	0.9311	0.0144	0.0464	0.9012	0.0174	0.0678	0.8948	0.0180
100%	0.00	0.0201	0.3203	0.0930	0.0208	0.3038	0.0930	0.0231	0.2991	0.0930
	2.00	0.0229	0.4804	0.0726	0.0250	0.4558	0.0738	0.0303	0.4486	0.0742
	4.00	0.0284	0.6405	0.0522	0.0318	0.6077	0.0547	0.0410	0.5981	0.0554
	6.00	0.0360	0.8006	0.0318	0.0412	0.7596	0.0355	0.0554	0.7477	0.0366
	8.00	0.0461	0.9608	0.0114	0.0533	0.9115	0.0163	0.0736	0.8972	0.0178

Table G-4 Aerodynamic data at A = 0.05c and ω = 1.00 rad/s

λ	h/c	0.3			0.5			1.0		
	α	C_D	C_L	C_mac	C_D	C_L	C_mac	C_D	C_L	C_mac
0	0.00	0.0195	0.3167	0.0930	0.0202	0.3016	0.0930	0.0225	0.2976	0.0930
	2.00	0.0217	0.4750	0.0729	0.0239	0.4523	0.0740	0.0293	0.4465	0.0743
	4.00	0.0270	0.6334	0.0527	0.0304	0.6031	0.0550	0.0395	0.5953	0.0556
	6.00	0.0339	0.7917	0.0326	0.0392	0.7539	0.0360	0.0534	0.7441	0.0369
	8.00	0.0436	0.9500	0.0125	0.0506	0.9047	0.0170	0.0711	0.8929	0.0182
25%	0.00	0.0239	0.3213	0.0930	0.0250	0.3073	0.0930	0.0273	0.3022	0.0930
	2.00	0.0298	0.4819	0.0725	0.0317	0.4610	0.0736	0.0369	0.4533	0.0740
	4.00	0.0378	0.6425	0.0521	0.0410	0.6146	0.0541	0.0497	0.6044	0.0549
	6.00	0.0477	0.8032	0.0316	0.0528	0.7683	0.0347	0.0667	0.7555	0.0359
	8.00	0.0595	0.9638	0.0111	0.0668	0.9219	0.0153	0.0869	0.9066	0.0168
50%	0.00	0.0209	0.3132	0.0930	0.0219	0.3046	0.0930	0.0152	0.2990	0.0930
	2.00	0.0244	0.4698	0.0731	0.0268	0.4568	0.0738	0.0173	0.4485	0.0742
	4.00	0.0302	0.6264	0.0533	0.0342	0.6091	0.0546	0.0222	0.5979	0.0554
	6.00	0.0380	0.7830	0.0334	0.0443	0.7614	0.0353	0.0295	0.7474	0.0366
	8.00	0.0482	0.9396	0.0135	0.0571	0.9137	0.0161	0.0403	0.8969	0.0178
75%	0.00	0.0141	0.3080	0.0930	0.0244	0.3019	0.0930	0.0183	0.2977	0.0930
	2.00	0.0143	0.4619	0.0735	0.0324	0.4528	0.0740	0.0235	0.4466	0.0743
	4.00	0.0171	0.6159	0.0540	0.0440	0.6037	0.0550	0.0326	0.5954	0.0556
	6.00	0.0224	0.7699	0.0346	0.0594	0.7546	0.0359	0.0452	0.7443	0.0369
	8.00	0.0313	0.9239	0.0151	0.0784	0.9056	0.0169	0.0621	0.8932	0.0182
100%	0.00	0.0193	0.3164	0.0930	0.0200	0.3014	0.0930	0.0223	0.2976	0.0930
	2.00	0.0215	0.4745	0.0729	0.0237	0.4521	0.0740	0.0290	0.4463	0.0743
	4.00	0.0266	0.6327	0.0528	0.0301	0.6028	0.0550	0.0392	0.5951	0.0556
	6.00	0.0335	0.7909	0.0327	0.0388	0.7535	0.0360	0.0530	0.7439	0.0369
	8.00	0.0431	0.9491	0.0126	0.0502	0.9042	0.0171	0.0706	0.8927	0.0182

Table G-5 Aerodynamic data at A = 0.05c and ω = 1.25 rad/s

λ	h/c	0.3			0.5			1.0		
	α	C_D	C_L	$C_m$ac	C_D	C_L	$C_m$ac	C_D	C_L	$C_m$ac
0	0.00	0.0192	0.3110	0.0930	0.0200	0.3006	0.0930	0.0223	0.2970	0.0930
	2.00	0.0213	0.4666	0.0733	0.0236	0.4509	0.0741	0.0289	0.4456	0.0743
	4.00	0.0260	0.6221	0.0536	0.0298	0.6012	0.0552	0.0389	0.5941	0.0557
	6.00	0.0326	0.7776	0.0339	0.0382	0.7514	0.0362	0.0526	0.7426	0.0370
	8.00	0.0446	0.9331	0.0142	0.0496	0.9017	0.0173	0.0707	0.8911	0.0184
25%	0.00	0.0243	0.3160	0.0930	0.0256	0.3075	0.0930	0.0279	0.3020	0.0930
	2.00	0.0308	0.4740	0.0729	0.0328	0.4612	0.0736	0.0379	0.4530	0.0740
	4.00	0.0391	0.6320	0.0528	0.0426	0.6150	0.0541	0.0510	0.6040	0.0549
	6.00	0.0493	0.7900	0.0328	0.0548	0.7687	0.0347	0.0684	0.7550	0.0359
	8.00	0.0645	0.9480	0.0127	0.0692	0.9224	0.0152	0.0895	0.9060	0.0169
50%	0.00	0.0211	0.3074	0.0930	0.0222	0.3051	0.0930	0.0247	0.3021	0.0930
	2.00	0.0246	0.4611	0.0736	0.0273	0.4576	0.0737	0.0329	0.4531	0.0740
	4.00	0.0304	0.6148	0.0541	0.0350	0.6102	0.0545	0.0446	0.6042	0.0549
	6.00	0.0383	0.7685	0.0347	0.0454	0.7627	0.0352	0.0603	0.7552	0.0359
	8.00	0.0525	0.9223	0.0153	0.0583	0.9153	0.0160	0.0798	0.9063	0.0168
75%	0.00	0.0126	0.3015	0.0930	0.0140	0.2986	0.0930	0.0171	0.2976	0.0930
	2.00	0.0121	0.4523	0.0740	0.0156	0.4479	0.0742	0.0220	0.4464	0.0743
	4.00	0.0142	0.6030	0.0550	0.0200	0.5972	0.0555	0.0307	0.5952	0.0556
	6.00	0.0189	0.7538	0.0360	0.0270	0.7465	0.0367	0.0429	0.7440	0.0369
	8.00	0.0324	0.9045	0.0170	0.0375	0.8958	0.0179	0.0598	0.8928	0.0182
100%	0.00	0.0190	0.3108	0.0930	0.0198	0.3004	0.0930	0.0221	0.2970	0.0930
	2.00	0.0209	0.4662	0.0733	0.0233	0.4506	0.0741	0.0286	0.4455	0.0743
	4.00	0.0256	0.6216	0.0536	0.0294	0.6009	0.0552	0.0386	0.5940	0.0557
	6.00	0.0320	0.7770	0.0339	0.0377	0.7511	0.0363	0.0521	0.7425	0.0370
	8.00	0.0441	0.9324	0.0142	0.0491	0.9013	0.0173	0.0698	0.8910	0.0184

Table G-6 Aerodynamic data at A = 0.15c and ω = 0.25 rad/s

λ	h/c	0.3			0.5			1.0		
	α	C_D	C_L	C_mac	C_D	C_L	C_mac	C_D	C_L	C_mac
0	0.00	NaN	NaN	NaN	0.0216	0.3199	0.0930	0.0232	0.3009	0.0930
	2.00	NaN	NaN	NaN	0.0260	0.4799	0.0726	0.0307	0.4513	0.0741
	4.00	NaN	NaN	NaN	0.0339	0.6399	0.0523	0.0416	0.6018	0.0551
	6.00	NaN	NaN	NaN	0.0445	0.7998	0.0319	0.0564	0.7522	0.0362
	8.00	NaN	NaN	NaN	0.0597	0.9598	0.0115	0.0750	0.9027	0.0172
25%	0.00	NaN	NaN	NaN	0.0244	0.3090	0.0930	0.0268	0.3036	0.0930
	2.00	NaN	NaN	NaN	0.0308	0.4635	0.0735	0.0360	0.4554	0.0739
	4.00	NaN	NaN	NaN	0.0397	0.6180	0.0539	0.0488	0.6073	0.0547
	6.00	NaN	NaN	NaN	0.0512	0.7725	0.0343	0.0654	0.7591	0.0355
	8.00	NaN	NaN	NaN	0.0665	0.9270	0.0148	0.0857	0.9109	0.0164
50%	0.00	NaN	NaN	NaN	0.0211	0.2988	0.0930	0.0237	0.3009	0.0930
	2.00	NaN	NaN	NaN	0.0254	0.4482	0.0742	0.0313	0.4514	0.0741
	4.00	NaN	NaN	NaN	0.0323	0.5977	0.0554	0.0424	0.6019	0.0551
	6.00	NaN	NaN	NaN	0.0416	0.7471	0.0366	0.0574	0.7523	0.0362
	8.00	NaN	NaN	NaN	0.0553	0.8965	0.0178	0.0760	0.9028	0.0172
75%	0.00	NaN	NaN	NaN	0.0167	0.2979	0.0930	0.0192	0.2961	0.0930
	2.00	NaN	NaN	NaN	0.0189	0.4469	0.0743	0.0248	0.4442	0.0744
	4.00	NaN	NaN	NaN	0.0241	0.5958	0.0556	0.0339	0.5922	0.0558
	6.00	NaN	NaN	NaN	0.0318	0.7448	0.0368	0.0467	0.7403	0.0372
	8.00	NaN	NaN	NaN	0.0437	0.8937	0.0181	0.0645	0.8883	0.0186
100%	0.00	NaN	NaN	NaN	0.0216	0.3200	0.0930	0.0232	0.3009	0.0930
	2.00	NaN	NaN	NaN	0.0260	0.4799	0.0726	0.0307	0.4513	0.0741
	4.00	NaN	NaN	NaN	0.0339	0.6399	0.0522	0.0417	0.6017	0.0551
	6.00	NaN	NaN	NaN	0.0446	0.7999	0.0319	0.0564	0.7522	0.0362
	8.00	NaN	NaN	NaN	0.0597	0.9599	0.0115	0.0750	0.9026	0.0172

Table G-7 Aerodynamic data at A = 0.15c and ω = 0.50 rad/s

λ	h/c	0.3			0.5			1.0		
	α	C_D	C_L	C_mac	C_D	C_L	C_mac	C_D	C_L	C_mac
0	0.00	NaN	NaN	NaN	0.0209	0.3138	0.0930	0.0225	0.2981	0.0930
	2.00	NaN	NaN	NaN	0.0248	0.4708	0.0731	0.0296	0.4471	0.0743
	4.00	NaN	NaN	NaN	0.0323	0.6277	0.0532	0.0400	0.5962	0.0555
	6.00	NaN	NaN	NaN	0.0423	0.7846	0.0332	0.0543	0.7452	0.0368
	8.00	NaN	NaN	NaN	0.0594	0.9415	0.0133	0.0723	0.8943	0.0181
25%	0.00	NaN	NaN	NaN	0.0266	0.3111	0.0930	0.0292	0.3058	0.0930
	2.00	NaN	NaN	NaN	0.0349	0.4667	0.0733	0.0401	0.4588	0.0737
	4.00	NaN	NaN	NaN	0.0457	0.6223	0.0536	0.0546	0.6117	0.0544
	6.00	NaN	NaN	NaN	0.0589	0.7779	0.0339	0.0730	0.7646	0.0350
	8.00	NaN	NaN	NaN	0.0779	0.9334	0.0141	0.0949	0.9175	0.0157
50%	0.00	NaN	NaN	NaN	0.0216	0.2970	0.0930	0.0244	0.3023	0.0930
	2.00	NaN	NaN	NaN	0.0261	0.4455	0.0744	0.0323	0.4534	0.0740
	4.00	NaN	NaN	NaN	0.0332	0.5939	0.0557	0.0439	0.6045	0.0549
	6.00	NaN	NaN	NaN	0.0427	0.7424	0.0370	0.0593	0.7557	0.0358
	8.00	NaN	NaN	NaN	0.0589	0.8909	0.0184	0.0783	0.9068	0.0168
75%	0.00	NaN	NaN	NaN	0.0113	0.2902	0.0930	0.0144	0.2933	0.0930
	2.00	NaN	NaN	NaN	0.0117	0.4354	0.0749	0.0183	0.4400	0.0746
	4.00	NaN	NaN	NaN	0.0146	0.5805	0.0567	0.0257	0.5866	0.0562
	6.00	NaN	NaN	NaN	0.0204	0.7256	0.0386	0.0368	0.7333	0.0379
	8.00	NaN	NaN	NaN	0.0337	0.8707	0.0204	0.0525	0.8799	0.0195
100%	0.00	NaN	NaN	NaN	0.0209	0.3136	0.0930	0.0224	0.2980	0.0930
	2.00	NaN	NaN	NaN	0.0247	0.4703	0.0731	0.0295	0.4470	0.0743
	4.00	NaN	NaN	NaN	0.0322	0.6271	0.0532	0.0399	0.5960	0.0555
	6.00	NaN	NaN	NaN	0.0421	0.7839	0.0333	0.0541	0.7450	0.0368
	8.00	NaN	NaN	NaN	0.0591	0.9407	0.0134	0.0721	0.8940	0.0181

Table G-8 Aerodynamic data at A = 0.15c and ω = 1.00 rad/s

λ	h/c	0.3			0.5			1.0		
	α	C_D	C_L	C_mac	C_D	C_L	C_mac	C_D	C_L	C_mac
0	0.00	NaN	NaN	NaN	0.0192	0.3041	0.0930	0.0201	0.2836	0.0930
	2.00	NaN	NaN	NaN	0.0219	0.4562	0.0738	0.0255	0.4254	0.0754
	4.00	NaN	NaN	NaN	0.0279	0.6082	0.0546	0.0339	0.5672	0.0577
	6.00	NaN	NaN	NaN	0.0365	0.7603	0.0354	0.0459	0.7090	0.0400
	8.00	NaN	NaN	NaN	0.0511	0.9124	0.0162	0.0646	0.8508	0.0224
25%	0.00	NaN	NaN	NaN	0.0279	0.3166	0.0930	0.0312	0.3005	0.0930
	2.00	NaN	NaN	NaN	0.0401	0.4748	0.0729	0.0444	0.4507	0.0741
	4.00	NaN	NaN	NaN	0.0547	0.6331	0.0528	0.0615	0.6010	0.0552
	6.00	NaN	NaN	NaN	0.0716	0.7914	0.0326	0.0823	0.7512	0.0363
	8.00	NaN	NaN	NaN	0.0901	0.9497	0.0125	0.1055	0.9014	0.0173
50%	0.00	NaN	NaN	NaN	0.0233	0.3076	0.0930	0.0259	0.3038	0.0930
	2.00	NaN	NaN	NaN	0.0291	0.4614	0.0736	0.0350	0.4557	0.0738
	4.00	NaN	NaN	NaN	0.0374	0.6152	0.0541	0.0476	0.6076	0.0547
	6.00	NaN	NaN	NaN	0.0487	0.7690	0.0347	0.0641	0.7595	0.0355
	8.00	NaN	NaN	NaN	0.0624	0.9228	0.0152	0.0849	0.9114	0.0163
75%	0.00	NaN	NaN	NaN	-.0006	0.2895	0.0930	0.0046	0.2908	0.0930
	2.00	NaN	NaN	NaN	-.0032	0.4343	0.0749	0.0053	0.4361	0.0748
	4.00	NaN	NaN	NaN	-.0028	0.5791	0.0568	0.0102	0.5815	0.0566
	6.00	NaN	NaN	NaN	0.0009	0.7239	0.0387	0.0189	0.7269	0.0384
	8.00	NaN	NaN	NaN	0.0135	0.8686	0.0206	0.0358	0.8723	0.0203
100%	0.00	NaN	NaN	NaN	0.0187	0.3033	0.0930	0.0195	0.2831	0.0930
	2.00	NaN	NaN	NaN	0.0211	0.4549	0.0739	0.0247	0.4247	0.0754
	4.00	NaN	NaN	NaN	0.0268	0.6066	0.0547	0.0329	0.5663	0.0578
	6.00	NaN	NaN	NaN	0.0351	0.7582	0.0356	0.0445	0.7079	0.0402
	8.00	NaN	NaN	NaN	0.0496	0.9099	0.0165	0.0632	0.8494	0.0225

Table G-9 Aerodynamic data at A = 0.15c and ω = 1.25 rad/s

λ	h/c	0.3			0.5			1.0		
	α	C_D	C_L	C_mac	C_D	C_L	C_mac	C_D	C_L	C_mac
0	0.00	NaN	NaN	NaN	0.0186	0.3003	0.0930	0.0194	0.2801	0.0930
	2.00	NaN	NaN	NaN	0.0211	0.4505	0.0741	0.0242	0.4201	0.0756
	4.00	NaN	NaN	NaN	0.0263	0.6007	0.0552	0.0319	0.5602	0.0582
	6.00	NaN	NaN	NaN	0.0340	0.7509	0.0363	0.0427	0.7002	0.0408
	8.00	NaN	NaN	NaN	0.0478	0.9010	0.0174	0.0600	0.8403	0.0234
25%	0.00	NaN	NaN	NaN	0.0273	0.3174	0.0930	0.0315	0.3012	0.0930
	2.00	NaN	NaN	NaN	0.0412	0.4761	0.0728	0.0459	0.4518	0.0740
	4.00	NaN	NaN	NaN	0.0575	0.6348	0.0526	0.0643	0.6023	0.0551
	6.00	NaN	NaN	NaN	0.0762	0.7935	0.0324	0.0865	0.7529	0.0361
	8.00	NaN	NaN	NaN	0.0957	0.9522	0.0123	0.1103	0.9035	0.0171
50%	0.00	NaN	NaN	NaN	0.0242	0.3086	0.0930	0.0269	0.3042	0.0930
	2.00	NaN	NaN	NaN	0.0306	0.4628	0.0735	0.0363	0.4563	0.0738
	4.00	NaN	NaN	NaN	0.0396	0.6171	0.0540	0.0495	0.6084	0.0546
	6.00	NaN	NaN	NaN	0.0513	0.7714	0.0344	0.0667	0.7605	0.0354
	8.00	NaN	NaN	NaN	0.0656	0.9257	0.0149	0.0884	0.9127	0.0162
75%	0.00	NaN	NaN	NaN	-.0066	0.2881	0.0930	-.0004	0.2900	0.0930
	2.00	NaN	NaN	NaN	-.0108	0.4321	0.0750	-.0011	0.4350	0.0749
	4.00	NaN	NaN	NaN	-.0116	0.5762	0.0570	0.0029	0.5800	0.0567
	6.00	NaN	NaN	NaN	-.0085	0.7202	0.0390	0.0104	0.7250	0.0386
	8.00	NaN	NaN	NaN	0.0044	0.8643	0.0210	0.0271	0.8700	0.0205
100%	0.00	NaN	NaN	NaN	0.0179	0.3000	0.0930	0.0187	0.2799	0.0930
	2.00	NaN	NaN	NaN	0.0200	0.4500	0.0741	0.0233	0.4199	0.0756
	4.00	NaN	NaN	NaN	0.0250	0.6000	0.0552	0.0307	0.5598	0.0583
	6.00	NaN	NaN	NaN	0.0323	0.7500	0.0364	0.0413	0.6998	0.0409
	8.00	NaN	NaN	NaN	0.0464	0.9000	0.0175	0.0579	0.8397	0.0235

Appendix H **Code example for dynamic analysis**

Here is an example of a code developed in MATLAB™ platform to do dynamic analysis of a WIGE craft configuration. The solution, as explained in the body of this thesis, is based on the system of equations of motion with no forced treatment involved. This is only applicable due to the quasi-static approach adopted by this thesis.

```
%%%%%%%%%%%%%%%%%%%%%%%%%%%%%%%%%%%%%%%%%%%%%%%%%%%%%%%%%%%%%%%%%%%%%%%%%%%%%%%%
%% This is an example code that can be used to run simple dynamic analysis %%
%%%%%%%%%%%%%%%%%%%%%%%%%%%%%%%%%%%%%%%%%%%%%%%%%%%%%%%%%%%%%%%%%%%%%%%%%%%%%%%%
%%%%%%%%%%%%%%%%%%%%%%%%%%%%%%%%%%%%%%%%%%%%%%%%%%%%%%%%%%%%%%%%%%%%%%%%%%%%%%%%

%% Call data file
filename = 'Filename1.xlsx';        % This is the file name in xlxs
gen = xlsread(filename,1,'B:B');    % This is general configuration data
der = xlsread(filename,2,'B:B');    % This is the data of the derivatives

%% Explain the general configuration data
mass = gen(1,1);
chord = gen(2,1);
area_w = gen(3,1);
rho = gen(4,1);
gravity = gen(5,1);
Ue = gen(6,1);
Iy = gen(7,1);

%% Dimensionalise the data of the vehicle's derivatives
Xu_ = der(1,1)*(0.5*rho*area_w*Ue);
Xw_ = der(2,1)*(0.5*rho*area_w*Ue);
Xq_ = der(3,1);
Xwd_ = der(4,1);
Xh_ = der(5,1)*(0.5*rho*area_w*(Ue^2)/chord);
%
Zu_ = der(6,1)*(0.5*rho*area_w*Ue);
Zw_ = der(7,1)*(0.5*rho*area_w*Ue);
Zq_ = der(8,1)*(0.5*rho*area_w*Ue*chord);
Zwd_ = der(9,1)*(0.5*rho*area_w*chord);
Zh_ = der(10,1)*(0.5*rho*area_w*(Ue^2)/chord);
%
Mu_ = der(11,1);
Mw_ = der(12,1)*(0.5*rho*area_w*Ue*chord);
Mq_ = der(13,1)*(0.5*rho*area_w*Ue*(chord^2));
Mwd_ = der(14,1)*(0.5*rho*area_w*(chord^2));
Mh_ = der(15,1)*(0.5*rho*area_w*(Ue^2));


%% Determine the matrix components
A11 = mass;
A12 = -Xwd_;
A13 = 0;
A21 = 0;
A22 = mass-Zwd_;
A23 = 0;
A31 = 0;
A32 = -Mwd_;
```

```
A33 = Iy;
%
B11 = -Xu_;
B12 = -Xw_;
B13 = -Xq_;
B21 = -Zu_;
B22 = -Zw_;
B23 = -Zq_-(mass*Ue);
B31 = -Mu_;
B32 = -Mw_;
B33 = -Mq_;
%
C11 = 0;
C12 = 0;
C13 = mass*gravity;
C21 = 0;
C22 = 0;
C23 = 0;
C31 = 0;
C32 = 0;
C33 = 0;
%
D11 = -Xh_;
D21 = -Zh_;
D31 = -Mh_;

%% Set the matrices of EOM
A = [A11 A12 A13; A21 A22 A23; A31 A32 A33];
B = [B11 B12 B13; B21 B22 B23; B31 B32 B33];
C = [C11 C12 C13; C21 C22 C23; C31 C32 C33];
D = [D11; D21; D31];

%% Determine the matrices and Laplace variables for state space
Ass = [A zeros(3,2); zeros(2,3) eye(2)];
Bss = [-B -C(:,3) -D; 0 0 1 0 0; 0 -1 0 Ue 0];
%
H = Ass\Bss;
%
s = eig(H);

%% Determine the frequency natural and damping ratio
for k = 1:length(s)
    M_s(k) = s(k);
    omega(k) = ((real(s(k)))^2 + (imag(s(k)))^2)^(0.5);
    zeta(k)  = -real(s(k))/omega(k);
end
```

Appendix I **Stability derivatives of the Ekranoplan 'Orlyonok' A90 (at constant C_L)**

I.1 Freestream condition

Table I-1 Stability derivatives for freestream condition

Derivatives	h/c						
	0.1	0.2	0.3	0.4	0.5	0.75	1.0
Xu	-0.0447	-0.0521	-0.0584	-0.0640	-0.0692	-0.0811	-0.0920
Xw	0.5507	0.4953	0.4579	0.4241	0.3924	0.2693	0.2449
Xq	0.0000	0.0000	0.0000	0.0000	0.0000	0.0000	0.0000
$X\dot{w}$	0.0000	0.0000	0.0000	0.0000	0.0000	0.0000	0.0000
Xh	-0.0021	-0.0022	-0.0022	-0.0022	-0.0023	-0.0023	-0.0023
Zu	-1.2943	-1.2943	-1.2943	-1.2943	-1.2943	-1.2943	-1.2943
Zw	-5.0150	-4.6285	-4.4726	-4.3978	-4.3573	-4.9443	-4.3452
Zq	-2.8580	-2.8580	-2.8580	-2.8580	-2.8580	-2.8580	-2.8580
$Z\dot{w}$	-0.1469	-0.2876	-0.4162	-0.5342	-0.6443	-0.8881	-1.1068
Zh	0.5057	0.2237	0.1130	0.0638	0.0153	0.0154	0.0154
Mu	0.0000	0.0000	0.0000	0.0000	0.0000	0.0000	0.0000
Mw	-0.6453	-0.5867	-0.5629	-0.5512	-0.5448	-0.5409	-0.5413
Mq	-6.1400	-6.1400	-6.1400	-6.1400	-6.1400	-6.1400	-6.1400
$M\dot{w}$	-0.3155	-0.6180	-0.8942	-1.1477	-1.3842	-1.9080	-2.3779
Mh	0.0350	0.0169	0.0088	0.0051	0.0012	0.0012	0.0012

I.2 Oscillating condition

Table I-2 Stability derivatives at A = 0.05c and ω = 0.25 rad/s

Derivatives	λi = 0			λi = 25%			λi = 50%		
	h/c = 0.3	h/c = 0.5	h/c = 1.0	h/c = 0.3	h/c = 0.5	h/c = 1.0	h/c = 0.3	h/c = 0.5	h/c = 1.0
Xu	-0.0580	-0.0689	-0.0916	-0.0633	-0.0741	-0.0968	-0.0589	-0.0696	-0.0923
Xw	0.4534	0.3906	0.2465	0.4385	0.3750	0.2297	0.4548	0.3900	0.2436
Xq	0.0000	0.0000	0.0000	0.0000	0.0000	0.0000	0.0000	0.0000	0.0000
$X\dot{w}$	0.0000	0.0000	0.0000	0.0000	0.0000	0.0000	0.0000	0.0000	0.0000
Xh	-0.0018	-0.0021	-0.0021	-0.0019	-0.0021	-0.0022	-0.0022	-0.0022	-0.0022
Zu	-1.2943	-1.2943	-1.2943	-1.2943	-1.2943	-1.2943	-1.2943	-1.2943	-1.2943
Zw	-4.6341	-4.4007	-4.3398	-4.5757	-4.4054	-4.3604	-4.4787	-4.3669	-4.3493
Zq	-2.8580	-2.8580	-2.8580	-2.8580	-2.8580	-2.8580	-2.8580	-2.8580	-2.8580
$Z\dot{w}$	-0.3924	-0.6340	-1.1090	-0.4012	-0.6335	-1.1016	-0.4153	-0.6421	-1.1052
Zh	0.1678	0.0214	0.0218	0.1251	0.0167	0.0169	0.0852	0.0087	0.0087
Mu	0.0000	0.0000	0.0000	0.0000	0.0000	0.0000	0.0000	0.0000	0.0000
Mw	-0.5871	-0.5513	-0.5405	-0.5780	-0.5516	-0.5432	-0.5638	-0.5462	-0.5418
Mq	-6.1400	-6.1400	-6.1400	-6.1400	-6.1400	-6.1400	-6.1400	-6.1400	-6.1400
$M\dot{w}$	-0.8430	-1.3620	-2.3826	-0.8619	-1.3610	-2.3666	-0.8923	-1.3794	-2.3744
Mh	0.0127	0.0017	0.0018	0.0096	0.0013	0.0014	0.0066	0.0007	0.0007

Derivatives	λi = 75%			λi = 100%		
	h/c = 0.3	h/c = 0.5	h/c = 1.0	h/c = 0.3	h/c = 0.5	h/c = 1.0
Xu	-0.0528	-0.0638	-0.0869	-0.0580	-0.0689	-0.0917
Xw	0.4747	0.4082	0.2604	0.4533	0.3906	0.2466
Xq	0.0000	0.0000	0.0000	0.0000	0.0000	0.0000
$X\dot{w}$	0.0000	0.0000	0.0000	0.0000	0.0000	0.0000
Xh	-0.0021	-0.0022	-0.0023	-0.0018	-0.0021	-0.0022
Zu	-1.2943	-1.2943	-1.2943	-1.2943	-1.2943	-1.2943
Zw	-4.5098	-4.3513	-4.3266	-4.6339	-4.4007	-4.3401
Zq	-2.8580	-2.8580	-2.8580	-2.8580	-2.8580	-2.8580
$Z\dot{w}$	-0.4102	-0.6451	-1.1135	-0.3924	-0.6340	-1.1089
Zh	0.1184	0.0109	0.0110	0.1677	0.0213	0.0217
Mu	0.0000	0.0000	0.0000	0.0000	0.0000	0.0000
Mw	-0.5689	-0.5443	-0.5388	-0.5871	-0.5513	-0.5405
Mq	-6.1400	-6.1400	-6.1400	-6.1400	-6.1400	-6.1400
$M\dot{w}$	-0.8812	-1.3859	-2.3922	-0.8430	-1.3620	-2.3823
Mh	0.0092	0.0009	0.0009	0.0127	0.0017	0.0017

Table I-3 Stability derivatives at A = 0.05c and ω = 0.5 rad/s

Derivatives	λi = 0			λi = 25%			λi = 50%		
	h/c = 0.3	h/c = 0.5	h/c = 1.0	h/c = 0.3	h/c = 0.5	h/c = 1.0	h/c = 0.3	h/c = 0.5	h/c = 1.0
Xu	-0.0573	-0.0681	-0.0907	-0.0679	-0.0787	-0.1011	-0.0598	-0.0704	-0.0933
Xw	0.4571	0.3946	0.2507	0.4220	0.3597	0.2156	0.4515	0.3867	0.2399
Xq	0.0000	0.0000	0.0000	0.0000	0.0000	0.0000	0.0000	0.0000	0.0000
$X\dot{w}$	0.0000	0.0000	0.0000	0.0000	0.0000	0.0000	0.0000	0.0000	0.0000
Xh	-0.0013	-0.0015	-0.0015	-0.0018	-0.0021	-0.0021	-0.0022	-0.0022	-0.0022
Zu	-1.2943	-1.2943	-1.2943	-1.2943	-1.2943	-1.2943	-1.2943	-1.2943	-1.2943
Zw	-4.6170	-4.3869	-4.3294	-4.6559	-4.4257	-4.3726	-4.4900	-4.3777	-4.3570
Zq	-2.8580	-2.8580	-2.8580	-2.8580	-2.8580	-2.8580	-2.8580	-2.8580	-2.8580
$Z\dot{w}$	-0.3948	-0.6372	-1.1131	-0.3935	-0.6293	-1.0975	-0.4137	-0.6396	-1.1023
Zh	0.1661	0.0205	0.0208	0.1482	0.0190	0.0193	0.0853	0.0096	0.0097
Mu	0.0000	0.0000	0.0000	0.0000	0.0000	0.0000	0.0000	0.0000	0.0000
Mw	-0.5846	-0.5493	-0.5390	-0.5821	-0.5543	-0.5447	-0.5654	-0.5477	-0.5429
Mq	-6.1400	-6.1400	-6.1400	-6.1400	-6.1400	-6.1400	-6.1400	-6.1400	-6.1400
$M\dot{w}$	-0.8481	-1.3688	-2.3914	-0.8454	-1.3519	-2.3578	-0.8888	-1.3741	-2.3681
Mh	0.0126	0.0016	0.0017	0.0099	0.0015	0.0015	0.0066	0.0008	0.0008

Derivatives	λi = 75%			λi = 100%		
	h/c = 0.3	h/c = 0.5	h/c = 1.0	h/c = 0.3	h/c = 0.5	h/c = 1.0
Xu	-0.0466	-0.0582	-0.0819	-0.0573	-0.0680	-0.0907
Xw	0.4900	0.4221	0.2737	0.4574	0.3949	0.2509
Xq	0.0000	0.0000	0.0000	0.0000	0.0000	0.0000
$X\dot{w}$	0.0000	0.0000	0.0000	0.0000	0.0000	0.0000
Xh	-0.0024	-0.0023	-0.0023	-0.0018	-0.0021	-0.0021
Zu	-1.2943	-1.2943	-1.2943	-1.2943	-1.2943	-1.2943
Zw	-4.4692	-4.3320	-4.3135	-4.6160	-4.3862	-4.3291
Zq	-2.8580	-2.8580	-2.8580	-2.8580	-2.8580	-2.8580
$Z\dot{w}$	-0.4159	-0.6491	-1.1179	-0.3949	-0.6373	-1.1132
Zh	0.1041	0.0091	0.0092	0.1659	0.0204	0.0207
Mu	0.0000	0.0000	0.0000	0.0000	0.0000	0.0000
Mw	-0.5633	-0.5418	-0.5373	-0.5845	-0.5492	-0.5389
Mq	-6.1400	-6.1400	-6.1400	-6.1400	-6.1400	-6.1400
$M\dot{w}$	-0.8934	-1.3944	-2.4016	-0.8484	-1.3692	-2.3916
Mh	0.0081	0.0007	0.0007	0.0126	0.0016	0.0017

Table I-4 Stability derivatives at A = 0.05c and ω = 1.00 rad/s

Derivatives	λi = 0			λi = 25%			λi = 50%		
	h/c = 0.3	h/c = 0.5	h/c = 1.0	h/c = 0.3	h/c = 0.5	h/c = 1.0	h/c = 0.3	h/c = 0.5	h/c = 1.0
Xu	-0.0547	-0.0654	-0.0878	-0.0761	-0.0830	-0.1084	-0.0621	-0.0730	-0.0961
Xw	0.4681	0.4078	0.2633	0.3904	0.3325	0.1905	0.4428	0.3768	0.2295
Xq	0.0000	0.0000	0.0000	0.0000	0.0000	0.0000	0.0000	0.0000	0.0000
$X\dot{w}$	0.0000	0.0000	0.0000	0.0000	0.0000	0.0000	0.0000	0.0000	0.0000
Xh	-0.0019	-0.0021	-0.0021	-0.0017	-0.0019	-0.0020	-0.0022	-0.0022	-0.0022
Zu	-1.2943	-1.2943	-1.2943	-1.2943	-1.2943	-1.2943	-1.2943	-1.2943	-1.2943
Zw	-4.5634	-4.3521	-4.3074	-4.6400	-4.4434	-4.3827	-4.5174	-4.3990	-4.3718
Zq	-2.8580	-2.8580	-2.8580	-2.8580	-2.8580	-2.8580	-2.8580	-2.8580	-2.8580
$Z\dot{w}$	-0.4024	-0.6451	-1.1217	-0.3928	-0.6257	-1.0948	-0.4097	-0.6349	-1.0968
Zh	0.1545	0.0168	0.0170	0.1406	0.0216	0.0219	0.0893	0.0115	0.0116
Mu	0.0000	0.0000	0.0000	0.0000	0.0000	0.0000	0.0000	0.0000	0.0000
Mw	-0.5768	-0.5443	-0.5359	-0.5867	-0.5567	-0.5457	-0.5693	-0.5507	-0.5449
Mq	-6.1400	-6.1400	-6.1400	-6.1400	-6.1400	-6.1400	-6.1400	-6.1400	-6.1400
$M\dot{w}$	-0.8644	-1.3859	-2.4098	-0.8439	-1.3442	-2.3521	-0.8802	-1.3639	-2.3563
Mh	0.0118	0.0013	0.0014	0.0106	0.0017	0.0018	0.0069	0.0009	0.0009

Derivatives	λi = 75%			λi = 100%		
	h/c = 0.3	h/c = 0.5	h/c = 1.0	h/c = 0.3	h/c = 0.5	h/c = 1.0
Xu	-0.0357	-0.0484	-0.0730	-0.0540	-0.0648	-0.0872
Xw	0.5091	0.4423	0.2954	0.4703	0.4097	0.2651
Xq	0.0000	0.0000	0.0000	0.0000	0.0000	0.0000
$X\dot{w}$	0.0000	0.0000	0.0000	0.0000	0.0000	0.0000
Xh	-0.0027	-0.0024	-0.0024	-0.0019	-0.0021	-0.0022
Zu	-1.2943	-1.2943	-1.2943	-1.2943	-1.2943	-1.2943
Zw	-4.4290	-4.3066	-4.3010	-4.5585	-4.3494	-4.3058
Zq	-2.8580	-2.8580	-2.8580	-2.8580	-2.8580	-2.8580
$Z\dot{w}$	-0.4212	-0.6541	-1.1213	-0.4030	-0.6457	-1.1222
Zh	0.0944	0.0054	0.0054	0.1531	0.0164	0.0166
Mu	0.0000	0.0000	0.0000	0.0000	0.0000	0.0000
Mw	-0.5580	-0.5387	-0.5360	-0.5761	-0.5439	-0.5357
Mq	-6.1400	-6.1400	-6.1400	-6.1400	-6.1400	-6.1400
$M\dot{w}$	-0.9049	-1.4051	-2.4089	-0.8658	-1.3871	-2.4109
Mh	0.0074	0.0004	0.0004	0.0117	0.0013	0.0013

Table I-5 Stability derivatives at A = 0.05c and ω = 1.25 rad/s

Derivatives	λi = 0			λi = 25%			λi = 50%		
	h/c = 0.3	h/c = 0.5	h/c = 1.0	h/c = 0.3	h/c = 0.5	h/c = 1.0	h/c = 0.3	h/c = 0.5	h/c = 1.0
Xu	-0.0529	-0.0641	-0.0866	-0.0791	-0.0899	-0.1112	-0.0627	-0.0745	-0.0974
Xw	0.4547	0.4131	0.2627	0.3560	0.3200	0.1759	0.4075	0.3703	0.2222
Xq	0.0000	0.0000	0.0000	0.0000	0.0000	0.0000	0.0000	0.0000	0.0000
$X\dot{w}$	0.0000	0.0000	0.0000	0.0000	0.0000	0.0000	0.0000	0.0000	0.0000
Xh	-0.0022	-0.0021	-0.0022	-0.0021	-0.0019	-0.0020	-0.0028	-0.0022	-0.0022
Zu	-1.2943	-1.2943	-1.2943	-1.2943	-1.2943	-1.2943	-1.2943	-1.2943	-1.2943
Zw	-4.4818	-4.3375	-4.2981	-4.5658	-4.4493	-4.3816	-4.4348	-4.4073	-4.3759
Zq	-2.8580	-2.8580	-2.8580	-2.8580	-2.8580	-2.8580	-2.8580	-2.8580	-2.8580
$Z\dot{w}$	-0.4144	-0.6485	-1.1253	-0.4038	-0.6251	-1.0959	-0.4224	-0.6331	-1.0954
Zh	0.1089	0.0152	0.0154	0.0872	0.0230	0.0234	0.0246	0.0127	0.0128
Mu	0.0000	0.0000	0.0000	0.0000	0.0000	0.0000	0.0000	0.0000	0.0000
Mw	-0.5647	-0.5422	-0.5346	-0.5753	-0.5570	-0.5453	-0.5569	-0.5519	-0.5455
Mq	-6.1400	-6.1400	-6.1400	-6.1400	-6.1400	-6.1400	-6.1400	-6.1400	-6.1400
$M\dot{w}$	-0.8903	-1.3931	-2.4176	-0.8675	-1.3430	-2.3543	-0.9075	-1.3601	-2.3532
Mh	0.0085	0.0012	0.0012	0.0067	0.0018	0.0019	0.0019	0.0010	0.0010

Derivatives	λi = 75%			λi = 100%		
	h/c = 0.3	h/c = 0.5	h/c = 1.0	h/c = 0.3	h/c = 0.5	h/c = 1.0
Xu	-0.0294	-0.0439	-0.0690	-0.0520	-0.0633	-0.0859
Xw	0.4775	0.4520	0.3038	0.4569	0.4154	0.2680
Xq	0.0000	0.0000	0.0000	0.0000	0.0000	0.0000
$X\dot{w}$	0.0000	0.0000	0.0000	0.0000	0.0000	0.0000
Xh	-0.0035	-0.0025	-0.0025	-0.0022	-0.0021	-0.0022
Zu	-1.2943	-1.2943	-1.2943	-1.2943	-1.2943	-1.2943
Zw	-4.3335	-4.2991	-4.2975	-4.4778	-4.3350	-4.2972
Zq	-2.8580	-2.8580	-2.8580	-2.8580	-2.8580	-2.8580
$Z\dot{w}$	-0.4359	-0.6554	-1.1219	-0.4150	-0.6490	-1.1256
Zh	0.0313	0.0043	0.0043	0.1079	0.0148	0.0150
Mu	0.0000	0.0000	0.0000	0.0000	0.0000	0.0000
Mw	-0.5442	-0.5379	-0.5358	-0.5641	-0.5419	-0.5345
Mq	-6.1400	-6.1400	-6.1400	-6.1400	-6.1400	-6.1400
$M\dot{w}$	-0.9364	-1.4079	-2.4102	-0.8915	-1.3942	-2.4182
Mh	0.0025	0.0003	0.0003	0.0084	0.0012	0.0012

Table I-6 Stability derivatives at A = 0.15c and ω = 0.25 rad/s

Derivatives	λi = 0			λi = 25%			λi = 50%		
	h/c = 0.3	h/c = 0.5	h/c = 1.0	h/c = 0.3	h/c = 0.5	h/c = 1.0	h/c = 0.3	h/c = 0.5	h/c = 1.0
Xu	NaN	-0.0681	-0.0914	NaN	-0.0789	-0.1057	NaN	-0.0699	-0.0931
Xw	NaN	0.3712	0.2449	NaN	0.3588	0.1977	NaN	0.3764	0.2406
Xq	NaN	0.0000	0.0000	NaN	0.0000	0.0000	NaN	0.0000	0.0000
$X\dot{w}$	NaN	0.0000	0.0000	NaN	0.0000	0.0000	NaN	0.0000	0.0000
Xh	NaN	-0.0016	-0.0046	NaN	-0.0024	-0.0025	NaN	-0.0024	-0.0024
Zu	NaN	-1.2943	-1.2943	NaN	-1.2943	-1.2943	NaN	-1.2943	-1.2943
Zw	NaN	-4.6167	-4.3556	NaN	-4.4654	-4.4020	NaN	-4.3154	-4.3570
Zq	NaN	-2.8580	-2.8580	NaN	-2.8580	-2.8580	NaN	-2.8580	-2.8580
$Z\dot{w}$	NaN	-0.5856	-1.1025	NaN	-0.6202	-1.0865	NaN	-0.6545	-1.1022
Zh	NaN	0.0770	-0.6472	NaN	0.0225	0.0228	NaN	-0.0091	-0.0090
Mu	NaN	0.0000	0.0000	NaN	0.0000	0.0000	NaN	0.0000	0.0000
Mw	NaN	-0.5838	-0.5429	NaN	-0.5603	-0.5487	NaN	-0.5384	-0.5429
Mq	NaN	-6.1400	-6.1400	NaN	-6.1400	-6.1400	NaN	-6.1400	-6.1400
$M\dot{w}$	NaN	-1.2581	-2.3685	NaN	-1.3324	-2.3342	NaN	-1.4062	-2.3680
Mh	NaN	0.0058	0.0494	NaN	0.0018	0.0018	NaN	-0.0007	-0.0007

Derivatives	λi = 75%			λi = 100%		
	h/c = 0.3	h/c = 0.5	h/c = 1.0	h/c = 0.3	h/c = 0.5	h/c = 1.0
Xu	NaN	-0.0526	-0.0762	NaN	-0.0607	-0.0914
Xw	NaN	0.4249	0.2826	NaN	0.4234	0.2448
Xq	NaN	0.0000	0.0000	NaN	0.0000	0.0000
$X\dot{w}$	NaN	0.0000	0.0000	NaN	0.0000	0.0000
Xh	NaN	-0.0023	-0.0023	NaN	-0.0024	-0.0026
Zu	NaN	-1.2943	-1.2943	NaN	-1.2943	-1.2943
Zw	NaN	-4.2934	-4.2796	NaN	-4.6135	-4.3554
Zq	NaN	-2.8580	-2.8580	NaN	-2.8580	-2.8580
$Z\dot{w}$	NaN	-0.6578	-1.1309	NaN	-0.5855	-1.1025
Zh	NaN	0.0078	0.0078	NaN	0.0772	0.0821
Mu	NaN	0.0000	0.0000	NaN	0.0000	0.0000
Mw	NaN	-0.5364	-0.5326	NaN	-0.5838	-0.5428
Mq	NaN	-6.1400	-6.1400	NaN	-6.1400	-6.1400
$M\dot{w}$	NaN	-1.4132	-2.4297	NaN	-1.2579	-2.3687
Mh	NaN	0.0006	0.0006	NaN	0.0059	0.0066

Table I-7 Stability derivatives at A = 0.15c and ω = 0.5 rad/s

Derivatives	λi = 0			λi = 25%			λi = 50%		
	h/c = 0.3	h/c = 0.5	h/c = 1.0	h/c = 0.3	h/c = 0.5	h/c = 1.0	h/c = 0.3	h/c = 0.5	h/c = 1.0
Xu	NaN	-0.0655	-0.0890	NaN	-0.0944	-0.1172	NaN	-0.0719	-0.0957
Xw	NaN	0.3621	0.2552	NaN	0.2688	0.1519	NaN	0.3479	0.2308
Xq	NaN	0.0000	0.0000	NaN	0.0000	0.0000	NaN	0.0000	0.0000
$X\dot{w}$	NaN	0.0000	0.0000	NaN	0.0000	0.0000	NaN	0.0000	0.0000
Xh	NaN	-0.0018	-0.0019	NaN	-0.0020	-0.0021	NaN	-0.0026	-0.0025
Zu	NaN	-1.2943	-1.2943	NaN	-1.2943	-1.2943	NaN	-1.2943	-1.2943
Zw	NaN	-4.5282	-4.3142	NaN	-4.5040	-4.4394	NaN	-4.2897	-4.3776
Zq	NaN	-2.8580	-2.8580	NaN	-2.8580	-2.8580	NaN	-2.8580	-2.8580
$Z\dot{w}$	NaN	-0.6046	-1.1191	NaN	-0.6132	-1.0738	NaN	-0.6611	-1.0943
Zh	NaN	0.0650	0.0684	NaN	0.0221	0.0225	NaN	-0.0231	-0.0227
Mu	NaN	0.0000	0.0000	NaN	0.0000	0.0000	NaN	0.0000	0.0000
Mw	NaN	-0.5707	-0.5368	NaN	-0.5649	-0.5535	NaN	-0.5344	-0.5458
Mq	NaN	-6.1400	-6.1400	NaN	-6.1400	-6.1400	NaN	-6.1400	-6.1400
$M\dot{w}$	NaN	-1.2988	-2.4042	NaN	-1.3173	-2.3070	NaN	-1.4202	-2.3510
Mh	NaN	0.0050	0.0055	NaN	0.0017	0.0018	NaN	-0.0019	-0.0018

Derivatives	λi = 75%			λi = 100%		
	h/c = 0.3	h/c = 0.5	h/c = 1.0	h/c = 0.3	h/c = 0.5	h/c = 1.0
Xu	NaN	-0.0334	-0.0595	NaN	-0.0652	-0.0888
Xw	NaN	0.4398	0.3298	NaN	0.3632	0.2562
Xq	NaN	0.0000	0.0000	NaN	0.0000	0.0000
$X\dot{w}$	NaN	0.0000	0.0000	NaN	0.0000	0.0000
Xh	NaN	-0.0027	-0.0026	NaN	-0.0018	-0.0019
Zu	NaN	-1.2943	-1.2943	NaN	-1.2943	-1.2943
Zw	NaN	-4.1742	-4.2310	NaN	-4.5240	-4.3129
Zq	NaN	-2.8580	-2.8580	NaN	-2.8580	-2.8580
$Z\dot{w}$	NaN	-0.6854	-1.1482	NaN	-0.6054	-1.1196
Zh	NaN	-0.0136	-0.0131	NaN	0.0642	0.0676
Mu	NaN	0.0000	0.0000	NaN	0.0000	0.0000
Mw	NaN	-0.5200	-0.5266	NaN	-0.5701	-0.5366
Mq	NaN	-6.1400	-6.1400	NaN	-6.1400	-6.1400
$M\dot{w}$	NaN	-1.4726	-2.4666	NaN	-1.3007	-2.4053
Mh	NaN	-0.0011	-0.0010	NaN	0.0050	0.0055

Table I-8 Stability derivatives at A = 0.15c and ω = 1.00 rad/s

Derivatives	λi = 0			λi = 25%			λi = 50%		
	h/c = 0.3	h/c = 0.5	h/c = 1.0	h/c = 0.3	h/c = 0.5	h/c = 1.0	h/c = 0.3	h/c = 0.5	h/c = 1.0
Xu	NaN	-0.0589	-0.0804	NaN	-0.1124	-0.1352	NaN	-0.0792	-0.1030
Xw	NaN	0.3951	0.2642	NaN	0.1952	0.0831	NaN	0.3510	0.1966
Xq	NaN	0.0000	0.0000	NaN	0.0000	0.0000	NaN	0.0000	0.0000
$X\dot{w}$	NaN	0.0000	0.0000	NaN	0.0000	0.0000	NaN	0.0000	0.0000
Xh	NaN	-0.0014	-0.0016	NaN	-0.0014	-0.0016	NaN	-0.0022	-0.0023
Zu	NaN	-1.2943	-1.2943	NaN	-1.2943	-1.2943	NaN	-1.2943	-1.2943
Zw	NaN	-4.3856	-4.1025	NaN	-4.5906	-4.3717	NaN	-4.4455	-4.4029
Zq	NaN	-2.8580	-2.8580	NaN	-2.8580	-2.8580	NaN	-2.8580	-2.8580
$Z\dot{w}$	NaN	-0.6364	-1.2102	NaN	-0.5960	-1.1048	NaN	-0.6248	-1.0856
Zh	NaN	0.0873	0.0936	NaN	0.0657	0.0693	NaN	0.0160	0.0162
Mu	NaN	0.0000	0.0000	NaN	0.0000	0.0000	NaN	0.0000	0.0000
Mw	NaN	-0.5498	-0.5057	NaN	-0.5765	-0.5420	NaN	-0.5573	-0.5491
Mq	NaN	-6.1400	-6.1400	NaN	-6.1400	-6.1400	NaN	-6.1400	-6.1400
$M\dot{w}$	NaN	-1.3671	-2.5999	NaN	-1.2804	-2.3736	NaN	-1.3422	-2.3322
Mh	NaN	0.0069	0.0079	NaN	0.0050	0.0056	NaN	0.0013	0.0013

Derivatives	λi = 75%			λi = 100%		
	h/c = 0.3	h/c = 0.5	h/c = 1.0	h/c = 0.3	h/c = 0.5	h/c = 1.0
Xu	NaN	0.0035	-0.0268	NaN	-0.0567	-0.0782
Xw	NaN	0.4895	0.3628	NaN	0.4004	0.2687
Xq	NaN	0.0000	0.0000	NaN	0.0000	0.0000
$X\dot{w}$	NaN	0.0000	0.0000	NaN	0.0000	0.0000
Xh	NaN	-0.0031	-0.0030	NaN	-0.0014	-0.0016
Zu	NaN	-1.2943	-1.2943	NaN	-1.2943	-1.2943
Zw	NaN	-4.1457	-4.1781	NaN	-4.3726	-4.0948
Zq	NaN	-2.8580	-2.8580	NaN	-2.8580	-2.8580
$Z\dot{w}$	NaN	-0.6880	-1.1641	NaN	-0.6392	-1.2132
Zh	NaN	-0.0054	-0.0054	NaN	0.0860	0.0921
Mu	NaN	0.0000	0.0000	NaN	0.0000	0.0000
Mw	NaN	-0.5185	-0.5211	NaN	-0.5480	-0.5047
Mq	NaN	-6.1400	-6.1400	NaN	-6.1400	-6.1400
$M\dot{w}$	NaN	-1.4782	-2.5008	NaN	-1.3732	-2.6064
Mh	NaN	-0.0004	-0.0004	NaN	0.0069	0.0078

Table I-9 Stability derivatives at A = 0.15c and ω = 1.25 rad/s

Derivatives	λi = 0			λi = 25%			λi = 50%		
	h/c = 0.3	h/c = 0.5	h/c = 1.0	h/c = 0.3	h/c = 0.5	h/c = 1.0	h/c = 0.3	h/c = 0.5	h/c = 1.0
Xu	NaN	-0.0561	-0.0765	NaN	-0.1183	-0.1414	NaN	-0.0833	-0.1068
Xw	NaN	0.4109	0.2904	NaN	0.1510	0.0519	NaN	0.3358	0.1780
Xq	NaN	0.0000	0.0000	NaN	0.0000	0.0000	NaN	0.0000	0.0000
$X\dot{w}$	NaN	0.0000	0.0000	NaN	0.0000	0.0000	NaN	0.0000	0.0000
Xh	NaN	-0.0013	-0.0015	NaN	-0.0014	-0.0015	NaN	-0.0022	-0.0022
Zu	NaN	-1.2943	-1.2943	NaN	-1.2943	-1.2943	NaN	-1.2943	-1.2943
Zw	NaN	-4.3302	-4.0504	NaN	-4.6055	-4.3847	NaN	-4.4614	-4.4110
Zq	NaN	-2.8580	-2.8580	NaN	-2.8580	-2.8580	NaN	-2.8580	-2.8580
$Z\dot{w}$	NaN	-0.6493	-1.2336	NaN	-0.5934	-1.1008	NaN	-0.6216	-1.0831
Zh	NaN	0.0873	0.0936	NaN	0.0662	0.0697	NaN	0.0182	0.0184
Mu	NaN	0.0000	0.0000	NaN	0.0000	0.0000	NaN	0.0000	0.0000
Mw	NaN	-0.5417	-0.4982	NaN	-0.5783	-0.5435	NaN	-0.5593	-0.5500
Mq	NaN	-6.1400	-6.1400	NaN	-6.1400	-6.1400	NaN	-6.1400	-6.1400
$M\dot{w}$	NaN	-1.3948	-2.6503	NaN	-1.2749	-2.3648	NaN	-1.3354	-2.3269
Mh	NaN	0.0070	0.0080	NaN	0.0051	0.0056	NaN	0.0014	0.0015

Derivatives	λi = 75%			λi = 100%		
	h/c = 0.3	h/c = 0.5	h/c = 1.0	h/c = 0.3	h/c = 0.5	h/c = 1.0
Xu	NaN	0.0215	-0.0113	NaN	-0.0533	-0.0929
Xw	NaN	0.5003	0.3840	NaN	0.4151	0.3013
Xq	NaN	0.0000	0.0000	NaN	0.0000	0.0000
$X\dot{w}$	NaN	0.0000	0.0000	NaN	0.0000	0.0000
Xh	NaN	-0.0033	-0.0033	NaN	-0.0030	-0.0034
Zu	NaN	-1.2943	-1.2943	NaN	-1.2943	-1.2943
Zw	NaN	-4.1158	-4.1597	NaN	-4.3237	-4.0558
Zq	NaN	-2.8580	-2.8580	NaN	-2.8580	-2.8580
$Z\dot{w}$	NaN	-0.6935	-1.1687	NaN	-0.6505	-1.2349
Zh	NaN	-0.0086	-0.0086	NaN	0.0866	0.0929
Mu	NaN	0.0000	0.0000	NaN	0.0000	0.0000
Mw	NaN	-0.5154	-0.5195	NaN	-0.5409	-0.4978
Mq	NaN	-6.1400	-6.1400	NaN	-6.1400	-6.1400
$M\dot{w}$	NaN	-1.4899	-2.5109	NaN	-1.3975	-2.6530
Mh	NaN	-0.0007	-0.0007	NaN	0.0070	0.0079

Appendix J **Eigenvalues of the Ekranoplan 'Orlyonok' A90 (at constant C_L)**

Table J-1 Short period at A = 0.05c

h/c	λi	ω = 0.25 rad/s		ω = 0.50 rad/s		ω = 1.00 rad/s		ω = 1.25 rad/s	
		Real	Img.	Real	Img.	Real	Img.	Real	Img.
0.3	0	-0.7031	0.8703	-0.7021	0.8674	-0.7010	0.8553	-0.7081	0.8229
	25%	-0.7110	0.8414	-0.7155	0.8526	-0.7120	0.8557	-0.7221	0.8199
	50%	-0.7149	0.8107	-0.7158	0.8120	-0.7169	0.8170	-0.7297	0.7759
	75%	-0.7074	0.8311	-0.7083	0.8197	-0.7078	0.8110	-0.7193	0.7699
	100%	-0.7031	0.8702	-0.7021	0.8672	-0.7010	0.8540	-0.7081	0.8220
	No Osc.	-0.7136 ± 0.8113i							
0.5	0	-0.7485	0.7467	-0.7477	0.7447	-0.7461	0.7392	-0.7454	0.7369
	25%	-0.7505	0.7446	-0.7514	0.7476	-0.7523	0.7502	-0.7523	0.7511
	50%	-0.7499	0.7369	-0.7505	0.7385	-0.7516	0.7416	-0.7519	0.7429
	75%	-0.7479	0.7366	-0.7469	0.7340	-0.7459	0.7302	-0.7456	0.7292
	100%	-0.7485	0.7466	-0.7477	0.7446	-0.7460	0.7388	-0.7453	0.7365
	No Osc.	-0.7497 ± 0.7351i							
1.0	0	-0.7884	0.6817	-0.7880	0.6801	-0.7876	0.6762	-0.7875	0.6746
	25%	-0.7919	0.6818	-0.7921	0.6838	-0.7921	0.6853	-0.7916	0.6855
	50%	-0.7940	0.6776	-0.7943	0.6788	-0.7948	0.6811	-0.7947	0.6819
	75%	-0.7913	0.6762	-0.7908	0.6744	-0.7911	0.6722	-0.7912	0.6717
	100%	-0.7885	0.6817	-0.7880	0.6800	-0.7876	0.6760	-0.7875	0.6744
	No Osc.	-0.7943 ± 0.6765i							

Table J-2 Phugoid at A = 0.05c

h/c	λi	ω = 0.25 rad/s		ω = 0.50 rad/s		ω = 1.00 rad/s		ω = 1.25 rad/s	
		Real	Img.	Real	Img.	Real	Img.	Real	Img.
0.3	0	-0.0404	0.2621	-0.0401	0.2606	-0.0371	0.2519	-0.0228	0.2187
	25%	-0.0271	0.2328	-0.0297	0.2564	-0.0304	0.2446	-0.0135	0.2035
	50%	-0.0152	0.2002	-0.0152	0.2006	-0.0161	0.2046	0.0063	0.1397
	75%	-0.0261	0.2265	-0.0218	0.2151	-0.0187	0.2069	0.0056	0.1464
	100%	-0.0403	0.2621	-0.0400	0.2604	-0.0368	0.2509	-0.0226	0.2179
	No Osc.	-0.0161 ± 0.2022i							
0.5	0	0.0051	0.1348	0.0053	0.1333	0.0064	0.1280	0.0069	0.1257
	25%	0.0069	0.1288	0.0061	0.1321	0.0051	0.1355	0.0046	0.1374
	50%	0.0098	0.1172	0.0096	0.1187	0.0090	0.1218	0.0085	0.1235
	75%	0.0091	0.1202	0.0101	0.1176	0.0125	0.1122	0.0135	0.1106
	100%	0.0051	0.1347	0.0053	0.1332	0.0065	0.1275	0.0071	0.1251
	No Osc.	0.0105 ± 0.1148i							
1.0	0	0.0057	0.1344	0.0059	0.1329	0.0069	0.1277	0.0075	0.1255
	25%	0.0075	0.1285	0.0067	0.1317	0.0057	0.1351	0.0053	0.1369
	50%	0.0101	0.1172	0.0099	0.1187	0.0094	0.1217	0.0090	0.1233
	75%	0.0095	0.1201	0.0103	0.1175	0.0124	0.1122	0.0133	0.1106
	100%	0.0058	0.1343	0.0060	0.1328	0.0071	0.1272	0.0077	0.1249
	No Osc.	0.0106 ± 0.1147i							

Table J-3 Subsidence mode at A = 0.05c

h/c	λi	ω = 0.25 rad/s	ω = 0.50 rad/s	ω = 1.00 rad/s	ω = 1.25 rad/s
0.3	0	-0.02081	-0.02057	-0.02001	-0.02181
	25%	-0.02329	-0.0221	-0.02648	-0.02921
	50%	-0.02365	-0.02384	-0.02446	-0.03107
	75%	-0.02087	-0.02059	-0.02013	-0.03045
	100%	-0.02082	-0.02055	-0.01989	-0.02169
	No Osc.	-0.0235			
0.5	0	-0.02844	-0.02818	-0.0278	-0.02791
	25%	-0.02949	-0.02969	-0.03002	-0.03019
	50%	-0.0299	-0.03005	-0.03039	-0.03019
	75%	-0.0294	-0.02961	-0.03107	-0.03192
	100%	-0.02845	-0.02818	-0.02782	-0.02793
	No Osc.	-0.0301			
1.0	0	-0.03331	-0.03287	-0.03186	-0.03177
	25%	-0.03359	-0.03416	-0.03481	-0.03519
	50%	-0.03236	-0.03275	-0.03352	-0.03357
	75%	-0.03238	-0.03221	-0.03274	-0.03328
	100%	-0.0333	-0.03286	-0.03182	-0.03167
	No Osc.	-0.0322			

Table J-4 Short period at A = 0.15c

h/c	λi	ω = 0.25 rad/s		ω = 0.50 rad/s		ω = 1.00 rad/s		ω = 1.25 rad/s	
		Real	Img.	Real	Img.	Real	Img.	Real	Img.
0.3	0	NaN	NaN	NaN	NaN	NaN	NaN	NaN	NaN
	25%	NaN	NaN	NaN	NaN	NaN	NaN	NaN	NaN
	50%	NaN	NaN	NaN	NaN	NaN	NaN	NaN	NaN
	75%	NaN	NaN	NaN	NaN	NaN	NaN	NaN	NaN
	100%	NaN	NaN	NaN	NaN	NaN	NaN	NaN	NaN
	No Osc.	NaN							
0.5	0	-0.7481	0.7976	-0.7449	0.7816	-0.7261	0.7755	-0.7215	0.7688
	25%	-0.7535	0.7537	-0.7572	0.7562	-0.7508	0.7848	-0.7522	0.7860
	50%	-0.7517	0.7229	-0.7544	0.7135	-0.7539	0.7484	-0.7546	0.7508
	75%	-0.7443	0.7293	-0.7419	0.7073	-0.7366	0.7102	-0.7352	0.7065
	100%	-0.7476	0.7983	-0.7448	0.7808	-0.7254	0.7734	-0.7212	0.7680
	No Osc.	-0.7497 ± 0.7351i							
1.0	0	-0.7669	0.7077	-0.7687	0.6972	-0.7415	0.6795	-0.7372	0.6727
	25%	-0.7932	0.6883	-0.7966	0.6914	-0.7741	0.7001	-0.7752	0.7013
	50%	-0.8011	0.6714	-0.8077	0.6681	-0.7957	0.6859	-0.7957	0.6873
	75%	-0.7887	0.6702	-0.7925	0.6577	-0.7851	0.6568	-0.7847	0.6546
	100%	-0.7668	0.7078	-0.7689	0.6967	-0.7415	0.6781	-0.7378	0.6714
	No Osc.	-0.7943 ± 0.6765i							

Table J-5 Phugoid at A = 0.15c

h/c	λi	ω = 0.25 rad/s		ω = 0.50 rad/s		ω = 1.00 rad/s		ω = 1.25 rad/s	
		Real	Img.	Real	Img.	Real	Img.	Real	Img.
0.3	0	NaN	NaN	NaN	NaN	NaN	NaN	NaN	NaN
	25%	NaN	NaN	NaN	NaN	NaN	NaN	NaN	NaN
	50%	NaN	NaN	NaN	NaN	NaN	NaN	NaN	NaN
	75%	NaN	NaN	NaN	NaN	NaN	NaN	NaN	NaN
	100%	NaN	NaN	NaN	NaN	NaN	NaN	NaN	NaN
	No Osc.	NaN							
0.5	0	-0.0130	0.1971	-0.0092	0.1840	-0.0183	0.1994	-0.0190	0.1978
	25%	0.0047	0.1371	0.0060	0.1373	-0.0056	0.1852	-0.0045	0.1859
	50%	0.0171	0.0880	0.0239	0.0569	0.0080	0.1287	0.0072	0.1318
	75%	0.0108	0.1151	0.0245	0.0813	0.0245	0.0970	0.0299	0.0941
	100%	-0.0148	0.1974	-0.0089	0.1832	-0.0180	0.1980	-0.0189	0.1972
	No Osc.	0.0105 ± 0.1148i							
1.0	0	-0.0159	0.1938	-0.0114	0.1814	-0.0227	0.1953	-0.0238	0.1938
	25%	0.0057	0.1367	0.0062	0.1368	-0.0075	0.1827	-0.0068	0.1834
	50%	0.0150	0.0875	0.0162	0.0518	0.0087	0.1285	0.0080	0.1316
	75%	0.0108	0.1151	0.0218	0.0802	0.0229	0.0967	0.0278	0.0935
	100%	-0.0160	0.1940	-0.0111	0.1806	-0.0223	0.1940	-0.0205	0.1929
	No Osc.	0.0106 ± 0.1147i							

Table J-6 Subsidence mode at A = 0.15c

h/c	λi	ω = 0.25 rad/s	ω = 0.50 rad/s	ω = 1.00 rad/s	ω = 1.25 rad/s
0.3	0	NaN	NaN	NaN	NaN
	25%	NaN	NaN	NaN	NaN
	50%	NaN	NaN	NaN	NaN
	75%	NaN	NaN	NaN	NaN
	100%	NaN	NaN	NaN	NaN
	No Osc.	NaN			
0.5	0	-0.02623	-0.02644	-0.0229	-0.02167
	25%	-0.02978	-0.03246	-0.03784	-0.04032
	50%	-0.03298	-0.0376	-0.03168	-0.0318
	75%	-0.02944	-0.04099	-0.04221	-0.04864
	100%	-0.02377	-0.0264	-0.02246	-0.02119
	No Osc.	-0.0301			
1.0	0	-0.03541	-0.03413	-0.03203	-0.03025
	25%	-0.0353	-0.03685	-0.04594	-0.04801
	50%	-0.02936	-0.02221	-0.03587	-0.03642
	75%	-0.03165	-0.03625	-0.04074	-0.04642
	100%	-0.03543	-0.03407	-0.03154	-0.0345
	No Osc.	-0.0322			